UNIVERSIDADE FEDERAL DO CEARÁ
INSTITUTO DE CIÊNCIAS DO MAR
PÓS-GRADUAÇÃO EM CIÊNCIAS MARINHAS TROPICAIS

ADRIANA PEREIRA DO NASCIMENTO

GEOQUÍMICA FORENSE APLICADA AOS MÚLTIPLOS DERRAMAMENTOS DE ÓLEO NA COSTA DO CEARÁ, BRASIL, DE 2019 A 2022

Fortaleza
2025

ADRIANA PEREIRA DO NASCIMENTO

GEOQUÍMICA FORENSE APLICADA AOS MÚLTIPLOS DERRAMAMENTOS DE ÓLEO NA COSTA DO CEARÁ, BRASIL, DE 2019 A 2022

Tese apresentada ao Programa de Pós-Graduação em Ciências Marinhas Tropicais da Universidade Federal do Ceará, como requisito parcial à obtenção do título de Doutor em Ciências Marinhas Tropicais. Área de concentração: Utilização e Manejo de Ecossistemas Marinhos e Estuarinos.

Orientador: Prof. Dr. Rivelino Martins Cavalcante.

Orientador: Prof. Dr. Laercio Lopes Martins.

FORTALEZA

2025

Dados Internacionais de Catalogação na Publicação
Universidade Federal do Ceará
Sistema de Bibliotecas
Gerada automaticamente pelo módulo Catalog, mediante os dados fornecidos pelo(a) autor(a)

N193g Nascimento, Adriana Pereira do.
Geoquímica forense aplicada aos múltiplos derramamentos de óleo na costa do Ceará, Brasil, de 2019 a 2022 / Adriana Pereira do Nascimento. – 2025.
268 f. : il. color.

Tese (doutorado) – Universidade Federal do Ceará, Instituto de Ciências do Mar, Programa de Pós-Graduação em Ciências Marinhas Tropicais, Fortaleza, 2025.
Orientação: Prof. Dr. Rivelino Martins Cavalcante.
Coorientação: Prof. Dr. Laercio Lopes Martins.

1. Poluiçaõ costeira. 2. Geoquímica ambiental. 4. Fingerprint. 5. Biomarcadores. I. Título.

CDD 551.46

ADRIANA PEREIRA DO NASCIMENTO

GEOQUÍMICA FORENSE APLICADA AOS MÚLTIPLOS DERRAMAMENTOS DE ÓLEO NA COSTA DO CEARÁ, BRASIL, DE 2019 A 2022

Tese ou Dissertação apresentada ao Programa de Pós-Graduação em Ciências Marinhas Tropicais da Universidade Federal do Ceará, como requisito parcial à obtenção do título de Doutor em Ciências Marinhas Tropicais. Área de concentração: Utilização e Manejo de Ecossistemas Marinhos e Estuarinos.

Aprovada em: 29/04/2025.

BANCA EXAMINADORA

_____

Prof. Dr. Rivelino Martins Cavalcante (Orientador)

Universidade Federal do Ceará - UFC

_____

Prof. Dr. Laercio Lopes Martins (Coorientador)

Universidade Estadual do Norte Fluminense - UENF

_____

Prof. Dr. André Henrique Barbosa de Oliveira

Universidade Federal do Ceará - UFC

_____

Profa. Dra. Georgiana Feitosa da Cruz

Universidade Estadual do Norte Fluminense - UENF

_____

Prof. Dr. Boniek Gontijo Vaz

Universidade Federal de Goiás - UFG

_____

Prof. Dr. Tristan Charles Clitandre Rousseau

Universidade Federal do Ceará - UFC

Aos meus pais, *in memoriam*:

José Marcelo e Zeneide Pereira.

AGRADECIMENTOS

Agradeço a Deus por ter me dado força em toda a trajetória da minha vida; pela sabedoria, pelo discernimento, pela paciência e por colocar as pessoas certas no meu caminho. Sou também grata por me livrar do mal e por me amparar a cada passo. Sem a sua presença, eu não seria quem sou hoje. Obrigada, meu Deus!

Dedico esta tese aos meus pais, José Marcelo e Zeneide Pereira — em especial à minha mãe, que nunca mediu esforços para nos dar educação. Foi ali, sentada diante de uma máquina de costura, que ela nos ensinou o valor da luta, da honestidade, do respeito ao próximo e da persistência para conquistar nossos sonhos.

Agradeço também aos meus irmãos, Silvana, Dario e Marcelino, por todo o apoio e incentivo, especialmente nos momentos mais difíceis que vocês sempre estiveram ao meu lado, me aguentando com amor e paciência. E à minha sobrinha Lorena: muito obrigada, viu? Você me ajudou demais. Você é, e sempre será a Loreninha da tia.

Ao meu orientador, Prof. Dr. Rivelino Cavalcante, agradeço por ter aberto as portas do LACOR para a minha vida profissional. Sou grata por todas as oportunidades de aprendizado, pelo crescimento profissional e pessoal, e até mesmo pelos puxões de orelha. Como diz Cavalcante (2025), **“nós nascemos para brilhar”**. Que o LACOR brilhe por muitos anos — tenho muito orgulho de fazer parte dessa equipe comprometida, competente e extremamente divertida.

Quero expressar minha gratidão ao meu coorientador, Prof. Dr. Laercio Lopes. Agradeço por me ter apresentado ao desafiador mundo da geoquímica, pelas orientações, pela dedicação, pela amizade, pelas viagens e por compartilhar generosamente seu conhecimento comigo. Sua presença foi de grande importância para minha trajetória, sou profundamente grata pela oportunidade de ter caminhado ao seu lado ao longo de todo o processo.

Agradeço à coordenação do PPGMT, à Profa. Cristina Rocha-Barreira, pelo apoio, incentivo e orientação ao longo da jornada, e à secretária do programa, Isabella Abreu, sempre atenciosa e disponível. Aos técnicos administrativos, em especial a técnica do Lacor Viviane Lemos.

Aos colegas do LACOR (Duci, Rafael, Alessandra, Beatriz ABC, Beatriz Diniz, Camila, Lara, Junior, Gardilene, Elissandra), expresso minha sincera gratidão pela parceria, pelo apoio nos experimentos, pela troca de conhecimento, pelas risadas compartilhadas, pelos cafezinhos, almoços, sorvetes, caminhadas e pedaladas ao longo dessa jornada. Esta equipe é, de fato, incrível e não mede esforços quando se trata de colocar a mão na massa.

Agradeço, de forma especial, à Duciene Feitosa, pela parceria inestimável durante esses anos de doutorado. Você foi, sem dúvida, um presente que o doutorado me proporcionou, sempre ao meu lado com seu apoio incondicional e dedicação. Sua presença foi fundamental para meu crescimento pessoal e acadêmico.

Expresso meus agradecimentos à equipe do LEA, sob a coordenação do Prof. Dr. André Oliveira. Em especial, agradeço ao discente Rufino Andrade, que caminhou comigo em diversos momentos do doutorado. Sou grata pelas horas de bancada, pela troca de conhecimento e por sua constante disposição em ajudar. Você sempre foi muito prestativo, compartilhando seu conhecimento sem medir esforços. Muito obrigada por tudo, Rufino!

Agradeço à equipe de monitoramento do projeto Plástico/Óleo, em nome do Prof. Dr. Tommaso Giarrizzo (UFC), bem como ao discente Lúcio Brabo.

Agradeço à CAPES pelo fomento à bolsa de doutorado.

Agradeço também à equipe responsável pela coleta das amostras no ano de 2021, Alexandre Medeiros e Antônio Rodrigues. Muito obrigada pelo apoio.

Agradeço à Profa. Dra. Débora Azevedo e ao Dr. Vinícius Barreto (UFRJ) pela parceria nas análises por cromatografia gasosa e pelo aprendizado adquirido durante o período em que estive no LADETEC-LAGOA.

Ao Prof. Dr. Boniek Vaz e à Dra. Danielle Mitze (UFG), pela disponibilidade e pelo uso do equipamento FT-ICR MS, fundamental para a análise e o tratamento das minhas amostras.

Profa. Dra. Georgiana Cruz e ao Prof. Dr. Laercio Lopes, meu agradecimento por me receberem no LENEP/UENF, onde tive a oportunidade de vivenciar uma etapa de formação acadêmica.

Ao Prof. Dr. Jandyson e à discente Marília Gabriela (UFRPE), expresso minha sincera gratidão pela troca de conhecimentos, pelas análises realizadas no GC-MS e pela parceria no desenvolvimento do meu primeiro artigo.

São muitos os amigos, e para que ninguém fique de fora, agradeço a todos que torceram e continuam torcendo por mim. O apoio e os pensamentos de cada um de vocês sempre me trazem força nesta jornada que é a vida.

RESUMO

Em janeiro de 2019, o Brasil foi impactado pelo maior derramamento de óleo já registrado em oceanos tropicais, com mais de 5 mil toneladas de óleo atingindo a costa das regiões Nordeste e Sudeste. Em janeiro de 2022, um novo evento relacionado à mais de 11 toneladas de óleo derramado atingiu o litoral do Ceará. Em agosto de 2022, toneladas de *tarballs* contaminaram grande parte do litoral nordestino. Em adição, nos anos de 2021 e 2022, resíduos oleosos continuaram a chegar no litoral cearense. Neste contexto, este trabalho aplicou a geoquímica forense para investigar as características, origens e o nível de intemperismo de 56 amostras de óleo coletadas entre 2019 e 2022. Um primeiro artigo publicado abordou 16 amostras de *tarballs* coletadas em agosto de 2022, as quais apresentaram similaridade entre si de acordo com as razões diagnósticas baseadas em biomarcadores. As razões diagnósticas destas amostras, quando comparada à dos óleos dos eventos de 2019 e do início de 2022, apresentaram diferenças significativas, indicando origens e eventos distintos. Os *tarballs* apresentaram um perfil bimodal, com *n*-alcanos variando de *n*C13 a *n*C41, caracterizando-se como óleo cru parafínico (não combustível), termicamente maturo e de origem marinha. Os resultados obtidos por ESI(-) FT-ICR MS indicaram que essas amostras passaram por processos de biodegradação e fotooxidação, com abundância de ácidos graxos, o que é consistente com características cerosas. O segundo artigo apresenta os resultados de óleos coletados nos anos de 2021 e 2022 no Ceará. Das 32 amostras analisadas, 26 apresentaram alta abundância de *n*-alcanos de cadeia longa *(n*C31 a *n*C41), típicos de óleos parafínicos. Não foram detectados *n*-alcanos de baixo peso molecular (<*n*C31) e os isoprenóides pristano (Pr) e fitano (Fi). A análise dos biomarcadores, através das razões diagnósticas, indicou que 26 amostras não apresentam similaridade mútua, sugerindo múltiplas fontes. No entanto, três amostras de 2021 apresentam similaridade com o evento de 2019, e três amostras de 2022 com o evento ocorrido no início de 2022. A análise multivariada corroborou com os resultados obtidos pelos biomarcadores, revelando o agrupamento de seis amostras com os eventos de 2019 e início de 2022, além de dispersão significativa das demais amostras, que não apresentaram similaridade entre si e nem com os eventos passados. Quanto aos compostos aromáticos, não houve detecção de hidrocarbonetos policíclicos aromáticos (HPAs), apenas a presença dos triaromáticos esteróides (TAS). O estudo dos compostos polares ácidos por ESI(-) FT-ICR MS diferenciou cinco grupos: o óleo de 2019 apresentou as classes N_1, O_2, NS, O_1 e NO; o óleo do início de 2022 apresentou as classes N_1, O_2, O_3, O_1, NO e NO_2; os *tarballs* parafínicos apresentaram as classes N_1, O_2, O_1, O_4S e NS. A amostra P03#2021, similar ao óleo de 2019, apresentou maior abundância das classes O_2, O_3, O_3S e O_4. As três amostras de 2022, associadas ao evento do início de 2022, apresentaram as classes O_2, O_4S, O_6 e O_6S, indicando ação da fotooxidação. As distribuições de DBE *vs* número de carbonos para as classes N_1 e O_2 mostraram maior abundância entre C20 e C40, padrão incomum em óleo cru, sugerindo que esses resíduos passaram por processos térmicos. Este estudo evidenciou a vulnerabilidade do litoral cearense à chegada contínua de resíduos petrolíferos, os quais têm se acumulado e impactado o meio ambiente de forma silenciosa.

Palavras-chave: poluição costeira; geoquímica ambiental; *fingerprint*; biomarcadores.

ABSTRACT

In January 2019, Brazil was impacted by the largest oil spill ever recorded in tropical oceans, with over 5,000 tons of oil reaching the coasts of the Northeast and Southeast regions. In January 2022, a new incident involving more than 11 tons of spilled oil affected the coast of Ceará. In August 2022, tons of tarballs contaminated large portions of the northeastern coastline. In addition, during 2021 and 2022, oily residues continued to wash up along the Ceará coast. In this context, this study applied forensic geochemistry to investigate the characteristics, origins, and degree of weathering of 56 oil samples collected between 2019 and 2022. The first published article addressed 16 *tarball*s samples collected in August 2022, which showed mutual similarity based on biomarker-derived diagnostic ratios. When compared to oils from the 2019 and early 2022 events, these samples exhibited significant differences, indicating distinct sources and spill events. The *tarballs* displayed a bimodal profile, with *n*-alkanes ranging from *n*C13 to *n*C41, characterizing them as paraffinic crude oil (non-fuel), thermally mature, and of marine origin. Results obtained through ESI(-) FT-ICR MS indicated that the samples had undergone biodegradation and photooxidation, with a high abundance of fatty acids, consistent with waxy characteristics. The second article presents results from oil samples collected in Ceará during 2021 and 2022. Of the 32 samples analyzed, 26 showed a high abundance of long-chain *n*-alkanes (*n*C31 to *n*C41), typical of paraffinic oils. No low molecular weight *n*-alkanes (<*n*C31) or the isoprenoids pristane (Pr) and phytane (Ph) were detected. Biomarker analysis using diagnostic ratios indicated that 26 samples did not show mutual similarity, suggesting multiple sources. However, three samples from 2021 showed similarity to the 2019 event, and three samples from 2022 were linked to the early 2022 spill. Multivariate analysis supported the biomarker results, revealing that six samples clustered with the 2019 and early 2022 events, while the remaining samples showed significant dispersion and no similarity with each other or with past events. As for aromatic compounds, no polycyclic aromatic hydrocarbons (PAHs) were detected—only the presence of triaromatic steroids (TAS). The analysis of polar acidic compounds by ESI(-) FT-ICR MS revealed five distinct groups: the 2019 oil exhibited the classes N_1, O_2, NS, O_1, and NO; the early 2022 oil showed the classes N_1, O_2, O_3, O_1, NO, and NO_2; and the paraffinic *tarballs* were characterized by the classes N_1, O_2, O_1, O_4S, and NS. Sample P03#2021, which was similar to the 2019 oil, showed higher abundances of O_2, O_3, O_3S, and O_4 classes. The three 2022 samples associated with the early 2022 event presented the classes O_2, O_4S, O_6, and O6S, indicating photooxidation. The DBE vs. carbon number distributions for the N_1 and O_2 classes showed higher abundances between C20 and C40, an uncommon pattern for crude oil, suggesting that these residues had undergone thermal processes. This study highlighted the vulnerability of the Ceará coastline to the continuous arrival of petroleum residues, which have been silently accumulating and impacting the environment.

Keywords: coastal pollution, environmental geochemistry; *fingerprint*; biomarkers.

LISTA FIGURAS

LISTA DE TABELAS

LISTA DE ABREVIATURAS E SIGLAS

FT-ICR MS - Espectrometria de massas de ressonância ciclotrônica de íons com transformada de Fourier

OPEP - Organização dos Países Exportadores de Petróleo

EPI - Equipamento de proteção individual

SEMACE - Secretaria de meio ambiente do Ceará

FID - Detector de ionização de chama

UFRPE - Universidade Federal Rural de Pernambuco

Pr - Pristano

Fi - Fitano

EM - Espectrometria de massas

EMBRAPA - Empresa Brasileira de Pesquisa Agropecuária

IBAMA - Instituto Brasileiro do Meio Ambiente

CG - Cromatografia gasosa

EI - Impacto eletrônico

APCI - Ionização química à pressão atmosférica

APPI - Fotoionização à pressão atmosférica (*Atmospheric Pressure Photoionization Ionization*)

ESI - *Electrospray Ionization*

DPR - Desvio padrão relativo

SUMÁRIO

1 INTRODUÇÃO GERAL

Esta tese está estruturada em quatro capítulos. O primeiro capítulo abrange a introdução, a revisão da literatura, os objetivos do estudo, a caracterização da área de estudo, a descrição da metodologia e as referências bibliográficas. O segundo e o terceiro capítulo consistem em artigos científicos resultantes da pesquisa. O artigo apresentado no segundo capítulo, publicado no periódico *Marine Environmental Research,* em 2025, investiga os *tarballs* parafínicos que atingiram a costa do Nordeste do Brasil no final de 2022. O terceiro capítulo apresenta os resultados da investigação geoquímica de amostras de resíduos de petróleo coletadas em duas campanhas na costa cearense durante os anos de 2021 e 2022. O quarto capítulo reúne a conclusão geral do trabalho e as considerações finais. Por fim, são apresentadas as referências bibliográficas e os apêndices A e B, referentes aos materiais suplementares dos artigos dos capítulos dois e três, respectivamente.

1.1 INTRODUÇÃO

Os derramamentos de petróleo ocorrem tanto por exsudações naturais quanto por atividades da indústria petrolífera, incluindo o transporte de óleo e seus derivados, perfuração de poços, colisões acidentais, naufrágios de petroleiros, falhas em oleodutos e em plataformas de extração, causando impactos adversos na socioeconomia e nos recursos ecológicos, entre outros (Bi *et al*., 2021; Keramea *et al*., 2021). Os derramamentos de petróleo registrados na região Nordeste do Brasil configuram-se como um problema de grandes proporções nos âmbitos social, econômico e ecológico, devido à alta frequência dos eventos, ao expressivo volume de óleo envolvido e à ampla extensão geográfica afetada. Tais episódios têm provocado impactos significativos em áreas legalmente protegidas, bem como em diversas comunidades costeiras que dependem diretamente dos recursos marinhos para sua subsistência (Soares *et al*., 2022).

Em 2019, a costa nordeste do Brasil foi atingida pelo maior derramamento de óleo já registrado em oceanos tropicais (Oliveira *et al*., 2020; Lourenço *et al*., 2022; Reddy *et al*., 2022), com mais de 5.000 toneladas de óleo recolhidas em mais de onze estados afetados (IBAMA, 2022; Soares *et al*., 2022). Esse evento foi tão expressivo que, ainda em 2020 e 2021, materiais oleosos relacionados ao derramamento de 2019 continuaram chegando às praias brasileiras (Lima *et al*., 2023). Em janeiro de 2022, manchas de óleo não associadas ao evento de 2019 surgiram na costa do estado do Ceará, atingindo uma extensão de aproximadamente 400 km, com mais de 8.000 litros de óleo coletados (Azevedo et al., 2022; Soares *et al*., 2022). Mais recentemente, no final de 2022, bolas de alcatrão (*tarballs*) foram observadas ao longo de toda a costa do Nordeste brasileiro (Mello *et al*., 2023; Pereira *et al*., 2023; Nascimento *et al*., 2025).

Os *tarballs* são bolas de alcatrão com variações de cor, forma, tamanho e composição química, podendo ter origem em exsudações naturais (Corrick *et al*., 2021; Kvenvolden e Cooper, 2003) ou em fontes antropogênicas, resultantes da liberação de petróleo no oceano (Warnock *et al*., 2015). Essas estruturas apresentam forma aproximadamente esférica, geralmente com menos de 10 cm de diâmetro (Kvenvolden e Cooper, 2003). Podem ser formadas a partir de petróleo líquido transformado em material oleoso mais consistente por intemperismo e outros processos físicos (Warnock *et al*., 2015), podendo persistir no oceano por longos períodos. Esses resíduos são transportados para regiões costeiras por meio das ondas e correntes marinhas (Butler *et al*., 1998), afetando os ecossistemas marinhos e as zonas costeiras, além de impactar diretamente as comunidades locais (Warnock *et al*., 2015). A poluição por derramamentos de óleo em ambientes costeiros representa uma preocupação significativa para o ecossistema marinho global, uma vez que esses resíduos contêm compostos tóxicos e poluentes (Shinde *et al*., 2020), além de abrigarem diversas bactérias e fungos associados, os quais podem ser potenciais agentes patogênicos para humanos e animais (Shinde *et al*., 2017).

Após ser derramado no ambiente, o petróleo é submetido a vários processos físicos, químicos e biológicos que alteram sua composição química,

processos esses conhecidos como intemperismo (Stout e Wang, 2016; Wang *et al*., 1999). O betume parafínico, que forma os *tarballs* parafínicos, é relativamente resistente aos processos de intemperismo, permitindo que permaneçam por períodos prolongados no oceano (Edwards *et al*., 2018). Os compostos parafínicos podem retardar os efeitos do intemperismo nos *tarballs* devido à diminuição da dispersão do óleo (Blumer *et al*., 1973) e à proteção proporcionada pela parafina na coluna de água durante o transporte pelas correntes marinhas (Lourenço *et al*., 2020).

Para a avaliação de óleos derramados, a geoquímica forense tem sido aplicada para ajudar a determinar sua origem, o tempo de exposição dos óleos e os processos intempéricos que atuaram nesses resíduos (Kaplan, 1997). A geoquímica forense baseia-se principalmente nos princípios científicos da geoquímica orgânica (Kaplan, 1997), permitindo obter a impressão digital química do petróleo derramado utilizando técnicas analíticas convencionais e avançadas de alta resolução, como a cromatografia gasosa (Stout e Wang, 2007) e, mais recentemente, a espectrometria de massas por ressonância ciclotrônica de íons com transformada de Fourier (FT-ICR MS; Prince e Walters, 2022). Essas técnicas envolvem a avaliação de fatores que influenciam a impressão digital química do óleo derramado, incluindo a gênese, o refino, os processos intempéricos e a mistura no meio ambiente sofridos por esses óleos (Stout e Wang, 2007). Este conceito tem sido amplamente utilizado para estudar os derramamentos de petróleo no Nordeste do Brasil nos últimos anos (Azevedo *et al*., 2022; Carregosa *et al*., 2021; Lima *et al*., 2020, 2021, 2023; Oliveira *et al*., 2020; Reddy *et al*., 2022; Pereira *et al*., 2023; Martins *et al*., 2024; Nascimento *et al*., 2025).

Destacando a extensão e a recorrência dos derramamentos de resíduos de petróleo na costa do Nordeste brasileiro, este trabalho propõe a aplicação da geoquímica forense como ferramenta para investigar a origem, as características e os efeitos intempéricos dos diferentes resíduos de petróleo registrados no litoral do estado do Ceará nos anos de 2019 a 2022.

1.2 OBJETIVOS

1.2.1 Objetivo Geral

Investigar a composição química de materiais oleosos encontrados ao longo do litoral do estado do Ceará, Nordeste do Brasil, entre 2019 e 2022, com base nos compostos saturados, aromáticos e polares, visando identificar a origem, a similaridade e os efeitos do intemperismo, por meio da aplicação dos conceitos da geoquímica forense.

1.2.2 Objetivos específicos

Para alcançar o objetivo geral, têm-se os seguintes objetivos específicos:

- Monitorar a presença de materiais oleosos em *beachrocks* — formações rochosas — e em faixas de areia nas praias do estado do Ceará, entre 2019 e 2022, através da: **(i)** coleta de *tarballs* parafínicos associados ao evento ocorrido no final de 2022 no Nordeste brasileiro; **(ii)** coleta de resíduos oleosos identificados ao longo de toda a costa cearense nos anos de 2021 e 2022.
- Avaliar as amostras de óleo derramado, por meio de razões diagnósticas obtidas a partir de biomarcadores saturados e aromáticos resistentes, analisados por técnicas cromatográficas gasosas, com o objetivo de: **(i)** verificar a similaridade entre as amostras coletadas, a fim de identificar os óleos que apresentam características semelhantes; **(ii)** Identificar possíveis perfis de combustíveis presentes nas amostras.
- Aplicar os compostos polares ácidos analisados pela técnica de espectrometria de massas com ressonância ciclotrônica de íons com transformada de Fourier (FT-ICR MS) para complementar a investigação geoquímica forense dos óleos derramados, incluindo a investigação dos processos intempéricos atuantes.

1.3 **REFERENCIAL TEÓRICO**

1.3.1 Derramamentos de óleo: contexto global e implicações ambientais

1.3.1.1 Ocorrências globais de derramamentos de óleo: históricos e perspectivas

O petróleo permanece como uma das principais fontes de energia global desde o século XX, sendo responsável, juntamente com o carvão e o gás natural, por cerca de 80% da matriz energética mundial projetada para 2030 (Alcoforado, 2023). Apesar dos crescentes apelos por transições energéticas sustentáveis, a dependência estrutural do petróleo ainda é marcante, o que torna inevitável os riscos ambientais associados à sua cadeia produtiva, especialmente no transporte marítimo.

A indústria petrolífera, enfrentando o desafio de equilibrar produtividade com sustentabilidade ambiental, é atualmente responsável por mais de dois terços da energia mundial (Heidari *et al*., 2022; Kamyk *et al*., 2021; Keramea *et al*., 2021). A crescente demanda projetada pela Organização dos Países Exportadores de Petróleo (OPEP), estimada em 105,2 milhões de barris por dia em 2025 (OPEP, 2023), reforça a expansão do transporte marítimo de petróleo. Como resultado, a segurança dos petroleiros torna-se cada vez mais relevante, especialmente diante dos inúmeros derramamentos de petróleo registrados ao longo da história (Chen *et al*., 2019). A Figura 1 apresenta o número de derramamentos de petróleo de navios tanques, de 1970 a 2024 (ITOPF, 2024).

Figura 1. Número de derramamentos de óleo de 1970 a 2024.

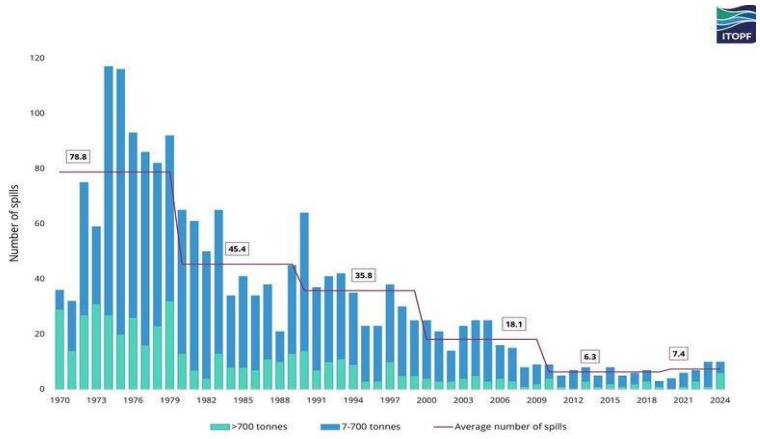

Fonte: ITOPF (2024).

Segundo dados da *International Tanker Owners Pollution Federation* (ITOPF, 2024), apenas em 2024 foram registrados seis grandes derramamentos (>700 toneladas) e quatro de médio porte (7–700 toneladas). A distribuição geográfica dos eventos entre a América do Sul, América do Norte, Ásia e Europa evidenciaram a abrangência global do problema. Os incidentes envolveram principalmente óleo combustível, resultando em cerca de 10.000 toneladas de resíduos oleosos derramados no ambiente marinho. Os desastres relacionados ao transporte de petróleo, embora menos frequentes nas últimas décadas, continuam sendo relevantes pelo seu potencial destrutivo.

De acordo com estudos realizados por Dong *et al*. (2022), a análise de 563.705 imagens de satélite resultou na elaboração do primeiro mapa global de manchas de óleo nos oceanos, acompanhado de um inventário detalhado das principais fontes persistentes, como exsudações naturais, plataformas e oleodutos. Os resultados indicaram que aproximadamente 90% das manchas estavam localizadas a menos de 160 quilômetros de áreas costeiras, o que evidencia a vulnerabilidade dessas regiões. Além disso, foram identificados 21 cinturões com alta densidade de manchas, que coincidem significativamente com rotas de navegação marítima. Esses dados sugerem que boa parte dos derramamentos tem origem antrópica, especialmente associada ao tráfego de navios petroleiros e outras embarcações comerciais.

Atividades como operações de produção de petróleo em alto-mar, incluindo perfuração, além de vazamentos e derramamentos de navios-tanque e embarcações, contribuem para aproximadamente 8% da quantidade total de resíduos de petróleo que chegam à superfície do oceano (Board *et al*., 2003; Chen *et al*., 2018; Lorenz, 2020). Porém, desde 1970, observa-se uma tendência de queda no número de acidentes e na quantidade de óleo derramado por petroleiros. Antes da década de 1990, esses índices variavam significativamente a cada ano. A partir dessa década, estabilizaram-se em níveis baixos e com redução contínua. Mais de 90% dos acidentes e do volume total de óleo derramado ocorreram antes de 1990. Os dados evidenciam uma expressiva diminuição desses eventos após esse período (Chen *et al*., 2019). Esses

incidentes não apenas colocam em risco a saúde e a vida de tripulações, ocorrem também perdas ambientais com sérios impactos sobre os ecossistemas. Uma vez derramado no oceano, o óleo tende a se espalhar e se deslocar com as correntes costeiras e os ventos, contaminando praias e ecossistemas associados (Galieriková e Materná 2020; Zanhg *et al*., 2016; Caballer e Oñate, 2017).

Ao longo das últimas décadas, diversos desastres associados ao transporte de petróleo e seus derivados em mares e oceanos foram registrados. Dentre eles, destacam-se o acidente com o super petroleiro *Torrey Canyon*, que colidiu contra rochas ao largo da costa da Cornualha, em águas britânicas, em 1967. Este evento resultou no derramamento de aproximadamente 119.328 toneladas de petróleo bruto, o que causou a morte de mais de 25.000 aves e outros organismos marinhos (Chen *et al*., 2018; Galieriková e Materná, 2020; Wells, 2017). Em 1989, o petroleiro *Exxon Valdez* encalhou no recife Bligh, localizado na baía de Prince William, no Alasca, provocando o derramamento de 42 milhões de litros de óleo cru. O incidente resultou na contaminação de aproximadamente 1.990 km de costa e causou uma significativa mortalidade da vida marinha local (Peterson *et al*., 2003). Em 2002, o petroleiro *Prestige* sofreu uma falha estrutural grave nos tanques de carga e afundou a 222 km da costa das Ilhas Cíes, no noroeste da Espanha. Como resultado, mais de 60.000 toneladas de petróleo foram derramadas, contaminando aproximadamente 1.300 km de costa (Albaigés *et al*., 2006). Em 2010, uma explosão na plataforma *Deepwater Horizon*, no norte do Golfo do México, com profundidade de 1.522 metros, liberou cerca de 3,19 milhões de barris de petróleo nos oceanos ao longo de 87 dias (Beyer *et al*., 2016). Já em 2017, as embarcações BW Maple, uma transportadora de gás de petróleo liquefeito, e MT Dawn Kanchipuram, transportadora de óleo lubrificante, colidiram ao norte de Chennai, no sul da Índia, resultando no derramamento de 75 toneladas de petróleo e impactando uma área de 25 milhas da costa (Han *et al*., 2018). Em 13 de março de 2025, no Equador, ocorreu o rompimento do sistema de oleodutos (SOTE) na província de Esmeraldas, resultando no derramamento de mais de 25.000 barris de petróleo. O vazamento se espalhou por 86 km a partir do local do incidente,

afetando mais de 15 municípios. Como consequência, cinco rios próximos ao Oceano Pacífico foram contaminados (Oil & Gás Journal, 2025).

Ao longo das últimas décadas, as estatísticas sobre a frequência de derramamentos de petróleo superiores a sete toneladas por navios-tanque indicam uma expressiva redução. Na década de 1970, a média anual era de aproximadamente 79 ocorrências, número que caiu mais de 90% na década de 2010, chegando a 6,3, e se mantendo em patamares semelhantes na década atual. Contudo, em termos de volume derramado, os dados anuais podem ser significativamente distorcidos por eventos isolados de grande magnitude. Exemplos como o *Atlantic Empress* (1979), com 287.000 toneladas derramadas; o *Castillo de Bellver* (1983), com 252.000 toneladas; o *ABT Summer* (1991), com 260.000 toneladas; e o *Sanchi* (2018), com 113.000 toneladas, ilustram essa situação (ITOPF, 2024). O vazamento da *Deepwater Horizon*, em 2010, que liberou cerca de 3,19 milhões de barris de petróleo no oceano, reforçando como um único acidente pode alterar drasticamente os índices de volume anual (Beyer *et al*., 2016). Apesar da expressiva redução na frequência desses desastres, os impactos ambientais decorrentes de grandes vazamentos permanecem significativos, evidenciando a necessidade de monitoramento constante e do contínuo aperfeiçoamento das estratégias de prevenção e resposta.

1.3.1.2 Panorama dos derramamentos de petróleo no Brasil

Nas últimas décadas, o Brasil tem enfrentado diversos derramamentos de petróleo que causaram impactos ambientais significativos, especialmente em áreas costeiras. Esses eventos não apenas revelam os riscos inerentes às atividades de exploração, transporte e refino de petróleo, mas também suscitam importantes debates acadêmicos acerca das causas, consequências e das respostas institucionais a esses acidentes.

Historicamente, destacam-se casos que marcaram o cenário ambiental brasileiro, como o vazamento do petroleiro Tarik Iba Ziyad em 1975, na Baía de Guanabara, Rio de Janeiro, que resultou no derramamento de seis mil toneladas de óleo. No início dos anos 2000, episódios como o rompimento de dutos da

Petrobras, que causaram o vazamento de milhões de litros de óleo na Baía de Guanabara e nos rios Barigui e Iguaçu, ampliaram a preocupação com a segurança das infraestruturas petrolíferas (Meniconi *et al*., 2000; CETESB, 2005). Outros acidentes, como o derramamento em São Sebastião (SP) em 2000 e o vazamento da Chevron em 2011 na Bacia de Campos, reforçaram o alerta sobre os potenciais danos ambientais e a necessidade de aprimorar os mecanismos de prevenção e mitigação.

No contexto mais atual, o derramamento de 2019 na costa nordeste do Brasil representa um marco que reabriu debates sobre a vulnerabilidade dos ecossistemas marinhos e as limitações dos sistemas de monitoramento e controle ambiental (Oliveira, *et al*., 2020; Reddy *et al*., 2022; Zacharias *et al*., 2023). Desde então, outros eventos têm sido registrados, como o derramamento de óleo em janeiro de 2022 no Estado do Ceará (Azevedo *et al*., 2022). A chegada dos *tarballs* parafínicos ao longo do litoral nordestino em agosto de 2022 (Mello *et al*., 2023; Nascimento *et al*., 2025; 2022; Pereira *et al*., 2023). Esses episódios recentes ressaltam a necessidade em aprofundar a investigação sobre os derramamentos de óleo ocorridos no Brasil, sobretudo aqueles que se sucederam a partir de 2019, tema que tem ganhado crescente atenção na área acadêmica e que será explorado nos tópicos seguintes.

1.3.1.3 Derramamento de petróleo no Brasil em 2019: consequências, desafios e debates

O derramamento de óleo ocorrido em 2019 foi o maior desastre ambiental relacionado a petróleo já registrado na América do Sul e em regiões tropicais, devido à sua ampla extensão geográfica e à sobreposição com ecossistemas de elevada relevância ecológica (Soares *et al*., 2020; 2022; Magalhães *et al*., 2022). No final de agosto daquele ano, manchas de óleo de origem desconhecida surgiram inicialmente no litoral da Paraíba, dando início a um grande derramamento ao longo do litoral brasileiro. Esse acidente configura-se como o maior derramamento de óleo em extensão e duração já registrado no Brasil

(Soares *et al*., 2020; Lourenço *et al*., 2020). Nos meses seguintes, o óleo atingiu toda a costa nordestina, além dos litorais dos estados do Espírito Santo e do Rio de Janeiro. De uma área monitorada que ultrapassa 4.000 km de extensão, aproximadamente 1.000 km da costa brasileira foram diretamente afetados pelo óleo (Soares *et al*., 2022; IBAMA, 2020). Mais de 4.000 toneladas de resíduos de petróleo, cuja origem permanece desconhecida, chegaram à costa nordeste do país desde o final de agosto, contaminando centenas de praias, estuários, recifes e manguezais ao longo de uma extensão de 2.500 km (Escobar, 2019; Cavalcante *et al*., 2024).

O óleo derramado em 2019 foi classificado como pesado e altamente intemperizado, ou seja, passou por processos químicos, físicos e biológicos ao longo do tempo, apresentando como principais características alta viscosidade, alta densidade e baixas concentrações de compostos voláteis (Reddy *et al*., 2022; Oliveira *et al*., 2022). Com base nessas propriedades, o IBAMA (2020) aponta os principais comportamentos previstos do óleo no ambiente marinho e seus prováveis impactos sobre a flora e fauna marinhas: baixos níveis de evaporação, o que implica em concentrações reduzidas de hidrocarbonetos no ar próximo às manchas; alta persistência no ambiente, indicando que o óleo não se degrada facilmente; densidade próxima à da água do mar, o que possibilita seu afundamento ao encontrar água salobra ou quando misturado a areia e outros sedimentos; baixa toxicidade potencial para organismos marinhos, devido às baixas concentrações de compostos aromáticos presentes; e potencial para sufocação física dos organismos marinhos que entrem em contato direto com o material, decorrente da alta viscosidade e densidade do óleo. A Figura 2 apresenta imagens ilustrativas do derramamento de óleo ocorrido em 2019.

Figura 2. Amostras do derramamento de petróleo no ano de 2019 nos estados da Bahia e Ceará, a) Praia de Ituberá e b) Praia do Balbino.

Fonte: IBAMA (2020).

À medida em que as manchas e ondas de óleo chegavam à costa do Nordeste, muitos voluntários locais se mobilizaram espontaneamente, tanto individual quanto coletivamente, movidos por forças humanitárias e ambientais para limpar as praias, todos expostos a substâncias tóxicas como (HPAs e BTEX), colocando em risco sua própria saúde. Nos primeiros dias, quando os poluentes começaram a chegar ao litoral, a maioria desses voluntários não tinha conhecimento sobre como lidar com o desastre, nenhuma orientação de autoridades, nem acesso a equipamentos de proteção individual (EPI) (Araújo *et al*., 2020; Euzébio *et al*., 2019; Aguilera *et al*., 2010; Oliveira *et al*., 2020).

Os impactos ambientais foram extensos, com efeitos sobre a biodiversidade marinha ainda não totalmente quantificados. Pesquisas indicam danos a espécies de peixes, invertebrados, tartarugas-marinhas e corais, além da contaminação de habitats críticos (Magalhães *et al*., 2022; Souza *et al*., 2022). As comunidades tradicionais — como pescadores artesanais e marisqueiras — foram severamente afetadas, tanto no aspecto econômico quanto na saúde, pela manipulação direta dos resíduos oleosos sem o uso de equipamentos adequados de proteção (Araújo *et al*., 2021; Pereira *et al*., 2023).

Um ano após o início do desastre ambiental, a Marinha do Brasil divulgou que o petróleo encontrado no litoral brasileiro era de origem venezuelana, e que

o vazamento teria ocorrido a aproximadamente 700 quilômetros da costa, com o óleo permanecendo submerso por cerca de 40 dias antes de atingir o litoral (Oliveira *et al*., 2020; Reddy *et al*., 2022). Ainda segundo a Marinha, a origem do óleo de uma embarcação que navegava em alto-mar e que realizou despejo ilegal de óleo (descarga intencional) ou que acidentalmente liberou o óleo. Essa embarcação não foi identificada, mesmo com indícios, a certeza do navio que lançou esse óleo não foi confirmada. Foram aproximadamente 2,5 milhões de toneladas de petróleo venezuelano, mas não se sabe quão precisa é essa estimativa e quanto desse óleo derramado chegou às regiões costeiras (Soares *et al*., 2020; Escobar, 2019).

Apesar dessas conclusões, a ausência de responsabilização formal e a escassez de informações públicas detalhadas sobre o ocorrido reforçaram o caráter enigmático do evento, contribuindo para debates contínuos sobre a governança ambiental, a segurança da navegação e os limites da capacidade de monitoramento em águas jurisdicionais brasileiras (Freitas *et al*., 2022; BRASIL, 2019; De Moura *et al*., 2023). Esse episódio não apenas evidenciou lacunas nas estratégias de prevenção e resposta a desastres ambientais no Brasil, como também impulsionou novas discussões sobre a vulnerabilidade da costa brasileira a incidentes similares. Diante disso, os eventos de derramamento de petróleo registrados nos anos subsequentes, particularmente em 2022, merecem atenção específica e serão analisados nas seções seguintes.

1.3.1.4 Presença de manchas de óleo no estado do Ceará no início de 2022: registros, análises e lacunas investigativas

No mês de fevereiro de 2022, ocorreram registros de manchas de óleo ao longo da costa do estado do Ceará (Figura 3). De acordo com informações do Projeto de Planejamento Costeiro e Marinho do Ceará, desenvolvido no âmbito do Programa Cientista-Chefe Meio Ambiente (FUNCAP/SEMA/SEMACE), em colaboração com o Gerenciamento Costeiro do Estado do Ceará (GERCO/SEMA/PRAIA LIMPA), até o dia 18 de fevereiro de 2022, um total de

65 praias, distribuídas em 14 municípios litorâneos cearenses, haviam sido impactadas.

A Superintendência Estadual do Meio Ambiente (SEMACE), alinhada ao Grupo de Articulação Interinstitucional criado na época do incidente de manchas de óleo ocorrido no ano de 2019, atualiza informações acerca do trabalho de recebimento do material recolhido pelas prefeituras. Na ocasião, 8.200 litros de material foram recolhidos e destinados a descarte.

Figura 3. Amostras de petróleo derramados nas praias do estado do Ceará em fevereiro de 2022.

Fonte: Azevedo *et al.* (2022).

Estudos de geoquímica forense realizados por Azevedo *et al*. (2022) e Nascimento *et al.* (2023) comprovaram que este óleo não tinha correlação com o óleo derramado em 2019, sendo, portanto, relacionado a um novo incidente. Assim, nos derramamentos de óleo: um em 2019 (Reddy *et al*., 2022) e outro no início de 2022, (Azevedo *et al*., 2022) determinou o perfil químico de seis amostras de 2022 e as comparou com os óleos derramados em 2019 com base na geoquímica forense (Kaplan *et al*., 1997). Como resultados, os perfis cromatográficos por GC-FID, caracterizados como “impressões digitais”, com *n*-alcanos variando de *n*C17 a *n*C34. Observou-se, ainda, que os isoprenóides pristano (Pr) e fitano (Fi) apresentaram abundâncias muito baixas ou não foram detectados (Figura 4).

A ausência de hidrocarbonetos de baixo peso molecular (<C17) nos cromatogramas é atribuída, muito provavelmente, ao processo de evaporação,

que é o principal mecanismo de intemperismo responsável pela degradação inicial dos óleos derramados quando expostos ao ambiente (Stout *et al*., 2016; Albaigés *et al*., 2018; Lima *et al*., 2021; Filewood *et al*., 2022). A presença de elevação da linha de base nos cromatogramas CG- FID nas amostras de óleo é caraterística da mistura complexa não resolvida (UCM), indicando a ocorrência de biodegradação ou fotooxidação (Stout *et al*., 2016; Albaigés *et al*., 2018; Filewood *et al*., 2022).

Figura 4. Cromatogramas GC-FID representativos das amostras de óleo do início de 2022 (amostra P05#22) e 2019 (amostra P01#19).

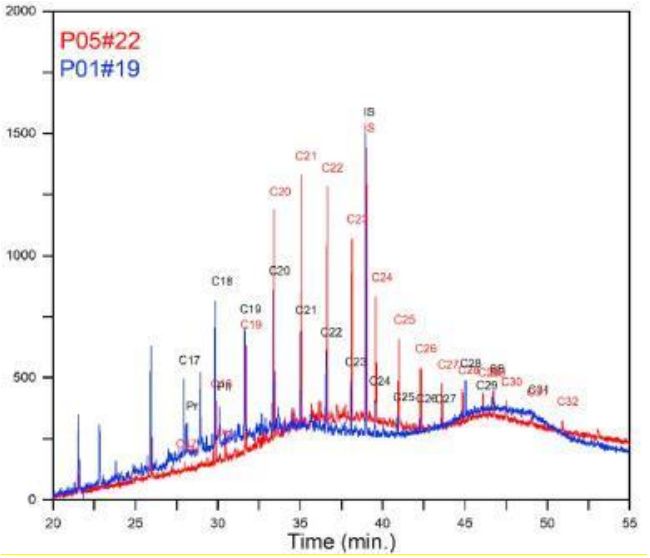

Fonte: Azevedo *et al*. (2022).

Ainda segundo Azevedo *et al*., 2022, a abundância de *n*-alcanos *n*C17 a *n*C34 indicou que a amostra de óleo coletada em 2022 não é o mesmo material do óleo que chegou à praia do Nordeste do Brasil em 2019, pois esses hidrocarbonetos não teriam sido preservados no ambiente por tanto tempo (Stout *et al*., 2016), a menos que tivessem a mesma fonte que continuou a liberar o petróleo, o que é improvável.

Com o objetivo de investigar a possível correlação entre os derramamentos de óleo ocorridos em 2019 e no início de 2022, foram realizadas análises de compostos mais resistentes à degradação, como os biomarcadores alifáticos terpanos e esteranos. Essas análises foram conduzidas por meio de

cromatografia gasosa bidimensional (GC×GC) (Figura 5). Os resultados obtidos por Azevedo *et al*. (2022) revelaram a presença de compostos típicos de petróleo bruto que, provavelmente, não passaram por processos industriais ou métodos de refino voltados à obtenção de óleos combustíveis. Foi identificada uma gama completa de biomarcadores alifáticos, incluindo hopanos, esteranos e diasteranos (Figura 5). A semelhança observada entre os perfis cromatográficos dos biomarcadores nas análises por GC×GC-FID (Figuras 5a e c) sugere que as amostras de óleo analisadas compartilham a mesma origem, indicando que o óleo encontrado ao longo dos 130 km da costa leste do estado do Ceará, em 2022, teve como provável fonte o mesmo evento ou incidente registrado anteriormente.

Figura 5. Cromatografia gasosa bidimensional das amostras de 2019 e início de 2022.

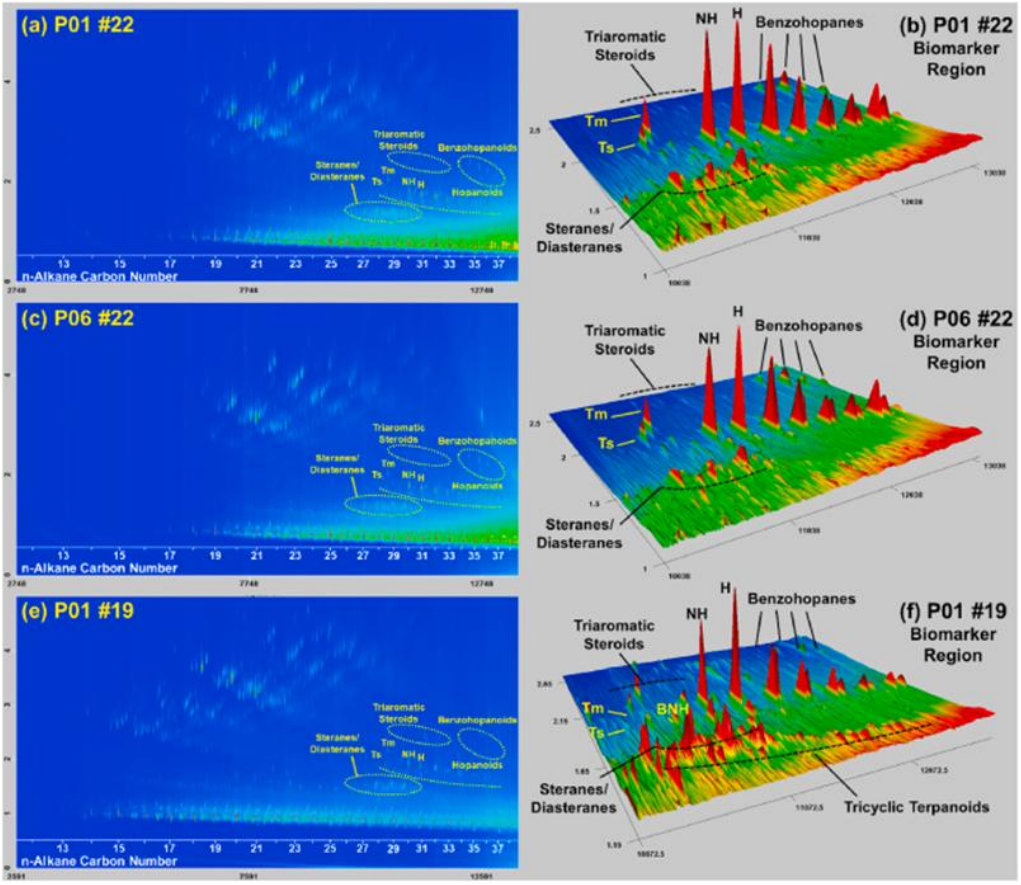

Fonte. Azevedo *et al.* (2022).

1.3.1.5 A chegada de *tarballs* parafínicos nas praias do Nordeste do Brasil em agosto de 2022: ocorrências, hipóteses e caminhos da pesquisa atual

Em agosto de 2022 chegaram resíduos oleosos nas praias do Nordeste brasileiro, esses resíduos oleosos atingiram praias do nordeste brasileiro, incluindo os estados do Alagoas, Bahia, Ceará, Paraíba, Pernambuco e Rio Grande do Norte (BRASIL, 2022). No estado de Pernambuco, mais de 400 quilos do material foram recolhidos em 12 cidades do litoral do estado, de acordo com a Agência Pernambucana do Meio Ambiente (CPRH). No estado do Ceará, os materiais oleosos chegaram em setembro de 2022, atingindo muitas praias, sendo grande parte destas regiões turísticas, como as praias do Futuro, Morro Branco, Cumbuco, Porto das Dunas entre outras. Para se ter uma dimensão da quantidade de óleo, cerca de 2,8 kg de material oleoso foi coletado em 3,4 Km de faixa de areia da Praia do Futuro no primeiro dia da chegada do óleo na região (Bastos *et al*., 2022; DIÁRIO DO NORDESTE, 2022; Nascimento *et al*., 2025).

Os óleos apresentavam características bem diferentes dos óleos do início de 2022 e de 2019. Eles tinham forma de bolas, os chamados *tarballs* (Corrick *et al*., 2021; Kvenvolden e Cooper, 2003), e foram encontradas aderidas a grande parte desses *tarballs* organismos marinhos do tipo Lepas (*L. anatifera Linnaeus*, 1758). As Lepas são organismos filtrantes, as quais são utilizadas como alimentos por muitos animais e até pelo homem (Mello *et al*., 2023; Feitosa *et al*., 2024). A Figura 6a, b e c apresenta três imagens da presença das Lepas aderidas aos *tarballs* quando coletados no final de 2022.

Figura 6. *Tarballs* coletados no final de 2022 nas praias do Ceará.

Fonte. Mello *et al.* (2022).

Segundo nota técnica divulgada pelo MCTI – Ministério da Ciência e Tecnologia (BRASIL, 2022), os resíduos oleosos que atingiram o litoral nordestino em agosto de 2022 apresentam características distintas de petróleo cru, as análises desses resíduos oleosos indicaram a ocorrência de um novo evento, possivelmente relacionado ao descarte de água oleosa proveniente da lavagem de tanques de navios petroleiros em alto-mar. Óleos parafínicos encontrados nos mares e oceanos geralmente estão associados à lavagem de tanques de navios petroleiros, prática comum que pode liberar resíduos de petróleo bruto com alto teor de *n*-alcanos de cadeia longa. Esses compostos, pouco solúveis e de baixa volatilidade, se solidificam em contato com a água fria do mar, formando *tarballs* que podem flutuar por semanas antes de atingir a costa (Corrêa *et al*., 2024; Nascimento *et al*., 2025; Pereira *et al*., 2023). A composição geoquímica desses resíduos indicou que estes não passaram por processos de refino, confirmando sua origem de resíduos aderidos às superfícies internas de tanques de navios (Mello *et al*., 2023). Quando descartados irregularmente, representam uma forma recorrente e crônica de poluição marinha associada ao tráfego marítimo internacional.

Em estudos realizados por pesquisadores da Universidade Federal de Sergipe (UFS) e da Universidade Federal Rural de Pernambuco (UFRPE), os óleos encontrados nas praias dos dois estados nordestinos estão associados ao derramamento de material proveniente de depósitos de parafina em tanques de armazenamento de óleo bruto. Em relação se este óleo derramado em setembro de 2022 é o mesmo do início de 2022, estudos realizados por Nascimento *et a*l. (2023) e Pereira *et al.* (2023) mostraram que esses óleos não se relacionam com os derramados no início do ano de 2022 e nem de 2019, indicando que o óleo do final de 2022 caracterizou-se por um novo evento de derramamento de óleo na costa brasileira.

1.3.2 Processos intempéricos

Quando um vazamento de petróleo acontece no mar, o óleo normalmente se espalha e se move na superfície do mar com o vento e as correntes, passando por uma série de transformações químicas e físicas. Esses processos são chamados coletivamente de intemperismo e determinam o destino desses resíduos de óleo. O intemperismo modifica a impressão digital química do óleo derramado, fazendo com que esse óleo não corresponda ao original encontrado nos eventos (Wang e Stout, 2016).

A modificação das características químicas desses óleos dificulta na caracterização do *fingerprinting*, isso porque os biomarcadores presentes no petróleo são compostos úteis para a identificação química, pois retêm todo ou a maior parte do esqueleto de carbono original do produto natural, e essa similaridade estrutural revela mais informações sobre a fonte do petróleo do que outros compostos presentes no mesmo. Assim, a análise qualitativa da impressão digital química do óleo derramado, das fontes candidatas poderá ter melhor sucesso a partir de uma comparação visual entre várias impressões digitais espectroscópicas e cromatográficas quando a assinatura do óleo não está desgastada, isto é, não sofreu com os processos intempéricos (Douglas *et al*., 2016; ITOPF, 2024).

Os processos intempéricos mais importantes após o vazamento de óleo em águas superficiais doces ou marinhas incluem o espalhamento, a evaporação, a dissolução, a dispersão na coluna d'água, formação de emulsões de água em óleo, oxidação fotoquímica, degradação microbiana, adsorção a partículas em suspensão e encalhe na costa ou sedimentação em sedimentos do fundo (Figura 7).

Figura 7. Processos de intemperismo atuando no mar.

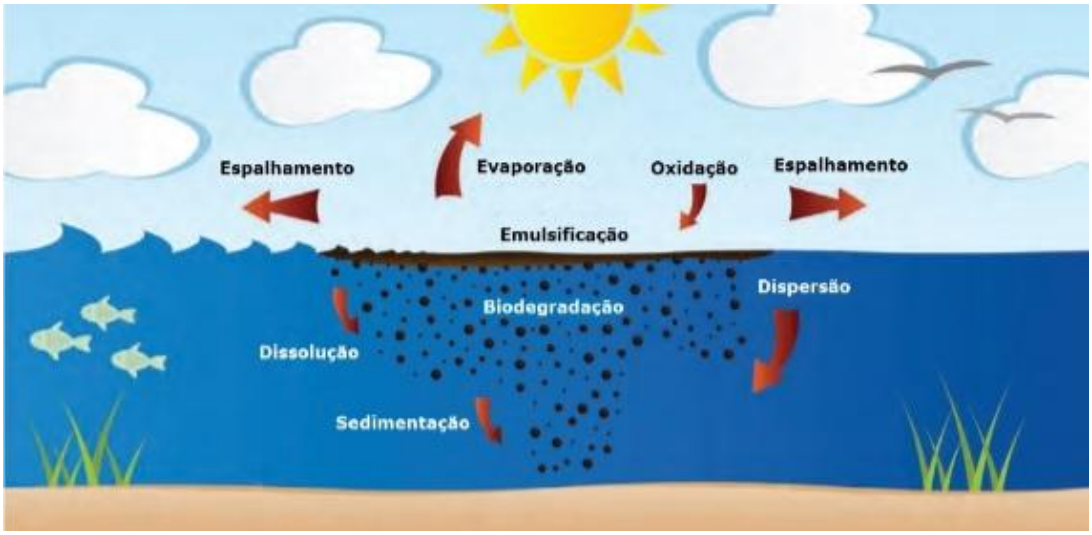

Fonte. ITOPF, 2011.

1.3.2.1 Evaporação

A evaporação é um dos principais processos de intemperismo que afetam a composição química/impressão digital do óleo derramado nas primeiras horas ou dias seguintes a um derramamento de óleo em meio aquoso. Embora as condições específicas do derramamento (por exemplo, espessura, formação de mousse, velocidade do vento e temperatura ambiente da água/ar) afetem a taxa de evaporação, em todas as condições, a propensão à evaporação é, em última análise, governada pela pressão de vapor de seus constituintes individuais. O efeito da evaporação na impressão digital de um óleo derramado dependerá de sua composição original, como exemplo, um combustível como a gasolina pode

evaporar completamente em poucas horas, eliminando efetivamente sua impressão digital, enquanto um combustível pesado ou óleo bruto sofrerá perdas mínimas ou alterações em sua impressão digital (Wang e Stout, 2016; TARR *et al*., 2023; ITOPF, 2024).

1.3.2.2 Dissolução

A dissolução é relativamente insignificante em comparação com a evaporação na maioria dos derramamentos em águas superficiais (Mackay e Mcauliffe, 1989; Payne *et al*., 1987; Neff, 1990) e terá pouco efeito na impressão digital química de um óleo derramado. Porém, para compreender o processo de dissolução, é importante reconhecer o impacto do óleo derramado na biota, que pode absorver hidrocarbonetos dissolvidos mais facilmente (ITOPF, 2024; Tarr *et al*., 2023).

1.3.2.3 Biodegradação

A taxa de perda de massa devido à biodegradação é mais lenta do que a da evaporação ou dissolução. Dessa forma, os efeitos da biodegradação na impressão digital química de um óleo derramado não são observados em curto prazo após o vazamento, isso porque o efeito da biodegradação dependerá da natureza do óleo derramado e das condições do derramamento. Assim, após um derramamento de petróleo bruto ou refinado em solos, sedimentos ou águas abertas, diferentes classes de hidrocarbonetos são degradadas simultaneamente, mas em taxas amplamente distintas pela microbiota nativa. Os *n*-alcanos de baixo peso molecular são os primeiros a ser biodegradados mais rapidamente, seguidos por isoalcanos e *n*-alcanos de maior peso molecular, olefinas, monoaromáticos, HPAs e, finalmente, cicloalcanos, resinas e asfaltenos altamente condensados (Stout e Wang, 2016; Tarr *et al*., 2023; ITOPF, 2024).

1.3.2.4 Fotooxidação

A exposição de petróleo bruto e seus derivados à radiação solar leva a diversas reações de fotooxidação de radicais livres que produzem uma variedade de compostos contendo oxigênio, incluindo peróxidos, aldeídos, cetonas, álcoois, carbonilas, sulfóxidos, epóxidos e ácidos graxos. Esses compostos polares formados durante a degradação do petróleo apresentam maior solubilidade em água em comparação aos compostos originais, favorecendo sua dissolução preferencial. Paralelamente, moléculas fotossensíveis de maior massa molecular podem sofrer reticulação via fotooxidação, tornando-se insolúveis e aumentando a viscosidade do óleo. A taxa de fotooxidação do petróleo está associada à intensidade da radiação ultravioleta solar, sendo pouco influenciada pela temperatura ambiente. A fotooxidação também afeta hidrocarbonetos aromáticos policíclicos (HPAs), podendo alterar grupos inteiros de compostos, como os esteróides triaromáticos, ou isômeros específicos, como metil-pirenos e benzofluorenos, onde alguns desses são utilizados na caracterização química de óleos derramados (Stout e Wang, 2016; Tarr *et al*., 2023; ITOPF, 2024).

1.3.2.5 Emulsificação

Entre os vários processos de intemperismo, a formação de emulsões (mousse) é o único que promove a persistência do óleo na superfície da água e na praia – e, simultaneamente, retarda o processo de intemperismo. Emulsões de petróleo formam frequentemente uma crosta composta por materiais asfaltênicos oxidados, que atuam como barreira física, limitando processos de dissolução, evaporação, fotooxidação e biodegradação dos hidrocarbonetos presentes na fase oleosa. Essa barreira contribui para a preservação do perfil químico do óleo emulsionado em relação ao óleo não emulsionado. Como consequência, resíduos intemperizados, como mousse, piche e pavimento asfáltico acumulados na zona costeira, podem reter hidrocarbonetos voláteis e compostos biodegradáveis por longos períodos. Esse fenômeno influencia a

persistência ambiental do petróleo derramado (Stout e Wang, 2016; Tarr *et al*., 2023; ITOPF, 2024).

1.3.2.6 Dispersão

Ocorre quando a ação das ondas faz com que uma mancha superficial se desfaça em gotas de óleo que se misturam e se espalham pela coluna d'água. Essas gotas naturalmente dispersas são maiores do que as observadas com o uso de dispersantes e podem flutuar de volta à superfície, onde se recombinam para formar outra mancha. Alguma dispersão natural ocorre com todos os óleos, especialmente os leves. Em mares agitados, os óleos leves podem até ser completamente dispersos por esse processo (Stout e Wang, 2016; Tarr *et al*., 2023; ITOPF, 2024).

1.3.3 Composição química do petróleo e seus principais constituintes

O petróleo é uma mistura complexa essencialmente de hidrocarbonetos que existe naturalmente nos estados gasoso (gás natural), líquido (petróleo cru) e sólido (asfalto). É derivado de uma variedade de materiais orgânicos que são quimicamente convertidos ao longo de longos períodos (centenas de milhões de anos), sob diferentes condições geológicas e térmicas. O petróleo cru é composto principalmente de carbono e hidrogênio, mas também contém pequenas quantidades de enxofre, oxigênio e nitrogênio, bem como traços de metais (Wang *et al*., 1995; Speight, 2014). Analisar a composição dos óleos derramados, geralmente derivados de petróleo cru, é fundamental para compreender seu comportamento no ambiente marinho. Esses óleos são formados por misturas complexas de hidrocarbonetos, cujas características químicas variam conforme a origem geológica e o grau de intemperismo. A identificação destes compostos permite rastrear a fonte do óleo e avaliar seu potencial de impacto ambiental. Assim, a análise composicional é essencial em casos de poluição por derramamento (Wang e Fingas, 2003; Stout e Payne, 2016).

Os principais componentes do petróleo investigados em estudos ambientais e forenses são os hidrocarbonetos saturados, os aromáticos e as resinas. Os saturados, como os *n*-alcanos e isoprenóides, são úteis na inferência de origem e grau de biodegradação; os aromáticos, por sua vez, incluem compostos tóxicos e persistentes como os HPAs, sendo indicadores importantes de risco ambiental; já as resinas, compostos mais polares, contribuem para a caracterização do óleo e podem influenciar sua solubilidade e comportamento em ambientes aquáticos.

1.3.3.1 *n*-Alcanos

Os *n*-alcanos têm fórmula geral C_nH_{2n+2}, possuem cadeias abertas e sem ramificações, com ligações simples entre seus átomos como o *n*C16 (Figura 8). Os *n*-alcanos são amplamente utilizados em estudos de geoquímica orgânica e forense de óleos derramados (Tissot e Welte, 1984; Peters *e* Moldowan, 2005; Hunt *et al*., 2002). O estudo dos *n*-alcanos auxilia na determinação de parâmetros relacionados ao grau de evolução térmica das rochas geradoras, tipo e origem da matéria orgânica, isso por estarem presentes em fontes de matéria orgânica como (plantas, bactérias e fitoplânctons). Os *n*-alcanos de cadeia longa, com número de carbonos variando de *n*C25 a *n*C31, são predominantemente derivados de plantas terrestres. Em contraste, os *n*-alcanos de cadeia curta, entre *n*C15 e *n*C17, são característicos de fontes marinhas (Peters e Moldowan, 2005). O uso das razões dos isoprenóides (*n*C17/Pr e *n*C18/Fi) são normalmente utilizados para avaliar o grau de biodegradação dos petróleos (Stout e Wang, 2016).

Figura 8. *n*-alcano C16.

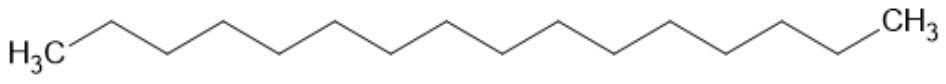

Fonte. Elaborada pelo autor.

1.3.3.2 Isoprenóides (Pristano e Fitano)

Os isoprenóides mais estudados em avaliações do petróleo e seus derivados são o pristano (2,6,10,14-tetra-metilpentadecano; Pr) e o fitano (2,6,10,14- tetra-metilhexadecano; Fi). A maioria dos isoprenóides regulares com 20 ou menos átomos de carbono, incluindo o pristano e o fitano, origina-se principalmente da degradação da cadeia lateral do fitol da clorofila (A) durante os estágios iniciais da diagênese (Rontani e Volkman, 2003), esses caminhos estão representados na Figura 9, onde o pristano é formado principalmente por oxidação e descarboxilação do fitol, enquanto o fitano resulta de processos de desidratação e subsequente redução. Assim, o pristano e o fitano para alguns óleos são normalmente os membros mais abundantes de toda uma série de isoprenóides regulares ligados à cabeça-cauda no petróleo (Peters e Moldowan, 2005).

A razão pristano/fitano (Pr/Fi) é amplamente utilizada como indicador das condições redox do ambiente deposicional da matéria orgânica. Valores de Pr/Fi inferiores a 1 sugerem ambientes anóxicos, enquanto valores superiores a 1 indicam deposição sob condições óxicas. Essa razão é particularmente útil na inferência do paleoambiente deposicional e na caracterização geoquímica de óleos e rochas geradoras. No entanto, sua interpretação deve ser realizada em conjunto com outros parâmetros geoquímicos (Peters e Moldowan, 2005).

Figura 9. Isoprenóides pristano e fitano.

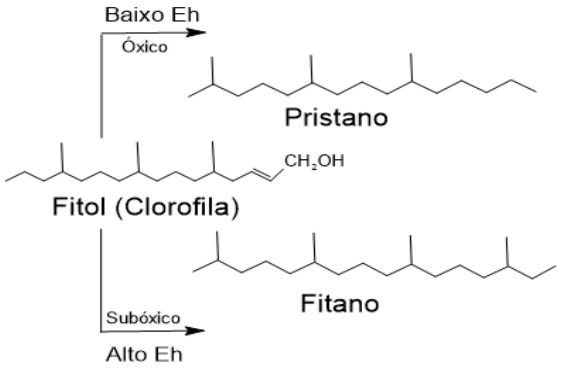

Fonte. Elaborado pelo autor.

1.3.3.3 Terpanos

Os terpanos constituem uma classe de biomarcadores de grande relevância na geoquímica orgânica. São derivados principalmente de precursores bacterianos do tipo poliprenóide, os quais compõem a membrana celular de procariontes (Waples e Machihara, 1991). Os terpanos mais comuns encontrados em petróleo e sedimentos são os tricíclicos, tetracíclicos e pentacíclicos (Peters *et al*., 2005).

Os terpanos tricíclicos são amplamente encontrados em óleos e extratos de rochas sedimentares marinhas e lacustres (Aquino Neto *et al*., 1982; Chicarelli *et al*., 1988; Kruge *et al*., 1990; Hunt *et al*., 2002; Peters, 2000). Já os terpanos pentacíclicos têm sido utilizados em correlações óleo/óleo e óleo/rocha geradores, na avaliação do paleoambiente deposicional, na análise do grau de maturação térmica e como indicadores do nível de biodegradação, devido à sua maior resistência quando comparados a outras classes de compostos do petróleo (Martins *et al*., 2014). Esses compostos derivam de reações de redução e desidratação do bacteriohopanoterol, originado de membranas de organismos procarióticos, que ocorrem durante a diagênese, contêm de 27 a 35 átomos de carbono e apresentam o íon de fragmentação *m/z* 191 como principal marcador (Peters et al., 2005).

Os terpanos tetracíclicos constituem uma série mais restrita do que os tricíclicos, cujos compostos mais comuns variam entre *n*C24 e *n*C27 (Nunes *et al*., 2017). São mais resistentes à biodegradação do que os hopanos (Aquino Neto *et al*., 1982) e, por isso, são utilizados ocasionalmente em correlações de petróleos brutos alterados (Seifert e Moldowan, 1980). A abundância do terpano tricíclico *n*C24 está relacionada a ambientes de deposição de carbonatos e evaporitos (Connan et al., 1986); contudo, de acordo com Waples e Machihara (1991), não é clara a existência de uma única origem para o *n*C24 tetracíclico, uma vez que este também está associado a alginatos ou à matéria orgânica terrestre.

Os terpanos pentacíclicos constituem a classe de biomarcadores mais estudada e utilizada entre os biomarcadores cíclicos. Por apresentarem muitos centros quirais em suas estruturas, possuem a capacidade de formar diferentes derivados estereoquímicos, cujas abundâncias são utilizadas como parâmetros indicativos do ambiente deposicional, da evolução térmica e/ou do nível de biodegradação (Peters *et al*., 2005). Nesta classe de terpanos, incluem-se compostos hopanóides e não hopanóides. Entre os não hopanóides, destacam-se os terpanos pentacíclicos, o gamacerano e os oleanano (Figuras 10 a e b).

Figura 10. Estruturas representativas dos terpanos pentacíclicos com esqueleto hopano (A) e não-hopanóide (B).

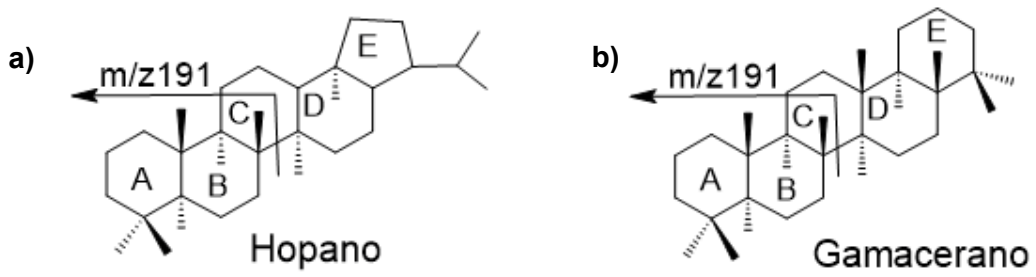

Fonte. Elaborado pelo autor.

1.3.3.4 Esteranos

Os esteranos têm de 27 a 29 átomos de carbono em sua cadeia fechada, incluindo os esteranos regulares, os esteranos rearranjados ou diasteranos. Dentre eles, os esteranos regulares da série homóloga C27, C28 e C29 (Colestano, Ergostano e Estigmastano) são os mais comuns e mais utilizados nas avaliações de petróleo em função da sua alta especificidade (Wang e Stout, 2006). Os esteróis dos organismos eucariotas são precursores dos esteranos nas rochas geradoras e no petróleo (Mackenzie *et al*., 1981; Moldowan *et al*., 1991). Devido ao grande número de centros assimétricos nos esteróis, são possíveis misturas muito complexas de estereoisômeros.

Grande parte dos esteranos (Figura 11 a, b e c) constituintes do petróleo originou-se a partir dos esteróis presentes nas membranas lipídicas dos

organismos eucariotas. A configuração biológica [14α,17α (H) -20R] ditada pelo esterol precursor e seu produto saturado é instável durante a catagênese e é convertida nas configurações geológicas (14β,17β (H)-20S, 14β,17β (H)-20SR, 14α,17α (H)-20S) através de isomerização (Gallotta, 2014).

Figura 11. Estruturas representativas dos esteranos.

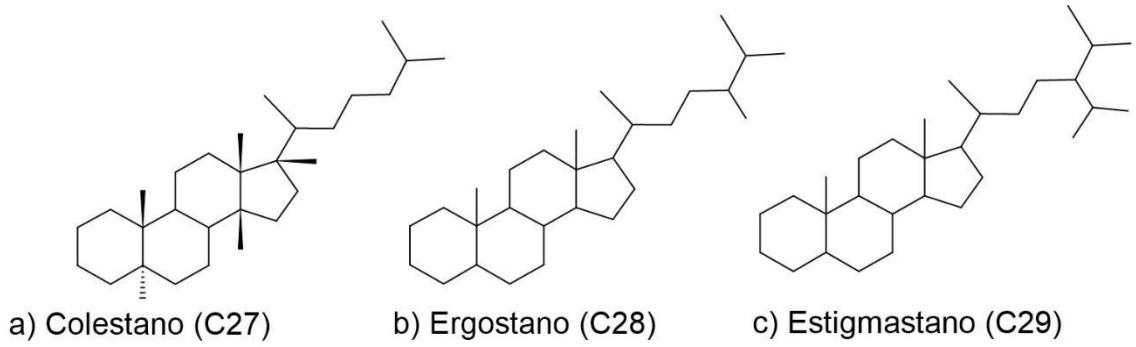

Fonte. Elaborado pelo autor.

1.3.3.5 Esteroides aromáticos

Os esteróides aromáticos são hidrocarbonetos naftênicos aromáticos, que consistem em estruturas mistas de anéis aromáticos e saturados de 6 ou 5 carbonos (Figura 12). A análise por CG-MS revelou a presença de duas famílias principais de componentes de hidrocarbonetos monoaromáticos esteróides e hidrocarbonetos triaromáticos esteróides (Mackenzie *et al*., 1981; Barakat, 1994; Li e Jiang, 2001). Os esteróides monoaromáticos do anel C (MAS) são compostos por dois anéis de ciclohexano (A+B) e um anel de ciclopentano fundidos com um anel aromático (anel C) na sua estrutura molecular. Os triaromáticos esteróides (TAS) têm estruturas moleculares semelhantes ao (MAS), com a principal diferença de que os seus anéis ciclohexano A e B são substituídos por anéis aromáticos (Yang *et al*., 2013).

A abundância de esteróides monoaromáticos em relação aos triaromáticos fornece informações através de correlações geoquímicas, para a avaliação da maturidade do petróleo bruto (Yang *et al*., 2013; Seifert e Moldowan, 1978; Lu *et al*., 1992; Barakat, 1994; Brocks *et al*., 2003; Zhao *et al*., 2005; Oliveira *et al*., 2012).

Os homólogos C26-28 TAS são considerados muito resistentes a uma grande variedade de condições de intemperismo em escalas geológicas, incluindo a biodegradação no reservatório, e degradam-se apenas em condições extremas como mostra escala de Peters e Moldowan (Volkman *et al*., 1984; Peters *et al*., 2005). Eles foram provavelmente formados por aromatização e perda de um grupo metilo dos esteranos regulares C27-C29 durante o processo de diagênese e processos térmicos (Moldowan e Fago, 1986; Peters *et al*., 2005).

Figura 12. Estereoisomeria e fragmentação em massa de esteróides triaromáticos e esteróides monoaromáticos do anel C.

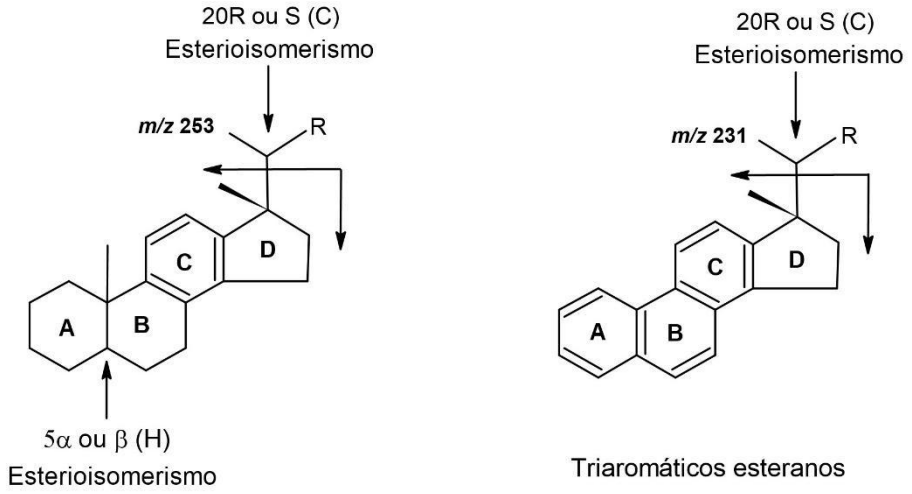

Fonte: Elaborada pelo autor**.**

Os esteróides aromáticos são monitorados pelo íon fragmento característico de *m/z* 231 para triaromáticos e de *m/z* 253 para os monoaromáticos esteróides, e confirmados por íons de *m/z* 215 e *m/z* 143, respectivamente (Peters *et al*., 2005; Yang *et al*., 2013).

1.3.3.6 Hidrocarbonetos Policíclicos Aromáticos (HPAs)

Os hidrocarbonetos são denominados aromáticos quando apresentam em sua cadeia pelo menos um anel aromático, enquanto isso os poliaromáticos, mais conhecidos como Hidrocarbonetos Policíclicos Aromáticos (HPAs)

apresentam dois ou mais anéis benzênicos fundidos com cinco ou seis átomos de carbono, chamados de HPAs parentais. Esses anéis podem apresentar ramificações de cadeias alifáticas ou heteroátomos como enxofre e oxigênio, sendo estes denominados HPAs alquilados (Cavalcante *et al*., 2020; Cheng *et al*., 2019; Behera *et al*., 2018; Yin *et al*., 2022). Como os HPAs são poluentes orgânicos persistentes, eles têm recebido atenção por apresentarem características tóxicas, mutagênicas, cancerígenas e teratogênicas, assim a Agência de Proteção Ambiental Americana (USEPA) classificou 16 HPAs como prioritários devido a estes riscos (Figura 13).

Figura 13. Estruturas moleculares dos 16 HPAs prioritários segundo a Agência de Proteção Ambiental dos Estados Unidos (USEPA).

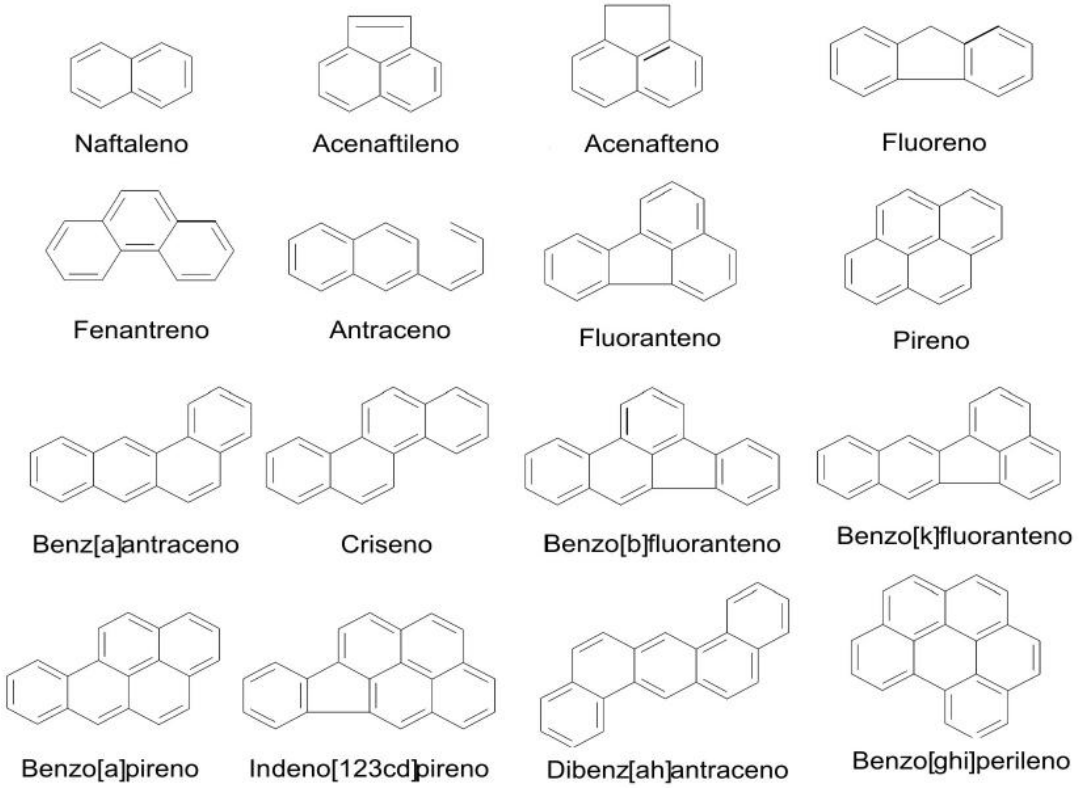

Fonte. EMBRAPA (2009); UESPA (2014).

Em geral, as emissões de HPAs no meio ambiente podem ocorrer através de três possíveis fontes: pirolítica, petrogênica e diagenética. Os HPAs de origem petrogênica são formados por processos diagenéticos, que neste caso, remetem a condições de baixa temperatura relativa, sobre escalas geológicas de tempo,

esses HPAs exibem um padrão de distribuição em forma de sino (*bell shaped*) (Wang e Fingas, 2003; Yunker *et al*., 2011). Por outro lado, os HPAs de origem pirolítica, resultam da combustão incompleta de matéria orgânica sob condições de intervalos de baixa a alta temperatura, baixa pressão e curto tempo de formação, geralmente apresentam a distribuição dos HPAs alquilados homólogos com HPAs parentais mais abundantes (com o perfil de distribuição de C0->>C1->C2->C3->C4-, chamada de distribuição inclinada), (Cavalcante *et al*., 2002; EMBRAPA, 2009; Neff *et a*l., 1979).

1.3.3.7. Compostos Polares no Petróleo (N, O e S)

Os compostos heteroatômicos, relatados como compostos polares, incluem espécies contendo átomos de N, S e O, ligados a sistemas aromáticos e naftênicos. Esses compostos correspondem a 15% do petróleo, e a presença de alguns desses compostos no óleo pode levar a problemas que afetam todo o setor petrolífero, que vão desde alteração das propriedades físicas e químicas do petróleo bruto, envenenamento do catalisador, instabilidade dos produtos, depósitos de nafteno, corrosão de equipamentos em refinarias (dutos e tanques), até perda da capacidade de fluxo com a redução da temperatura, entre outros (Vanini *et al*., 2020). Estes são tipicamente encontrados em frações de resinas e asfaltenos (Rocha *et a*l., 2019).

Os principais compostos oxigenados presentes no petróleo são os ácidos naftênicos e os fenóis. Os ácidos naftênicos são definidos como ácidos carboxílicos que incluem uma ou mais estruturas de anel saturado, sendo os anéis de cinco e seis membros mais comuns. Além dos ácidos contendo anéis, os ácidos carboxílicos lineares são frequentemente incluídos na classe de ácidos naftênicos (Dalmaschio *et al*., 2014). Os ácidos naftênicos são responsáveis por processos corrosivos em tanques de armazenamento, que têm sua corrosividade associada ao índice de acidez total (TAN). Valores elevados de TAN indicam maior concentração desses ácidos, o que eleva o potencial corrosivo do petróleo ou de seus derivados (Speight, 2014). Já os fenóis contribuem para a coloração escura, odor forte e formação de emulsões estáveis

devido à imiscibilidade entre água e petróleo. Ambos estão concentrados na fração asfaltênica, a mais pesada do petróleo, sendo objetos de destaque em estudos que visam compreender os efeitos desses compostos nas propriedades física e químicas e nos desafios operacionais dos processos de refino (Barrow *et al*., 2003; Rocha *et al*., 2019; Gruber *et al*., 2012).

Além dos compostos oxigenados, o petróleo contém outros componentes polares importantes, como as espécies nitrogenadas básicas e não - básicas. Os compostos básicos são representados pelos seguintes grupos de compostos: piridina, alguns pirróis, azo-(bases médias), aminas primárias (bases fortes), *n*-alquil- indóis e alquil-aril-aminas (bases fracas). Já os compostos não-básicos são representados pelos: são representados pelos indóis, carbazóis, piridinas, pirróis e a maior parte das amidas, esses compostos representam menos de 30% do total de compostos orgânicos nitrogenados presentes no petróleo. Os carbazóis são os compostos mais abundantes (Looij *et al*., 1998; Dalmaschio *et al*.,2014; Furimsky *et al*., 2005; Rocha *et al*., 2011). A figura 14 apresenta as principais classes de heterocompostos.

Figura 14. Exemplos de compostos contendo heteroátomos comumente encontrados no petróleo.

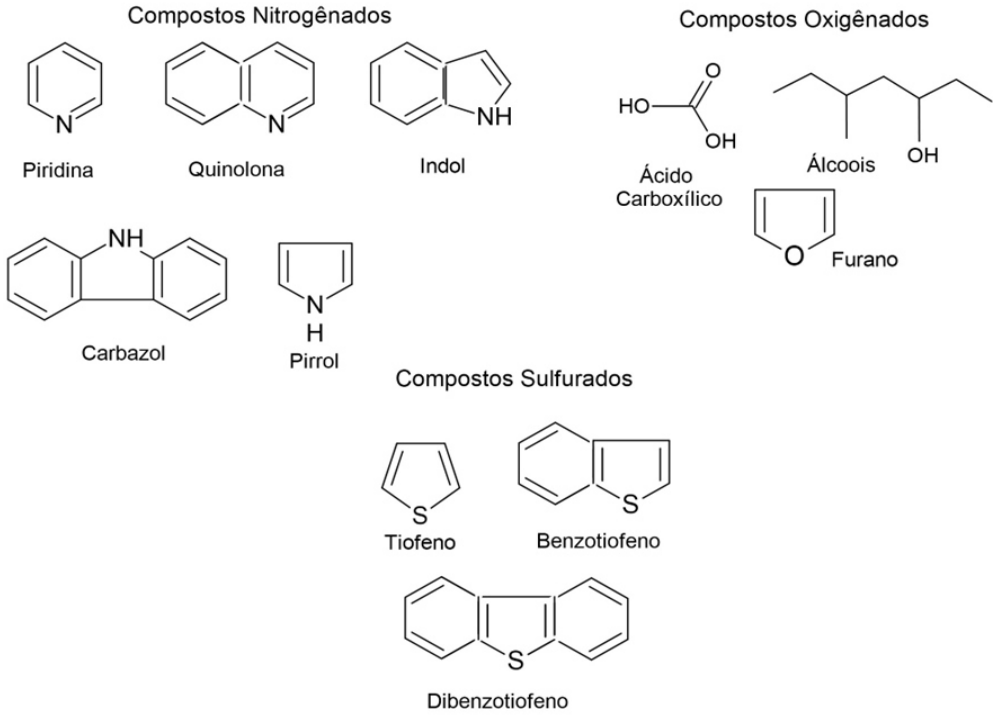

Fonte. Elaborado pelo autor.

Dentre os compostos sulfurados presentes no petróleo, os organossulfurados se destacam por sua abundância e são geralmente classificados em duas categorias: ácidos, que incluem mercaptanas, tiofenóis e ciclo-tióis; e não ácidos, como dissulfetos e derivados de tiofeno. Os tiofenos, por sua vez, apresentam estruturas aromáticas complexas, tais como benzo-, dibenzo- e naftobenzotiofenos, sendo considerados os compostos sulfurados majoritários nas amostras de petróleo. Frequentemente, esses compostos encontram-se associados a outros heteroátomos, como nitrogênio (N) e oxigênio (O), originando estruturas mistas do tipo SO, NS e NOS, entre outras (Rocha *et al*., 2019; Looij *et al.,* 1998; Orr e Damsté, 1990).

1.3.4 Técnicas analíticas aplicadas para análise de petróleo

A aplicação de técnicas analíticas torna-se essencial para a análise química à nível molecular de óleos derramados e fornecer respostas precisas quanto à sua origem, seu grau de degradação e outros processos relevantes. Dessa forma, métodos analíticos vêm sendo empregados em estudos científicos e periciais, com o objetivo de oferecer subsídios confiáveis nas análises para ações de remediação ambiental, como também em processos de responsabilização legal (Oliveira *et al*., 2020).

Nesse contexto, três técnicas analíticas têm sido amplamente utilizadas nos estudos sobre derramamentos de óleo. A cromatografia gasosa com detector por ionização de chama (GC-FID) é amplamente utilizada para quantificação de hidrocarbonetos totais do petróleo, sendo eficiente na obtenção de perfis de *n*-alcanos. Já a cromatografia gasosa acoplada à espectrometria de massas (GC-MS) permite a identificação de compostos específicos, como os biomarcadores (Hyun *et al*., 2018). No entanto, a elevada complexidade dos componentes do petróleo e a presença de compostos polares, que não são passíveis de análise por CG, apresentam desafios para as abordagens tradicionais. Assim, surge a petroleômica, ferramenta para se obter mais informações composicionais de frações do petróleo não passíveis de CG,

utilizando técnicas de espectrometria de massas de alta resolução, como espectrometria de massas por ressonância ciclotrônica de íons com transformada de Fourier (FT-ICR MS; Chen *et al*., 2019; Acter *et al*., 2023; Price e Walters, 2022).

O uso de técnicas convencionais, como a cromatografia gasosa, incluindo o GC-FID e o GC-MS, tem sido amplamente empregado na análise de óleos derramados, fornecendo informações relevantes sobre as alterações composicionais decorrentes do intemperismo de hidrocarbonetos e HPAs. No entanto, limitações como a coeluição de compostos e a impossibilidade de análise de frações polares não voláteis ou termicamente instáveis evidenciam a necessidade de sua integração com métodos com maior resolução e abrangência, especialmente em contextos de análise forense ambiental, como evidenciam diversos estudos voltados à caracterização de óleos derramados em ambientes costeiros (Lima *et al*., 2023; Pereira et al., 2023; Nascimento *et al*., 2025; Maki e Harayama, 2001; Prince e Walters, 2022);

1.3.4.1 Cromatografia gasosa com detector de ionização de chama (GC-FID)

A cromatografia gasosa com detecção por ionização de chama (GC-FID) é amplamente empregada na análise de óleos derramados devido à sua alta eficiência na quantificação de hidrocarbonetos totais do petróleo (TPH), *n*-alcanos e isoprenóides. Sua sensibilidade, reprodutibilidade e ampla faixa linear tornam essa técnica ideal para investigações ambientais, sobretudo na avaliação de alterações composicionais provocadas por processos intempéricos, como evaporação, oxidação e biodegradação (Wang *et al*., 1999; Wang e Fingas, 2003). Como resultado de suas análises, o GC-FID gera perfis cromatográficos característicos, frequentemente denominados “impressões digitais” (*fingerprints*), que possibilitam a identificação e diferenciação entre óleos de distintas origens, sendo particularmente úteis na correlação óleo/óleo e óleo/fonte em estudos forenses e ambientais (Hyun *et al*., 2018; CEN EN 15522-

2:2023). As Figuras 15 a e b exemplificam cromatogramas do GC-FID de amostras de óleos derramados nos anos de 2019 e 2022 na costa brasileira.

Figura 15. Cromatogramas GC-FID de amostras dos derramamentos de 2019 (a) e 2022 (b).

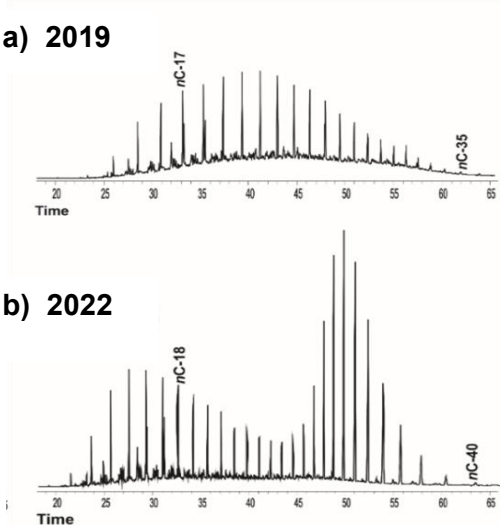

Fonte. Azevedo *et al* (2022); Nascimento *et al* (2025).

Os cromatogramas gerados por GC-FID apresentam distribuições características de *n*-alcanos, geralmente variando de *n*C9 a *n*C40, e permitem comparações diretas com padrões de referência ou óleos previamente caracterizados. A técnica também possibilita a avaliação da UCM (*Unresolved Complex Mixture*), cuja intensificação indica ação avançada de biodegradação ou outros processos intempéricos (Hyun *et al*., 2018). Além disso, quando combinada a outras técnicas, como a cromatografia gasosa acoplada à espectrometria de massas (GC-MS), pode ser mais eficazmente aplicada por meio da correlação com biomarcadores geoquímicos, como hopanos e esteroides (Peters *et al*., 2000).

Estudos forenses de contaminação ambiental frequentemente adotam o GC-FID como ferramenta de triagem em análises rotineiras de solos, sedimentos e amostras de água contaminadas por petróleo. No contexto de derramamentos costeiros, como o registrado no Brasil em 2019, o uso do GC-FID demonstrou eficácia na identificação de hidrocarbonetos totais e *n*-alcanos, os quais foram

utilizados como marcadores primários para determinar a origem do óleo e seu estágio de degradação (Oliveira *et al*., 2020). No caso do derramamento da *Deepwater Horizon*, Aeppli *et al*. (2012) e McKenna *et al*. (2013) analisaram sedimentos oleosos, utilizando inicialmente GC-FID, para determinar se estes óleos haviam sofrido intemperismo. Dessa forma, o GC-FID permanece como uma técnica indispensável no monitoramento de áreas impactadas por hidrocarbonetos, oferecendo robustez analítica e simplicidade operacional.

1.3.4.2 Cromatografia gasosa acoplada à espectrometria de massas (GC-MS)

A cromatografia gasosa acoplada à espectrometria de massas (GC-MS) é amplamente reconhecida como ferramenta essencial na análise de óleos derramados, por permitir a identificação e quantificação de hidrocarbonetos alifáticos, incluindo os biomarcadores de petróleo, e aromáticos, mesmo em amostras altamente degradadas. Estudos realizados durante o desastre do *Deepwater Horizon* demonstraram que o GC-MS, operando em modo de monitoramento seletivo de íons (SIM), é eficaz na detecção de compostos-chave essenciais para caracterizar a origem do óleo e monitorar seu grau de degradação ambiental (Wang *et al*., 2012; Hall *et al*., 2013; Aeppli *et al*., 2012; 2014: McKenna *et al*., 2013).

Além disso, os dados obtidos das análises por GC-MS têm sido integrados à métodos multivariados, combinando razões diagnósticas de biomarcadores com análises estatísticas, como a Análise de Componentes Principais (PCA) (Sudol *et al*., 2020), o que amplia a robustez da correlação entre amostras ambientais e possíveis fontes. Normas internacionais, como a CEN EN 15522-2:2023, também consolidam esse tipo de análise como padrão para investigações de derramamentos de óleo. O GC-MS tem sido amplamente utilizado em investigações de contaminação ambiental costeira no Brasil, incluindo os episódios de derramamento registrados no Nordeste em 2019 e 2022. Trabalhos recentes demonstraram a aplicação eficaz da técnica na caracterização de resíduos oleosos coletados em praias, com foco na

identificação de marcadores moleculares como hopanos, esteranos e hidrocarbonetos policíclicos aromáticos (HPAs) alquilados — compostos que indicam origem petrogênica dos contaminantes e sugerem sua proveniência a partir de óleo pesado (Azevedo *et al*., 2022; Martins *et al*., 2024; Oliveira *et al*., 2020; Brandão *et al*., 2021; Bontempo *et al*., 2020; Bérgamo *et al*., 2023; Martins *et al*., 2023; Stout e Wang, 2016). Nesses estudos, a seleção de íons de fragmentação específicos, como *m/z* 191 (terpanos; Figura 16 a), *m/z* 217 (esteranos; Figura 16 b) e *m/z* 231 (esteranos triaromáticos), é essencial para a detecção seletiva e a construção de cromatogramas de íons característicos, possibilitando uma identificação precisa dos compostos presentes. Esses dados não apenas corroboram com a eficiência da técnica para análises forenses, também reforçam sua importância em avaliações de risco ambiental.

Figura 16. Cromatogramas *m/z* 191 do óleo de 2019 e *m/z* 217 do óleo de 2022.

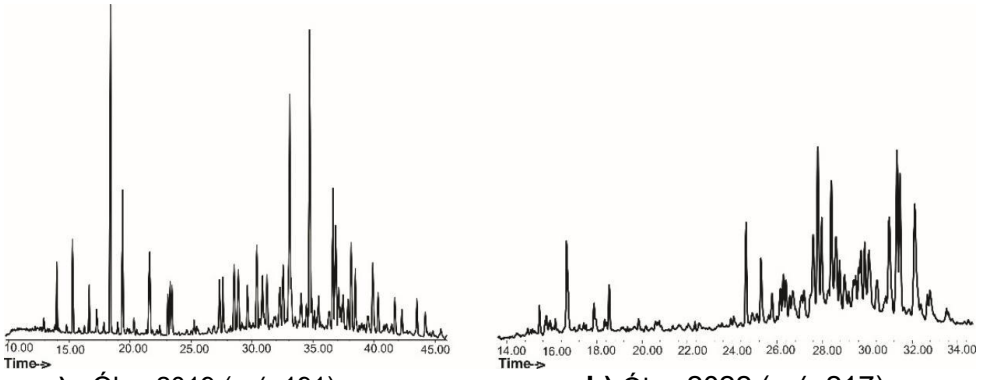

Fonte. Nascimento *et al.* (2025).

A cromatografia gasosa acoplada à espectrometria de massas (GC-MS) permanece como uma das técnicas mais eficazes para a caracterização detalhada de óleos, mesmo em estágios avançados de degradação. Sua aplicação tem sido fundamental na detecção de hidrocarbonetos, incluindo os HPAs alquilados e biomarcadores resistentes, permitindo inferências sobre a origem e o estado de alteração dos resíduos oleosos (Arey *et al*., 2007; Reddy *et al*., 2012). A elevada seletividade e sensibilidade dessa técnica é

indispensável em estudos ambientais, periciais e industriais voltados à análise de derramamentos de petróleo.

1.3.4.3 Espectrometria de massas de alta resolução (FT-ICR MS)

A espectrometria de massas de ultra-alta resolução revolucionou a compreensão da composição do petróleo, permitindo a caracterização de componentes individuais em frações inteiras, sem a necessidade de separação cromatográfica prévia. Esses instrumentos oferecem grande potencial para caracterizar a maioria dos compostos polares de alto peso molecular ainda não identificados no petróleo, bem como resíduos que foram alterados por processos intempéricos (Prince e Walters, 2022; Huba e Gardinali, 2016; Qin *et al*., 2024).

Assim, a espectrometria de massas por ressonância ciclotrônica de íons com transformada de Fourier (FT-ICR MS) apresenta resolução e acurácia de massa acima de 1.000.000 em *m/z* 400, permitindo a identificação de dezenas de milhares de fórmulas moleculares em uma única análise. Essa capacidade torna possível caracterizar diretamente frações complexas de petróleo, como resinas e asfaltenos, sem a necessidade de separação cromatográfica prévia, acessando compostos pesados, polares e pouco voláteis que não são detectados por técnicas convencionais, como GC-MS uni e bidimensional (Marshall e Rodgers, 2008; Rodović *et al*., 2019: Wise *et al*,.2022).

O FT-ICR MS oferece análise em uma ampla faixa de massa (*m/z*), poder de resolução de massa e precisão de massa. Este foi aplicado pela primeira vez ao petróleo por meio da ionização eletrônica do petróleo destilado. No entanto, o campo magnético relativamente baixo (3,0 T), limitada a faixa *m/z*, a necessidade de volatilizar a amostra, limitada faixa de peso molecular (especialmente para espécies contendo heteroátomos) e a ionização eletrônica produz extensa fragmentação (especialmente de cadeias alquílicas; Mckenna *et al*., 2013). No entanto, os recentes desenvolvimentos em FT-ICR MS (Figura 17) e fontes de íons lançaram uma nova luz sobre a imensa complexidade do petróleo bruto, tornando possível resolver e identificar milhares de compostos a partir de uma única amostra de óleo cru (Rocha *et al*., 2019).

A espectrometria de massas com foco na Petroleômica tem como seus pilares a fontes de ionização, que permite análises de moléculas complexas, um analisador com altíssima resolução e exatidão e um sistema de processamento dos dados (Rocha *et al*., 2019). As principais fontes de ionização empregadas na análise do petróleo e suas frações são a ionização por impacto eletrônico (EI), ionização química à pressão atmosférica (APCI), fotoionização à pressão atmosférica (APPI) e *electrospray* (ESI), onde cada uma tem a capacidade de ionizar diferentes compostos, respeitando a polaridade e massa molecular de cada espécie.

As técnicas de APCI, APPI e ESI são classificadas como técnicas de ionização à pressão atmosférica (API), visto que elas não operam sob vácuo e possuem característica de serem técnicas de ionização brandas, ou seja, geram pouca ou nenhuma fragmentação. Desta forma, a técnica de APCI, é utilizada na ionização de espécies com polaridade intermediária e com massa até 1500 Da. A técnica de APPI utiliza fótons gerados por uma lâmpada de descarga ultravioleta para ionizar o analito e a técnica de *electrospray* ioniza moléculas polares com massas elevadas, neste caso, ao contrário do que acontece com APCI e APPI, as espécies são ionizadas ainda em solução (Rocha *et al*., 2019; Hoffmann e Stroobant, 2007; Marshall, 2008).

Figura 17. Espectrometria de massa por ressonância ciclotrônica de íons com transformada de Fourier (FT-ICR MS) para caracterização química do petróleo e seus derivados.

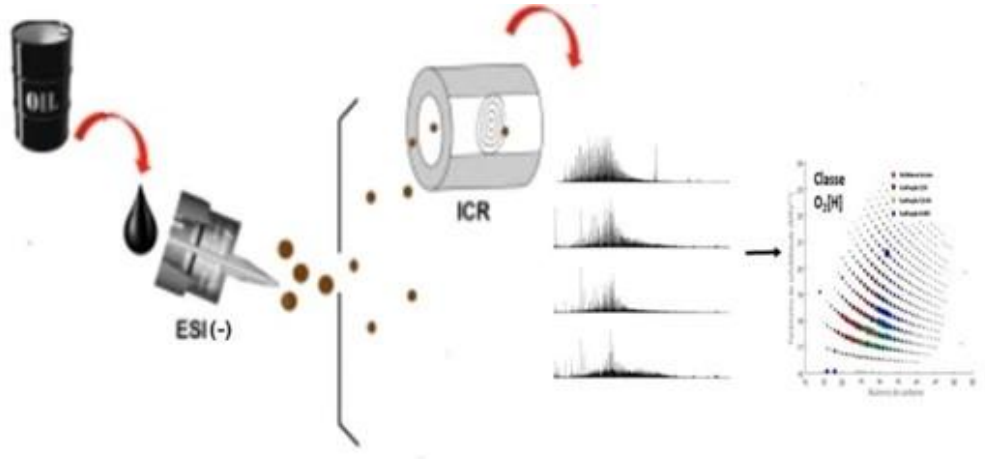

Fonte: Adaptado de Vanini *et al*. (2020) e Pinto *et al*. (2022).

O FT-ICR MS tem se mostrado particularmente importante em estudos sobre derramamentos de óleo, permitindo o monitoramento de mudanças moleculares causadas por processos intempéricos como a fotooxidação, a biodegradação e a formação de agregados orgânicos oleosos (*marine oil snow*; Rodović *et al*., 2019). A análise de parâmetros como o defeito de massa (*mass defect*), o número de insaturações (DBE) e a presença de heteroátomos (O, N, S) fornece uma "impressão digital química" detalhada do petróleo, auxiliando na diferenciação entre fontes distintas e na avaliação do grau de degradação do óleo em ambientes costeiros (Corilo *et al*., 2013; Lima *et al*., 2023). Esses atributos mostram o quanto essa técnica é uma ferramenta essencial e inovadora em análises forenses e ambientais de derramamentos de óleo, complementando os estudos de outras técnicas cromatográficas convencionais (Prince e Walters, 2022).

No contexto da pesquisa no Brasil, diversos estudos têm aplicado técnicas de espectrometria de massas de alta resolução para caracterização detalhada de óleos derramados, com ênfase na elucidação da composição molecular e na identificação de marcadores específicos que permitam inferir a origem e o grau de intemperismo do material. Essa abordagem tem sido particularmente relevante na investigação de derramamentos de petróleo em áreas costeiras, fornecendo informações mais abrangente sobre a distribuição de compostos polares, incluindo ácidos orgânicos e frações resinosas e asfálticas. Assim, de acordo com Lima *et al*. (2020; 2021), em seus estudos utilizando óleos brasileiros simulando a ação de processos intempéricos, bem como *tarballs* coletados em praias, pode-se observar o aumento na abundância relativa de compostos das classes O_2, O_3 e O_4, o que sugeriu que a fotooxidação teve um papel importante na oxidação dos óleos derramados. Já para os *tarballs*, os perfis de classes de heteroátomos obtidos por FT-ICR MS indicaram intemperismo extensivo para todas as amostras, com biodegradação e fotooxidação como os processos mais importantes sofridos pelo óleo derramado.

Em estudo realizado por Reddy *et al*. (2022), com óleos derramados no ano de 2019 no Brasil, o uso do FT-ICR MS permitiu identificar que o óleo derramado continha compostos com ponto de ebulição alto, indicativo de mistura de petróleo bruto com outros derivados de petróleo ou de alteração térmica. Já estudos realizados por Nascimento *et al*. (2025) e Pereira *et al*. (2023), com *tarballs* parafínicos que chegaram ao litoral do Nordeste brasileiro no final de 2022, mostraram que a avaliação dos compostos polares ácidos por ESI(-) FT-ICR MS revelou que esses óleos sofreram biodegradação e fotooxidação, pelo menos em sua extensão inicial. Eles também apresentaram alta abundância de ácidos graxos, DBE 1 da classe O_2, consistentes com suas características cerosas.

A capacidade de diferenciar amostras com base em assinaturas moleculares únicas em estudos da geoquímica forense tem-se fortalecido com a aplicação das técnicas de espectrometria de massas de alta resolução, incluindo o FT-ICR MS, auxiliando não apenas na identificação de fontes, mas também para um melhor entendimento das alterações químicas provocadas pelos processos intempéricos, como biodegradação e fotooxidação (Prince e Walters, 2022). As contribuições dessa técnica evidenciam seu papel estratégico na compreensão dos impactos ambientais e na formulação de respostas mais eficazes frente a eventos de derramamento de petróleo.

1.4 MATERIAL E MÉTODOS

1.4.1 Área de Estudo

Neste trabalho, foram analisadas 56 amostras de resíduos oleosos coletadas ao longo da costa do estado do Ceará e de mais cinco estados do nordeste brasileiro no período de 2019 a 2022 (Tabela 1). Incluem-se nesse estudo, quatro amostras referentes ao evento de 2019 (1 a 4, Tabela 1; Reddy *et al*., 2022), 19 amostras coletadas no monitoramento do ano de 2021 (5 a 23, Tabela 1) na costa litoral cearense, três amostras coletadas no início de 2022, referentes ao evento ocorrido no estado do Ceará (24 a 26, Tabela 1; Azevedo *et al*., 2022), 13 amostras coletadas no monitoramento do litoral do Ceará no período de maio a setembro de 2022 (27 a 39, Tabela 1) e 17 amostras coletadas no final de 2022 referentes à chegada de *tarballs* parafínicos (45 a 53, Tabela 1; Nascimento *et al*., 2022; Nascimento *et al*., 2025; Pereira *et al*., 2023). Além das amostras do estado do Ceará, foram analisadas oito amostras de resíduos dos estados de Alagoas, Bahia, Paraíba e Rio Grande do Norte (54 a 61, Tabela 1, Nascimento *et al*., 2025; Pereira *et al*., 2023), relacionadas ao evento dos *tarballs* parafínicos do final de 2022.

Tabela 1. Localização das amostras de óleo coletadas nos anos de 2019 a 2022.

Nº	**Amostras**	
	Evento de 2019	**Praia/Estado**
1	P01#2019	Cumbuco/CE
2	P02#2019	Mangue do Rio Jaguaribe
3	P03#2019	Paracuru/CE
4	P04#2019	Paracuru/CE
	Monitoramento de 2021	
5	P01E#2021	Barra nova/CE
6	P03E#2021	Pontal de Maceió/CE
7	P04E#2021	Barra/CE
8	P06E#2021	Cano quebrada/CE
9	P07E#2021	Iguape/CE
10	P08E#2021	Sabiaguaba/CE
11	P10E#2021	Pecém /CE
12	P11E#2021	Icaraí/CE

13	P12E#2021	Cumbuco/CE
14	P14W#2021	Taíba/CE
15	P16W#2021	Lagoinha/CE
16	P17W#2021	Paracuru/CE
17	P20W#2021	Caetanos de cima/CE
18	P21W#2021	Mundaú/CE
19	P22W#2021	Icaraí de amontada/CE
20	P23W#2021	Almofala/CE
21	P24W#2021	Bitupitá/CE
22	P28W#2021	Jericoacoara/CE
23	P34W#2021	Caetenos/CE
	Evento de 2022.1	
24	P01E#22 (01)	Sabiaguaba/CE
25	P04E#22 (01)	Cumbe/CE
26	P05E#22 (01)	Canoa Quebrada/CE
	Monitoramento de 2022	
27	P01E#22 (02)	Sabiaguaba/CE
28	P02E#22 (02)	Porto das Dunas/CE
29	P05E#22 (02)	Canoa quebrada/CE
30	P06E#22 (02)	Canto verde/CE
31	P01W#22 (03)	Cumbuco/CE
31	P02W#22(03) S03	Taíba/CE
33	P03W#22(03)	Paracuru/CE
34	P04W#22(03)	Flecheiras/CE
35	P01W#22(04) S01	Bitupitá/CE
36	P01W#22(04) S03	Bitupitá/CE
37	P01W#22(04) S05	Bitupitá/CE
38	P01W#(05) S01	Jericoacoara/CE
39	P01W#(05) S03	Jericoacoara/CE
	Evento de 2022.2	
45	P01W#22(06) S01	Praia do Futuro/CE
46	P01W#22 (07)	Icaraí/CE
47	P02W#22 (07)	Cumbuco/CE
48	P03W#22 (07)	Pecém/CE
49	P01W#22 (08)	Futuro/CE
50	P01W#22 (09)S01	Flecheiras/CE
51	P02W#22 (09)	Almofala/CE
52	P01W#22 (10)	Paracuru/CE
53	P01W#22 (11)	Peroba/CE
54	P01W#22 (12)	Albino/BA
55	P02W#22 (12)	Costa/BA
56	P01W#22 (13)	Barra Formosa/RN
57	P02W#22 (13)	Tabatinga/RN
58	P01W#22 (15)	Candeias/PE

59	P02W#22 (15)	Olinda/PE
60	P03W#22 (15)	Maragogi/AL
61	P04W#22 (15)	Pina/AL

Fonte: Elaborado pelo autor, 2025.

A Figura 18 representa o mapa de localização das amostras monitoradas nos anos de 2021 e 2022 e dos eventos de 2019, 2022.1 e 2022.2 no estado do Ceará. Já a Figura 19 representa o mapa de localização dos *tarballs* coletados nos estados de Alagoas, Bahia, Ceará, Pernambuco e Rio Grande do Norte.

Figura 18. Mapa de Localização das amostras monitoradas nos anos de 2021, 2022 e das amostras dos eventos de 2019, 2022.1 e 2022.2.

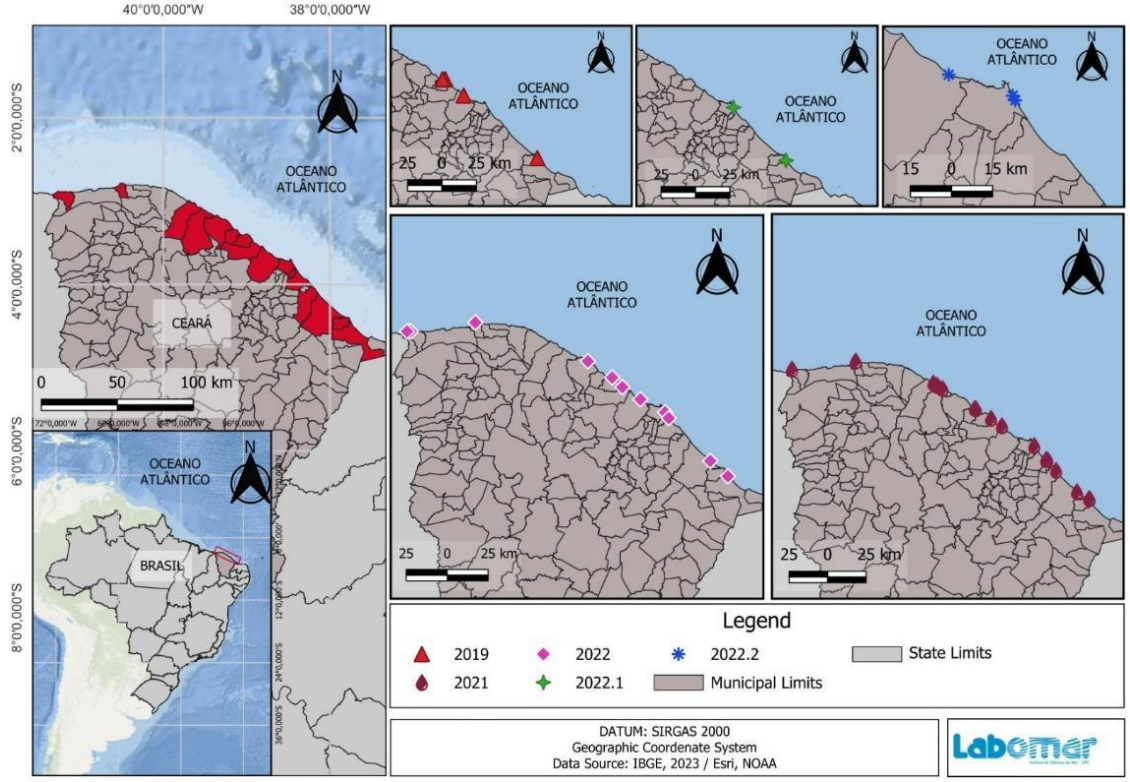

Fonte: Elaborado por Pinheiro (2025).

Figura 19. Localização das amostras de óleo de *tarballs* dos estados do Ceará, Alagoas, Bahia, Sergipe, Rio Grande do Norte e Pernambuco.

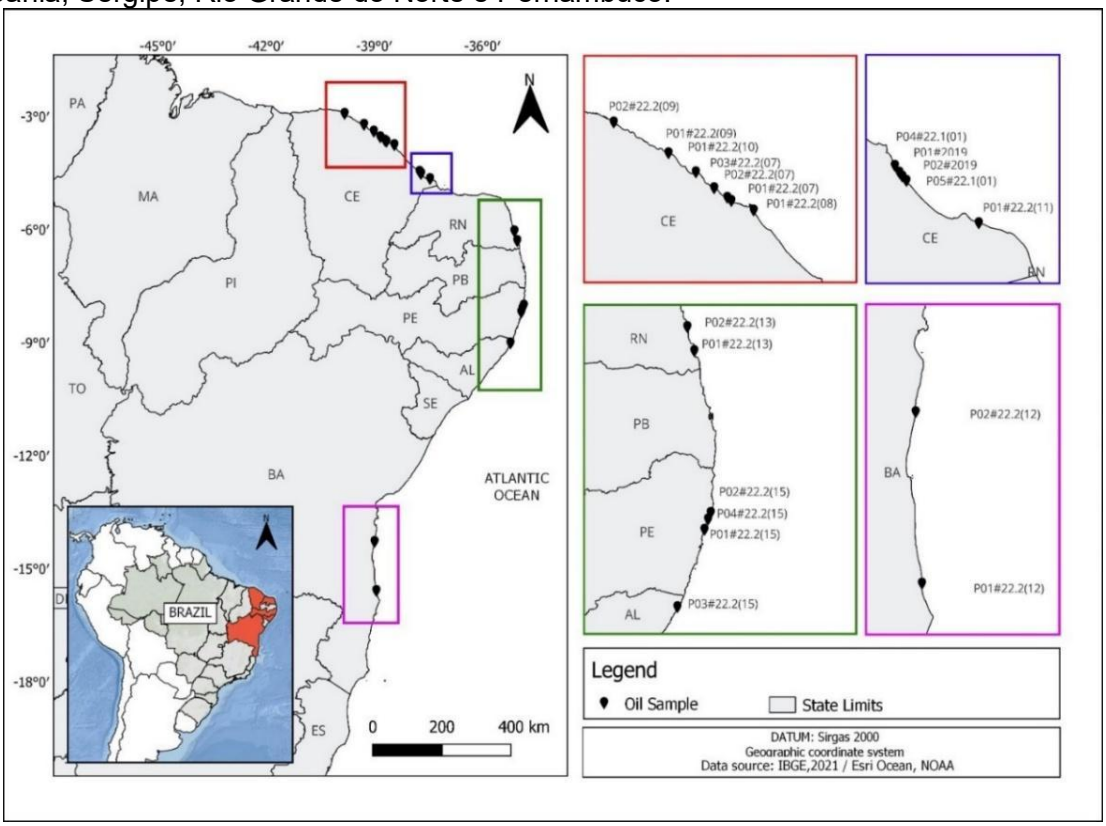

Fonte: Elaborado por Pinheiro (2025).

1.4.2 Procedimento Experimental

Nestas etapas serão descritos os procedimentos adotados para as análises das amostras de óleo derramado. Detalha-se as etapas extração, precipitação do asfalteno e a cromatografia líquida, onde a metodologia SARA é aplicada para separação do petróleo em classes de compostos (Saturados, Aromáticos, Resinas e Asfaltenos). Os procedimentos experimentais foram estruturados de modo a assegurar a reprodutibilidade e a confiabilidade dos resultados obtidos. Essa abordagem visa garantir a robustez e a validade das inferências realizadas. A Figura 20 representa o fluxograma das etapas de análises experimentais que foram aplicados para a análise das amostras.

Todas as vidrarias foram inicialmente lavadas com sabão Dinâmicatec a 3% e enxaguadas com água destilada. Em seguida, foram enxaguadas com uma solução de potassa alcoólica e posteriormente lavadas dez vezes com água. Após essa etapa, as vidrarias foram enxaguadas com uma solução de ácido acético a 10% e novamente lavadas cerca de dez vezes com água corrente. Por fim, as vidrarias foram enxaguadas com água destilada e secas em estufa. Após a secagem, as vidrarias foram rinsadas com diclorometano PA.

Figura 20. Fluxograma do processo de extração, precipitação, e análises das amostras de óleo.

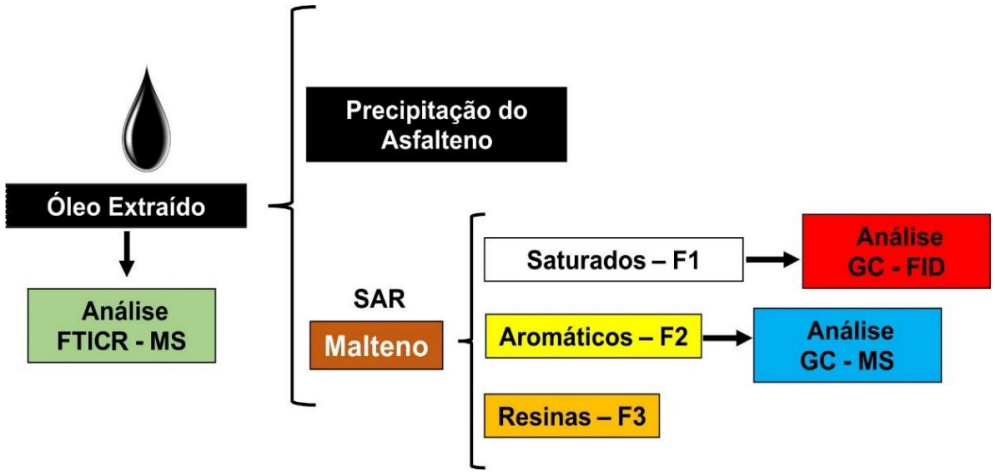

Fonte: Elaborado pelo autor.

1.4.3 Extração

A etapa de extração tem como objetivo retirar impurezas como sedimentos, folhas e todo qualquer material que esteja aderido a amostra de óleo derramado (Figura 21). Todas as amostras foram pesadas, cerca de 1,0 g, e adicionado 6 mL de diclorometano (grau HPLC). A amostra foi agitada em vórtex e centrifugada, esse procedimento foi realizado cinco vezes. Após cada centrifugação, o sobrenadante foi retirado e acondicionado em um balão de fundo redondo. Após a realização deste procedimento, o óleo foi roto evaporado para retirada de todo solvente e concentração da amostra de óleo (Carregosa *et al*., 2021). O óleo extraído foi guardado em frasco âmbar sob refrigeração para ser usado nas etapas posteriores.

Figura 21. Etapas do processo de extração do óleo.

Fonte: Elaborado pelo autor.

1.4.4 Precipitação do asfalteno

Cerca de 300 mg de óleo foi utilizado na precipitação de asfalteno. A amostra de óleo pesada foi adicionada 12 mL de *n*-hexano (grau HPLC), e esta foi levada ao banho ultrassônico por 10 min, seguido por centrifugação. Esse processo foi realizado cinco vezes (Martins *et al.*, 2021). Ao final de cada centrifugação, o sobrenadante (malteno) foi retirado e acondicionado em um balão de fundo redondo. Após realizado este procedimento, o malteno foi roto evaporado e guardado em vial de 4 mL em refrigeração, até sua utilização em etapas futuras (Figura 22).

Figura 22. Fluxograma de precipitação do asfalteno.

Fonte. Elaborado pelo autor.

1.4.5 Cromatografia líquida em coluna

A etapa de Cromatografia líquida em coluna foi realizada em duas etapas (Figura 23). A primeira etapa tem a preparação da amostra e ambientação da coluna com 8 g sílica gel, alumina, sulfato de sódio (1 g) e lã de vidro. Cerca de 40 mg de malteno foi pesado em uma placa de Petri. A esta amostra foram adicionadas algumas gotas de diclorometano (HPLC) e um pouco de alumina para formar uma pasta. Após mistura, o material é deixado para evaporação de todo solvente.

Figura 23. Fluxograma do processo de cromatografia líquida.

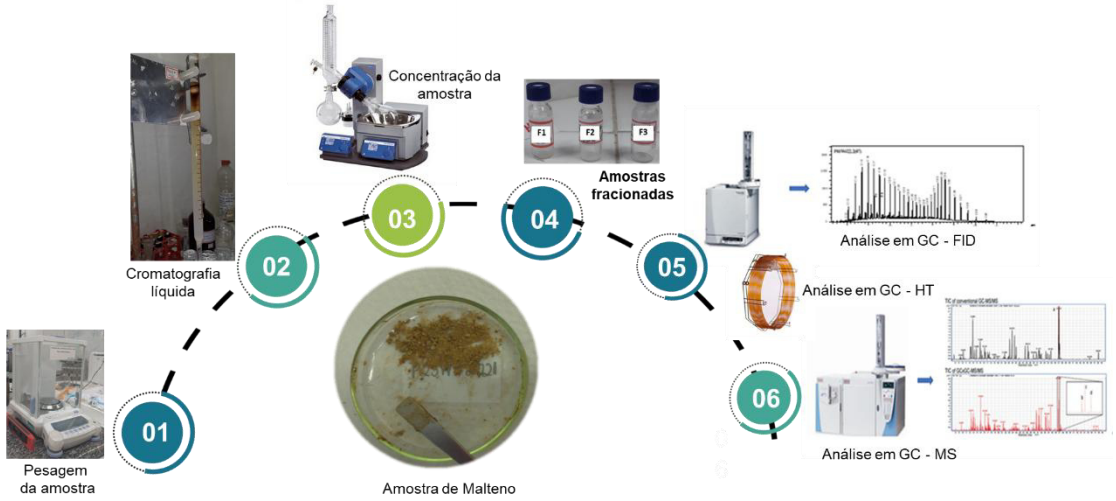

Fonte. Elaborado pelo autor.

Já na etapa 2, após empacotamento da coluna com sílica gel e sulfato de sódio anidro, são realizadas três eluições:

a) Fração de saturados (F1), utilizando 30 mL de *n*-hexano, coletado em um balão de fundo redondo .

b) Fração de aromáticos (F2), utilizando 30 mL de uma mistura de *n*-hexano com diclorometano (8:2), coletado a fração em balão de fundo redondo.

c) Fração de resinas (F3), utilizando 30 mL de uma mistura de diclorometano e metanol (9:1), coletado a fração em balão de fundo redondo.

Após a coleta de cada fração, estas foram levadas ao roto evaporador para remoção dos solventes e concentração das frações. Após roto evaporação, as amostras foram acondicionadas em vial de 2 mL previamente limpo e

guardadas sob refrigeração (Terra *et al*., 2019). Todos os solventes usados têm grau cromatográfico HPLC da Sigma-Aldrich Chemical.

Além da cromatografia líquida para as amostras, também foi realizado o mesmo procedimento para as amostras de branco para todas as frações. O branco foi constituído de todos os reagentes presentes na cromatografia líquida em coluna (sílica gel, alumina, sulfato de sódio anidro). Esse procedimento é importante pois permite avaliar possíveis contaminações durante o preparo e a análise em laboratório das amostras. O branco atuou como controle de qualidade, revelando interferências oriundas de reagentes, materiais ou equipamentos. Esse procedimento assegura a confiabilidade dos resultados, garantindo que os hidrocarbonetos detectados sejam exclusivamente da amostra. Dessa forma, a inclusão do branco fortalece a rastreabilidade e a precisão dos dados obtidos

1.4.6 Cromatografia gasosa com detector de ionização de chama (GC-FID) para análise da fração saturada (F1)

Para análise dos *n*-alcanos e isoprenóides pristano e fitano, a fração saturada foi analisada por cromatografia gasosa com detetor de ionização de chama (GC-FID) da Thermo - Focus GC com coluna capilar Agilent J&W DB-5 (30 m × 0,25 mm i.d. × 0,25 µm df). Utilizou-se nitrogênio como gás de arraste, com um fluxo constante de 1 mL min^{-1}. O forno do GC- FID foi mantido isotermicamente a 50 °C durante 5 min, depois aquecido de 50 a 300 °C a 6 min^{-1}, com a temperatura final mantida durante 17,67 min (tempo total de 63 min.).

A temperatura do injetor foi de 280 ºC e o FID foi regulado para 300 ºC. O volume de injeção da amostra foi de 1 µL, em modo splitless, utilizando *n*-hexano como solvente (grau HPLC). Os *n*-alcanos (*n*C8 a *n*C40) e os isoprenóides (pristano e fitano) foram identificados e quantificados por padronização externa. O padrão analítico foi adquirido à AccuStandard (*Hydrocarbon Window Defining Standard*, DRH-008S-R^2, que é uma mistura de *n*-alcanos e isoprenóides acima referidos).

1.4.7 Cromatografia gasosa acoplada à espectrometria de massas (GC-MS) para análise das frações saturados e biomarcadores (F1 e F2)

Para avaliar os biomarcadores saturados e aromáticos, a fração de malteno foi analisada por cromatografia gasosa/espectrómetro de massa de quadrupolo (GCMS-QP2010 SE, Shimadzu, Japão) com o procedimento realizado com ionização de elétrons (EI) a 70 eV, acoplado a um amostrador automático (AOC-6000 Plus, Shimadzu, Japão). A separação cromatográfica foi efetuada utilizando uma coluna capilar HP-5ms Ultra Inert (30 m × 0,25 mm d.i. × 0,25 µm df; 5%-fenil-metilpolissiloxano). O forno de GC foi aquecido de 70º a 325 °C a uma taxa de 20 °C min^{-1}, mantendo-se a temperatura final durante 10 minutos. O volume de injeção da amostra foi de 1 µL em modo split (1:20).

As temperaturas do injetor, da fonte de íons e da interface foram de 300, 250 e 300 °C, respectivamente. Utilizou-se Hélio como gás de arrastamento a um caudal constante de 1 mL min^{-1}. As amostras foram analisadas nos modos de aquisição de varredura completa e monitoramento de íons selecionados (SIM). No modo SIM, os íons fragmentos *m/z* 83, 85, 191 e 217 foram monitorados para avaliar os compostos saturados alquilciclohexanos, *n*-alcanos/hidrocarbonetos ramificados, terpanos tri e pentacíclicos e esteranos e diasteranos. Os *m/z* 178, 192 e 231 foram monitorizados para avaliar os compostos aromáticos fenantreno e antraceno, metilfenantrenos e metilantraceno, e esteróides triaromáticos (TAS), respetivamente (Carregosa *et al*., 2021). Os dados obtidos após as análises foram processados utilizando o software GC- ES v. 4.20 (SHIMADZU, JAPÃO).

1.4.8. Espectrometria de massas de ressonância ciclotrônica de íons com transformada de Fourier (FT-ICR MS) para avaliação dos compostos polares ácidos

Para avaliar os compostos polares ácidos, o óleo total extraído foi analisado por ESI(-) FT-ICR MS. 10 mg de óleo foram dissolvidos em 10 mL de tolueno. Da solução de reserva para análise ESI(-), 500 µL foram recolhidos e transferidos para um balão contendo 500 µL de metanol com 25 µL (2,5%) de

NH4OH. Os solventes metanol, tolueno e hidróxido de amónio eram de qualidade HPLC adquiridos a J.T. Baker (Phillipsburg, NJ, EUA) e Sigma-Aldrich (Steinheim, Alemanha), respectivamente.

As aquisições de FT-ICR MS foram efetuadas com um SolariX 2xR 7T (Bruker Daltonics - Bremen, Alemanha) acoplado a uma fonte ESI de modo negativo. O gás de secagem utilizado foi o azoto com um caudal de 4,0 L min-1 e uma temperatura de 200 °C e gás de nebulização com 1,0 bar. As amostras foram injetadas utilizando uma bomba de seringa com um caudal de 240 μL h^{-1}. Os íons foram acumulados na célula de colisão durante 0,005 s e transferidos para a célula ICR em 0,6 $^{-1}$ ms. Os espectros foram previamente analisados no LTQ Fleet para verificar a distribuição gaussiana. Foram adquiridos conjuntos de dados 8MW utilizando o modo de magnitude com a gama de deteção *m/z* 150 - 2000. Foi utilizada a detecção 2ω (quadrupolo) para obter uma resolução elevada a uma velocidade de varrimento rápida. Para cada amostra, foram adquiridos 300 exames para obter espectros com excelentes valores de sinal/ruído. Para os dados apodizados, o poder de resolução medido em *m/z* 400 foi de 880 000. Para a aquisição dos espectros de uma amostra, o tempo de aquisição transiente foi de 2,5 segundos. Os dados foram calibrados internamente utilizando uma série homóloga de classe de nitrogênio neutro (N_1) utilizando o software Data Analysis 4.2 (BRUKER DALTONICS GMBH, BREMEN, Alemanha).

Na fase de processamento, as fórmulas moleculares são inicialmente atribuídas a partir dos espectros recalibrados. Para isto, foi utilizado o *software* Composer64 (Versão 1.5.3 Sierra Analytica, Modesto, EUA). Em geral, as condições de processamento foram semelhantes para todas as amostras. No entanto, o limiar de intensidade, a abundância mínima e os novos parâmetros de abundância mínima variaram de acordo com a intensidade do ruído de cada espectro. Estes três parâmetros foram utilizados para definir um limite de abundância relativa, de modo a que apenas fossem atribuídas fórmulas moleculares a sinais de intensidade superior ao limite pré-estabelecido. Os

elementos permitidos foram ^{12}C, ^{1}H, ^{16}O, ^{14}N e ^{32}S. O erro de fórmula máximo permitido foi de 0,5 ppm.

REFERÊNCIAS

ACTER, THAMINA; SON, SEUNGWOO; KIM, DONGHWI; YIM, UN HYUK; BARROW, MARK P.; SHI, Quan; UDDIN, Nizam; KIM, Sunghwan. *Environmental petroleomics – application of ultrahigh-resolution mass spectrometry for molecular-level understanding of the fate of spilled oils*. Trends in Environmental Analytical Chemistry, v. 40, p. e00212, 2023. DOI: 10.1016/j.teac.2023.e0021

AEPPLI, C., C.A. CARMICHAEL, R.K. NELSON, K.L. LEMKAU, W.M. GRAHAM, M.C. REDMOND, D.L. VALENTINE, AND C.M. REDDY. 2012. Oil weathering after the Deepwater Horizon disaster led to the forma-tion of oxygenated residues. Environmental Science & Technology 46(16):8,799–8,807, http://dx.doi.org/10.1021/es3015138.

AGUILERA, F; MÉNDEZ, J; PÁSARO, E; LAFFON, Review on the effects of exposure to spilled oils on human health. Analyticalsciencejournals.onlinelibrary.wiley.com First published: 14 April 2010. https://doi.org/10.1002/jat.1521

ALBAIGÉS, J; BAYONA, J. M. Sources and Fate of Organic Contaminants in the Marine Environment. Marine Organic Matter: Biomarkers, Isotopes and DNA. Chapter First Online:22 December 2005. DOI:10.1007/698_2_010.

ALCOFORADO, A. G. O futuro da energia requerido para o mundo.30 de novembro, 2023. https://www.linkedin.com/pulse/o-futuro-da-energia-requerido-para-mundo-fernando-a-g-alcoforado-diejf/

AQUINO NETO, F. R.; RESTLÉ, A.; CONNAN, J.; ALBRECHT, P.; OURISSON, G., 1982. Novel tricyclic terpanes (C19, C20) in sediments and petroleums. Tetrahedron Lett., v. 23, p. 2027-2030.

ARRUDA, T. R; LEITE, J; BRUNO, R. de C; MARQUES, C. S; BERNARDES, P. C; MAGALHÃES, C. G; PINHEIRO, P. F. Emerging techniques for extraction and characterization of natural compounds. In: GREEN PRODUCTS IN FOOD SAFETY.: Elsevier, 2023. cap. 2, p. 29–79. https://doi.org/10.1016/B978-0-323-95590-4.00009-6

AREY, J. S.; GUSTAFSON, T. L.; RITCHIE, K. et al. Comprehensive two-dimensional gas chromatography of weathered crude oil. *Environmental Science & Technology*, Washington, v. 41, n. 15, p. 5738–5746, 2007. DOI: 10.1021/es070390j.

ARAUJO, E. M; RAMALHO, A. C. W; MELO, P. W. Artisanal fishers, consumers and the environment: immediate consequences of the oil spill in Pernambuco, Northeast Brazil. Cad. Saúde Pública 2020; 36(1):e 00230319. https://doi.org/10.1590/0102-311X00230319

AREKHI, M., TERRY, L.G., JOHN, G.F., CLEMENT, T.P. Environmental fate of petroleum biomarkers in Deepwater Horizon oil spill residues over the past 10 years. Sci. Total Environ. 2021. 791, 148056. https://doi.org/10.1016/j.scitotenv.2021.148056.

AZEVEDO, R.A., BEZERRA, K.M.M., NASCIMENTO, R.F., NELSON, R.K., REDDY, C.M., NASCIMENTO, A.P., OLIVEIRA, A.H.B., MARTINS, L.L.,

BARAKAT, ASSEM O. Computerized GC/MS detection of monoaromatic and triaromatic steroid hydrocarbons in Alamein crude oil. *Journal of High Resolution Chromatography*, v. 17, n. 7, p. 493–496, jul. 1994. https://doi.org/10.1002/jhrc.1240170708

BARKER, C**.** Origin, composition and properties of petroleum. In: Donaldson, Erle C.; Chilingarian, G. V.; YEN, Teh Fu (ed.). *Enhanced oil recovery. I: fundamentals and analysis*. Amsterdam: Elsevier, 1985. (Developments in Petroleum Science, v. 17, pt. A), cap. 2, p. 11–45. https://doi.org/10.1016/S0376-7361(08)70564-8

BÉRGAMO, D.B., SOARES, M.O., CRAVEIRO, N., MAGALHÃES, K.M., ZANARDI-LAMARDO, E., YOGUI, G.T., ROJAS, L.A.V., LIMA, M.C.S., ROSA FILHO, J.S., 2023. Tar balls as afloating substrate for long-distance species dispersal. Mar. Pollut. Bull. 196, 115654. https://doi.org/10.1016/j.marpolbul.2023.11565432.

BEYER, J; TRANNUM, H. C.; BAKKE, T; HODSON, P. V.; COLLIER, T. K. Environmental effects of the Deepwater Horizon oil spill: A review. *Marine Pollution Bulletin*, v. 110, n. 1, p. 28–51, 2016. https://doi.org/10.1016/j.energy.2020.119707

BEHERA, B. K**;** DAS, A**;** SARKAR, D. J**;** WEERA, T , PABUDI**;** P. P. KUMAR**;** DAS, B. K**;** THAVAMANI, P**;** RAMANATHAN, R**;** BANSAL, V. Polycyclic aromatic hydrocarbons (PAHs) in inland aquatic ecosystems: Perils and remedies through biosensors and bioremediation. *Environmental Pollution*, v. 241, p. 212–233, out. 2018. https://doi.org/10.1016/j.envpol.2018.05.016

BI, H**;** AN, C**;** OWENS, E**;** LEE, K**;** CHEN, Z**;** MULLIGAN, C**;** TAYLOR, E**;** BOUFADEL, MICHEL. A framework for the evaluation and selection of shoreline surface washing agents in oil spill response. *Journal of Environmental Management*, v. 287, p. 112346, 1 jun. 2021. https://doi.org/10.1016/j.jenvman.2021.112346

BLUMER, M., EHRHARDT AND JONE, J.H., 1973. The environmental assessments fate of Stranded crude oil. Deep-sea Res. 20, 239-259. https://doi.org/10.1016/0011-7471(73)90014-4.

BOURBONNIERE, R.A., MEYERS, P.A. Sedimentary geolipid records of historical changes in the watersheds and productivities of Lakes Ontario and Erie. Limnol.Oceanogr .1996. 41, 352–359. https://doi.org/10.4319/lo.1996.41.2.0352.

BONTEMPO FILHO, Eduardo B.; COUTINHO, Roberto Q.; BARBOSA, José Antonio; BARCELLOS, Roberto L.; GIACHETI, Heraldo Luiz; RAMOS, Germano Mário S. Temporal monitoring of contamination in three sandy beaches from the 2019 oil spill near Cabo de Santo Agostinho, Northeastern Brazil. *Journal of Coastal Research*, [S.l.], v. 95, p. 697–701, 2020. DOI: 10.2112/SI95-136.1.

BUTLER, J.N., Wells, P.G., Johson, S., Manock, J.J. Beach tar on bermuda: Recent observations and implications for global monitoring. Mar. Pollut. Bull. 1998. 36, 458-463. https://doi.org/10.1016/S0025-326X(98)00005-8.

BARROW, M. P.; MCDONNELL, L. A.; FENG, X; WALKER, J; DERRICK, P. J. Determination of the nature of naphthenic acids present in crude oils using nanospray Fourier transform ion cyclotron resonance mass spectrometry: the continued battle against corrosion. Analytical Chemistry, v. 75, n. 4, p. 860–866, 2003. https://doi.org/10.1021/ac020388b

BRUM, H, D; CAMPOS-SILVA, J, V; OLIVEIRA, E, G. Brazil oil spill response: Government inaction. SCIENCE**,** 10 Jan 2020. Vol 367, Issue 6474 pp.155-156. DOI: 10.1126/science.aba0369

BRANDÃO, A. C.; MACHADO, K. S.; COSTA, L. M. et al. Composição geoquímica dos resíduos oleosos coletados no litoral do Brasil em 2019: evidências da origem do petróleo. *Brazilian Journal of Geochemistry*, v. 38, n. 4, p. 1–14, 2021. DOI: 10.21715/bjgeo.v38.4.1.

CAVALCANTE, R.M., 2022. Is there a similarity between the 2019 and 2022 oil spills that occurred on the coast of Ceará (Northeast Brazil)? An analysis based on forensic environmental geochemistry. Environ. Pollut. 315, 120283. https://doi.org/10.1016/j.envpol.2022.120283.

CAVALCANTE, R. M.; LIMA, A. D. F.; SOUZA, A. D. M.; ALKIMIN, G. D.; SANTANA, L. M. B. M.; MELLO, L. C.; SOARES, M. O. Oil spill impacts on marine food webs: lessons from contamination in tropical coasts. In: Baird, Daniel; Elliott, Michael (org.). Treatise on estuarine and coastal science. 2. ed. Oxford: Elsevier, 2024. v. 4, p. 706–734. http://dx.doi.org/10.1016/B978-0-323-90798-9.00071-8

CAVALCANTE, R. (org.). *Contaminantes orgânicos em ambientes aquáticos* [livro eletrônico]. Fortaleza: Imprensa Universitária, 2020. Il. color. PDF. (Coleção de Estudos da Pós-Graduação).

CABALLERO, GONZALO; SOTO-OÑATE, David. Environmental crime and judicial rectification of the Prestige oil spill: the polluter pays. *Marine Policy*, v. 84, p. 213–219, 2017. DOI: https://doi.org/10.1016/j.marpol.2017.07.012.

CARREGOSA, J.C., SANTOS, I.R.D., DE SÁ, M.S., SANTOS, J.M., WISNIEWSKI, A., 2021. Multiple reaction monitoring tool applied in the geochemical investigation of a mysterious oil spill in northeast Brazil. An. Acad. Bras. Cienc. 93, 1–20. https://doi.org/10.1590/0001-376520212021017.

CEN, 2012. European Committee for Standardisation (CEN) (2012) CEN/TR 15522–2:2012: Oil Spill Identification. Waterborne Petroleum and Petroleum Products. Part 2: Analytical Methodology and Interpretation of Results Based on GCFID and GC-MS Low Resolution Analyses. CEN, Brussels

COCCARO, G, M. Avaliação geoquímica molecular de petróleos brasileiros aplicada no setor petrolífero e em estudos forenses. Trabalho de conclusão de curso, UFRJ, 2023.

CONNAN, J., BOUROULLEC, J., DESSORT, D., ALBRECHT, P. “The microbial input in carbonate-anhydrite facies of a sabkha palaeoenvironment from Guatemala: a molecular approach”, Organic Geochemistry, 1986. v.10, pp. 29-50. https://doi.org/10.1016/0146-6380(86)90007-0.

CORILO, YURI E.; PODGORSKI, DAVID C.; MCKENNA, AMY M.; LEMKAU, KARIN L.; REDDY, CHRISTOPHER M.; MARSHALL, ALAN G.; RODGERS, RYAN P. Oil spill source identification by principal component analysis of electrospray ionization Fourier transform ion cyclotron resonance mass spectra. *Environmental Science & Technology*, [S.l.], v. 47, n. 10, p. 5064–5071, 2013. DOI: 10.1021/es4008716.

CHEN, J; ZHANG, W; WAN, Z; LI, S; HUNG, T; FEI, Y. Oil spills from global tankers: Status review and future governance. J. Chen et al. / Journal of Cleaner Production 227 ,2019, 20 e32. https://doi.org/10.1016/j.jclepro.2019.04.020.

CHENG, B., LIU, H., CAO, Z., WU, X., AND CHEN, Z. (2020). Origin of deep oil accumulations in carbonate reservoirs within the north tarim basin: Insights from molecular and isotopic compositions. Org. Geochem. 39, 103931. doi:10.1016/j. orggeochem.2019.103931. https://doi.org/10.1016/j.orggeochem.2019.103931
CHRISTENSEN, J. H.; TOMASI, G.; STOUT, S. A. Chemical fingerprinting of petroleum biomarkers in assessing weathering and source correlation of crude oil residues. *Environmental Forensics*, v. 5, n. 4, p. 293–305, 2004. DOI: 10.1080/15275920490500613.

CHICARELLI, M. I.; AQUINO NETO, F. R.; ALBRECHT, P**.** Occurrence of four stereoisomeric tricyclic terpane series in immature Brazilian shales. *Geochimica et Cosmochimica Acta*, v. 52, n. 8, p. 1955–1959, ago. 1988. https://doi.org/10.1016/0016-7037(88)90176-7

CETESB – COMPANHIA AMBIENTAL DO ESTADO DE SÃO PAULO**.** *Breve história do petróleo no Brasil e em São Paulo e principais acidentes*. São Paulo: CETESB, 2005. Disponível em: https://cetesb.sp.gov.br/emergencias-quimicas/wp-content/uploads/sites/22/2013/12/Principais-Acidentes-Brasil-.pdf. Acesso em: 12 abr. 2025.

CHEN, H., MCKENNA, A.M., NILES, S.F., FRYE, J.W., GLATTKE, T.J., RODGERS, R.P., 2022. Time-dependent molecular progression and acute toxicity of oil-soluble, interfacially- active, and water-soluble species reveals their rapid formation in the photodegradation of Macondo Well Oil. Sci. Total Environ. 813, 151884. https://doi.org/10.1016/j.scitotenv.2021.151884

CHEN, H., HOU, A., CORILO, Y.E., LIN, Q., LU, J., MENDELSSOHN, I.A., ZHANG, R., RODGERS, R.P., MCKENNA, A.M. 4 years after the Deepwater Horizon spill: molecular transformation of Macondo Well oil in Louisiana salt marsh sediments revealed by FT-ICR mass spectrometry, 2016. Environ. Sci. Technol. 50, 9061-9069. https://doi.org/10.1021/acs.est.6b0115633.

CORILO, Y.E., PODGORSKI, D.C., MCKENNA, A.M., LEMKAU, K L., REDDY, C.M., MARSHALL, A.G., RODGERS, R.P. Oil spill source identification by principal component analysis of electrospray ionization Fourier transform ion cyclotron resonance mass spectra. 2013. Anal. Chem. 85, 9064-9069. https://doi.org/10.1021/ac401604u.

CORRICK, A.J., HALL, P.A., TREFRY, C., MCKIRDY, D.M., ROSS, S.G.A.S. The natural hydrocarbon loading of the South Australian coastline .2021. Mar. Pollut. Bull. 166, 112198. https://doi.org/10.1016/j.marpolbul.2021.112198

CORRÊA, Antônia M.; CAMPOS, Felipe F.; TENÓRIO, Marcus F.; RODRIGUES, Alice M. S.; PÉREZ, Carlos D.; THOMPSON, Fabiano; BATISTA, Andressa S.; GATTS, Pedro V.; DE REZENDE, Carlos E.; LEAL, Kátia Z.; BERNARDES, Marcelo C. Hydrocarbon composition of oils spilt on the Brazilian coast in 2019 and 2022. *Marine Pollution Bulletin*, v. 207, art. no. 116821, 2024. DOI: https://doi.org/10.1016/j.marpolbul.2024.116821

COLLINS, J. A.; CARR, A. S.; SCHEFU, E; BOOM, A; SEALY, J. Investigation of organic matter and biomarkers from Diepkloof Rock Shelter, South Africa: insights into Middle Stone Age site usage and palaeoclimate. *Journal of Archaeological Science*, v. 85, p. 51–65, set. 2017. DOI: https://doi.org/10.1016/j.jas.2017.07.003.

DALMASCHIO, G. P.; MALACARNE, M.M.; ALMEIDA, V. M. D. L. DE; PEREIRA, T. M. C.; GOMES, A. O.; CASTRO, E. V. R. DE; GRECO, S. J.; VAZ, B. G.; ROMÃO, W. Characterization of polar compounds in a true boiling point distillation system using electrospray ionization FT-ICR mass spectrometry. Fuel, v. 115, p. 190–202, Jan. 2014. https://doi.org/10.1016/j.fuel.2013.07.008

DE MOURA, NÁJLA VILAR AIRES; DE CARVALHO JÚNIOR, Osmar Abílio. Gestão ambiental de vazamentos de óleo no mar territorial brasileiro e o uso do sensoriamento remoto. *Espaço Aberto*, Rio de Janeiro, v. 13, n. 2, p. 85–100, set. 2023. DOI: 10.36403/espacoaberto.2023.57435. Disponível em: https://revistas.ufrj.br/index.php/EspacoAberto/article/view/57435.

DIDYK, B.M., SIMONEIT, B.R.T., BRASSELL, S.C., EGLINTON, G. Organic geochemical indicators of palaeoenvironmental conditions of sedimentation. Nature 272, 216–22, 1978. https://doi.org/10.1038/272216a0.

DIÁRIO DO NORDESTE**.** *Manchas de óleo voltam a aparecer na Praia do Futuro e mais 9 locais do Ceará*. Fortaleza, 24 set. 2022. Disponível em: https://diariodonordeste.verdesmares.com.br/ceara/manchas-de-oleo-voltam-a-aparecer-na-praia-do-futuro-e-mais-9-locais-do-ceara-veja-lista-1.3281775. Acesso em: 12 abr. 2025.

DOUGLAS, G. S.; STOUT, S. A.; UHLER, A. D.; MCCARTHY, K. J.; EMSBO-MATTINGLY, STEPHEN. D. Advantages of quantitative chemical fingerprinting in oil spill identification and allocation of mixed hydrocarbon contaminants. In: FINGAS, Mervin (ed.). *Standard Handbook Oil Spill Environmental Forensics: Fingerprinting and Source Identification*. 2. ed: Elsevier, 2016. cap. 17, p. 789–847. https://doi.org/10.1016/B978-0-12-803832-1.00017-9

DONG, YANZHU; LIU, YONGXUE; HU, CHUANMIN; MACDONALD, IAN R.; LU, YINGCHENG. Chronic oiling in global oceans. *Science*, Washington, DC, v. 376, n. 6599, p. 1300–1304, 2022. DOI: https://doi.org/10.1126/science.abm5940.

ESCOBAR, H. Mystery oil spill threatens marine sanctuary in Brazil. *Science*, Washington, v. 366, n. 6466, p. 672, 8 nov. 2019. https://doi.org/10.1126/science.366.6466.672

EDWARDS, D.S., MCKIRDY, D.M., ROWLAND, S.J., HEATH, D.J., GRAY, P.S. Waxy bitumen stranding in southern Australia: A geochemical study of multiple oil families and their likely origins, 2018. Org. Geochem. 118, 132-151. https://doi.org/10.1016/j.orggeochem.2017.12.010

EMBRAPA – EMPRESA BRASILEIRA DE PESQUISA AGROPECUÁRIA. *Manual de conservação de solos e água para o Estado do Pará*. Belém, PA: EMBRAPA Amazônia Oriental, 2009.

EMBRAPA- Passo a passo para o uso do cromatógrafo gasoso modelo GC-CP3800 Varian para análises de gases de efeito estufa (GEEs). Belém, PA: Embrapa Amazônia Oriental, 2014. 68 p. (Documentos / Embrapa Amazônia Oriental, ISSN 1983-0513; 403). Disponível em: https://www.infoteca.cnptia.embrapa.br/bitstream/doc/986671/1/DOC403.pdf. Acesso em: 13 abr. 2025.

EUZÉBIO, C. S.; RANGEL, G. S.; MARQUE, S. R. C. Derramamento de petróleo e seus impactos no ambiente e na saúde humana. *Revista Brasileira de Ciências (2019)* 947820190472

EMSBO-MATTINGLY, STEPHEN D., ERIC LITMAN. Polycyclic aromatic hydrocarbon homolog and isomer fingerprinting. Standard handbook oil spill environmental forensics. Academic Press, 2016. 255-312. https://doi.org/10.1016/B978-0-12- 803832-1.00005-2. G1, 2022.

FREITAS, MARIANA SANTOS FIGUEIREDO DE; MARTINS, ADRIELLE BEATRICE DO Ó; FERNANDES, GABRIELA ANDRADE SOUZA; COMBI, TATIANE. Mysterious oil spill in Brazil (2019–2020): what lessons can we learn from previous events? In**:** RIO OIL & GAS EXPO AND CONFERENCE**,** 2022, Rio de Janeiro. *Anais eletrônicos.* Rio de Janeiro: Instituto Brasileiro de Petróleo e Gás, 2022. ISSN 2525-7579. Disponível em: https://www.ibp.org.br/publicacoes/mysterious-oil-spill-in-brazil-2019-2020-what-lessons-can-we-learn-from-previous-events/.

FEITOSA, ALICE F. ; MENEZES, ÍCARO B.H.M.P. ; DUARTE, OSCAR S. ; S'B' SALMITO-VANDERLEY, CARMINDA ; CARNEIRO, PEDRO B.M. ; AZEVEDO, RUFINO N.A. ; OLIVEIRA, ANDRÉ H.B. ; LUZ, ANA C.S. ;NASCIMENTO, ADRIANA P. ; NASCIMENTO, RONALDO F. ; MARTINS, LAERCIO L. ; CAVALCANTE, RIVELINO M. ; FEITOSA, CAROLINE V. . The impact of chronic and acute problems on sea turtles: The consequences of the oil spill and ingestion of anthropogenic debris on the tropical semi-arid coast of Ceará, Brazil. AQUATIC TOXICOLOGY, v. 269, p. 106867, 2024. http://dx.doi.org/10.1016/j.aquatox.2024.106867

FILEWOOD, T; KWOK, H; BRUNSWICK, P; YAN, J; OLLINIK, J. E.; COTE, C; KIM, M; AGGELEN, GV; HELBING, C. C.; SHANG, D**.** Investigating the fate of polycyclic aromatic sulfur heterocycle compounds in spilled oils with a microcosm weathering experiment. *Environmental Systems Research*, v. 11, n. 6, 2022. https://doi.org/10.1186/s40068-022-00252-w

FURIMSKY, E; MASSOTH, F, E. *Hydrodenitrogenation of Petroleum*. Catalysis Reviews – Science and Engineering, v. 47, n. 3, p. 297–489, 2005. DOI: https://doi.org/10.1081/CR-200057492.

FRYSINGER, G. S.; GAINES, R. B.; XU, L; REDDY, C. M**.** Resolving the unresolved complex mixture in petroleum-contaminated sediments. *Environmental Science & Technology*, v. 37, n. 8, p. 1653–1662, 12 mar. 2003. https://doi.org/10.1021/es026379p

GALLOTTA, F. D.C. Avaliação dos níveis de concentração e identificação de fontes de hidrocarbonetos na Bacia do Alto Iguaçu: estudo de caso pós derrame acidental de óleo na Refinaria Presidente Getúlio Vargas*. 2006. 140 f. Tese* (Doutorado em Geociências – Geoquímica) – Instituto de Química, Universidade Federal Fluminense, Niterói, 2014.

GALIERIKOVÁ, A; MATERNA, M. World seaborne trade with oil: one of main cause for oil spills? *Transportation Research Procedia*, v. 44, p. 297–304, 2020. DOI: https://doi.org/10.1016/j.trpro.2020.02.039.

G1, 2022. https://g1.globo.com/pe/pernambuco/noticia/2022/10/06/sobe-quantidade-de-bolotas-de-oleo-recolhidas-em-praias-do-litoral-de-pernambuco.ghtml

GUO, W; HE, M; YANG, Z; LIN, C; QUAN, X**.** Characteristics of petroleum hydrocarbons in surficial sediments from the Songhuajiang River (China): spatial and temporal trends. *Environmental Monitoring and Assessment*, v. 179, n. 1–4, p. 81–92, ago. 2011. https://doi.org/10.1007/s10661-010-1720-0

GOUGH, M. A.; ROWLAND, S. J. Characterization of unresolved complex mixtures of hydrocarbons in petroleum. *Nature*, Londres, v. 344, p. 648–650, 12 abr. 1990. https://doi.org/10.1038/344648a0.

GRUBER, L. D. A; DAMASCENO, F. C; CARAMÃO, E. B; JACQUES, R. A. A; GELLER, A M; CAMPOS, M. C. V. Ácidos naftênicos no petróleo. Química Nova, v. 35, n. 7, p. 1423-1433, 2012. https://doi.org/10.1590/S0100-40422012000700025

GROB R. L.; BARRY, E. F**.** *Modern Practice of Gas Chromatography*. 4. ed. Hoboken: John Wiley & Sons, 2004. 896 p.

HALL, G. J.; WANG, Z.; LI, K. et al. Petroleum fingerprinting of Macondo well oil in marine environments. *Marine Pollution Bulletin*, v. 73, n. 1, p. 245–258, 2013. DOI: 10.1016/j.marpolbul.2013.05.028.

HAN, Y; NAMBI, I. M.; CLEMENT, T. P**.** Environmental impacts of the Chennai oil spill accident – A case study. *Science of the Total Environment*, Oxford, v. 626, p. 795–806, 2018. https://doi.org/10.1016/j.scitotenv.2018.01.128

HARRIS, D, C. Quantitative Chemical Analysis, Editora:W.H. Freeman and Company, 2010.

HAGE, D. S.; CARR, J. D. *Química analítica e análise quantitativa*. São Paulo: Pearson, 2012.

HAKIMI, M.H., KUMAR, A., SINGH, A.K., LASHIN, A., RAHIM, A., VARFOLOMEEV, M.A., YELWA, N.A., MUSTAPHA, K.A., 2023. Geochemistry and organic petrology of the bituminite shales from the Kapurdi mine, Rajasthan of NW India: implications for 34 waxy oil generation potential. J. Pet. Explor. Prod. Technol. 13, 505–521. https://doi.org/10.1007/s13202-022-01597-9

HEGAZI, H, A., ANDERSSON, T, J., ABU-ELGHEIT, A, M., EL-GAYAR, M.SH., 2004. Sourcediagnostic and weathering indicators of tar balls utilizing acyclic, polycyclic and Sheterocyclic components. Chemosphere 55, 1053–1065. https://doi.org/10.1016/j.chemosphere.2004.01.019

HEIDARI, H.; AKBARI, M.; SOUHANKAR, A.; HAFEZI, R. Review of global energy trends towards 2040 and recommendations for Iran oil and gas sector. International Journal of Environmental Science and Technology, v. 19, n. 8, p. 8007–8018, 2022. Disponível em: https://doi.org/10.1007/s13762-022-03963-w

HOLBA, A.G., TEGELAAR, E., ELLIS, L., SINGLETARY, M.S., ALBRECHT, P., 2000. Tetracyclic polyprenoids: indicators of freshwater (lacustrine) algal input. Geology 28, 251–254. https://doi.org/10.1130/0091-7613(2000)28<251:TPIOFL>2.0.CO;2

HOFFMANN, E. DE; STROOBANT, V**.** *Mass spectrometry: principles and applications*. 3. ed. Chichester: John Wiley & Sons, 2007.

HUBA, ANNA KATARINA; GARDINALI, PIERO R. Characterization of a crude oil weathering series by ultrahigh-resolution mass spectrometry using multiple ionization modes. *Science of the Total Environment*, [s.l.], v. 563–564, p. 600–610, set. 2016. DOI: 10.1016/j.scitotenv.2016.03.233 .

HUANG, W.-Y., MEINSCHEIN, W.G., 1979. Sterols as ecological indicators. Geochim. Cosmochim. Acta 43, 739-745. https://doi.org/10.1016/0016-7037(79)90257-6

HUNT, J, M; PHILP, R. P; KVENVOLDEN, K, A. Early developments in petroleum geochemistry. Organic Geochemistry. Volume 33, Issue 9, September 2002, Pages 1025-1052. https://doi.org/10.1016/S0146-6380(02)00056-6

HUBA, A.K., GARDINALI, P.R. Characterization of a crude oil weathering series by ultrahigh-resolution mass spectrometry using multiple ionization modes, 2016. Sci. Total Environ. 563, 600-610. https://doi.org/10.1016/j.scitotenv.2016.03.233

HYUN, B.; LEE, H.; CHANG, Y. S. *Source identification and weathering evaluation of crude oil in contaminated soils using GC–FID and GC–MS. Chemosphere*, Oxford, v. 200, p. 607–615, 2018. DOI: 10.1016/j.chemosphere.2018.02.120. Acesso em: 21 jun. 2025.

IBAMA**.** Desmobilização das ações de resposta ao incidente de poluição por óleo nas praias do Brasil: cartilha informativa. Brasília: IBAMA, 2020. Disponível em: https://www.ibama.gov.br/phocadownload/emergenciasambientais/2020/manchasdeoleo/ibama-manchasdeoleo-desmobilizacao-cartilha_v2.pdf. Acesso em: 12 abr. 2025.

IBAMA. *Sobre as manchas de óleo*. Brasília, 2022. Disponível em: https://www.gov.br/ibama/pt-br/assuntos/fiscalizacao-e-protecao-

ambiental/emergencias-ambientais/manchasdeoleo/sobre/sobre. Acesso em: 12 abr. 2025.

ITOPF. *Estatísticas de derramamento de petroleiros em 2024*. Disponível em: https://www.itopf.org/knowledge-resources/data-statistics/oil-tanker-spill-statistics-2024/.

KAMYK, J; KOT-NIEWIADOMSKA, A; GALOS, K**.** The criticality of crude oil for energy security: A case of Poland. *Energy*, Oxford, v. 220, p. 119707, 2021. Disponível em: https://doi.org/10.1016/j.energy.2020.119707.

KAPLAN, I.R., GALPERIN, Y., LU, S.-T., LEE, R.-P., 1997. Forensic environmental geochemistry: differentiation of fuel-types, their sources and release time. Org. Geochem. 27, 289-317. https://doi.org/10.1016/S0146-6380(97)87941-7.

KAPLAN, ISAAC; LU, SHAN-TAN; LEE, RU-PO; WARRICK, GREG. Polycyclic hydrocarbon biomarkers confirm selective incorporation of petroleum in soil and kangaroo rat liver samples near an oil well blowout site in the western San Joaquin Valley, California. *Environmental Toxicology and Chemistry*, v. 15, n. 5, p. 696–707, mai 1996. DOI: https://doi.org/10.1002/etc.5620150513.

KERAMEA, P**;** SPANOUDAKI, K**;** ZODIATIS, G**;** GIKAS, G**;** SYLAIOS, G**.** Oil spill modeling: a critical review on current trends, perspectives, and challenges. *Journal of Marine Science and Engineering*, v. 9, n. 2, p. 181, 2021. https://doi.org/10.3390/jmse9020181

KIM, S., STANFORD, L.A., RODGERS, R.P., MARSHALL, A.G., WALTERS, C.C., QIAN, K., WENGER L.M, MANKIEWICZ, P., 2005. Microbial alteration of the acidic and neutral polar NSO compounds revealed by Fourier transform ion cyclotron resonance mass 35 spectrometry. Org. Geochem. 36, 1117-1134. https://doi.org/10.1016/j.orggeochem.2005.03.010.

KRAJEWSKI, L.C., LOBODIN, V.V., JOHANSEN, C., BARTGES, T.E., MAKSIMOVA, E.V., MACDONALD, I.R., MARSHALL, A.G., 2018. Linking natural oil seeps from the Gulf of Mexico to their origin by use of Fourier transform ion cyclotron resonance mass spectrometry. Environ. Sci. Technol. 52, 1365-1374 https://doi.org/10.1021/acs.est.7b04445

KVENVOLDEN, K.A., COOPER, C.K., 2003. Natural seepage of crude oil into marine environment. *Geo-Marine Letters*, v. 23, p. 140–146, 2003. https://doi.org/10.1007/s00367-003-0135-0

KRUGE, M. A.; HUBERT, J. F.; AKES, R. J.; MERINEY, P. E., 1990. Biological markers in Lower Jurassic synrift lacustrine black shales, Hartford basin, Connecticut, U.S.A. Org. Geochem, v. 15, p. 281-289.

LIMA, B.D., MARTINS, L.L., PEREIRA, V.B., FRANCO, D.M.M., SANTOS, I.R., SANTOS, J.M., VAZ, B.G., AZEVEDO, D.A., CRUZ, G.F., 2023. Weathering impacts on petroleum biomarker, aromatic, and polar compounds in the spilled oil at the northeast coast of Brazil over time. Mar. Pollut. Bull. 189, 114744. https://doi.org/10.1016/j.marpolbul.2023.114744

LIMA, B.D., MARTINS, L.L., SOUZA, E.S., PUDENZI, M.A., DA CRUZ, G.F., 2021.Monitoring Chemical compositional changes of simulated spilled Brazilian oils under tropical climate conditions by multiple analytical techniques. Mar. Pollut. Bull. 164, 111985. https://doi.org/10.1016/j.marpolbul.2021.111985.

LIMA, B.D., MARTINS, L.L., SANTOS, L.C., SOUZA, E.S., PUDENZI, M.A., NASCIMENTO, H.L., EBERLIN, M.N., CRUZ, G.F., 2020. Geochemical Investigation of Tar Balls Collected in a Brazilian Beach Using Biomarkers, Ni/V, δ13C Ratios and Ultra-High Resolution FT-ICR Mass Spectrometry. J. Braz. Chem. Soc. 31, 673-682.https://doi.org/10.21577/0103-5053.2019023136.

LOURENÇO, R.A., COMBI, T., ALEXANDRE, M.R., SASAKI, S.T., ZANARDI-LAMARDO, E., YOGUI, G.T., 2020. Mysterious oil spill along Brazil's northeast and southeast seaboard (2019–2020): Trying to find answers and filling data gaps. Mar. Pollut. Bull. 156, 111219. https://doi.org/10.1016/j.marpolbul.2020.111219

LOOIJ, V F.; LAAN, D, V. D.; P.; STORK, W. H. J.; DICAMILLO, D. J.; SWAIN, J. K *parameters in deep hydrodesulfurization of diesel fuel*. Applied Catalysis A: General, v. 170, n. 1, p. 1–12, 25 maio 1998. https://doi.org/10.1016/S0926-860X(98)00028-3

LORENZ, AMA. Ocean oil spills and their impact. *FairPlanet*, 17 jun. 2020. Disponível em: https://www.fairplanet.org/story/ocean-oil-spills-and-its-impact/

LU, S. T., AND KAPLAN, I. R. 1992. Diterpanes, triterpanes, steranes, and aromatic hydrocarbons in natural bitumens and pyrolysates from different humic coal. Geochimica et Cosmochimica Acta 5: 2761–2788.

MAGALHÃES, KARINE MATOS; CARREIRA, RENATO SILVA; ROSA FILHO, JOSÉ SOUTO; ROCHA, PEDRO PALMEIRA; SANTANA, FRANCISCO MARCANTE; YOGUI, GILVAN TAKESHI. Polycyclic aromatic hydrocarbons (PAHs) in fishery resources affected by the 2019 oil spill in Brazil: short-term environmental health and seafood safety. *Marine Pollution Bulletin*, v. 175, art. no. 113334, 2022. DOI: https://doi.org/10.1016/j.marpolbul.2022.113334.

MARTINS, L.L.; PEREIRA, V.B.; NASCIMENTO, A.P.; AZEVEDO, R.N.A.; OLIVEIRA, A.H.; TEIXEIRA, C.E.P.; AZEVEDO, D.A.; DA CRUZ, G.F.; CAVALCANTE, R.M.; GIARRIZZO, T. Forensic Geochemistry Reveals International Ship Dumping as a Source of New Oil Spill in Brazil's Coastline (Bahia) in Late 2023. *Environmental Science & Technology*. 2024, 58, 21, 9328–9338. https://doi.org/10.1021/acs.est.4c01520

MARTINS, L.L., SCHULZ, H.-M., NOAH, M., POTZ, S., RIBEIRO, H.J.P.S., CRUZ, G.F., 2021. New paleoenvironmental proxies for the Irati black shales (Paraná Basin, Brazil) based on acidic NSO compounds revealed by ultra-high resolution mass spectrometry. Org. Geochem. 151, 104152. https://doi.org/10.1016/j.orggeochem.2020.104152.

MARTINS, L.L., CRUZ, G.F.D., SANTOS, L.C., PUDENZI, M.A., EBERLIN, M.N., 2019. Avaliação da extensão da biodegradação de petróleos brasileiros com ênfase nos *n*- alquilciclohexanos. Quim. Nova 42, 289-295. https://doi.org/10.21577/0100- 4042.20170328.

MARTINS, L.L., PUDENZI, M.A., DA CRUZ, G.F., NASCIMENTO, H.D., EBERLIN, M. N., 2017. Assessing biodegradation of Brazilian crude oils via characteristic profiles of O_1 and O_2 compound classes: petroleomics by negative-ion mode electrospray ionization Fourier transform ion cyclotron resonance mass spectrometry. Energy Fuel 31, 6649- 6657. https://doi.org/10.1021/acs.energyfuels.7b00109.

MARTINS, L, L. SOUZA, E, S; CRUZ, G, F. Terpanos pentacíclicos como indicadores de heterogeneidades composicionais em reservatório de petróleo biodegradado. Quim. Nova, Vol. 37, No. 8, 1263-1268, 2014. https://doi.org/10.5935/0100-4042.20140222

MARSHALL, A. G.; RODGERS, R.P. Petroleomics : Chemistry of the underworld. Procedings of the Nacional Academy of Sciences, v. 105, n. 47, p. 18090–19095, 2008. https://doi.org/10.1073/pnas.0805069105

MACKENZIE, A. S.; HOFFMANN, C. F.; MAXWELL, J. R. Molecular parameters of maturation in the Toarcian shales, Paris Basin, France—III. Changes in aromatic steroid hydrocarbons. *Geochimica et Cosmochimica Acta*, v. 45, n. 8, p. 1345-1355, ago. 1981. https://doi.org/10.1016/0016-7037(81)90227-1

MACKAY, D; MCAULIFFE, C. D. Fate of hydrocarbons discharged at sea. *Oil and Chemical Pollution*, v. 5, n. 1, p. 1–20, 1989. DOI: https://doi.org/10.1016/S0269-8579(89)80002-6.

MAKI, H.; SASAKI, T.; HARAYAMA, S. Photo-oxidation of biodegraded crude oil and toxicity of the photo-oxidized products. *Chemosphere*, [S.l.], v. 44, n. 5, p. 1145–1151, 2001. DOI: 10.1016/S0045-6535(00)00287-1.

MCKENNA, A. M.; NELSON, R.; REDDY, C. M.; SAVORY, J. J.; KAISER, N. K.; FITZSIMMONS, J. E.; MARSHALL, A. G.; RODGERS, R. P. Expansion of the analytical window for oil spill characterization by ultrahigh resolution mass spectrometry: beyond gas chromatography. Analytical Chemistry, Washington, v. 86, n. 6, p. 2013, Environmental Science & Technology, № 13, p.7530-

7539. Publisher: American Chemical Society (ACS). https://doi.org/10.1021/es305284t

MELLO, L.C., NASCIMENTO, A.P., LOPES, B.D., LIMA, A.D.F., BEZERRA, L.E.A., MENDES, L.F., BASTOS, L.M., NOSSOLD, A.B.S., MARTINS, M.M., MARTINS, L.L., CAVALCANTE, R.M., 2023. Tarballs on the Brazilian coast in late 2022 sustain Lepas anatifera Linnaeus, 1758 (Crustacea: Cirripedia): Occurrence and risk of petroleum hydrocarbon ingestion. Sci. Total Environ. 896, 164981. https://doi.org/10.1016/j.scitotenv.2023.164981.

MELLO, M.R., TELNAES, N., GAGLIANONE, P.C., CHICARELLI, M.I., BRASSELL, S.C., MAXWELL, J.R., 1988. Organic geochemical characterization of depositional palaeoenvironments of source rocks and oils in Brazilian marginal basins. Org. Geochem. 13, 31–45. https://doi.org/10.1016/B978-0-08-037236-5.50009-9.

MENICONI, M. F. G; G, I. T; C, M. E. ROCHA; B, S. M; S, GILSON, C; MASSONE, C. G. Brazilian oil spills chemical characterization: case studies. *Journal of the Brazilian Chemical Society*, [S.l.], v. 21, n. 2, p. 303–321, 2010. Disponível em: https://doi.org/10.1590/S0103-50532010000200026.

MOLDOWAN, J. Michael; LEE, Cathy Y.; WATT, David S.; JEGANATHAN, Alwarsamy; SLOUGUI, Nacer-Eddine; GALLEGOS, Emilio J. Analysis and occurrence of C₂₆-steranes in petroleum and source rocks. *Geochimica et Cosmochimica Acta*, [S.l.], v. 55, n. 4, p. 1065–1081, abr. 1991. DOI: https://doi.org/10.1016/0016-7037(91)90164-Z

MOLDOWAN, J. MICHAEL; FAGO, FREDERICK J. Structure and significance of a novel rearranged monoaromatic steroid hydrocarbon in petroleum. *Geochimica et Cosmochimica Acta*, v. 50, n. 3, p. 343–351, mar. 1986. DOI: https://doi.org/10.1016/0016-7037(86)90188-2.

NASCIMENTO, A. P.; AZEVEDO, R. N. A.; PEREIRA, M. G. A.; FRANCO, D. M. M.; VAZ, B, G.; OLIVEIRA, A. H. B.; SANTOS, J. M.; CAVALCANTE, R. M.; MARTINS, LAERCIO. L. Forensic environmental geochemistry to reveal the extent, characteristics, and fate of waxy tarballs spilled over the northeast coast of Brazil in 2022. *Marine Environmental Research*, v. 204, p. 105, fev. 2025. DOI: 10.1016/j.marenvres.2024.106105. Disponível em: https://www.sciencedirect.com/science/article/pii/S0141113624005397

NASCIMENTO, A.P., AZEVEDO, R.N.A., PEREIRA, M.G.A., OLIVEIRA, A.H.B., SANTOS, J.M., CAVALCANTE, R.M., MARTINS, L.L., 2023. Is there a correlation between the waxy tarballs stranded on the coast of Northeast Brazil in late 2022 with previous oil spills? Annals of the XVI Latin American Congress on Organic Geochemistry (ALAGO 2023), p. 205.

NASCIMENTO, R. F. DO; LIMA, A. C. A. DE; BARBOSA, P. G. A; SILVA, V. P. A da. Cromatografia gasosa: aspectos teóricos e práticos. Fortaleza: Imprensa

Universitária, 2018. 334 p. (Estudos da Pós-Graduação). ISBN 978-85-7485-326-0.

NEFF, J. M. 1979. Polycyclic Aromatic Hydrocarbons in the Aquatic Environment. Applied Science Publishers Ltd., London, 1979, 262 pp. https://www.osti.gov/etdeweb/biblio/5162466

NUNES, N. M. M**;** ADE, M. V. B**;** RODRIGUES, R**;** ASSIS, FERNANDA, B**;** NASCIMENTO, F**;** LEITE, R. T. N**.** Oil Biodegradation in Siliciclastic Reservoir: an Example from Paleogene, Oliva Block, North of Santos Basin, Brazil / Biodegradação de Óleo em Reservatório Siliciclástico: um Exemplo do Paleógeno, Bloco Oliva, Norte da Bacia de Santos, Brasil. *Anuário do Instituto de Geociências - UFRJ*, Rio de Janeiro, v. 40, n. 3, p. 222–231, 2017. ISSN 0101-9759. Disponível em: https://revistas.ufrj.br/index.php/aigeo/article/view/13194.

O GLOBO. Equador declara emergência por vazamento de petróleo em oleoduto que afeta meio milhão de pessoas. 19 mar. 2025. Disponível em: https://oglobo.globo.com/mundo/noticia/2025/03/19/equador-declara-emergencia-por-vazamento-de-petroleo-em-oleoduto-que-afeta-meio-milhao-de-pessoas.ghtml. Acesso em: 15 abr. 2025.

OLDENBURG, T.B.P., BROWN, M., BENNETT, B., LARTER, S.R., 2014. The impact of thermal maturity level on the composition of crude oils , assessed using ultra-high resolution mass spectrometry. Org. Geochem. 75, 151–168. https://doi.org/10.1016/j.orggeochem.2014.07.002

OIL & GAS JOURNAL**.** SOTE pipeline rupture triggers one of Ecuador's largest oil spills. *Oil & Gas Journal*, 2025. Disponível em: https://www.ogj.com/general-interest/hse/article/55278287/sote-pipeline-rupture-triggers-one-of-ecuadors-largest-oil-spills. Acesso em: 12 abr. 2025.

OLIVEIRA, O.M., QUEIROZ, A.F.D.S., CERQUEIRA, J.R., SOARES, S.A., GARCIA, K.S., PAVANI FILHO, A., ROSA, M.L.S., SUZART, C.M., PINHEIRO, L.L., MOREIRA, I.T., 2020. Environmental disaster in the northeast coast of Brazil: forensic geochemistry in the identification of the source of the oily material. Mar. Pollut. Bull. 160, 111597. https://doi.org/10.1016/j.marpolbul.2020.111597.

OLIVEIRA, C. R., OLIVEIRA, C., FERREIRA, A. A., AZEVEDOA, D. A., AND AQUINO NETO, F. R. 2012. Characterization of aromatic steroids and hopanoids in marine and lacustrine crude oils using comprehensive two dimensional gas chromatography coupled to time–of–flight mass spectrometry (GC×GC–TOFMS). Organic Geochemistry 53:131–136

ORGANIZAÇÃO DOS PAÍSES EXPORTADORES DE PETRÓLEO. *OPEP*. Viena: OPEP, [s.d.]. Disponível em: https://www.opec.org.

ORR, WILSON L.; DAMSTÉ, JAAP S. SINNINGHE. Geochemistry of sulfur in petroleum systems. In: Orr, William L.; White, Catherine M. (Ed.). Geochemistry of sulfur in fossil fuels. Washington, DC: American Chemical Society, 1990. cap. 1, p. 2-29. (ACS Symposium Series, v. 429). DOI: 10.1021/bk-1990-0429.ch001

PAYNE, J. R; CLAYTON JR., JOHN R.; KIRSTEIN, B. E**.** oil/suspended particulate material interactions and sedimentation. *spill science & technology bulletin*, v. 8, n. 2, p. 201–221, abr. 2003. doi: https://doi.org/10.1016/s1353-2561(02)00115-1.

PEREIRA, M.G.A., SANTOS, I.R., LIMA, I.F.S., COUTINHO, M.E.B., CARREGOSA, J.C., WISNIEWSKI, A., SANTOS, J.M., 2023. Geochemical Assessment of Tar Balls That Arrived in 2022 along the Northeast Coast of Brazil and Their Relationship with the 38 2019 Oil Spill Disaster. Energy Fuel 37, 16388–16395. https://doi.org/10.1021/acs.energyfuels.3c02472

PETERS, K. E**.** Petroleum tricyclic terpanes: predicted physicochemical behavior from molecular mechanics calculations. *Organic Geochemistry*, v. 31, n. 6, p. 497–507, jun. 2000. https://doi.org/10.1016/S0146-6380(00)00029-2

PETERS, K.E., WALTERS, C.C., MOLDOWAN, J.M., 2005. The Biomarker Guide: Biomarkersand Isotopes in the Petroleum Exploration and Earth History, 2nd ed., UniversityPress: Cambridge, vol. 2. Peters, K.E., Scheuerman, G.L., Lee, C.Y., Moldowan, J. M., Reynolds, R.N., Pena, M.M., 1992. Effects of refinery processes on biological markers. Energy Fuel 6, 560- 577. https://doi.org/10.1021/ef00035a005

PETERSON, C. H.; RICE, S. D.; SHORT, J. W.; ESLER, D; BODKIN, J. L.; BALLACHEY, B. E.; IRONS, D. B. Long-term ecosystem response to the Exxon Valdez oil spill. *Science*, Washington, DC, v. 302, n. 5653, p. 2082–2086, 2003. https://doi.org/10.1126/science.1084282

PINTO, F. E.; FONSECA, V. R.; SOUZA, L. M.; TERRA, L. A.; SUBRAMANIAN, S; SIMON, S; SJÖBLOM, J; PEREIRA, T. M.; LACERDA JR., V; ROMÃO, W. Asphaltenes subfractions characterization and calculation of their solubility parameter using ESI(-) FT-ICR MS: Part II. *Fael*, [S. l.], v. 312, p. 122864, 15 mar. 2022. https://doi.org/10.1016/j.fuel.2021.122864

PHILP, R.P., 1994. Geochemical characteristics of oils derived predominantly from terrigenous source materials. In: Scott, A.C., Fleet, A.J. (Eds.), Coal and CoalBearing Strata as Oil-Prone Source Rocks? Geological Society Special Publication 77, pp. 71–91.

PRINCE, R.C., WALTERS, C.C., 2022. Modern analytical techniques are improving our ability to follow the fate of spilled oil in the environment. Curr. Opin. Chem. Eng. 36, 1-8. https://doi.org/10.1016/j.coche.2021.100787

REDDY, C.M., NELSON R.K., HANKE, U.M., CUI, X., SUMMONS, R.E., VALENTINE, D.L., RODGERS, R.P., CHACÓN-PATIÑO, M.L., NILES, S.F., TEIXEIRA, C.E.P., BEZERRA, L.E.A., CAVALCANTE, R.M., SOARES, M.O., OLIVEIRA, A.H.B., WHITE, H.K., SWARTHOUT, R.F., LEMKAU, K.L., RADOVIĆ, J.R., 2022. Synergy of Analytical Approaches Enables a 39 Robust Assessment of the Brazil Mystery Oil Spill. Energy Fuel 36, 13688–13704. https://doi.org/10.1021/acs.energyfuels.2c00656

REDDY, C. M.; AREY, J. S.; SEEWALD, J. S. et al. Composition and fate of gas and oil released to the water column during the Deepwater Horizon oil spill. *Proceedings of the National Academy of Sciences*, v. 109, n. 50, p. 20229–20234, 2012. DOI: 10.1073/pnas.1101242108.

RONTANI, J-F; VOLKMAN, J. K**.** Phytol degradation products as biogeochemical tracers in aquatic environments. *Organic Geochemistry*, v. 34, n. 1, p. 1–35, jan. 2003. https://doi.org/10.1016/S0146-6380(02)00185-7

RODGERS, R. P.; SCHAUB, T. M.; MARSHALL, A. G. Petroleomics: MS returns to its roots. Analytical and bioanalytical chemistry, v. 77, p. 21A–27A, 2005. http://dx.doi.org/10.1021/ac053302y

ROCHA, Y. S., PEREIRA, R. C., & GRACIANO FILHO, J. M. (2019). Petroleomics: fundaments and application on the geochemical assessment of crude oil and source rock samples. Anuário do Instituto de Geociências, 42, pp. 196-208.https://doi.org/10.11137/2019_1_196_208

SEIFERT W. K.; MOLDOWAN, J. M., 1978. Applications of steranes, terpanes and.monoaromatics to the maturation, migration and source of crude oils. Geochim. Cosmochim. Acta, v. 42, p. 77-95. https://doi.org/10.1016/0016-7037(78)90219-3

SKOOG, D. A.; WEST, D. M.; HOLLER, J. F**.** *Fundamentos de química analítica*. São Paulo: Cengage Learning, 2006.

SPEIGHT, J. G**.** *The chemistry and technology of petroleum*. 5. ed. Boca Raton: CRC Press, 2014. eBook

SEIFERT, W.K. AND MOLDOWAN, J.M., 1980. The effect of thermal stress on source-rock quality as measured by hopane stereochemistry. Phys. Chem. Earth 12, 229–37. https://doi.org/10.1016/0079-1946(79)90107-1

SHINDE, V.L., SUNEEL, V., SHENOY, B.D., 2017. Diversity of bacteria and fungi associated with tarballs: Recent developments and future prospects. Mar. Pollut. Bull. 117, 28-33. https://doi.org/10.1016/j.marpolbul.2017.01.067

SHINDE, V.L., SUNEEL, V., RATHORE, C., SHENOY, B.D., 2020. Degradation of tarballs using associated bacterial consortia. Biotech 10, 1-10. https://doi.org/10.1007/s13205-020- 2095-8

SOARES, M. O; TEIXEIRA, C. E. P; BEZERRA, L.E.A; PAIVA, S.V; TAVARES, T.C. L; GARCIA, T.M; ARAÚJO, J.T; CAMPOS, C. C; FERREIRA, S.M.C; MATTHEWS-CASCON, H; FROTA, A; MONT'ALVERNE, T.C.F; SILVA. S.T; RABELO, E.F; BARROSO, C.Z; FREITAS, J.E.P;JÚNIOR MELO, M; CAMPELO, R.P.S; CAVALCANTE, R.M. Oil spill in South Atlantic (Brazil): Environmental and governmental disaster. Mar. Policy 2020; 115

SOARES, M.O., TEIXEIRA, C.E.P., BEZERRA, L.E.A., RABELO, E.F., CASTRO, I.B., CAVALCANTE, R.M., 2022. The most extensive oil spill registered in tropical oceans (Brazil): the balance sheet of a disaster. Environ. Sci. Pollut. Res. 29, 19869–19877. https://doi. org/10.1007/s11356-022-18710-4

SOUZA, CHRISTIANE SAMPAIO DE; MAFALDA JUNIOR, PAULO DE OLIVEIRA; KIKUCHI, RUY KENJI PAPA DE; DOMINGUEZ, JOSÉ MARIA LANDIM. Assessment of the Brazilian Coast oil-spill impact in the fish eggs and larvae development from the tropical continental shelf. *Regional Studies in Marine Science*, v. 56, p. 102635, 2022. DOI: https://doi.org/10.1016/j.rsma.2022.102635.

SUDOL, PAIGE E.; PIERCE, KARISA M.; PREBIHALO, SARAH E.; SKOGERBOE, KRISTEN J.; WRIGHT, BOB W; SYNOVEC, ROBERT E. Development of gas chromatographic pattern recognition and classification tools for compliance and forensic analyses of fuels: A review. *Analytica Chimica Acta*, [S.l.], v. 1102, p. 1–14, 2020. DOI: 10.1016/j.aca.2019.12.054.

STOUT, S.A., DOUGLAS, G.S., UHLER, A.D., 2016. Chemical fingerprinting of gasoline and distillate fuels. In Standard Handbook Oil Spill Environmental Forensics (pp. 509- 564). Academic Press. http://dx.doi.org/10.1016/B978-0-12-809659-8.00011-5

STOUT, S. A., ZHENDI, W. Chemical fingerprinting methods and factors affecting petroleum fingerprints in the environment. Standard handbook oil spill 40 environmental forensics. Academic Press, 2016. 61-129. https://doi.org/10.1016/B978-0-12-803832-1.00003-9

STOUT, S.A., WANG, Z., 2007. Chemical fingerprinting of spilled or discharged petroleum – methods and factors affecting petroleum fingerprints in the environment. Oil Spill Environmental Forensics, 1-53. https://doi.org/10.1016/B978-012369523-9.50005-7

STOUT, S; WANG, Z. Standard handbook oil spill environmental forensics: fingerprinting and source identification. *2. ed. Cambridge: Academic Press,* 2016. 1142 p. ISBN 978-0-12-809659-8.

STOUT, Scott A.; WANG, Zhendi (ed.). *Oil spill environmental forensics: case studies*. 1. ed. Amsterdam: Elsevier, 2018. 804 p. ISBN 9780128044346. DOI: 10.1016/C2015-0-04091-4.

TARR, M. A.; ZITO, P; OVERTON, E. B; OLSON, G. M.; ADHIKARI, P. L.; REDDY, C. M. *Weathering of oil spilled in the marine environment*. Oceanography, [S.l.], v. 29, n. 3, p. 126–135, 2016. DOI: 10.5670/oceanog.2016.77. Disponível em: https://doi.org/10.5670/oceanog.2016.77.

TERRA, W.S., MARTINS, L.L., DA CRUZ, G.F., 2019. Avaliação da Eficiência de Diferentes Solventes Orgânicos na Precipitação de Asfaltenos de Petróleos Brasileiros e Uhler, A.D., Stout, S.A., Douglas, G.S., Healey, E.M., Emsbo-Mattingly, S. D., 2016.Chemical character of marine heavy fuel oils and lubricants. In Standard handbook oil spill environmental forensics (pp. 641-683). Academic Press. https://doi.org/10.1016/B978-0-12-803832-1.00013-1

TISSOT, B. P.; WELTE, D. H. Petroleum formation and occurrence. 2. ed. Revised. Berlin; Heidelberg; New York; Tokyo: Springer-Verlag, 1984.

VAZ, B.G., SILVA, R.C., KLITZKE, C.F., SIMAS, R.C., LOPES NASCIMENTO, H.D., PEREIRA, R.C.L., GARCIA, D.F., EBERLIN, M.N., AZEVEDO, D.A., 2013. Assessing Biodegradation in the Llanos Orientales Crude Oils by Electrospray Ionization Ultrahigh Resolution and Accuracy Fourier Transform Mass Spectrometry and Chemometric Analysis. Energy Fuel 27, 1277−1284. https://doi.org/10.1021/ef301766r41

VANINI, G; BARRA, T. A.; SOUZA, L. M.; MADEIRA, N. C. L.; GOMES, A. O.; ROMÃO, W; AZEVEDO, D. A. Characterization of nonvolatile polar compounds from Brazilian oils by electrospray ionization with FT-ICR MS and Orbitrap-MS. *Fuel*, [S. l.], v. 282, n. 15, p. 118790, 15 dez. 2020. https://doi.org/10.1016/j.fuel.2020.118790

VOLKMAN, John K.; ALEXANDER, Robert; KAGI, Robert I.; ROWLAND, Steven J.; SHEPPARD, Peter N. Biodegradation of aromatic hydrocarbons in crude oils from the Barrow Sub-basin of Western Australia. *Organic Geochemistry*, v. 6, p. 619–632, jan. 1984. DOI: https://doi.org/10.1016/0146-6380(84)90084-6.

WANG, C., CHEN, B., ZHANG, B., HE, S., ZHAO, M., 2013. Fingerprint and weathering characteristics of crude oils after Dalian oil spill, China. Mar. Pollut. Bull. 71, 64–68. https://doi.org/10.1016/j.marpolbul.2013.03.034

WANG, Z.; FINGAS, M. F**.** Development of oil hydrocarbon fingerprinting and identification techniques. *Marine Pollution Bulletin*, v. 47, p. 423–452, 2003. https://doi.org/10.1016/S0025-326X(03)00215-7

WANG, Z; STOUT, S. A.; FINGAS, M**;** YANG, C; CHRISTENSEN, J. H**.** Crude oil and refined product fingerprinting: principles. In: Morrison, R.D.; Murphy, B. L. (ed.). *Environmental forensics: contaminant specific guide*. Amsterdam: Academic Press, 2006. cap. 16, p. 340–407. https://doi.org/10.1016/B978-012507751-4/50038-0

WANG, Z; STOUT, S. A.; FINGAS, M**.** Forensic fingerprinting of biomarkers for oil spill characterization and source identification. *Environmental Forensics*, v. 7, n. 2, p. 105–146, 2006. https://doi.org/10.1080/15275920600667104

WANG, C., CHEN, B., ZHANG, B., GUO, P., ZHAO, M., 2014. Study of weathering effects on the distribution of aromatic steroid hydrocarbons in crude oils and oil residues. Environ. Sci.: Processes Impacts 16, 2408-2414.https://doi.org/10.1039/C4EM00266K

WANG, Z., FINGAS, M., Page, D. S., 1999. Oil spill identification. J. Chromatogr. A 843, 369-411. https://doi.org/10.1016/S0021-9673(99)00120-X

WANG, Z.; FINGAS, M. *Development of oil hydrocarbon fingerprinting and identification techniques. Marine Pollution Bulletin*, Oxford, v. 47, n. 9–12, p. 423–452, 2003. DOI: 10.1016/S0025-326X(03)00215-7.

WANG, Z., FINGAS, M., 1995. Study of the Effects of Weathering on the Chemical Composition of a Light Crude Oil Using GC/MS GC/FID. J. MicrocolumnSeparations 7, 617-639. https://doi.org/10.1002/mcs.1220070609

WARNOCK, A.M., HAGEN, S.C., PASSERI, D.L., 2015. Marine Tar Residues: a Review.Water Air Soil Pollut 226, 1-24. https://doi.org/10.1007/s11270-015-2298-5

WARD, C. P.; OVERTON, E. B**.** How the 2010 Deepwater Horizon spill reshaped our understanding of crude oil photochemical weathering at sea: a past, present, and future perspective. *Environmental Science: Processes & Impacts*, Cambridge, v. 22, n. 5, p. 1125–1138, 2020. https://doi.org/10.1039/d0em00027b.

WAPLES, D. W.; MACHIHARA, T**.** Biomarkers as organic-facies indicators. In: b*iomarkers for geologists: a practical guide to the application of steranes and triterpanes in petroleum geology*. Tulsa, Okla.: American Association of Petroleum Geologists, 1991. cap. 5, p. 41–60. (Methods in Exploration Series, n. 9)

WELLS, P. G. The iconic Torrey Canyon oil spill of 1967 – Marking its legacy. Marine Pollution Bulletin, [S.l.], v. 115, n. 1–2, p. 1–2, 2017. https://doi.org/10.1016/j.marpolbul.2016.12.013

WENG, NA; WAN, S; WANG, H; ZHANG, S; ZHU, G; LIU, J; CAI, D; YANG, Y. Insight into unresolved complex mixtures of aromatic hydrocarbons in heavy oil via two-dimensional gas chromatography coupled with time-of-flight mass spectrometry analysis. *Journal of Chromatography A*, v. 1398, p. 94–107, 12 jun. 2015. https://doi.org/10.1016/j.chroma.2015.03.057

YANG, C; WANG, ZI; LIU, Y; YANG, Z; LI, YAN; SHAH, K; ZHANG, G; LANDRIAULT, M; HOLLEBONE, B; BROWN, C; LAMBERT, P; LIU, Z; TIAN, SI. Aromatic steroids in crude oils and petroleum products and their applications in forensic oil spill identification. Environmental Forensics, v. 14, n. 4, p. 278–293, 2013. https://doi.org/10.1080/15275922.2013.843617

YIN, F; GAO, C; SONG, Z; HAN, Y; HE, Z; ZHANG, L; SU, P; FENG, D; YANG, T; FU, J. Chemical signatures of polycyclic aromatic hydrocarbons in the emissions from in situ oil burns. *Marine Pollution Bulletin*, v. 184, p. 114194, nov. 2022. https://doi.org/10.1016/j.marpolbul.2022.114194

YUNKER, M.B., LACHMUTH, C.L., CRETNEY, W.J., FOWLER, B.R., DANGERFIELD, N., WHITE, L., ROSS, P.S., 2011. Biota - Sediment partitioning of aluminium smelter related PAHs and pulp mill related diterpenes by intertidal clams at Kitimat, British Columbia. Marine Environmental Research. V. 72, p. 105 – 126. https://doi.org/10.1016/j.marenvres.2011.06.004

ZAKARIA, P.M., OKUDA, T., TAKADA, H., 2001. Polycyclic Aromatic Hydrocarbon (PAHs) and Hopanes in Stranded Tar-balls on the Coasts of Peninsular Malaysia: Applications of Biomarkers for Identifying Sources of Oil Pollution. Mar. Pollut.Bull. 42, 1357-1366. https://doi.org/10.1016/S0025-326X(01)00165-5

ZACHARIAS, D. C; CRESPO, N. M; SILVA, N. P; ROCHA, R. P; GAMA, C. M; RIBEIRO, S. S. B. N.; HARARI, J. Oil reaching the coast: Is Brazil on the route of international oceanic dumping? *Marine Pollution Bulletin*, v. 196, art. 115624, 2023. DOI: https://doi.org/10.1016/j.marpolbul.2023.115624.

ZHAO, W., ZHANG, S., WANG, F., CHEN, J., XIAO, Z., SONG, F. 2005. Gas accumulation from oil cracking in the eastern Tarim Basin: A case study of the YN2 gas field. Organic Geochemistry 36:1602–1616.

ZHANG, H., WANG, C., ZHAO, R., YIN, X., ZHOU, H., TAN, L., WANG, J., 2016. New diagnostic ratios based on phenanthrenes and anthracenes for effective distinguishing heavy fuel oils from crude oils. Mar. Pollut. Bull. 106, 58-61. https://doi.org/10.1016/j.marpolbul.2016.03.03642

ZHANG, H-Y; JI, Q; FAN, Y. What drives the formation of global oil trade patterns? Energy Economics Volume 49, May 2015, Pages 639-648. https://doi.org/10.1016/j.eneco.2015.02.017

ZITO, P., CHEN, H., PODGORSKI, D.C., MCKENNA, A.M., TARR, M.A., 2014. Sunlight creates oxygenated species in water-soluble fractions of Deepwater horizon oil. J. Hazard. Mater. 280, 636-643. https://doi.org/10.1016/j.jhazmat.2014.08.059

CAPÍTULO 2

Artigo 1: *Publicado na Marine Environmental Research 204, 106878, 2025. DOI: https://doi.org/10.1016/j.marenvres.2024.106878*

FORENSIC ENVIRONMENTAL GEOCHEMISTRY TO REVEAL THE EXTENT, CHARACTERISTICS, AND FATE OF WAXY TARBALLS SPILLED OVER THE NORTHEAST COAST OF BRAZIL IN 2022

Abstract

This work applied the forensic environmental geochemistry assessment to evaluate the tarballs that contaminated the coast of Brazil in late 2022. Accordingly, saturated and aromatic biomarkers were analyzed by gas chromatography and acidic polar compounds by Fourier transform ion cyclotron resonance mass spectrometry (FT-ICR MS) of 16 tarball samples from beaches of five Brazilian states. All samples presented waxy characteristics and are from the same source, highlighting the large coast extension affected by this event (~ 3,000 km). However, they have distinct sources from the spilled oils stranded on the Brazilian coast in 2019 and early 2022. Biomarkers indicate their characteristics of mature and marine crude oils (not fuel). Furthermore, all samples presented low weathering levels, indicating their fate as a high-persistence contaminant in the environment. These tarballs likely originated from the washing processes of ship tanks and persisted drifting on the sea until they arrived on the Brazilian coast.

Keywords: Oil Spill; Tarball; Marine Pollution; Forensic Geochemistry; Biomarker; FT-ICR MS.

2.1 **Introduction**

In late 2022, tens of tons of mysterious tarballs were stranded on the northeast coast of Brazil (MCTI, 2022), contaminating many marine and seashore areas. The first oiled materials were found in the State of Pernambuco in late August (Pereira et al., 2023; Bérgamo et al., 2023), reaching the states of Bahia, Sergipe, Alagoas, Paraiba, Rio Grande do Norte, and Ceará in the following weeks (Mello et al., 2023).

Oil spills affecting Northeast Brazil have been an immeasurable social, economic, and ecological problem due to their high frequency, high amount of oil, and because they have been affecting large geographic extension, impacting a broad number of protected areas and coastal communities (Soares et al., 2022). In 2019, the northeast coast of Brazil experienced the largest oil spill on tropical oceans (Reddy et al., 2022), with more than 5,000 tons of oil affecting eleven states (Soares et al., 2022). During 2020 and 2021, oiled materials related to the 2019 event were still reaching the beaches of Brazil (Lima et al., 2023). In January 2022, spilled oil not associated with the 2019 event appeared once again on the coast of the State of Ceará, reaching an extension of 400 km and with more than 8,000 liters of oil collected (Azevedo et al., 2022; Soares et al., 2022). Most recently, in late 2022, puzzling tarballs appeared all over the coast of Northeast Brazil.

Tarballs are marine residues with varying color, shape, size, and chemical composition that can originate from natural seepages (Corrick et al., 2021; Kvenvolden and Cooper, 2003) or anthropogenic sources due to the release of

oil into the ocean (Warnock et al., 2015). They have roughly spherical shapes, usually less than 10 cm in diameter (Kvenvolden and Cooper, 2003). They can be formed by liquid petroleum transformed into more consistent oiled material by weathering and other physical processes (Warnock et al., 2015) and can persist in the ocean for a long time (Warnock et al., 2015). These conglomerated residues can be carried ashore by waves and currents (Butler et al., 1998), affecting the marine ecosystems and coastal areas with human and ecological impacts (Warnock et al., 2015). Tarballs pollution is a considerable concern to the global marine ecosystem as they have toxic and pollutant compounds (Shinde et al., 2020) and have many bacteria and fungi associated with them, including potential human and animal pathogens (Shinde et al., 2017).

After being released into the environment, petroleum undergoes several physical, chemical, and biological processes that affect its fate and chemical composition, known as weathering (Stout and Wang, 2016; Wang et al., 1999). This fate is dependent on the oil properties and the environmental conditions. The waxy bitumen, which forms the waxy tarballs, is relatively resistant to weathering processes, allowing them to survive prolonged periods in the ocean (Edwards et al., 2018). The waxy compounds can retard the weathering effects on the tarballs due to the decrease in oil dispersion (Blumer et al., 1973) and their protection by the wax in the water column during transport by marine currents (Lourenço et al., 2020).

Forensic environmental geochemistry has been applied to assess petroleum-related contaminants and spilled oils, determining their source, time of release,

and the acting weathering process (Kaplan, 1997). It is mainly based on the scientific principles of organic geochemistry (Kaplan, 1997), in which it can be obtained the chemical fingerprinting of the spilled oil using analytical techniques, mostly gas chromatography (GC) (Stout and Wang, 2007) and, more recently, high-resolution mass spectrometry, mainly Fourier transform ion cyclotron resonance mass spectrometry (FT-ICR MS) (Prince and Walters, 2022). It usually involves assessing the significant factors that influence the chemical fingerprint of the spilled oil, including the crude oil genesis, petroleum refining, weathering processes, and mixing in the environment (Stout and Wang, 2007). This concept has been widely employed to examine the oil spills in Northeast Brazil in recent years (Azevedo et al., 2022; Carregosa et al., 2021; Lima et al., 2020, 2021, 2023; Oliveira et al., 2020; Reddy et al., 2022).

FT-ICR MS is an ultra-high-resolution analytical technique that has been used in oil spill studies, expanding the analytical window and, consequently, allowing the analysis of non-volatile compounds that are not accessible by traditional chromatographic techniques (Chen et al., 2016; Corilo et al., 2013; Huba and Gardinali., 2016; Krajewski et al., 2018; McKenna et al., 2013). FT-ICR MS coupled with electrospray ionization (ESI) in negative ion mode enables the detection of acidic NSO compounds through the deprotonation process, including phenols (O_1 class), carboxylic acids (O_2 class), and pyrroles (N_1 class) (Kim et al., 2005; Martins et al., 2021; Oldenburg et al., 2014).

Drawing attention to the recurrent oiled material stranding the seashore of Brazil from multiple sources, this work aims to thoroughly assess the geochemical

characteristics of the tarballs that reached its northeastern coast in late 2022 through aliphatic and aromatic biomarkers and acidic polar compounds assessed by GC and FT-ICR MS. The forensic environment geochemistry concept was comprehensively applied on them to assess: (1) the extension of the Brazilian coast affected by this event; (2) possible similarities between the 2022 waxy tarballs and the spilled oils collected in 2019 and in early 2022; (3) their genesis, including the depositional environment and thermal maturity of their source rock; (4) if the oiled material is virgin crude oil or processed oil; (5) the weathering process acting on them and their fate.

2.2 Materials and methods

2.2.1 Samples

The set of samples encompasses 16 tarballs collected from late August to late October 2022 on distinct beaches from the states of Bahia, Sergipe, Alagoas, Rio Grande do Norte, and Cear´a, in the northeast of Brazil (Fig. 23, samples with codes 22.2). In addition, two spilled oil samples were collected in January 2022 in the State of Cear´a (samples with codes 22.1; Azevedo et al., 2022), and two samples from the 2019 oil spill event, also collected in the State of Cear´a (Fig. 23).

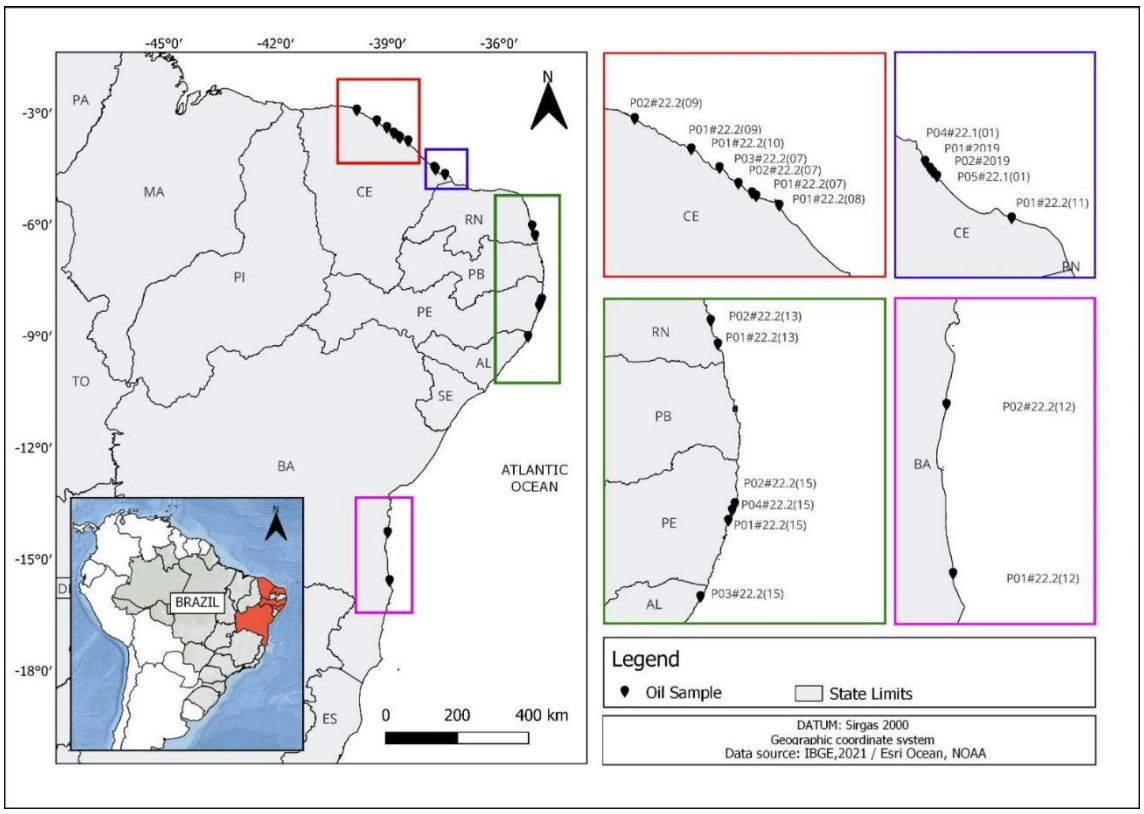

Fig. 23. Location of tarballs and spilled oil samples collected in 2019 and 2022 (see details in **Table S1, Appendence A**).

2.2.3 Extraction and separation

The oil extraction was performed from approximately 1.0 g of tarball samples (oil mixed with sediment) using dichloromethane as a solvent, which was stirred, centrifuged, and the organic phase was relocated to a flask and the solvent with the oil was roto-evaporated (Carregosa et al., 2021). The asphaltene precipitation was performed from 300 mg of extracted oil by 100 µl of dichloromethane mixed with 12 mL of *n*-hexane through an ultrasonic bath for 10 min, followed by centrifugation. The maltene fraction dissolved in the solvent was removed, and the precipitated asphaltene was washed five times with 12 mL of *n*-hexane to ensure maximum recovery of the maltene (Martins et al., 2021), then roto-

evaporated. Finally, approximately 40 mg of maltene were fractionated in saturated, aromatics, and resins by liquid column chromatography where each fraction was eluted with *n*-hexane, *n*-hexane:dichloromethane (8:2, *v:v*), and dichloromethane:methanol (9:1, *v:v*), respectively. After collecting each fraction, they are taken to the rotary evaporator to remove the solvents (Terra et al., 2019). All solvents were chromatographic/HPLC grade from Sigma-Aldrich Chemical.

2.2.4 GC-FID

To assess the *n*-alkanes and isoprenoids, the saturated fraction was analyzed by gas chromatography with a flame ionization detector (GC-FID) from Thermo – Focus GC with Agilent J&W DB-5 capillary column (30 m × 0.25 mm i.d. × 0.25 µm df). Nitrogen was used as a carrier gas, with a 1 mL min^{-1} constant flow. The GC oven was isothermally held at 50 °C for 5 min, then heated from 50º to 310 °C at 6 min^{-1}, with the final temperature held for 17.67 min (total time: 63 min.). The injector temperature was 280 ºC, and the FID was set at 300 ºC. The sample injection volume was 1 µL, in splitless mode, using *n*-hexane as a solvent (HPCL grade). The *n*-alkanes (*n*C8 to *n*C40) and isoprenoids (pristane and phytane) were identified and quantified by external standardization. The analytical standard was purchased from AccuStandard (Hydrocarbon Window Defining Standard, DRH-008S-R2, which is a mixture of the aforementioned *n*-alkanes and isoprenoids). The applied calibration curves cover the range from 0.50 to 10 ppm.

2.2.5 GC-MS

To assess the saturated and aromatic biomarkers, the maltene fraction was analyzed by gas chromatography/quadrupole mass spectrometer (GCMS-QP2010 SE, Shimadzu, Japan) with the procedure performed with Electron ionization (EI) at 70 eV, coupled to an automatic sampler (AOC-6000 Plus, Shimadzu, Japan). The chromatographic separation was done using an HP-5ms Ultra Inert capillary column (30 m × 0.25 mm i.d. × 0.25 μm df; 5%-phenyl-methylpolysiloxane). The GC oven was heated from 70 to 325 °C at a rate of 20 °C min^{-1}, with the final temperature held for 10 min. The sample injection volume was 1 μL in split mode (1:20). The injector, ion source, and interface temperatures were 300, 250, and 300 °C, respectively. Helium was used as carrier gas at a constant flow rate of 1 mL min^{-1}. Samples were analyzed in full scan and single ion monitoring (SIM) acquisition modes. In SIM mode, *m/z* 83, 85, 191, and 217 were monitored to assess the saturated compounds alkylcyclohexanes, *n*-alkanes/branched hydrocarbons, tri and pentacyclic terpanes, and steranes and diasteranes. The *m*/*z* 178, 192, and 231 were monitored to assess the aromatic compounds phenanthrene (P) and anthracene (A), methylphenanthrenes (MP) and methylanthracene (MA), and triaromatic steroids (TAS), respectively (Carregosa et al., 2021). The data obtained after the analyses were processed using GCMS solution v. 4.20 (Shimadzu, Japan).

2.2.6 ESI(-) FT-ICR MS

To assess the acidic polar compounds, the total extracted oil was analyzed by ESI(-) FT-ICR MS. 10 mg of oil was dissolved in 10 mL of toluene. From the stock solution for ESI(-) analysis, 500 μL was collected and transferred to a flask

containing 500 µL of methanol with 25 µL (2.5%) of NH_4OH. Solvents methanol, toluene, and ammonium hydroxide were HPLC grade purchased from J.T. Baker (Phillipsburg, NJ, USA) and Sigma-Aldrich (Steinheim, Germany), respectively.

FT-ICR MS were acquired using a 7T SolariX 2xR (Bruker Daltonics - Bremen, Germany) coupled to the negative mode ESI source. The drying gas used was nitrogen with a flow rate of 4.0 L min^{-1}, a temperature of 200 °C, and nebulization gas with 1.0 bar. Samples were injected using a syringe pump with a flow rate of 240 µL h^{-1}. Ions were accumulated in the collision cell for 0.005 s and transferred to the ICR cell in 0.6 - 1 ms. The spectra were previously analyzed in the LTQ Fleet to check the Gaussian distribution. 8MW datasets were acquired using magnitude mode with the detection range *m/z* 150 - 2000. 2ω (quadrupole) detection was used to provide high resolution at a fast scan rate. For each sample, 300 scans were acquired to obtain spectra with excellent signal/noise values. For the apodized data, the resolving power measured in *m/z* 400 was 880 000. For the acquisition of one sample spectra, the transient acquisition time was 2.5 seconds (**Fig. S1, Appendence A**). The data were internally calibrated using a homologous series of neutral nitrogen (N_1) class using Data Analysis 4.2 software (Bruker Daltonics GmbH, Bremen, Germany).

In the processing stage, molecular formulas are initially assigned from the recalibrated spectra. The Composer64 software (Version 1.5.3 Sierra Analytica, Modesto, USA) was used for this. In general, processing conditions were similar for all samples. However, the intensity threshold, minimum abundance, and new minimum abundance parameters varied according to the noise intensity of each

spectrum. These three parameters were used to define a limit of relative abundance so that only molecular formulas were assigned to peaks of intensity greater than the pre-established limit. Allowed elements were ^{12}C, ^{1}H, ^{16}O, ^{14}N, and ^{32}S. The maximum allowed formula error was 0.5 ppm.

3 Results and discussion

3.1 General characteristics of the waxy tarballs

The tarballs collected all over the Northeast coast of Brazil (**Fig. 24, Appendence A**), from the states of Bahia to Ceará, have a roughly spherical appearance, ranging from small materials (**Fig. 24b, Appendence A**) with less than 1 cm to large materials with more than 10 cm (**Fig. 24c** and **d**). They are soft black materials with an oil smell, which fluctuates on the seawater as pelagic tars (**Fig. S2, Appendence A**). The precipitation of a considerable visible amount of wax in the saturated fraction after the fractionation by liquid chromatography pointed out their waxy characteristics, in agreement with the high percentage of it (46 to 62%; **Fig. S3, Appendence A**). Part of the tarballs were found with the marine organisms goose barnacle species *Lepas anatifera* attached to them (Mello et al., 2023), which have cosmopolitan distribution mostly in oceanic waters, indicating that these materials come from the open Atlantic Ocean and that they have been drifting for at least a month due to the size of these organisms (more detail in Mello et al., 2023).

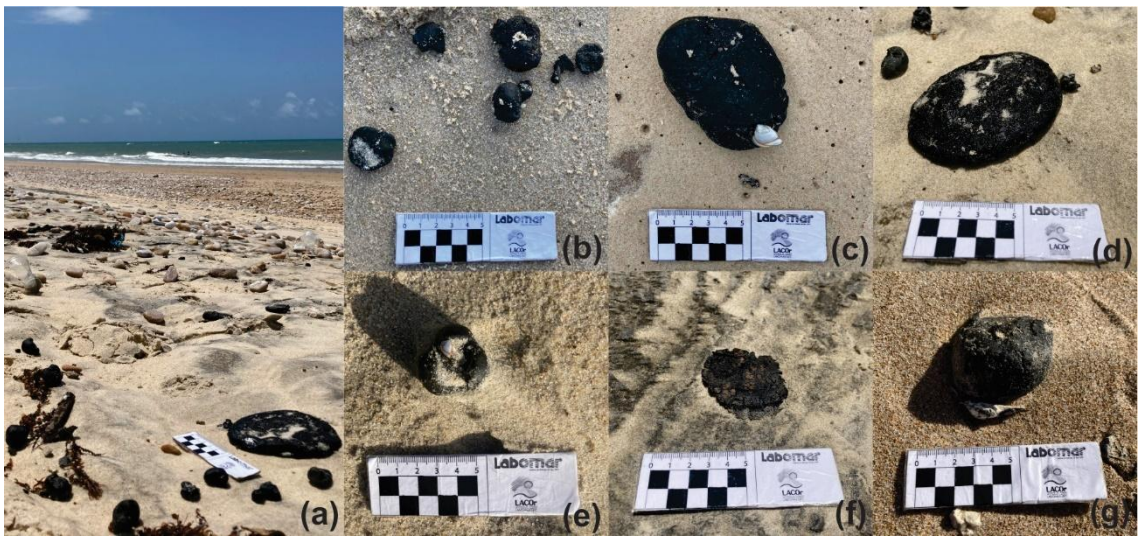

Fig. 24. Tarballs found in the first days of their appearance at the State of Ceará in late 2022: Cumbuco beach, September 24 (a); Futuro beach, September 23 (b); Icaraí beach, September 24 (c); Cumbuco beach, September 24 (d); Pecém beach, September 24 (e); Flecheiras beach, August 03 (f); Almofala beach, August 03 (g).

Approximately 2.8 Kg of tarballs (**Fig. S4, Appendence A**) were collected in 200 m of beach extension at the Futuro beach in their first appearance in the State of Ceará on September 23, 2022. Considering that Future Beach has an extension of eight km, it can be estimated that around 112 kg of tarballs were stranded on this beach on that day. The amount of tarball reaching the coast of Ceará on the first arrival can also be estimated as eight tons, considering its 573 km of extension. If we consider the coastal extension of Northeast Brazil, which is nearly 3,000 km, the amount of tarballs beaching Brazil could reach at least 42 tons. This amount is consistent with the seven tons collected only in the state of

Pernambuco (G1, 2022), with an extension of 187 km. Moreover, this amount can probably be higher since tarballs kept arriving in the following days in small amounts after the first arrivals. This is consistent with medium tanker spills (ITOPF, 2024).

3.2 Similarity among the Northeast Brazilian waxy tarballs

The GC-FID chromatogram of the 16 tarball samples collected in late 2022 shows a remarkably similar bimodal profile (**Fig. S5, Appendence A)** and **Fig.25**), with *n*-alkanes ranging from *n*C12 to *n*C40, maximizing at *n*C17 and *n*C33. The high abundance of long-chain *n*-alkanes (*n*C31 to *n*C40) corroborates their waxy characteristic, and together with no detection of UCM (unresolved complex mixture), it also points to little-weathering tarballs. Edwards et al. (2018) described similar characteristics in the stranding waxy tarballs in southern Australia, which pointed to the unusual amount of long-chain *n*-alkanes that resemble wax precipitated from marine crude oil during production (Philp, 1994). Pereira et al. (2023) and Bérgamo et al. (2023) have found similar profiles for tarball samples, but the studies were restricted for sampling in the state of Pernambuco, Northeast Brazil, between August and September 2022.

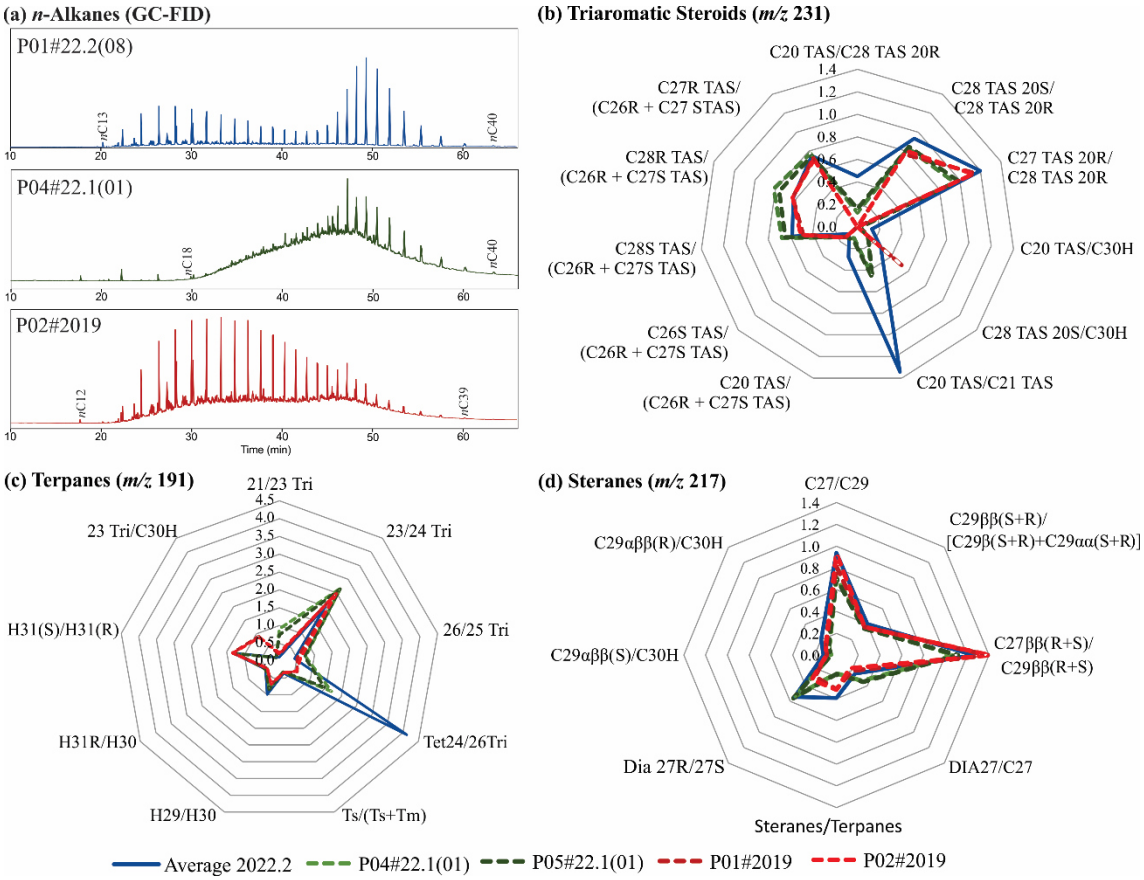

Fig. 25. GC-FID chromatograms representative for the tarballs and the 2022.1 and 2019 spilled oils (a). Radar plots comparing the diagnostic ratios of triaromatic steroids (b), tricyclic and pentacyclic terpanes (c), and steranes (d) for the average of the tarballs and the 2022.1 and 2019 spilled oils.

Some possible origins of the waxy tarballs are natural oil seeps (Edwards et al., 2018) or ship tank washing processes, where paraffin sticks to the walls during long transport trips (Zakaria et al., 2001). Tarballs derived from the washing process of tanks are usually rich in paraffin (Blumer et al., 1973) and have long-chain *n*-alkanes in high abundance (Zakaria et al., 2001).

The GC-FID chromatograms of the 2022.2 tarballs have notable distinct profiles from the chromatograms of the 2019 and 2022.1 spilled oils (**Fig. 25a**);

these last two already presented by Reddy et al. (2022), Azevedo et al. (2022), and Pereira et al. (2023). The ratios calculated using the *n*-alkanes and isoprenoids pristane/phytane (Pr/Ph), Pr/*n*C17, and Ph/*n*C18 (**Table S2, Appendence A**) showed low relative standard deviation (RSD) values (<5%) among the 16 tarballs; however, the ratios using a wider range of *n*-alkanes, such as terrigenous/aquatic ratio (TAR), carbon preference index (CPI), low molecular weight *n*-alkanes (LMW)/high molecular weight *n*-alkanes (HMW), and weathering index (WI) showed high RSD values (>30%) among them, primarily due to weathering effects. When the 2019 and 2022.2 samples are included in this comparison, the RSD values dramatically rise, ranging from 28.15 to 258.56% for these ratios. These differences suggest distinct sources for these three groups of spilled oils. However, as the diagnostic features from the GC-FID profiles are influenced by weathering processes, resistant molecular biomarkers are needed to assess the similarity among these spilled oils (Wang et al., 2013).

To investigate the similarity among the tarballs collected in 2022.2 and also the correlations of these tarballs with the spilled oils collected in 2019 and 2022.1, we applied diagnostic ratios based on molecular biomarkers resistant to weathering processes including the triaromatic steroids (TA), tricyclic and pentacyclic terpanes, and steranes (**Table S3**; mass chromatograms in **Figs. S6**, **S7**, and **S8**; representative mass spectrum in **Fig. S9**; Arekhi et al., 2021; Wang et al., 2013**, Appendence A**), which can be recalcitrant even under tropical climate conditions (Lima et al., 2021; 2023).

On the one hand, the radar plots of the diagnostic ratios for all 16 tarballs show good similarity (**Fig. S10, Appendence A**), corroborating the GC-FID results, with the RSD lower than 10% to 24 of the total 28 ratios. Exceptions are the ratios 21/23 Tri, 23/24 Tri, 26/25 Tri, and Tet24/26Tri (**Fig. S10b, Appendence A**), which can be explained by the higher susceptibility of the tricyclic terpanes to biodegradation when compared with the pentacyclic and steranes (Arekhi et al., 2021). The similarity of these samples confirms the great extension (approximately 3,000 km) of the Brazilian coast affected by this oil spill event, from the Bahia to Ceará states.

On the other hand, the radar plots of the diagnostic ratios for the average of the 16 tarballs (2022.2) compared with 2022.1 and 2019 spilled oils are remarkably different (**Fig. 25b**, **c**, and **d**), clearly indicating that these sets of samples originated from a distinct source and different events. The RSDs considering all 20 environmental oil samples are considerably higher than the RSD only of the 16 tarballs, reaching values up to 38.9% to the TAS, up to 106.5% to the terpanes, and up to 21.7% to the steranes.

3.3 Genesis of the waxy tarballs

The key chemical feature associated with the source, depositional environment, and maturity of the source rock of the crude oil is crucial in the chemical fingerprinting of spilled oils (Stout and Wang, 2007). Petroleum biomarkers resistant to weathering processes were assessed to investigate the geochemical information of the tarball genesis.

The thermal maturity of the source rock of the spilled oil samples was assessed by geochemical parameters based on the isomerization of asymmetric centers of hopanes and steranes (Peters et al., 2005). For instance, the biologically produced hopanes have the configuration 22R, which is converted gradually to a mixture of 22R and 22S diastereomers. So, the ratios H31S/(H31S + H31R) and H32S/(H32S + H32R) with values between 0.57 to 0.62 point out that the main phase of oil generation has been reached (Seifert and Moldowan, 1980). The tarball samples (2022.2) have the values of H31S/(H31S + H31R) and H32S/(H32S + H32R) ratios within the equilibrium zone (**Fig. 26a** and **Table S4 ,Appendence A**; 0.56 to 0.59 and 0.59 to 0.60, respectively), indicating that they are mature. The values are similar to those obtained for the 2019 oil [except the H32S/(H32S + H32R) ratio for sample P01#2019; **Table S4, Appendence A**] and 2022.1 spilled oils. The values of the carbon preference index (CPI) near 1.0 corroborate the maturity of the tarballs (**Table S4, Appendence A**; from 0.97 to 1.12) (Peters et al., 2005).

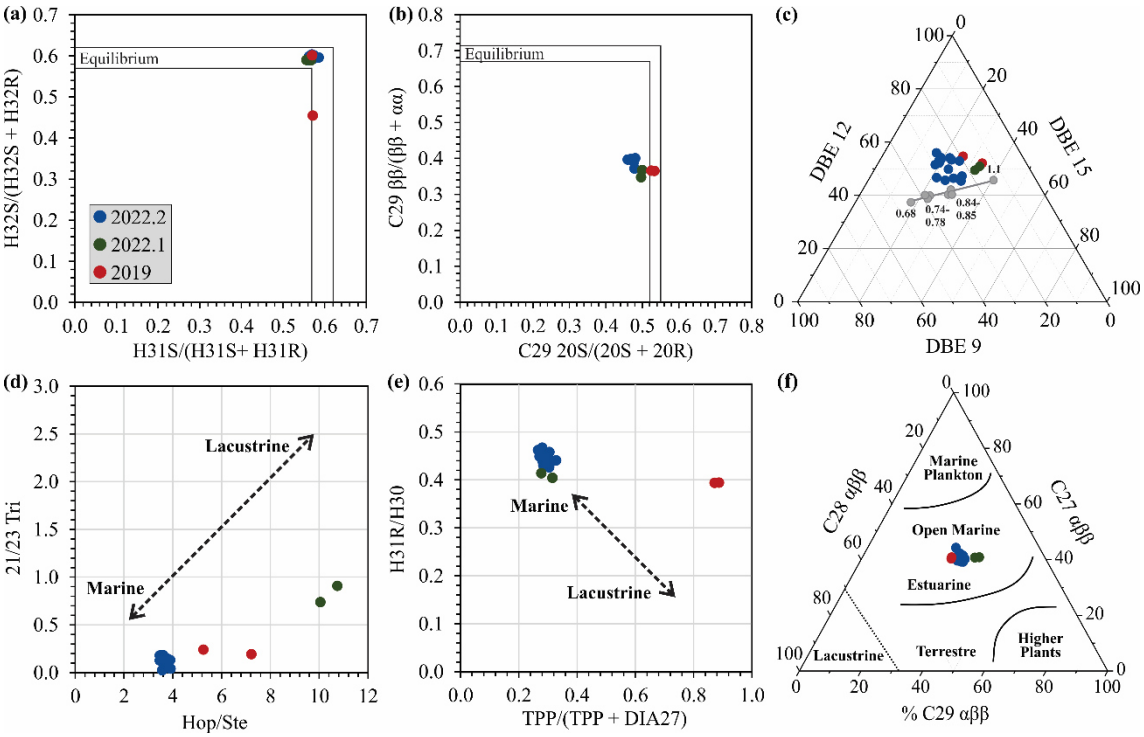

Fig. 26. Thermal maturity parameters based on isomerization of asymmetric centers in the C31 and C32 homohopanes (a) and C29 steranes (b), in addition to the triangular plot to assess maturity based on the relative distribution of carbazoles (DBE 9), benzocarbazoles (DBE 12), and dibenzocarbazoles (DBE 15) obtained from the ESI(-) FT-ICR MS analysis (Oldenburg et al., 2014). Numbers on the diagram indicate the values of the vitrinite reflectance equivalent (%Re) obtained by Oldenburg et al. (2014). Plots to assess the source and depositional environment: Hop/Ste against 21/23 Tri (d); TPP/(TPP + Dia27) (e); Triangular plot showing the relative distribution of C27, C28, and C29 regular steranes.

However, the values for the C29 20S/(20S + 20R) and C29 ββ/(ββ + αα) ratios indicate that the tarball samples are below the equilibrium zone (**Fig. 26b**), being still immature. In addition, they present lower maturity than the 2019 and

2022.1 spilled oil samples according to the C29 20S/(20S + 20R). The C29 ββ/(ββ + αα) presents values for all samples markedly lower than the equilibrium values, possibly because they are slower to reach equilibrium than the C29 20S/(20S + 20R), being more effective at higher levels of maturity.

The maturity was also assessed by the triangular plot based on the distribution of the carbazoles (DBE 9), benzocarbazoles (DBE 12), and dibenzocarbazoles (DBE 15) (**Fig. 26c**; Oldenburg et al., 2014) from the ESI(-) FT-ICR MS analysis. The tarball samples have reached the peak of the oil window [approximately 0.84-0.85 %Re compared with Oldenburg et al. (2014)], whereas the other spilled oil samples have a higher maturity.

Regarding the organic matter type and depositional environment of the source rocks of the oil that generated the tarballs, the bimodal distribution of the *n*-alkanes (**Fig. 26a** and **Fig. S5, Appendence A**) indicates a mixture of marine and terrestrial organic matter input (Hakimi et al., 2023). The high values of the Terrigenous/Aquatic ratio (0.49 to 0.76; **Table S5, Appendence A**) corroborate the significant terrigenous contribution (Bourbonniere and Meyers, 1996). In addition, the Pr/Ph ratio lower than 1 (0.58 to 0.70, **Table S5, Appendence A**) suggests marine organic matter deposited under anoxic conditions (Didyk et al., 1978).

The depositional paleoenvironment of the tarball source rocks was also assessed by geochemical parameters based on biomarkers (**Table S5, Appendence A**). The plot of 21/23 Tri against Hop/Ste (**Fig. 26d**) and H31R/H30 against TPP/(TPP + Dia27) (**Fig. 26e**) indicate that the tarballs are associated

with a marine source rock. Low 21/23 Tri (0.02 to 0.18 for the herein tarballs, **Table S5, Appendence A**) and low Hop/Ste (lower than 5, Mello et al., 1998; 3.46 to 3.90 for the herein tarballs, **Table S5, Appendence A**) are characteristics of marine oils (Bastos et al., 2022; Oliveira et al., 2020;). In addition, C31/30H ratio higher than 0.30 (Bastos et al., 2022; 0.43 to 0.47 for the herein tarballs, **Table S5, Appendence A**) is also associated with marine conditions, and the low abundance of C30 tetracyclic polyprenoid (TPP; 0.27 to 0.33 for the herein tarballs, **Table S5, Appendence A**) indicate low contribution of lacustrine algae to the source rock since the TPP is highly specific for algal input (*Botryococcus;* Holba et al., 2000).

Other biomarker ratios supported that marine characteristics of the oils, including the H29/H30 higher than 0.6 (Teixeira et al., 2014; 0.96 to 1.03 for the herein tarballs, **Table S5, Appendence A**) and HH35(S)/HH34(S) close or higher than 0.8 (Teixeira et al., 2014; 0.67 to 1.86 for the herein tarballs, **Table S5, Appendence A**). The tarball samples also have an abundance of C27 and C29 regular steranes close to each other (C27/C29 from 0.90 to 1.03 for the herein tarballs, **Table S5, Appendence A**), together with the relative distribution of C27, C28, and C29 regular steranes plotted in a triangular plot (**Fig. 26f**) corroborates an open marine to marine estuarine as the depositional environment of the source rocks of the tarballs (Huang and Meinschein, 1979). These results are consistent with the mixture of marine and terrestrial organic matter input highlighted by the bimodal distribution of the *n*-alkanes (**Fig. 25a** and **Fig. S5, Appendence A**) and the low salinity conditions indicated by the low values of the gammacerane ratio

(G/H, varying from 0.00 to 0.04 for the herein tarballs, **Table S5, Appendence A**).

3.4 Type of Oil

Although petroleum products maintain some of the chemical characteristics of the genesis (primary control), refining processes, such as distillation, hydrotreatment, and cracking, alter the distribution of some biomarkers and PAHs in the source oil and are considered a secondary control, influencing the chemical fingerprint of spilled oil and should be considered when analyzing spilled oil (Stout and Wang, 2016). So, most oil spill in marine environments is crude or refined oil (Stout and Wang, 2007). Accordingly, to understand the essential features of the accidents, it is fundamental to determine if the oily material is crude or refined oil (Bastos et al., 2022).

Anthracene was absent in all 16 analyzed tarballs, and 2-methylanthracene was detected only in three samples, with very low abundance (**Fig. 27a** and **Fig. 27b**; **Fig. S11** and **S12, Appendence A**), indicating that they probably did not undergo refining processes. These compounds, generally absent or in very low abundance in crude oils, are formed when the oil is exposed to thermal alteration processes, such as cracking (Emsbo-Mattingly and Litman, 2016; Stout and Douglas, 2016; Uhler et al., 2016). Another indication is the predominance of the 9/4 and 1-MP isomers, less thermally stable, about the 3 and 2-MP isomers, which are more thermally stable (**Fig. 27b**, **Fig. S11**, and **S12, Appendence A**). The 3 and 2-MP isomers tend to be enriched about 9/4 and 1 MP when exposed to some thermal alteration processes (Reddy et al., 2022; Uhler et al., 2016).

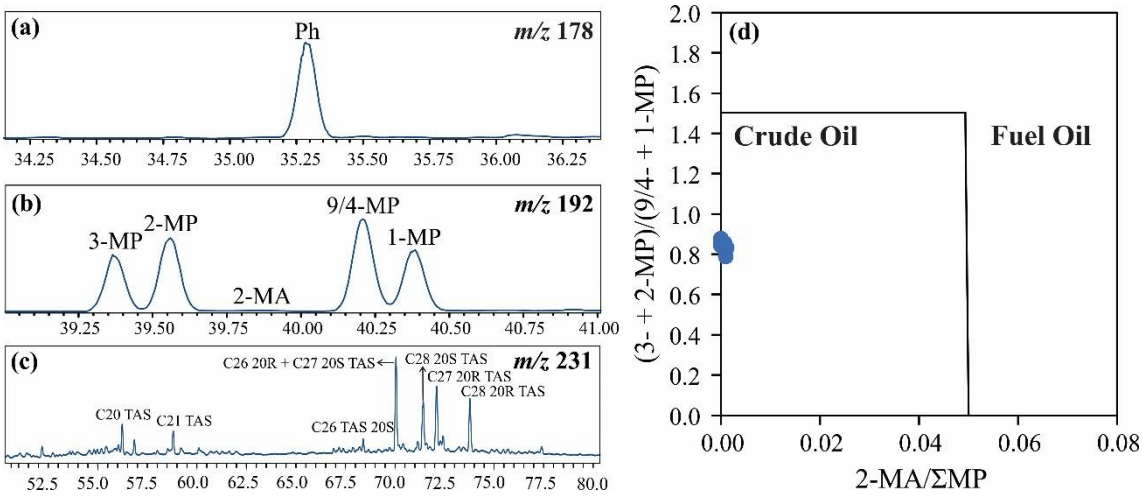

Fig. 27. Representative *m/z* 178 (a), *m/z* 192 (b), and *m/z* 231 (c) chromatograms of aromatic fractions of tarballs, showing the distribution of the phenanthrene, methylphenanthrenes, and triaromatic steroids (TAS), respectively. (d) The plot of (3- + 2-MP)/(9/4- + 1-MP) against 2-MA/∑MP to assess the type of oil. Ph = phenanthrene (*m/z* 178); An = anthracene (*m/z* 178); MP = methylphenanthrene (*m/z* 192); 2-MA = 2-methylanthracene (*m/z* 192); TAS = triaromatic steroids (*m/z* 231).

More evidence that the waxy tarballs are a crude oil product was obtained through the ratios suggested by Zhang et al. (2016) (**Table S6, Appendence A**), who used the compounds mentioned above to distinguish crude oils from heavy fuel oils (HFOs) that share similar physical properties and chromatographic characteristics (Zhang et al., 2016). A plot of the 2-MA/∑MP ratio against the (3- + 2-MP)/(9/4- + 1-MP) ratio was applied to assess whether the tarballs are raw or refined products (**Fig. 27d**). Zhang et al. (2016) showed that the 2-MA/∑MP ratio was below 0.05 for most of the 230 crude oils and above 0.05 for most of

the 210 HFOs studied in their work. In the present study, this ratio was possible to obtain for only three of the 16 samples of tarballs 2022.2, with values less than 0.05. The (3- + 2-MP) /(9/4- + 1-MP) ratio ranged from 0.79 to 0.88 for the 16 samples analyzed in this study, which are consistent with those observed in crude oils (<1.50). In addition, the other ratios that use the 2-MA [2-MA/3-MP; 2-MA/1-MP; 2-MA/(2 + 3-MP); 2-MA/(9/4 + 1-MP)] were also possible to calculate only for three of the 16 samples, with values close to or less than 0.01, which are characteristic of crude oils. These results are in agreement with the outcomes of Pereira et al. (2023), which indicated that two tarballs collected in the State of Pernambuco in August 2022 were related to virgin/unprocessed oils.

In addition, the hydrocracking process can destroy mono and triaromatic steroids (Peters et al., 1992), probably due to the elevated temperatures and pressures of the hydrogen. The high abundance of TAS in the 2022.2 oils (**Fig. 27c** and **Fig. S6, Appendence A**), which is best visualized through the ratios C20 TAS/C30H (0.12 to 0.15) and C28 TAS 20S/C30H (0.26 to 0.31; **Table S3, Appendence A**), corroborates this oil did not undergo this process.

3.5 Weathering and fate assessment

The fate of spilled oils in marine and coastal environments rests on their initial physical and chemical characteristics, the climatic and environmental conditions, and whether the oil remains at sea or is washed ashore (IPTOF, 2012). This fate is closely linked to the weathering processes that may change the chemical composition and properties of the spilled oil over time, which are even more

intense under tropical climate conditions, as occur in Northeast of Brazil (Lima et al., 2021; 2023). So, the effects of weathering should be taken into consideration in oil spill investigations and response operations (IPTOF, 2012).

3.6 Hydrocarbons by GC-FID and GC-MS

Through the analysis carried out using GC-FID, it was possible to visualize the still presence of low molecular weight *n*-alkanes (*n*C12-*n*C14) and the unresolved complex mixture (UCM) in very low abundance in the 16 tarball samples collected along the coast of Northeast Brazil (**Fig. 21a** and **Fig. S3, Appendence A**), which indicates that weathering processes (e.g., evaporation, dissolution, and biodegradation) probably affected them in low extension (Lourenço et al., 2020; Stout and Wang, 2016; Zito et al., 2014). This low UCM and the high abundance of *n*-alkanes (*n*C12 to *n*C41) directly influenced the high values observed for the resolved/UCM ratio (32.37 to 101.10%; **Table S2, Appendence A**), which corroborates the low degradation of these waxy tarballs, although these high values can also be attributed to their paraffinic characteristic (Edwards et al., 2018; Rostami and Amini-Rad 2019).

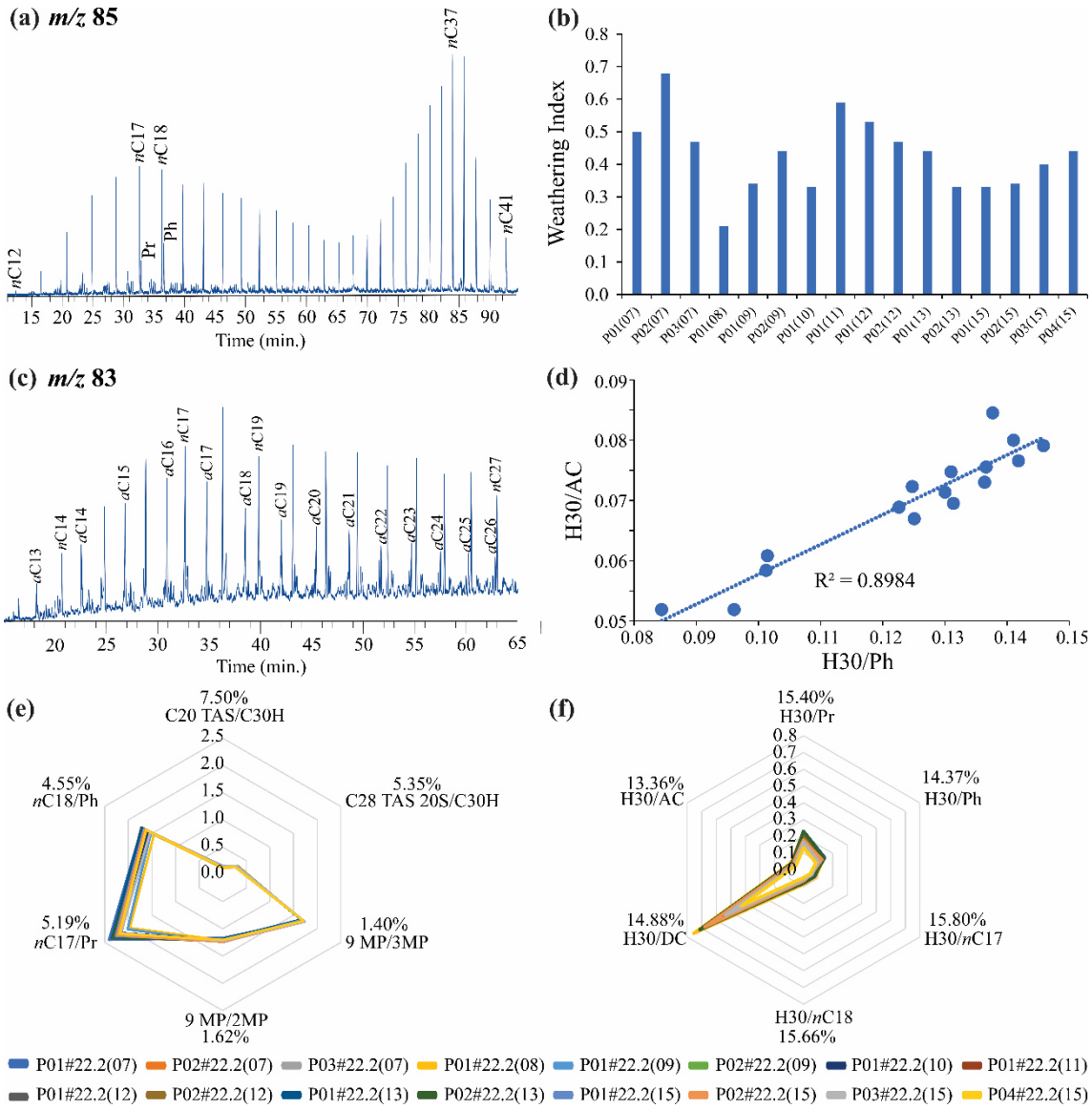

Fig. 28. Representative *m/z* 85 (a) and *m/z* 83 (c) chromatograms of aliphatic fractions of tarballs, showing the distribution of the *n*-alkanes and alkylcyclohexanes, respectively. Bar graph of the Weathering Index (WI) applied to assess the extent of weathering suffered by tarball samples (b). The plot of the H30/Ph against H30/AC to assess biodegradation (d). Radar plots comparing the diagnostic ratios for weathering assessment (e; f) for the tarballs.

The Weathering Index [WI = (*n*C10 + *n*C12 + *n*C14)/(*n*C22 + *n*C24 + *n*C26 + *n*C28)] was also applied (**Fig. 28b**), which tends to decrease with increasing weathering due to evaporation and dissolution of low molecular weight *n*-alkanes (Hegazi et al., 2004; Wang and Fingas, 1995). This index varied considerably among the 16 tarball samples (0.21 to 0.68; **Table S2, Appendence A**), showing a high RSD value (26.28%), indicating that the weathering processes of dissolution and evaporation acted at some level in these tarball samples, which is expected in tropical climate conditions.

Isoprenoids (e.g., pristane and phytane) are more resistant to biodegradation processes when compared to *n*-alkanes; therefore, the *n*C17/Pr and *n*C18/Ph ratios can be used as a cue for evaluating microbial degradation (Emsbo-Mattingly and Litman, 2016; Stout and Wang, 2016). Values >1 were obtained for the *n*C17/Pr (1.97 to 2.41) and *n*C18/Ph (1.46 to 1.72) ratios, which showed low RSD of 5.19 and 4.55%, respectively (**Fig. 28e** and **Table S7, Appendence A**), indicating that little biodegradation acted to remove the *n*-alkanes or acted in the same extension to all tarballs (Emsbo-Mattingly and Litman, 2016; Stout and Wang, 2016).

Edwards et al. (2018), studying waxy bitumen stranded on beaches in southern Australia, assigned empirical values of the degree of weathering varying from 0 to 5. In this work, the greater abundance of *n*C17 and *n*C18 over the pristane and phytane and the depletion observed for these compounds (**Fig. 28f**) point to the 0.5 degree of weathering for the tarballs, being slightly affected by weathering processes.

In addition, the normalization of biomarkers with 17⟨(H),21β(H)-C30 hopane (H30), which is highly recalcitrant, have been used to assess further the possible effects of biodegradation on the *n*-alkanes and isoprenoids (Arekhi et al., 2021). The calculated ratios H30/*n*C17 (0.05 to 0.08), H30/*n*C18 (0.05 to 0.09), H30/Pr (0.13 to 0.23), and H30/Ph (0.08 to 0.15) showed values of RSD 15.80, 15.40, 15.66, and 14.37% (**Fig. 28f** and **Table S7, Appendence A**), respectively, demonstrating that biodegradation likely acted at low extension in these tarballs.

The *n*-alkylcyclohexanes, which were detected in the 16 tarball samples (*a*C13 to *a*C26, **Fig. 28c** and **Fig. S13, Appendence A**), are more resistant to biodegradation when compared to *n*-alkanes and isoprenoids (Martins et al., 2019; Lima et al., 2023). Despite this higher resistance, the ratios H30/DC (0.43 to 0.75) and H30/AC (0.05 and 0.08; Martins et al., 2019; Lima et al., 2023) showed values of RSD 14.88 and 13.36% (**Fig. 28f** and **Table S7, Appendence A**), respectively, corroborating that biodegradation acted in different levels in these samples. The plot between the C30H/Ph ratio and the C30H/DC and C30H/AC ratios (Martins et al., 2019; **Fig. 28d** and **Fig. S14, Appendence A**) showed good correlations, with R^2 indices close to 0.9, which reinforces that these samples were probably affected to different degrees by biodegradation. With the increase in biodegradation, an increase in the values of these ratios are observed (Martins et al., 2019).

Regarding the aromatic compounds, 9-MP is more resistant to microbial biodegradation processes than the 2- and 3-MP isomers. Thus, biodegradation promotes increased ratios 9-MP/3-MP and 9-MP/2-MP (Lima et al., 2023).

Photooxidation may also affect these ratios since 2-MP would be more refractory than other MP isomers (Radovic et al., 2014; Lima et al., 2023). These ratios indicate that biodegradation and photooxidation acted similarly among the 16 tarball samples due to the low variations observed in the values of the ratios 9-MP/3-MP (1.66 to 1.74) and 9-MP/2-MP (1.17 to 1.25) and the low values of RSD 1.40 and 1.62%, respectively (**Fig. 28e** and **Table S7, Appendence A**).

The ratios C20 TAS/C30H and C28 TAS 20S/C30H can be applied to assess the effect of photooxidation on the composition of oils exposed to the environment, as triaromatic steroids are resistant to biodegradation; however, susceptible to photooxidation (Aeppli et al., 2014; Arekhi et al., 2021; Radovic et al., 2014; Wang et al., 2014). The similar values for these ratios among the 16 tarballs (0.12 to 0.15 and 0.26 to 0.31), with low values of RSD 7.50 and 5.45%, respectively (**Fig. 28e** and **Table S7, Appendence A**), indicated that photooxidation was probably not very active since it did not effectively affect the distribution of TAS present in the tarballs.

3.7 Acidic polar compounds by ESI(-) FT-ICR MS

The heteroatomic class distribution obtained from the ESI(-) FT-ICR MS analysis (relative abundance >2%) of the 16 tarball samples is presented in **Fig. 29a** (the heteroatomic class distribution with all classes is presented in **Table S8, Appendence A**). Despite previous analyses using biomarker compounds demonstrating that these samples share the same origin, their relative abundance of the heteroatomic classes varied among the 16 analyzed samples.

Some variations are also observed in the DBE distribution of the most abundant N_1, O_1, and O_2 classes (**Fig. S15, Appendence A**). This is probably due to the high susceptibility of acidic polar compounds (e.g., carboxylic acids, alcohols, and pyrroles) to weathering processes (Chen et al., 2016; Huba and Gardinali., 2016; Lima et al., 2021; Lima et al., 2023).

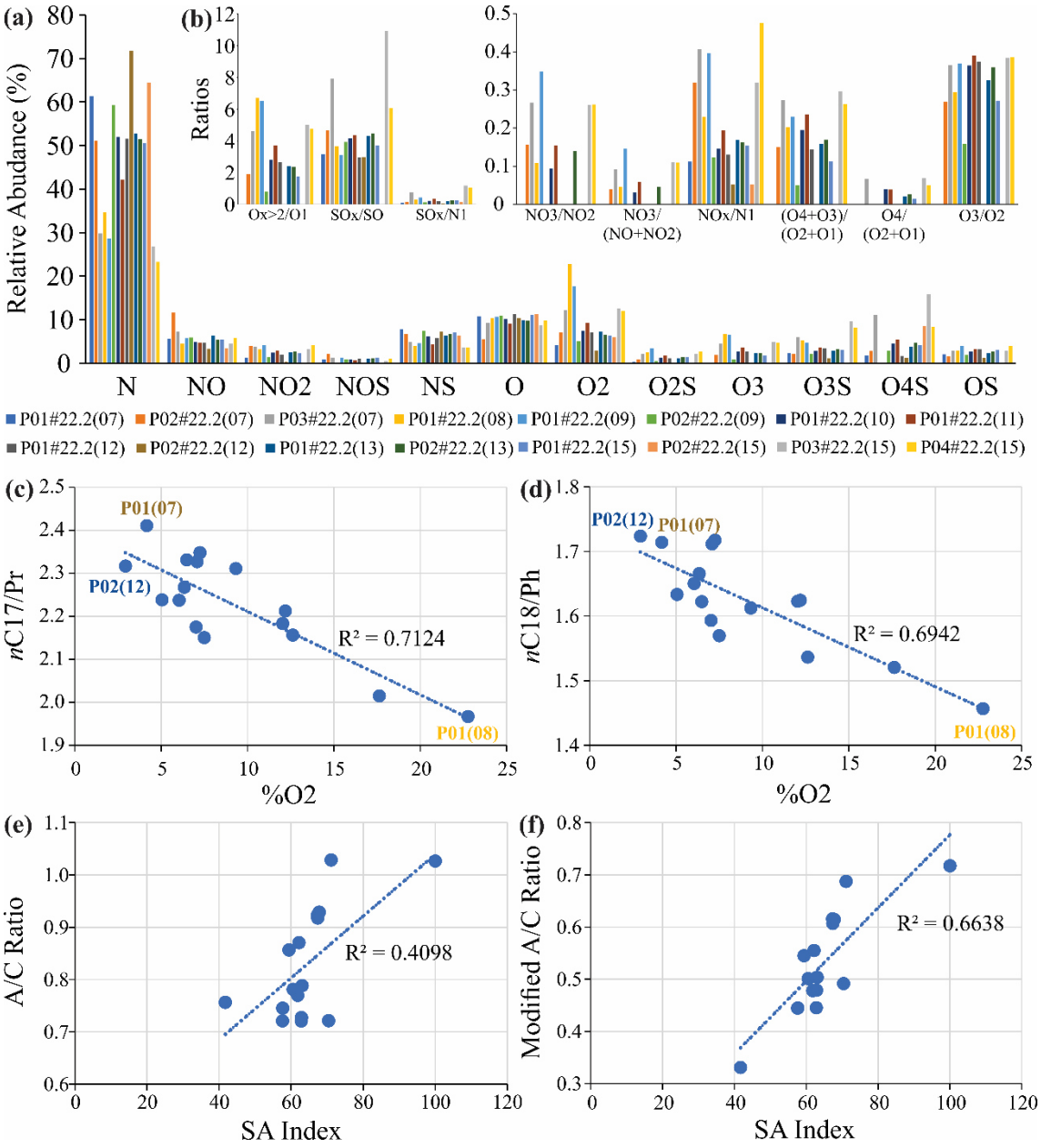

Fig. 29. Heteroatom class distribution of the tarballs assessed by ESI(-) FT-ICR MS (a). Bar charts showing the variation in heteroatom class ratios suggested by Lima et al. (2021) in the 16 tarballs collected on the coast of Brazil in late 2022 (b). Plots of the O_2 (%) obtained by ESI(-) FT-ICR MS against the *n*C17/Pr (c) and *n*C18/Ph (d) obtained by GC-FID. Plots of the SA Index against the A/C ratio

(e) and modified A/C ratio (f), which are biodegradation parameters based on O_2 compounds.

The variation in the abundance of oxygenated classes with more than two oxygen atoms (e.g., O_3, O_4, O_3S, O_4S, NO_3, N_3O_3, and N_3O_3S) in the 16 tarball samples (**Fig. 29a** and **Table S8, Appendence A**) indicate that photooxidation acted at some level in these tarballs since oil exposure to radiation generates an increase in the abundance of oxygenated classes (Aeppli, 2022; Chen et al., 2022; Lima et al., 2021; Zito et al., 2014). This is plausible since these tarballs were drifting on the sea for at least a month, since some of them had a growth Lepas Anatifera attached to them (Mello et al., 2023; Bérgamo et al., 2023), and they fluctuate on seawater, being exposed to the sunlight in Tropical areas.

Several ratios using the heteroatom classes were calculated to further assess the influence of biodegradation and photooxidation on the waxy tarballs. Their significant variation highlights the occurrence of these weathering processes at some extension (**Fig. 29b** and **Table S10, Appendence A**; Lima et al., 2021; 2023). For instance, the higher values for the SO_x/SO and SO_x/N ratios indicate that the P03#22.2(15) sample is probably the most affected by biodegradation. In contrast, the higher $O_{x>2}$/O ratio indicates that sample P01#22.2(08) would be the most affected by biodegradation (Lima et al., 2023). However, the high values of photooxidation ratios [NO_3/NO_2, $NO_3/(NO + NO_2)$, NO_x/N_1, $(O_4+O_3)/(O_2+O_1)$, $O_4/(O_2+O_1)$, O_3/O_2; **Fig. 29b**] obtained for samples P03#22.2(07), P01#22.2(09),

P01#22.2(11), P03#22.2(15), and P04#22.2(15) is an indication that they were probably the most affected by photooxidative processes (Lima et al., 2021).

In addition, the negative correlation in the variation of the O_2 class (%), which increases, and the *n*C17/Pr and *n*C18/Ph ratios (**Fig. 29c** and **d**), which tend to decrease with biodegradation, due to the formation of carboxylic acids and the higher resistance of the isoprenoids over the *n*-alkanes, respectively, corroborate the occurrence of biodegradation at least in low extension. The P01#22.2(08) sample was the most affected by biodegradation, whereas the P01#22.2(07) and P02#22.2(12) samples were the least affected.

The A/C ratio (DBE 1/DBE 2-4; Kim et al., 2005), modified A/C ratio (DBE 1/DBE 2-6; Vaz et al., 2013), which tend to reduce with increasing biodegradation, the SA index (% DBE 1-6; Vaz et al., 2013) and the modified SA index (% DBE 2-6; Martins et al., 2017), which tends to increase with the progression of biodegradation, were also applied to evaluate the effects of biodegradation on the waxy tarballs based on O_2 class. The plot using the SA index and the A/C and modified A/C ratios showed an increasing general tendency (**Fig. 29e** and **f**), with R^2 of 0.41 and 0.66, respectively. Here, it is worth noting an inverse tendency expected to biodegradation, with an increase in the SA index and the A/C ratios (positive correlation), indicating that acyclic acids could be generated, probably due to the paraffin characteristic of these tarballs, rich in *n*-alkanes that tend to be consumed to form fatty acids (Lima et al., 2023). The plot between the % DBE 1 and % DBE 1-6 (**Fig. S16, Appendence A**) facilitates the understanding of this observation, in which it is clear that all acid

compounds, fatty acids, and naphthenic acids, are being formed, probably by biodegradation.

4 Conclusions

The oil residues in the form of tarballs collected from 16 beaches in five states of Brazil in late 2022 have the same source, revealing the extensive coastline affected by the oil spill, with approximately 3,000 km. Additionally, it constitutes a new event with no correlations with the 2019 and early 2022 oil spills. We estimated that more than 42 tons of this new material were stranded on the shore, classifying the event as at least a medium tanker spill. This represents a silent and considerable contamination of the Brazilian coast due to oil discharging into the South Atlantic Ocean.

The tarballs have characteristics of a thermally mature and marine crude oil (not fuel oil). They present waxy aspects and low levels of weathering, including dissolution, evaporation, biodegradation, and photooxidation. This highlights their fate with high persistence even in tropical regions, showing that they can drift for long distances without being significantly degraded, amplifying the extension of contamination. In addition, the assessment of the acidic polar compounds by ESI(-) FT-ICR MS reveals that they suffered biodegradation and photooxidation, at least at the initial extension. They also have a high abundance of fatty acids (acyclic carboxylic acids), consistent with their waxy characteristics.

The comprehensive geochemical assessment of the waxy tarballs, together with the fact that they were drifting on the sea for at least a month due to the presence of the grown marine organisms goose barnacle species Lepas anatifera

attached to them and that they appear in the Northeast of Brazil as a specific event, not having any relationship with previous oil spills, indicated that these tarballs are likely originated from washing processes of ship tanks with crude oil, which were discharged intentionally or accidentally on the open Atlantic Ocean, and brought to the coast of Northeast Brazil by ocean currents.

Acknowledgments

This work was supported by the Federal University of Ceará (UFC) and performed with financial support provided by Fundação de Amparo à Ciência e Tecnologia do Estado de Pernambuco (FACEPE APQ APQ-0036-1.06/20) and Coordenação de Aperfeiçoamento de Pessoal de Nível Superior (CAPES), Brazil. Laercio L. Martins thanks the Postgraduate Program in Tropical Marine Sciences (PPGCMT) and the LABOMAR-UFC for the visiting professor position (Public Notice no. 04/2022 published in the DOU on 01/17/2022). Rivelino M. Cavalcante is grateful for the PQ-2 Grant (315281/2020-0-CNPq), INCT-AmbTropic phase II - oil spill (CNPq Process 465634/2014-1), and project “Dispersants and adsorbents for remediation of coastal areas affected by crude oil spills (Coast of Ceará, Northeast Brazil)” (440868/2020–3), both linked to MCTI Emergency Action to Combat the Oil Spill (2020), as well as Lemae/Finep/CNPq (380975/2022–0), Pronen/FUNCAP/CNPq (Pne-0112-00007.01.00/16), CNPq (440880/2020-3), Pronex (PR2 0101 00008 01 00/15), and also the CECAMP for the analysis of GC-FID.

References

AEPPLI, C., 2022. Recent advance in understanding photooxidation of hydrocarbons after oil spills. Curr. Opin. Chem. Eng. 36, 100763. https://doi.org/10.1016/j.coche.2021.100763

AEPPLI, C., NELSON, R.K., RADOVIC, J.R., CARMICHAEL, C.A., VALENTINE, D.L., REDDY, C.M., 2014. Recalcitrance and Degradation of Petroleum Biomarkers upon Abiotic and Biotic Natural Weathering of Deepwater Horizon Oil. Environ. Sci. Technol. 48, 6726−6734. https://doi.org/10.1021/es500825q

AREKHI, M., TERRY, L.G., JOHN, G.F., CLEMENT, T.P., 2021. Environmental fate of petroleum biomarkers in Deepwater Horizon oil spill residues over the past 10 years. Sci. Total Environ. 791, 148056. https://doi.org/10.1016/j.scitotenv.2021.148056

AZEVEDO, R.A., BEZERRA, K.M.M., NASCIMENTO, R.F., NELSON, R.K., REDDY, C.M., NASCIMENTO, A.P., OLIVEIRA, A.H.B., MARTINS, L.L., CAVALCANTE, R.M., 2022. Is there a similarity between the 2019 and 2022 oil spills that occurred on the coast of Ceará (Northeast Brazil)? An analysis based on forensic environmental geochemistry. Environ. Pollut. 315, 120283. https://doi.org/10.1016/j.envpol.2022.120283

BASTOS, L.P.H., CAVALCANTE, D.C., ALFERES, C.L.F., SILVA, D.B.N., FERREIRA, L.O., RODRIGUES, R., PEREIRA, E., 2022. Fingerprinting an oil spill event (August of 2021) in the oceanic Fernando de Noronha archipelago using biomarkers and stable carbon isotopes. Mar. Pollut. Bull. 185, 114316. https://doi.org/10.1016/j.marpolbul.2022.114316

BÉRGAMO, D.B., SOARES, M.O., CRAVEIRO, N., MAGALHÃES, K.M., ZANARDI-LAMARDO, E., YOGUI, G.T., ROJAS, L.A.V., LIMA, M.C.S., ROSA FILHO, J.S., 2023. Tar balls as a floating substrate for long-distance species dispersal. Mar. Pollut. Bull. 196, 115654. https://doi.org/10.1016/j.marpolbul.2023.115654

BLUMER, M., EHRHARDT AND JONE, J.H., 1973. The environmental assessments fate of Stranded crude oil. Deep-sea Res. 20, 239-259. https://doi.org/10.1016/0011-7471(73)90014-4

BOURBONNIERE, R.A., MEYERS, P.A., 1996. Sedimentary geolipid records of historical changes in the watersheds and productivities of Lakes Ontario and Erie. Limnol. Oceanogr. 41, 352–359. https://doi.org/10.4319/lo.1996.41.2.0352

BUTLER, J.N., WELLS, P.G., JOHSON, S., MANOCK, J.J., 1998. Beach tar on bermuda: Recent observations and implications for global monitoring. Mar. Pollut. Bull. 36, 458-463. https://doi.org/10.1016/S0025-326X(98)00005-8

CARREGOSA, J.C., SANTOS, I.R.D., DE SÁ, M.S., SANTOS, J.M., WISNIEWSKI, A., 2021. Multiple reaction monitoring tool applied in the

geochemical investigation of a mysterious oil spill in northeast Brazil. An. Acad. Bras. Cienc. 93, 1–20. https://doi.org/10.1590/0001-3765202120210171

CHEN, H., MCKENNA, A.M., NILES, S.F., FRYE, J.W., GLATTKE, T.J., RODGERS, R.P., 2022. Time-dependent molecular progression and acute toxicity of oil-soluble, interfacially-active, and water-soluble species reveals their rapid formation in the photodegradation of Macondo Well Oil. Sci. Total Environ. 813, 151884. https://doi.org/10.1016/j.scitotenv.2021.151884

CHEN, H., HOU, A., CORILO, Y.E., LIN, Q., LU, J., MENDELSSOHN, I.A., ZHANG, R., RODGERS, R.P., MCKENNA, A.M., 2016. 4 years after the Deepwater Horizon spill: molecular transformation of Macondo Well oil in Louisiana salt marsh sediments revealed by FT-ICR mass spectrometry. Environ. Sci. Technol. 50, 9061-9069. https://doi.org/10.1021/acs.est.6b01156

CORILO, Y.E., PODGORSKI, D.C., MCKENNA, A.M., LEMKAU, K L., REDDY, C.M., MARSHALL, A.G., RODGERS, R.P., 2013. Oil spill source identification by principal component analysis of electrospray ionization Fourier transform ion cyclotron resonance mass spectra. Anal. Chem. 85, 9064-9069. https://doi.org/10.1021/ac401604u

CORRICK, A.J., HALL, P.A., TREFRY, C., MCKIRDY, D.M., ROSS, S.G.A.S., 2021. The natural hydrocarbon loading of the South Australian coastline. Mar. Pollut. Bull. 166, 112198. https://doi.org/10.1016/j.marpolbul.2021.112198

DIDYK, B.M., SIMONEIT, B.R.T., BRASSELL, S.C., EGLINTON, G., 1978. Organic geochemical indicators of palaeoenvironmental conditions of sedimentation. Nature 272, 216–22. https://doi.org/10.1038/272216a0

EDWARDS, D.S., MCKIRDY, D.M., ROWLAND, S.J., HEATH, D.J., GRAY, P.S., 2018. Waxy bitumen stranding in southern Australia: A geochemical study of multiple oil families and their likely origins. Org. Geochem. 118, 132-151. https://doi.org/10.1016/j.orggeochem.2017.12.010

EMSBO-MATTINGLY, STEPHEN D; ERIC L. Polycyclic aromatic hydrocarbon homolog and isomer fingerprinting. Standard handbook oil spill environmental forensics. Academic Press, 2016. 255-312. https://doi.org/10.1016/B978-0-12-803832-1.00005-2.

G1, 2022. https://g1.globo.com/pe/pernambuco/noticia/2022/10/06/sobe-quantidade-de-bolotas-de-oleo-recolhidas-em-praias-do-litoral-de-pernambuco.ghtml

HAKIMI, M.H., KUMAR, A., SINGH, A.K., LASHIN, A., RAHIM, A., VARFOLOMEEV, M.A., YELWA, N.A., MUSTAPHA, K.A., 2023. Geochemistry and organic petrology of the bituminite shales from the Kapurdi mine, Rajasthan of NW India: implications for waxy oil generation potential. J. Pet. Explor. Prod. Technol. 13, 505–521. https://doi.org/10.1007/s13202-022-01597-9

HEGAZI, H, A., ANDERSSON, T, J., ABU-ELGHEIT, A, M., EL-GAYAR, M.Sh., 2004. Source diagnostic and weathering indicators of tar balls utilizing acyclic, polycyclic and S-heterocyclic components. Chemosphere 55, 1053–1065. https://doi.org/10.1016/j.chemosphere.2004.01.019

HOLBA, A.G., TEGELAAR, E., ELLIS, L., SINGLETARY, M.S., ALBRECHT, P., 2000. Tetracyclic polyprenoids: indicators of freshwater (lacustrine) algal input. Geology 28, 251–254. https://doi.org/10.1130/0091-7613(2000)28<251:TPIOFL>2.0.CO;2

HUANG, W.-Y., MEINSCHEIN, W.G., 1979. Sterols as ecological indicators. Geochim. Cosmochim. Acta 43, 739-745. https://doi.org/10.1016/0016-7037(79)90257-6

HUBA, A.K., GARDINALI, P.R., 2016. Characterization of a crude oil weathering series by ultrahigh-resolution mass spectrometry using multiple ionization modes. Sci. Total Environ. 563, 600-610. https://doi.org/10.1016/j.scitotenv.2016.03.233

ITOPF, 2011. Fate of Marine Oil Spills. Tech. Inf. Pap. 2 - Int. Tanker Owners Pollut. Fed. Ltd. https://www.itopf.org/knowledge-resources/documents-guides/tip-02-fate-of-marine-oil-spills/

KAPLAN, I.R., GALPERIN, Y., LU, S.-T., LEE, R.-P., 1997. Forensic environmental geochemistry: differentiation of fuel-types, their sources and release time. Org. Geochem. 27, 289-317. https://doi.org/10.1016/S0146-6380(97)87941-7

KIM, S., STANFORD, L.A., RODGERS, R.P., MARSHALL, A.G., WALTERS, C.C., QIAN, K., WENGER L.M, MANKIEWICZ, P., 2005. Microbial alteration of the acidic and neutral polar NSO compounds revealed by Fourier transform ion cyclotron resonance mass spectrometry. Org. Geochem. 36, 1117-1134. https://doi.org/10.1016/j.orggeochem.2005.03.010

KRAJEWSKI, L.C., LOBODIN, V.V., JOHANSEN, C., BARTGES, T.E., MAKSIMOVA, E.V., MACDONALD, I.R., MARSHALL, A.G., 2018. Linking natural oil seeps from the Gulf of Mexico to their origin by use of Fourier transform ion cyclotron resonance mass spectrometry. Environ. Sci. Technol. 52, 1365-1374. https://doi.org/10.1021/acs.est.7b04445

KVENVOLDEN, K.A., COOPER, C.K., 2003. Natural seepage of crude oil into marine environment. Geo-Mar 23, 140-146. https://doi.org/10.1007/s00367-003-0135-0

LIMA, B.D., MARTINS, L.L., PEREIRA, V.B., FRANCO, D.M.M., SANTOS, I.R., SANTOS, J.M., VAZ, B.G., AZEVEDO, D.A., CRUZ, G.F., 2023. Weathering impacts on petroleum biomarker, aromatic, and polar compounds in the spilled oil at the northeast coast of Brazil over time. Mar. Pollut. Bull. 189, 114744. https://doi.org/10.1016/j.marpolbul.2023.114744

LIMA, B.D., MARTINS, L.L., SOUZA, E.S., PUDENZI, M.A., DA CRUZ, G.F., 2021. Monitoring Chemical compositional changes of simulated spilled Brazilian oils under tropical climate conditions by multiple analytical techniques. Mar. Pollut. Bull. 164, 111985. https://doi.org/10.1016/j.marpolbul.2021.111985

LIMA, B.D., MARTINS, L.L., SANTOS, L.C., SOUZA, E.S., PUDENZI, M.A., NASCIMENTO, H.L., EBERLIN, M.N., CRUZ, G.F., 2020. Geochemical Investigation of Tar Balls Collected in a Brazilian Beach Using Biomarkers, Ni/V,

δ13C Ratios and Ultra-High Resolution FT-ICR Mass Spectrometry. J. Braz. Chem. Soc. 31, 673-682. https://doi.org/10.21577/0103-5053.20190231

LOURENÇO, R.A., COMBI, T., ALEXANDRE, M.R., SASAKI, S.T., ZANARDI-LAMARDO, E., YOGUI, G.T., 2020. Mysterious oil spill along Brazil's northeast and southeast seaboard (2019–2020): Trying to find answers and filling data gaps. Mar. Pollut. Bull. 156, 111219. https://doi.org/10.1016/j.marpolbul.2020.111219

MARTINS, L.L., SCHULZ, H.-M., NOAH, M., POTZ, S., RIBEIRO, H.J.P.S., CRUZ, G.F., 2021. New paleoenvironmental proxies for the Irati black shales (Paraná Basin, Brazil) based on acidic NSO compounds revealed by ultra-high resolution mass spectrometry. Org. Geochem. 151, 104152. https://doi.org/10.1016/j.orggeochem.2020.104152

MARTINS, L.L., CRUZ, G.F.D., SANTOS, L.C., PUDENZI, M.A., EBERLIN, M.N., 2019. Avaliação da extensão da biodegradação de petróleos brasileiros com ênfase nos *n*-alquilciclohexanos. Quim. Nova 42, 289-295. https://doi.org/10.21577/0100-4042.20170328

MARTINS, L.L., PUDENZI, M.A., DA CRUZ, G.F., NASCIMENTO, H.D., EBERLIN, M. N., 2017. Assessing biodegradation of Brazilian crude oils via characteristic profiles of O_1 and O_2 compound classes: petroleomics by negative-ion mode electrospray ionization Fourier transform ion cyclotron resonance mass spectrometry. Energy Fuel 31, 6649-6657. https://doi.org/10.1021/acs.energyfuels.7b00109

MCKENNA, A.M., NELSON, R.K., REDDY, C.M., SAVORY, J.J., KAISER, N.K., FITZSIMMONS, J. E., MARSHALL, A.G., RODGERS, R.P., 2013. Expansion of the analytical window for oil spill characterization by ultrahigh resolution mass spectrometry: beyond gas chromatography. Environ. Sci. Technol. 47, 7530-7539. https://doi.org/10.1021/es305284t

MCTI, 2022. https://www.gov.br/mcti/pt-br/acompanhe-o-mcti/noticias/2022/09/nota-tecnica-a-imprensa-residuos-de-oleo-encontrados-em-agosto-no-litoral-do-nordeste.

MELLO, L.C., NASCIMENTO, A.P., LOPES, B.D., LIMA, A.D.F., BEZERRA, L.E.A., MENDES, L.F., BASTOS, L.M., NOSSOLD, A.B.S., MARTINS, M.M., MARTINS, L.L., CAVALCANTE, R.M., 2023. Tarballs on the Brazilian coast in late 2022 sustain Lepas anatifera Linnaeus, 1758 (Crustacea: Cirripedia): Occurrence and risk of petroleum hydrocarbon ingestion. Sci. Total Environ. 896, 164981. https://doi.org/10.1016/j.scitotenv.2023.164981

MELLO, M.R., TELNAES, N., GAGLIANONE, P.C., CHICARELLI, M.I., BRASSELL, S.C., MAXWELL, J.R., 1988. Organic geochemical characterization of depositional palaeoenvironments of source rocks and oils in Brazilian marginal basins. Org. Geochem. 13, 31–45. https://doi.org/10.1016/B978-0-08-037236-5.50009-9

OLDENBURG, T.B.P., BROWN, M., BENNETT, B., LARTER, S.R., 2014. The impact of thermal maturity level on the composition of crude oils , assessed

using ultra-high resolution mass spectrometry. Org. Geochem. 75, 151–168. https://doi.org/10.1016/j.orggeochem.2014.07.002

OLIVEIRA, O.M., QUEIROZ, A.F.D.S., CERQUEIRA, J.R., SOARES, S.A., GARCIA, K.S., PAVANI FILHO, A., ROSA, M.L.S., SUZART, C.M., PINHEIRO, L.L., MOREIRA, I.T. 2020. Environmental disaster in the northeast coast of Brazil: forensic geochemistry in the identification of the source of the oily material. Mar. Pollut. Bull. 160, 111597. https://doi.org/10.1016/j.marpolbul.2020.111597

PEREIRA, M.G.A., SANTOS, I.R., LIMA, I.F.S., COUTINHO, M.E.B., CARREGOSA, J.C., WISNIEWSKI, A., SANTOS, J.M., 2023. Geochemical Assessment of Tar Balls That Arrived in 2022 along the Northeast Coast of Brazil and Their Relationship with the 2019 Oil Spill Disaster. Energy Fuel 37, 16388–16395. https://doi.org/10.1021/acs.energyfuels.3c02472

PETERS, K.E., WALTERS, C.C., MOLDOWAN, J.M., 2005. The Biomarker Guide: Biomarkers and Isotopes in the Petroleum Exploration and Earth History, 2nd ed., University Press: Cambridge, vol. 2.

PETERS, K.E., SCHEUERMAN, G.L., LEE, C.Y., MOLDOWAN, J. M., REYNOLDS, R.N., PENA, M.M., 1992. Effects of refinery processes on biological markers. Energy Fuel 6, 560-577. https://doi.org/10.1021/ef00035a005

PHILP, R.P., 1994. Geochemical characteristics of oils derived predominantly from terrigenous source materials. In: Scott, A.C., Fleet, A.J. (Eds.), Coal and Coal-Bearing Strata as Oil-Prone Source Rocks? Geological Society Special Publication 77, pp. 71–91.

PRINCE, R.C., WALTERS, C.C., 2022. Modern analytical techniques are improving our ability to follow the fate of spilled oil in the environment. Curr. Opin. Chem. Eng. 36, 1-8. https://doi.org/10.1016/j.coche.2021.100787

RADOVIĆ, J.R., AEPPLI, C., NELSON, R.K., JIMENEZ, N., REDDY, C.M., BAYONA, J.M., ALBAIGÉS, J., 2014. Assessment of photochemical processes in marine oil spill fingerprinting. Mar. Pollut. Bull. 79, 268-277. https://doi.org/10.1016/j.marpolbul.2013.11.029

REDDY, C.M., NELSON R.K., HANKE, U.M., CUI, X., SUMMONS, R.E., VALENTINE, D.L., RODGERS, R.P., CHACÓN-PATIÑO, M.L., NILES, S.F., TEIXEIRA, C.E.P., BEZERRA, L.E.A., CAVALCANTE, R.M., SOARES, M.O., OLIVEIRA, A.H.B., WHITE, H.K., SWARTHOUT, R.F., LEMKAU, K.L., RADOVIĆ, J.R., 2022. Synergy of Analytical Approaches Enables a Robust Assessment of the Brazil Mystery Oil Spill. Energy Fuel 36, 13688–13704. https://doi.org/10.1021/acs.energyfuels.2c00656

ROSTAMI, S., ABESSI, O., AMINI-RAD, H., 2019. Assessment of the toxicity, origin, biodegradation and weathering extent of petroleum hydrocarbons in surface sediments of Pars Special Economic Energy Zone, Persian Gulf. Mar. Pollut. Bull. 138, 302-311. https://doi.org/10.1016/j.marpolbul.2018.11.034

SEIFERT, W.K. AND MOLDOWAN, J.M., 1980. The effect of thermal stress on source-rock quality as measured by hopane stereochemistry. Phys. Chem. Earth 12, 229–37. https://doi.org/10.1016/0079-1946(79)90107-1

SHINDE, V.L., SUNEEL, V., RATHORE, C., SHENOY, B.D., 2020. Degradation of tarballs using associated bacterial consortia. Biotech 10, 1-10. https://doi.org/10.1007/s13205-020-2095-8

SHINDE, V.L., SUNEEL, V., SHENOY, B.D., 2017. Diversity of bacteria and fungi associated with tarballs: Recent developments and future prospects. Mar. Pollut. Bull. 117, 28-33. https://doi.org/10.1016/j.marpolbul.2017.01.067

SOARES, M.O., TEIXEIRA, C.E.P., BEZERRA, L.E.A., RABELO, E.F., CASTRO, I.B., CAVALCANTE, R.M., 2022. The most extensive oil spill registered in tropical oceans (Brazil): the balance sheet of a disaster. Environ. Sci. Pollut. Res. 29, 19869–19877. https://doi. org/10.1007/s11356-022-18710-4

STOUT, S.A., DOUGLAS, G.S., UHLER, A.D., 2016. Chemical fingerprinting of gasoline and distillate fuels. In Standard Handbook Oil Spill Environmental Forensics (pp. 509-564). Academic Press. http://dx.doi.org/10.1016/B978-0-12-809659-8.00011-5

STOUT, SCOTT A., ZHENDI WANG. Chemical fingerprinting methods and factors affecting petroleum fingerprints in the environment. Standard handbook oil spill environmental forensics. Academic Press, 2016. 61-129. https://doi.org/10.1016/B978-0-12-803832-1.00003-9

STOUT, S.A., WANG, Z., 2007. Chemical fingerprinting of spilled or discharged petroleum – methods and factors affecting petroleum fingerprints in the environment. Oil Spill Environmental Forensics, 1-53. https://doi.org/10.1016/B978-012369523-9.50005-7

TERRA, W.S., MARTINS, L.L., DA CRUZ, G.F., 2019. Avaliação da Eficiência de Diferentes Solventes Orgânicos na Precipitação de Asfaltenos de Petróleos Brasileiros e Análise das Frações Asfaltênicas e Maltênicas por Diferentes Técnicas Instrumentais. Rev. Virtual Quim. 11, 1344-1363. https://doi.org/10.21577/1984-6835.20190093

TEXEIRA, C.C., SIQUEIRA, C.Y.S., AQUINO NETO, F.R., MIRANDA, F.P., CERQUEIRA, J.R., VASCONCELOS, A.O., LANDAU, L., HERRERA, M., BANNERMAMAN, K., 2014. Source identification of sea surface oil with geochemical data in Cantarell, Mexico. Microchem. J. 117, 202-213. https://doi.org/10.1016/j.microc.2014.06.025

UHLER, A.D., STOUT, S.A., DOUGLAS, G.S., HEALEY, E.M., EMSBO-MATTINGLY, S. D., 2016. Chemical character of marine heavy fuel oils and lubricants. In Standard handbook oil spill environmental forensics (pp. 641-683). Academic Press. https://doi.org/10.1016/B978-0-12-803832-1.00013-1

VAZ, B.G., SILVA, R.C., KLITZKE, C.F., SIMAS, R.C., LOPES NASCIMENTO, H.D., PEREIRA, R.C.L., GARCIA, D.F., EBERLIN, M.N., AZEVEDO, D.A., 2013. Assessing Biodegradation in the Llanos Orientales Crude Oils by

Electrospray Ionization Ultrahigh Resolution and Accuracy Fourier Transform Mass Spectrometry and Chemometric Analysis. Energy Fuel 27, 1277−1284. https://doi.org/10.1021/ef301766r

WANG, C., CHEN, B., ZHANG, B., HE, S., ZHAO, M., 2013. Fingerprint and weathering characteristics of crude oils after Dalian oil spill, China. Mar. Pollut. Bull. 71, 64–68. https://doi.org/10.1016/j.marpolbul.2013.03.034

WANG, C., CHEN, B., ZHANG, B., GUO, P., ZHAO, M., 2014. Study of weathering effects on the distribution of aromatic steroid hydrocarbons in crude oils and oil residues. Environ. Sci.: Processes Impacts 16, 2408-2414. https://doi.org/10.1039/C4EM00266K

WANG, Z., FINGAS, M., Page, D. S., 1999. Oil spill identification. J. Chromatogr. A 843, 369-411. https://doi.org/10.1016/S0021-9673(99)00120-X

WANG, Z., FINGAS, M., 1995. Study of the Effects of Weathering on the Chemical Composition of a Light Crude Oil Using GC/MS GC/FID. J. Microcolumn Separations 7, 617-639. https://doi.org/10.1002/mcs.1220070609

WARNOCK, A.M., HAGEN, S.C., PASSERI, D.L., 2015. Marine Tar Residues: a Review. Water Air Soil Pollut 226, 1-24. https://doi.org/10.1007/s11270-015-2298-5

ZAKARIA, P.M., OKUDA, T., TAKADA, H., 2001. Polycyclic Aromatic Hydrocarbon (PAHs) and Hopanes in Stranded Tar-balls on the Coasts of Peninsular Malaysia: Applications of Biomarkers for Identifying Sources of Oil Pollution. Mar. Pollut. Bull. 42, 1357-1366. https://doi.org/10.1016/S0025-326X(01)00165-5

ZHANG, H., WANG, C., ZHAO, R., YIN, X., ZHOU, H., TAN, L., WANG, J., 2016. New diagnostic ratios based on phenanthrenes and anthracenes for effective distinguishing heavy fuel oils from crude oils. Mar. Pollut. Bull. 106, 58-61. https://doi.org/10.1016/j.marpolbul.2016.03.036

ZITO, P., CHEN, H., PODGORSKI, D.C., MCKENNA, A.M., TARR, M.A., 2014. Sunlight creates oxygenated species in water-soluble fractions of Deepwater horizon oil. J. Hazard. Mater. 280, 636-643. https://doi.org/10.1016/j.jhazmat.2014.08.059

CAPÍTULO 3

STUDY OF PETROLEUM RESIDUES ALONG THE CEARÁ COAST IN 2021 AND 2022: FORENSIC GEOCHEMISTRY TO ASSESS CHRONIC SEASHORE POLLUTION IN BRAZIL AFTER THE 2019 OIL SPILL

Artigo 2: *A ser submetido para a Marine Pollution Bulletin*

Abstract

This work aimed to investigate the occurrence, characteristics, and origin of petroleum residues contaminating the beaches of Ceará, Brazil, following the 2019 oil spill, using forensic geochemistry and testing correlation with known oil spill events. Two monitoring surveys were conducted in 2021 and 2022 to collect oil residues from distinct beaches over ~470 km of Brazilian coastline, sampling 19 and 13 oil residues, respectively. Ten spilled oil samples from 2019, 2022.1, and 2022.2 events were also used. Hydrocarbons were assessed by GC-FID and high-temperature GC-FID, saturated and aromatic biomarkers by GC-MS, and acidic polar compounds by ESI(-) FT-ICR MS. Multivariate statistical analysis was performed using PRIMER 7 with the PERMANOVA. Most 2021 and 2022 oil residues have a high abundance of long-chain *n*-alkanes (*n*C29 to *n*C52) and moderate to high unresolved complex mixture (UCM), indicating paraffinic and heavy petrogenic material. Diagnostic ratios based on tricyclic terpanes, steranes, and tetracyclic polyprenoids and principal coordinates and hierarchical clustering analysis showed that only three 2021 and three 2022 oil samples correlated with the 2019 and 2022.1 events, respectively. In addition, the other petroleum residues showed remarkable dissimilarities among them, indicating

multiple sources. PAHs and alkylcyclohexanes were generally not detected in the oil residues, but the triaromatic steranes were, which is similar to heavy petroleum residues. FT-ICR MS analysis also suggests their heavy residue characteristics. We hypothesize that the beached oils are residual waste from ship operations in the Atlantic Ocean dumped in the sea and brought to the Brazilian coast by oceanic currents. This research discloses that toxic petrogenic material has chronically contaminated the coast of Ceará.

Keywords: Oil Spill; Tarball; Coastal Pollution; Organic Geochemistry; Biomarker; FT-ICR MS.

1. Introduction

Crude oil is a critical raw material in contemporary society due to its extensive application as a primary fuel source across various sectors, including electric power generation, industrial processes, and transportation (Singh et al., 2020). Much of society depends on oil products; areas such as transport and industry are examples. Crude oil is available in some parts of the world, and due to the high global demand, it is predominantly transported by sea after it has been extracted. Maritime logistics, therefore, plays an essential role in the global distribution of this material (Govindarajan et al., 2021).

The growing demand for oil exploration and consumption in marine and terrestrial environments has increased the risk of spills caused by pipeline ruptures, ship accidents, and natural seepage, among other factors (ITOPF, 2024). Such incidents release crude oil into the environment, leading to significant ecological

impacts, including food chain contamination and damage to vegetation and coastal resources in marine ecosystems. (Purohit et al., 2024).

Oil spills of unidentified origin, often called "mystery" oil spills, frequently occur in rivers, open waters, and navigable coastal areas (Hettithanthri et al., 2022; Wang et al., 2023). These spills commonly result from accidental or intentional discharges from oil production platforms, floating storage units, coastal oil storage facilities, other industrial installations, as well as barges and vessels in transit (Stout et al., 2007; Ornitz and Champ, 2002; Li et al., 2016). These oil spills, in addition to crude oil, also consist of petroleum products such as light distillates, medium fuels, and heavy residues, each composed of different constituents (Yang et al., 2014). Among the most significant environmental disasters with oil spills in the world are the Deepwater Horizon (2010) and the Gulf War oil spill (1991), which have caused extensive environmental damage (Haseeba et al., 2025). These events released more than four million barrels of crude oil into marine ecosystems, severely impacting wildlife, coastal habitats, and the fishing industry, Environmental Protection Area (EPA; Clement et al., 2017).

In Brazil, the year 2019 is remembered as the most significant environmental tragedy in tropical oceans, when large quantities of oil reached the northeastern and parts of the southeastern coastline of Brazil, impacting over 1,000 locations (IBAMA, 2020). More than 5,000 tons of oil-contaminated residues were removed from affected beaches, mangroves, and coral reefs during this period, reflecting the extensive environmental impact of the spill (Oliveira et al., 2020; Brum et al.,

2020; Lourenço et al., 2020; Reddy et al., 2022; Zacharias et al., 2022). In the years 2020 and 2021, remnants of the oil from 2019 still reached the beaches of northeastern Brazil through the movements of winds and currents (Lima et al., 2023).

In early 2022, oiled materials reappeared mysteriously on the coast of Northeast Brazil, specifically in Ceará (Azevedo et al., 2022; Soares et al., 2022b). Initially, oil spots were found along a 130 km stretch of the eastern coast state, later spreading over 400 km westward (Soares et al., 2022b). Over again, in late 2022, tens of tons of mysterious tarballs were stranded on the northeast coast of Brazil (MCTI, 2022; Mello et al., 2023; Pereira et al., 2023; Nascimento et al., 2025), contaminating many marine and seashore areas. The first oiled materials were found in the State of Pernambuco in late August, reaching the states of Bahia, Sergipe, Alagoas, Paraiba, Rio Grande do Norte, and Ceará in the following weeks in an extension of ~3,000 km (Nascimento et al., 2025). These oils have characteristics of tarballs, which are marine residues with varying color, shape, size, and chemical composition that can originate from natural seepages (Clement et al., 2012; Corrick et al., 2021) or anthropogenic sources due to the release of oil into the ocean (Warnock et al., 2015). They can be formed by liquid petroleum transformed into more consistent oiled material by weathering and other physical processes and can persist in the ocean for a long time (Warnock et al., 2015).

Forensic geochemical investigation of oil spills is essential for finding their provenance, assessing their impact, and improving response strategies. Efficient

analytical methods are crucial for accurately characterizing oil spills and supporting pollution control laws that aim to protect public health and the environment (Kienhuis et al., 2016). Among several techniques, the most widely used to characterize the spilled oils and identify their sources is gas chromatography (GC). Key variables include changes in chromatographic profiles, the presence of a complex unresolved mixture (UCM), and variations in carbon number range (Chua et al., 2020) or coupled to mass spectrometry (MS) (Wang and Fingas, 1997; Rocha et al., 2022) which analyzes the most resistant biomarkers and oil. Additionally, statistical analyses assist in the correlations of the spilled oil with possible sources or other oils (Martins et al., 2024).

In this context, this work aimed to investigate the presence of petroleum residues over the coast of Ceará, Northeast of Brazil, in 2021 and 2022, assessing their characteristics and origin in a forensic geochemistry approach. It is also the aim to assess their fingerprint and their correlation with the oils of the known spill events of 2019, early 2022, and late 2022.

2. Materials and methods

2.1. Samples

The oil samples investigated in this work include 19 and 13 petroleum residues collected during two surveys conducted in 2021 and 2022, respectively, covering most of the extension of the State of Ceará (~488.28 km), Northeastern Brazil, as presented in the map in Figure 1 and detailed described in Table S1. In addition, ten oil samples from knowing oil spill events on the coast of Brazil were assessed, including four samples from the 2019 oil spill (Reddy et al., 2022),

three samples from the 2022.1 oil spill (Azevedo et al., 2022), and three samples from 2022.2 oil spill (Nascimento et al., 2025) (**Table S2**, **Appendence B**), totalizing 42 oil samples. Figure 2 shows representative pictures of the samples from the 2022 and 2021 surveys, as well as from the 2019, 2022.1, and 2022.2 events. The 2021 and 2022 petroleum residues were collected in various areas on the beaches of Ceará, including tarballs on the sediments and adhered to rocks (see additional pictures in **Figures S1** and **S2**, **Appendence B**).

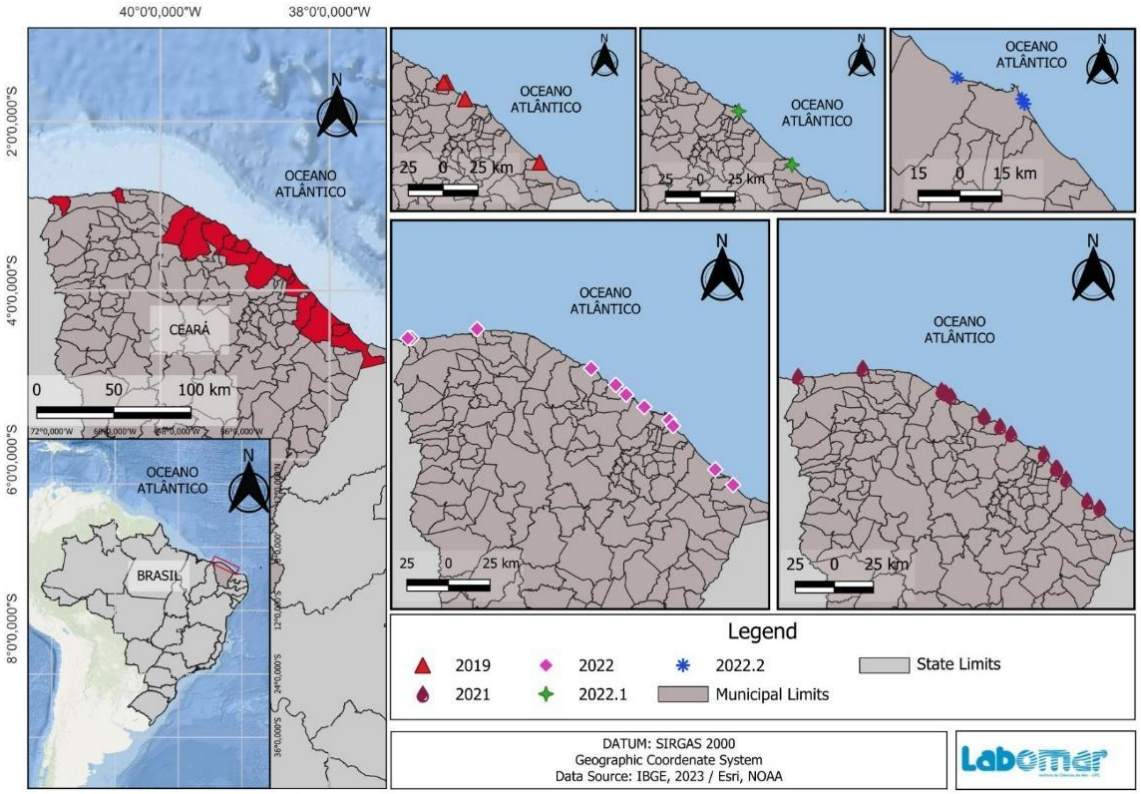

Figure 1. Location of tarballs and spilled oil samples collected in 2019, 2022.1, and 2022.2 events and in the 2021 and 2022 surveys.

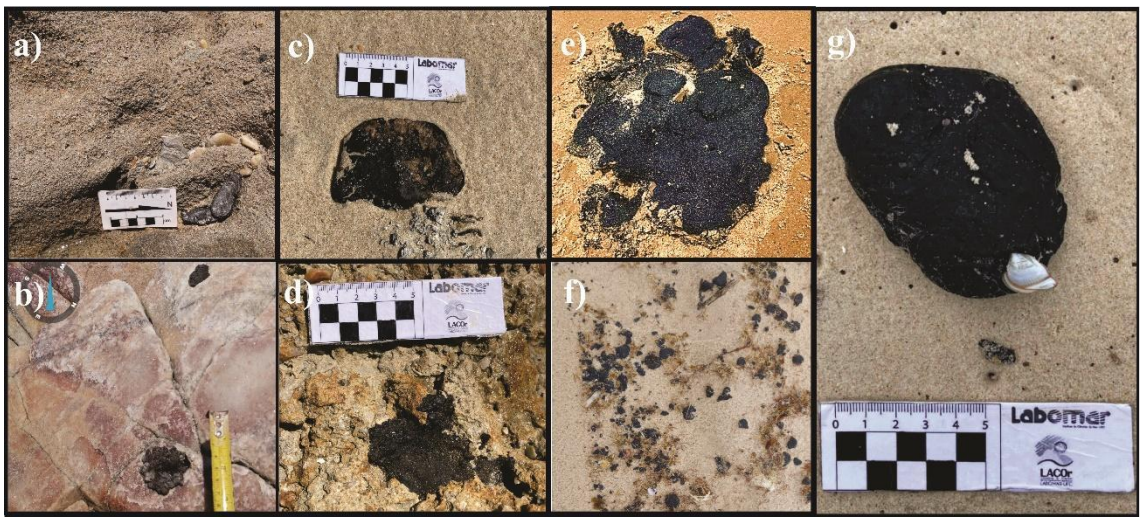

Figure 2. Representative pictures of the petroleum residue samples from the 2021 and 2022 surveys: P21#2021, Caetanos Beach (a); P08#2021(02), Sabiaguaba Beach (b); P03#2022(03), Paracuru Beach (c); P02#22(03)S03, Taíba Beach; and the 2019, 2022.1, and 2022.2 events collected over the Ceará coast: (d); P01#2019, Paracuru Beach (e); P05#22.1(01), Canoa Quebrada Beach (f); P07#22(02), Icaraí Beach (g).

1.1. Extraction and separation

Oil extraction was performed with approximately 1.0 g of the oil sample mixed with sediment, using dichloromethane as a solvent, which was stirred, centrifuged, and the organic phase was stored in a round-bottomed flask where the solvent was roto evaporated (Carregosa et al., 2021). Asphaltene precipitation was performed from 300 mg of oil, using 12 mL of *n*-hexane as solvent through an ultrasonic bath for 10 min, followed by centrifugation. The maltene fraction was removed, and the precipitated asphaltene was washed five times with 12 mL of *n*-hexane to ensure maximum maltene recovery (Martins et al., 2021), then roto-evaporated.

For the fractionation of maltene into saturate, aromatic, and resin fractions by liquid chromatography, 40 mg of maltene was used, in which each fraction was

eluted with *n*-hexane, *n*-hexane:dichloromethane (8:2, v:v) and dichloromethane:methanol (9:1, v:v), respectively (Terra et al., 2019). After collecting the fractions, they are taken to the rotary evaporator to remove the solvents. All solvents are chromatographic/HPLC grade from Sigma-Aldrich Chemical.

1.2. GC-FID

Gas chromatography with a flame ionization detector (GC-FID) was used for the analysis of *n*-alkanes and isoprenoids. The GC-FID was equipped with a Thermo Focus GC system with an Agilent J&W DB-5 capillary column (30 m × 0.25 mm i.d. × 0.25 μm df). Nitrogen served as the attractor gas at a constant flow rate of 1 mL min^{-1}. The GC oven program included an initial isothermal phase at 50 °C for 5 min, followed by heating at 6 °C min^{-1} to 310 °C, with a final hold at 310 °C for 17.67 min, for a total of 63 minutes. The injector temperature was 280 °C, where the FID operated at 300 °C. Splitless mode (1 μL) was used for sample injections using HPLC-grade *n*-hexane as the solvent. Analytical standards, including the Hydrocarbon Window Defining Standard (DRH-008S-R2) containing *n*-alkanes and isoprenoids, were obtained from AccuStandard.

1.3. High-temperature GC-FID

High-temperature gas chromatography (HT-GC), which employs advanced thermally stable GC columns and operates at oven temperatures up to 470°C, enables routine analysis of hydrocarbons ranging from C35 to C120, commonly

found in petroleum and related substances (Philp et al., 2015; Pereira et al., 1999; Coto et al., 2011). For detection, a flame ionization detector (FID) with a flame of air and hydrogen 2mL min^{-1} with a temperature of 400 ºC was used. Injection mode of 370 ºC, splitless with column DB-5HT (30 × 0,25mm × 0.10 µm). Injection starts at 100 °C maintained for 2 minutes, followed by heating at 10 °C min^{-1} up to 380 °C. Solvent used to solubilize the samples: carbon disulfide (CS_2).

1.4. GC-MS

The saturated and aromatic hydrocarbon fractions were analyzed using a quadrupole mass spectrometer (Agilent Technologies 5973) coupled to a gas chromatograph, equipped with a splitless injector (300 °C, 0.8 min purge). A 1 µL aliquot of each fraction was injected into an HP-5MS capillary column (30 m × 0.25 mm × 0.25 µm, 5% phenyl–95% methylpolysiloxane; details in Nascimento et al.[11]), with helium as the carrier gas at a constant flow rate of 1.0 mL min^{-1}. For the saturated hydrocarbons, the GC oven was programmed from 60 °C (2 min), ramped at 22 °C min^{-1} to 200 °C (3 min), then at 3 °C min^{-1} to 300 °C, held for 25 min. For aromatic fractions, the program was 70 °C (1 min), ramped at 22 °C min^{-1} to 110 °C (1 min), 1.5 °C min^{-1} to 200 °C, and finally 3 °C min^{-1} to 300 °C (10 min isotherm). The MS was operated in full scan mode (50–550 Da) and selected ion monitoring (SIM) mode, with compound identification based on published mass spectra (Martins et al., 2023; Lima et al., 2021). Data were acquired in full scan and single ion monitoring (SIM) modes. In SIM mode, *m/z* 83, 85, 191, and 217 were monitored to detect alkylcyclohexanes, *n*-

alkanes/branched hydrocarbons, tri- and pentacyclic terpanes, and steranes/diasteranes, respectively. For aromatic compounds, *m/z* 178, 192, 231, and 259 were monitored to quantify phenanthrene, anthracene, methylphenanthrenes, methylanthracene, and triaromatic steroids (TAS).

2.6. FT-ICR MS

To evaluate the polar acidic compounds, the extracted total oil was analyzed by ESI(-) FT-ICR MS, where 10 mg of oil was dissolved in 10 mL of toluene. From the stock solution for ESI(-) analysis, 500 µL were collected and transferred to a vial containing 500 µL of methanol with 25 µL (2.5%) of NH_4OH. All solvents used were HPLC grade purchased from J. T. Baker (Phillipsburg, NJ, USA) and Sigma-Aldrich (Steinheim, Germany), respectively. FT-ICR MS were acquired using a 7T SolariX 2xR (Bruker Daltonics - Bremen, Germany) coupled to the negative mode ESI source. The drying gas used was nitrogen with a flow rate of 4.0 L min^{-1}, a temperature of 200 °C, and nebulization gas with 1.0 bar.

Composer64 software (version 1.5.3 Sierra Analytica, Modesto, 196 USA) was used in the processing step, where molecular formulas were initially assigned to the recalibrated spectra. The processing conditions were similar for all samples. However, the intensity threshold, minimum abundance and new minimum abundance parameters varied according to the noise intensity of each spectrum. These three parameters were used to define a relative abundance limit so that only molecular formulas were assigned to peaks with intensity greater

than the pre-established limit. The allowed elements were ^{12}C, ^{1}H, ^{16}O, ^{14}N, and ^{32}S. The maximum allowed error of the formula was 0.5 ppm.

1.5. Statistical analysis

Multivariate statistical analysis of the diagnostic parameters used the diagnostic ratios of the 42 oil samples based on resistant biomarkers (terpanes and steranes) was performed using PRIMER 7 with the PERMANOVA add-on for data processing.

2. Results and discussion

2.1. Occurrence and characterization of the petroleum residues

During the spilled oil monitoring and collection surveys carried out in 2021 and 2022 on 13 and 10 beaches along the coast of Ceará, Brazil, a considerable amount of dark material similar to petroleum and its products was observed (**Figures 2**, **S1**, and **S2**, **Appendence B**). These oiled materials were on the beach sands or attached to beach rocks. They were usually black or dark brown, and the appearance was mostly very dry and weathered. In order to investigate if they are, in fact, petrogenic, in addition to their characteristics, origin, and possible correlation with previous oil spills on the Brazilian coast, 19 oil samples were collected during the 2021 survey, and 13 oil samples were collected during the 2022 survey (**Figure 1** and **Table S1**, **Appendence B**). For this, their chemical fingerprints were comprehensively assessed by GC techniques.

Similar monitoring was performed by Bontempo Filho et al. (2022) fourteen months after the 2019 oil spill, and various oil residues were found mixed with sand and adhered to rocks. They concluded that the oil residues are evidence of 2019 spilled oil persistence on the beaches. However, no chemical or geochemical assessment was performed to evaluate their correlation with the 2019 oil spill, although they suggested that in future research on that, to discard confusion from contaminants from ships navigating near the coastline zone of Brazil.

In general, the GC-FID chromatograms of 2021 and 2022 petroleum residues presented a high abundance of *n*-alkanes homologs series and considerable UCM, confirming their petrogenic nature (**Figures S3** and **S4**, **Appendence B**). The monitoring samples present a variable profile, with a distinct range of *n*-alkanes and UCM shapes, that can indicate different sources or exposure time in the environment, leading to distinct weathering levels. UCM is the lift of the baseline in the gas chromatogram (Wang et al., 2006). The UCM consists mainly of linear hydrocarbon chains connected at one or more branch points, providing strong evidence for petroleum contamination in sediment or water samples (Azevedo et al., 2007). The presence of UCM is one of the primary hints of contamination related to petroleum (Reddy et al., 2000).

In addition, most of the GC-FID chromatograms (**Figures S3** and **S4**, **Appendence B**), often called oil fingerprints from 2021 and 2022 surveys, presented related profiles, indicating that the samples may share a common source of waste. In all samples, the low molecular weight *n*-alkanes were not

detected (<*n*C31), and the isoprenoids pristane (Pr) and phytane (Ph) and a medium to high UCM, which could be attributed to the weathering processes such as evaporation and biodegradation (Lima et al., 2023). However, the medium to high *n*-alkanes (*n*C31 to *n*C41) are present in high abundance in these samples, which is not a usual profile for weathering samples. Moreover, normal alkanes degrade at faster rates than the isoprenoids (Peters and Moldowan, 2005; Stout and Wang, 2016). This profile may be related to petroleum products produced from crude oil distillation processes (Fingas et al., 2016) since the abundance and distribution profiles of petroleum hydrocarbons in organic petroleum products are often altered by the distillation and refining processes of their original feedstock oils (Yang et al., 2013). In addition, some of these samples present a bimodal UCM, characteristics of blended oils used as fuel (Douglas et al., 2016; Fingas, 2016).

A significant reduction in the abundance of *n*-alkylcyclohexanes was also observed for all oil samples from 2021 and 2022 monitoring (**Figures S7** and **S8, Appendence B**), corroborating the central hypothesis of a distillation cut. However, the possibility of absence due to the weathering process cannot be ruled out.

The presence of a high abundance of high molecular weight *n*-alkanes ranging from (*n*C31 to *n*C41) in the petroleum residues indicates a paraffinic material in accordance with their whitish saturated fraction (Nascimento et al., 2025). Similar profiles were observed in a tarball collected from the coast of the Bahia state in 2019 by Lobão et al. (2022) and in Ceará in 2019 by Reddy et al.

(2022). The waxy characteristics make these petrogenic contaminants even more resistant to weathering and persistent in the environment (Lourenço et al., 2020).

Three samples from the 2021 survey (P03#21, P07#21, and P08#21; **Figures 3a**, **S1b**, and **S1f**, **Appendence B**) presented distinct profiles from the others with no predominance of long-chain *n*-alkanes, in addition to no whitish saturated fraction. P03#21 sample presented no *n*-alkanes, while P07#21 and P08#21 samples presented medium to long-chain *n*-alkanes (*n*C17 to *n*C40). They all presented unresolved complex mixture (UCM), which can be related to weathering processes, such as biodegradation (Ramadass et al., 2020) or related to their genesis as the 2019 spilled oil that was already biodegraded and heavy before being spilled in the ocean (Reddy et al., 2022; Lima et al., 2023). Unlike the other samples, these three 2022 samples (P01#22(02), P02#22(02), and P02#22(03) S03) presented a GC-FID profile (**Figures 3c**, **S4g**, and **h**, **Appendence B**) different from the other samples monitored in 2022, with a profile ranging from *n*C17 to *n*C41 and a high UCM.

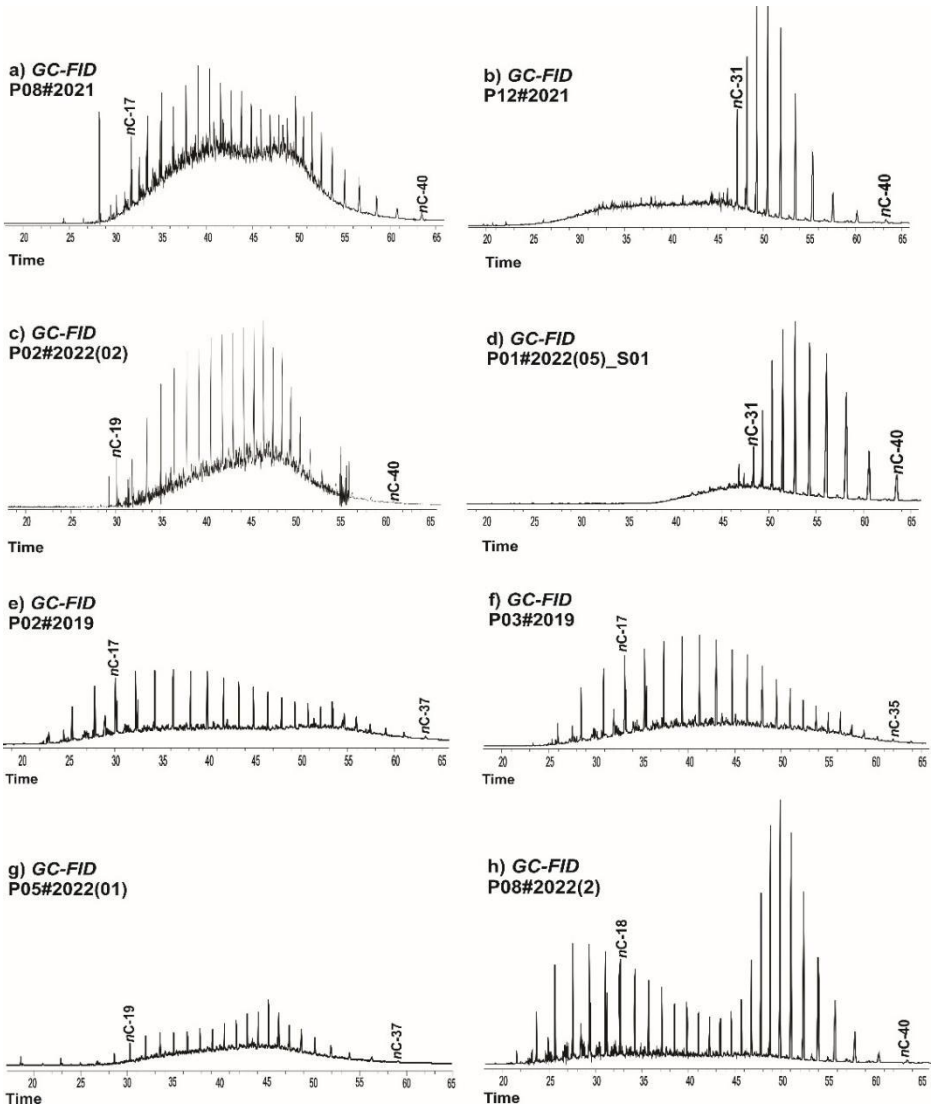

Figure 3. Representative gas chromatographic profiles from GC-FID comparing the oil samples collected on the coast of the state of Ceará in 2019, 2021, 2022.1, 2022.2, and 2022.

The spill events (**Figures 3e**, **g**, and **h**, **Appendence B**), respectively, P02#2019, P05#2022(01), and P08#2022(02) present distinct profiles, where sample P02#2019 (**Figure 3e**) presents a distribution of components with a carbon number range from *n*C13 to *n*C40, with normal *n*-alkanes and many other well-resolved compounds, over a smooth and continuous UCM.

The GC-FID chromatograms of the year 2019 did not exhibit a bimodal distribution, a characteristic that typically indicates mixtures of different types of oil or mixtures with background biogenic organic matter (Reddy et al., 2020; Lobão et al., 2022). Sample P05#22(01) (**Figure 3g**, **Appendence B**) has a GC-FID chromatographic profile with n-alkanes ranging from (*n*C17 to *n*C37), and the isoprenoids pristane (Pr) and phytane (Ph) occurring in very low abundances or not detected (Azevedo et al., 2022). The absence of low molecular weight hydrocarbons (<C17) in the chromatograms is probably due to evaporation, a predominant weathering process that initially degrades spilled oils exposed to the environment (Stout et al., 2016; Albaigés et al., 2018; Lima et al., 2021; Filewood et al., 2022). Moreover, the samples from 2019 and early 2022 are related to heavy fuel oil, originating from the mix of residual oil and a light cut (Azevedo et al., 2025; Reddy et al., 2019).

The sample P08#2022(2) presented a bimodal profile with *n*-alkanes range of (*n*C12 to *n*C40; **Figure 3h**, **Appendence B**), maximizing at *n*C17 and *n*C33. The high abundance of long-chain *n*-alkanes (*n*C31 to *n*C40) confirms its waxy characteristic and, together with the absence of UCM detection, also points to poorly weathered tarballs. Similar characteristics were observed by Pereira et al. (2024) and Nascimento et al. (2025) in tarballs spilled on beaches of the northeastern Brazilian coast and beaches in Australia (Edwards et al., 2017).

The petroleum residues monitored in 2021 and 2022 presented very peculiar characteristics, such as the presence of long-chain *n*-alkanes (> *n*C40); these oils presented a whitish saturated fraction, characterizing these oils as paraffinic.

Studies show that wax concentrates from several crude oils revealed an extremely complex mixture of hydrocarbons with C numbers much higher than C40, including *n*-alkanes, *n*-alkylcyclohexanes, *n*-alkylcyclopentanes, and several series of branched hydrocarbons, representing a significant fraction of the total oil, and when well preserved, they are relatively resistant to biodegradation (Hsieh et al., 2000; Boukadi et al., 2005.; Suaria et al., 2018).

The oil samples monitored in 2021 and 2022 (**Figure S6c** and **f, Appendence B**) subjected to HT-GC analysis shows significant concentrations of high molecular weight hydrocarbons, ranging from *n*C31 to *n*C45. These waxes can be characterized as microcrystalline waxes, dominated by high molecular weight hydrocarbons HMWHCs above > *n*C40, being the main contributors to the sludge at the bottom of the tank (Boukadi et al., 2005; Carlson et al., 1994; Misra et al., 1995.; Philp et al., 2015). These samples presented their saturated fraction whitish, thus indicating a paraffinic characteristic.

3.2. Similarity and origin of the petroleum residues

3.2.1. Correlation of the oils using saturated biomarkers

To investigate the correlation of the petroleum residue samples collected in 2021 and 2022 with other events that occurred in the state of Ceará in 2019, early 2022, and late 2022, diagnostic ratios based on resistant saturated biomarkers analyzed by GC-MS were calculated, and their values compared among the samples. These ratios were already applied in previous works investigating oil spills in Brazil (Lima et al., 2023; Martins et al., 2024; Nascimento et al., 2025), and it was shown to be very useful. Thus, twelve diagnostic ratios were applied

in this forensic geochemical study (**Tables S3**, **S4**, **S5**, and **S6**, **Appendence B**) using tricyclic and pentacyclic terpanes (*m/z* 191), steranes (*m/z* 217), triaromatic steroids (TAS, *m/z* 231), and tetracyclic polyprenoids (TPPs, *m/z* 259).

Among the 19 samples monitored in 2021, only P03#21, P07#21, and P08#21 samples presented a correlation with the 2019 oil spill samples (**Figure 4a**). Their mass chromatograms *m/z* 191 (**Figure S9b**, **e**, and **f**, **Appendence B**) with the terpanes distributions showed a noticed high abundance of the tricyclic terpane (Tr23), which constitutes a chemical signature that associates them with Venezuelan oil (Azevedo et al., 2022; Oliveira et al., 2020; Reddy et al., 2022). In addition, they have a significantly higher abundance of C30 hopane (H30) in comparison to the C29 hopane (H29), of 18α-22,29,30-trisnorneohopane (Ts) and 17α-22,29,30-trisnorhopane (Tm) (**Figure S9b**, **Appendence B**).

The relative standard deviation (RSD) values ranged from 2.39 to 19.82% (**Figure 4a**), thus demonstrating a positive correlation with the 2019 event. However, the high RPD value of the C28 20S/(20S + 20R) steranes ratio is more susceptible to biodegradation (Peters and Moldowan, 2005). Seven samples monitored in 2021 (**Figure 4c**) showed a correlation with each other. However, the high RSD values (18.7 to 138.8% for tricyclics, terpanes, and steranes) may be related to the susceptibility of these compounds to biodegradation (Arekhi et al., 2021). It can also be observed that the samples (**Figure S16a** and **b**, **Appendence B**) did not correlate with the 2019 and 2022.1 events or with themselves, indicating that these oily residues are from different sources and underwent weathering processes that modified their characteristics (Harriman et

al., 2017; Aeppli et al., 2012). These results show that most oily materials were not related to the known oil spill event of 2019 as expected (Bontempo Filho et al., 2022) but have multiple possible sources.

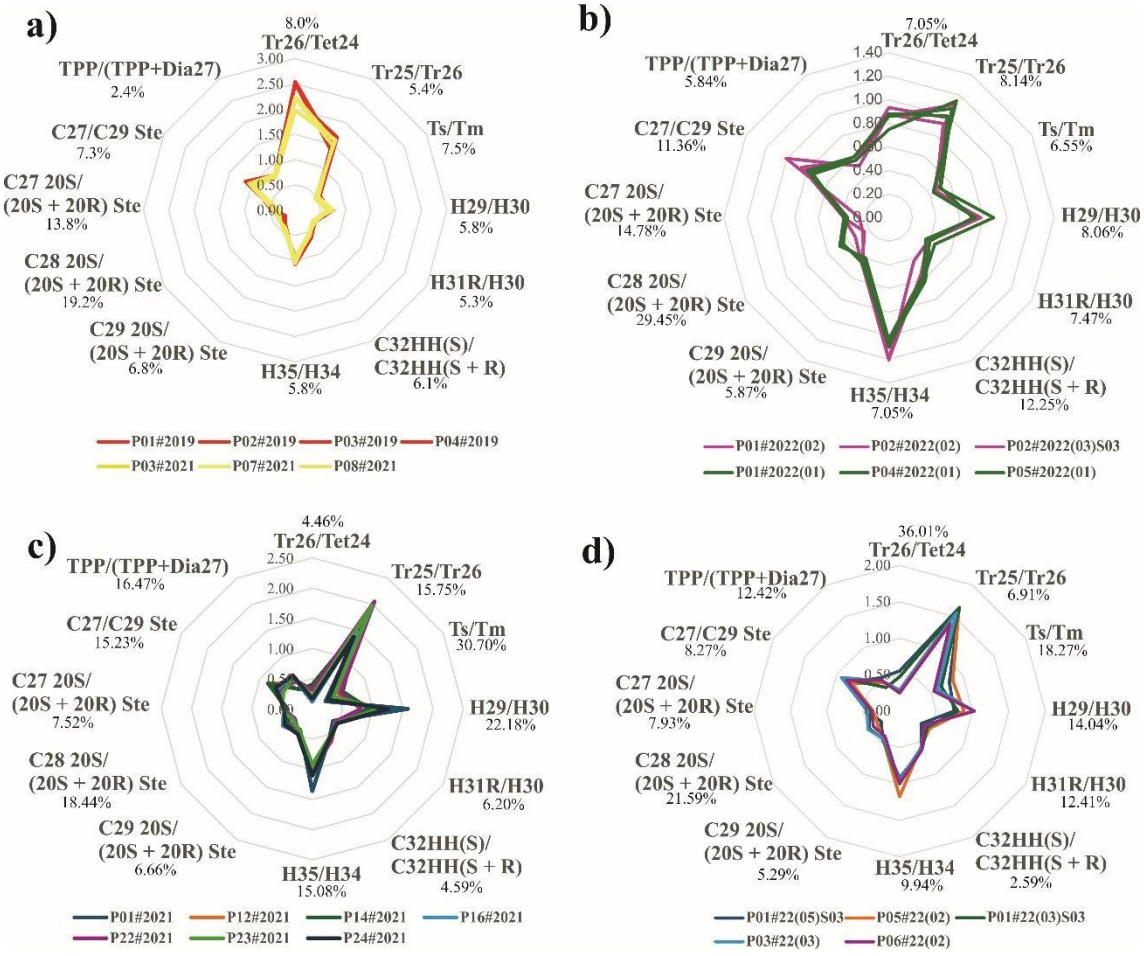

Figure 4. Radar plots comparing the diagnostic ratios based on the terpanes, steranes, and tetracyclic polyprenoids among the petroleum residue samples and the spilled oil samples from the 2019 and 2022 known events: correlation between the 2021 oil residues and the 2019 spilled oils (a); correlation between the 2022 oil residues and the 2022.1 spilled oils (b); correlation among seven 2021 oil residues (c); correlation among five 2022 oil residues (d).

Among the 13 samples monitored in 2022, only P01#2022(02), P02#2022(02), and P02#2022(03)S03) samples showed a correlation to the oils

spilled in early 2022 (**Figure 4b**) Remarkable similarities were observed in their mass chromatograms *m/z* 191, 217, and 259, related to the terpanes, steranes, and TPPs. The C30 hopane showed greater abundance compared to the C29 hopane. The C23 tricyclic terpanes (Tr 23) were in low abundance, and C24 tetracyclic terpane (Tet 24) showed greater abundance than the C26 tricyclic terpane isomers (Tr 26). These relationships show their correlation (Azevedo et al., 2022). C27 and 28 steranes with high RSD values, between 16.16% and 30.14%, may be related to the susceptibility of these compounds to weathering processes. One more group was formed based on the similarity of the samples from the 2022 monitoring (**Figure 4d**), demonstrating the extent of the multiple residues and oils released into the environment. Like that was observed for the samples from the 2021 monitoring, these results show that most of the oily materials collected in 2022 were not related to the known oil spill event of 2022 as expected but have multiple possible sources and are contaminating the coast of Brazil regularly.

The identification of the similarity of the petroleum residue samples collected in 2021 and 2022 through the multivariate PCO and HCA analyses of all oils confirmed what the biomarkers diagnostic ratios showed, the samples monitored in the years 2022 (P01#22(02), P02#22(02), and P02#22(03)_S03) grouped with the samples from the 2022.1 event and the samples P03#21, P07#21, and P08#21, grouped with the samples from the 2019 event (**Figure 5a** and **b**).

The samples from the 2021 and 2022 surveys that grouped among themselves using the biomarker compounds also showed similarities through the multivariate PCO and HCA (**Figure 5a** and **b**). The multivariate analysis confirms the existing correlations between the groups. However, the Tr26/Tec24 ratios and Tr25/Tr26 differed the most in the groups, which may be related to the weathering processes suffered by these oil residues. Another important piece of information is that the vast majority of samples that were statistically treated were samples collected two years after a major event that was in 2019. These samples remained in these environments being degraded by the weathering processes, thus leading to the modification of their characteristics.

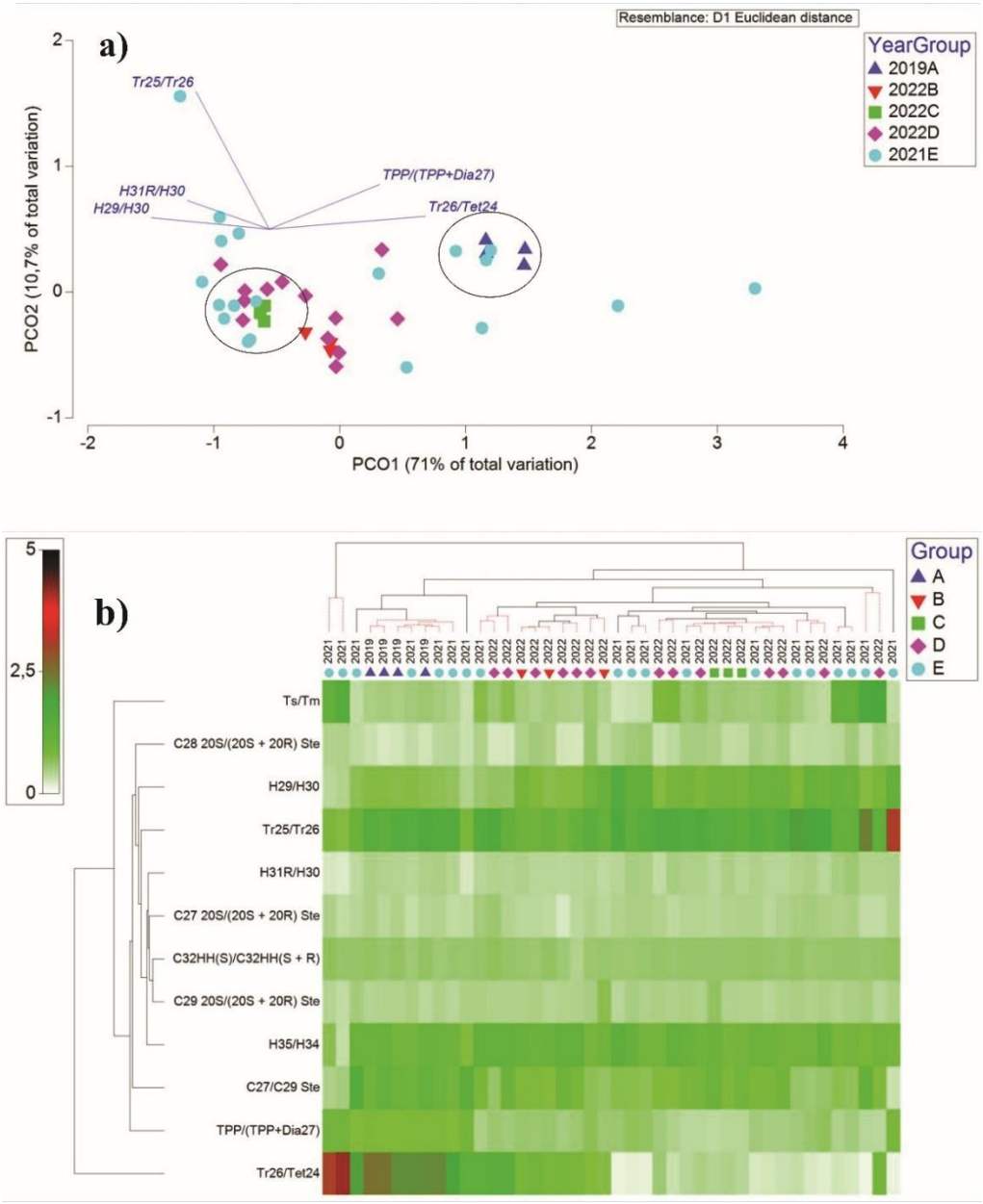

Figure 5. Principal component analysis (PCO) and Cluster analysis (HCA) showing relationships for everyone samples monitored in 2021 and 2022, from events in 2019, 2022.1 and 2022.2.

3.2.2. Correlation of the oils using the aromatic compounds

The chromatographic profile of the samples collected in 2022 and 2021 that do not correlate with the events of 2019 and 2022 present a very peculiar characteristic, with the presence of long-chain *n*-alkanes ranging from *n*C31 to

*n*C40, observed by GC-FID (**Figures S3** and **S4**, **Appendence B**). These samples that presented cuts in their profiles also showed a marked decrease in the abundance of *n*-alkylcyclohexanes (*m/z* 83) (**Figures S7** and **S8**, **Appendence B**), remaining predominantly high molecular weight *n*-alkanes. This compositional change may indicate that these oils underwent biodegradation processes, preferentially removing more labile compounds with lower molecular weight (Peters et al., 2005; Lima et al., 2019).

As the samples monitored in 2021 and 2022 were collected in a coastal region of Northeastern Brazil, where the semi-arid tropical climate is predominant, with high temperatures, intense solar radiation, and long periods of drought, these conditions favored the evaporation of volatile compounds and the oxidative degradation of hydrocarbons, where compounds such as *n*-alkylcyclohexanes tend to be rapidly degraded or removed (Lima et al., 2021).

The samples monitored in 2021 and 2022 that presented cuts with the absence of light and medium *n*-alkanes and the presence of high molecular weight *n*-alkanes also present a similar trend in the polycyclic aromatic hydrocarbons (PAHs) profile. The full scan mode showed that the conventional low and medium molecular weight PAHs were not detected (**Tables S7** and **S8; Figures S13** and **S14**, **Appendence B**), unlike the samples associated with known events (2019 and 2022.1), which presented a significant presence of these compounds already studied by Reddy et al. (2022), Azevedo et al. (2022), Nascimento et al. (2025), and Pereira et al. (2024). The compositional profile depleted in PAHs corroborates the possibility that these petroleum residues have

undergone some degree of refining, given the simultaneous absence of low molecular weight *n*-alkanes and PAHs, which is typical of derived products and not of crude oil (Wang et al., 1999).

These oils may be a mixture of distilled residues of petroleum derivatives such as lubricating oils that are distinguished from other refined products by presenting a UCM eluted in a range of high-boiling point hydrocarbons, where these oils generally contain very low concentrations of low molecular weight *n*-alkanes and aromatic compounds (Yang et al., 2016).

The monitored samples that correlated with the 2019 event (P03#2021, P07#2021, and P08#2021) and 2022.1 event (P01#2022(02), P02#2022(02), and P02#2022(03)SO3) also present a similar profile in the PAHs chromatogram. In general, they are characterized by the presence of the conventional aromatic compounds present in oil samples, such as phenanthrenes, dibenzothiophenes, chrysene, and their alkyl compounds, not detected in the other samples from the 2021 and 2022 monitoring (**Tables S7** and **S8; Figures S13** and **S14**, **Appendence B)**. The diagnostic ratios calculated using these PAHs compounds and the triaromatic steranes (TAS) corroborate their similarity. For the three 2021 oil samples that correlate with the 2019 event, only two of the ten ratios present an RSD higher than 10% (**Figure 6a**). For the three oil samples from the 2022 monitoring that correlate with the 2022.1 event, only three of the ten ratios present an RSD higher than 10% (**Figure 6a**).

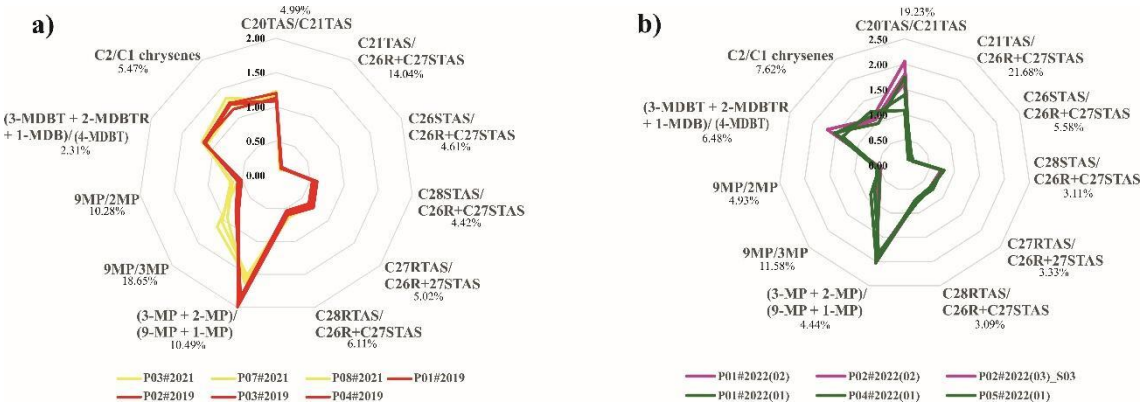

Figure 6. Radar plots comparing the diagnostic ratios based on the PAHs compounds and in the triaromatic steranes among the petroleum residue samples and the spilled oil samples from the 2019 and 2022 known events: correlation between the 2021 oil residues and the 2019 spilled oils (a); correlation between the 2022 oil residues and the 2022.1 spilled oils (b)

Triaromatic steranes (TAS) were detected in all samples monitored in 2021 and 2022, with medium to high abundance. According to Yang (2013), concentrations of aromatic steroids are particularly high in certain heavy crude oils. They may be undetectable in products derived from the distillation of light petroleum, such as aviation gasoline, kerosene, jet oil, and diesel. Their presence is variable in heavy fuels and lubricating oils, influenced by the refining processes employed, such as fluid catalytic cracking and hydrotreating, which can significantly modify the abundance and distribution of aromatic steroids in refined products.

According to the mass chromatogram *m/z* 231, the samples monitored in 2021 and 2022, which demonstrated geochemical correlation with the 2019 and 2022.1 events, present a cluster of intense peaks corresponding to triaromatic steroids and other polycyclic aromatic hydrocarbons and/or naphthenic

aromatics. The presence of these compounds suggests that the analyzed material may have been subjected to industrial processes, such as thermal or catalytic cracking and fractional distillation, as discussed by Pereira et al. (2023) and Yang et al. (2013). This evidence reinforces the hypothesis that much of the part of the samples does not represent crude oil but products derived from already processed petroleum or a mixture of residues. These results are essential for correctly interpreting the origin and processing history of the oily material found.

3.3. Characterization by ESI(-) FT-ICR MS

3.3.1. Correlation and weathering assessment

Acidic polar compounds (e.g., carboxylic acids, alcohols, and carbazoles) assessed by ESI(-) FT-ICR MS are usually detected in great abundance in spilled oils and can be degraded or formed by weathering processes, such as biodegradation and photooxidation (Chen et al., 2016; Huba and Gardinali., 2016; Lima et al., 2021, 2023). In this work, these polar compounds were evaluated to compare and check possible similarities and differences in the composition of the petroleum residues and spilled oils collected between 2019 and 2022 along the coast of Ceará, Northeastern Brazil. The possible influence of weathering processes on the distribution of acidic polar compounds was also evaluated.

The heteroatom class distribution of polar acidic compounds allowed distinguishing the two surveys (2021 and 2022) and the three oil spill events (2019, 2022.1, and 2022.2) of samples collected between 2019 and 2022 on the

coast of Ceará (**Figure 7a**). For the samples from the 2019 event, N_1 class is predominant, followed by O_2, NS, O_1, and NO classes, respectively (**Figure 7b**). The samples from the early 2022 oil spill (2022.1 samples, **Figure 7c**) are dominated by the compounds from N_1, O_2, O_3, O_1, NO, and NO_2 classes, respectively. For the 2022.2 event, N_1, O_2, O_1, O_4S, and NS classes are predominant (**Figure 7a**). Some differences observed in the class distribution of samples from the same oil spill event can be attributed to the susceptibility of acidic compounds to weathering processes, such as photooxidation and biodegradation (Chen et al., 2016; Lima et al., 2021, 2023).

With these results, the heteroatom class distribution of oil residues and spilled oils revealed a significant variation in acidic composition among the samples, which could be related to different sources or due to weathering processes. The similarities in the class distribution among the samples collected in 2019, 2022.1, and 2022.2 events (**Figure 7a** to **c**) corroborate with the biomarker analyses shown in this work and the previous studies (Azevedo et al., 2022; Nascimento et al., 2025; Reddy et al., 2022).

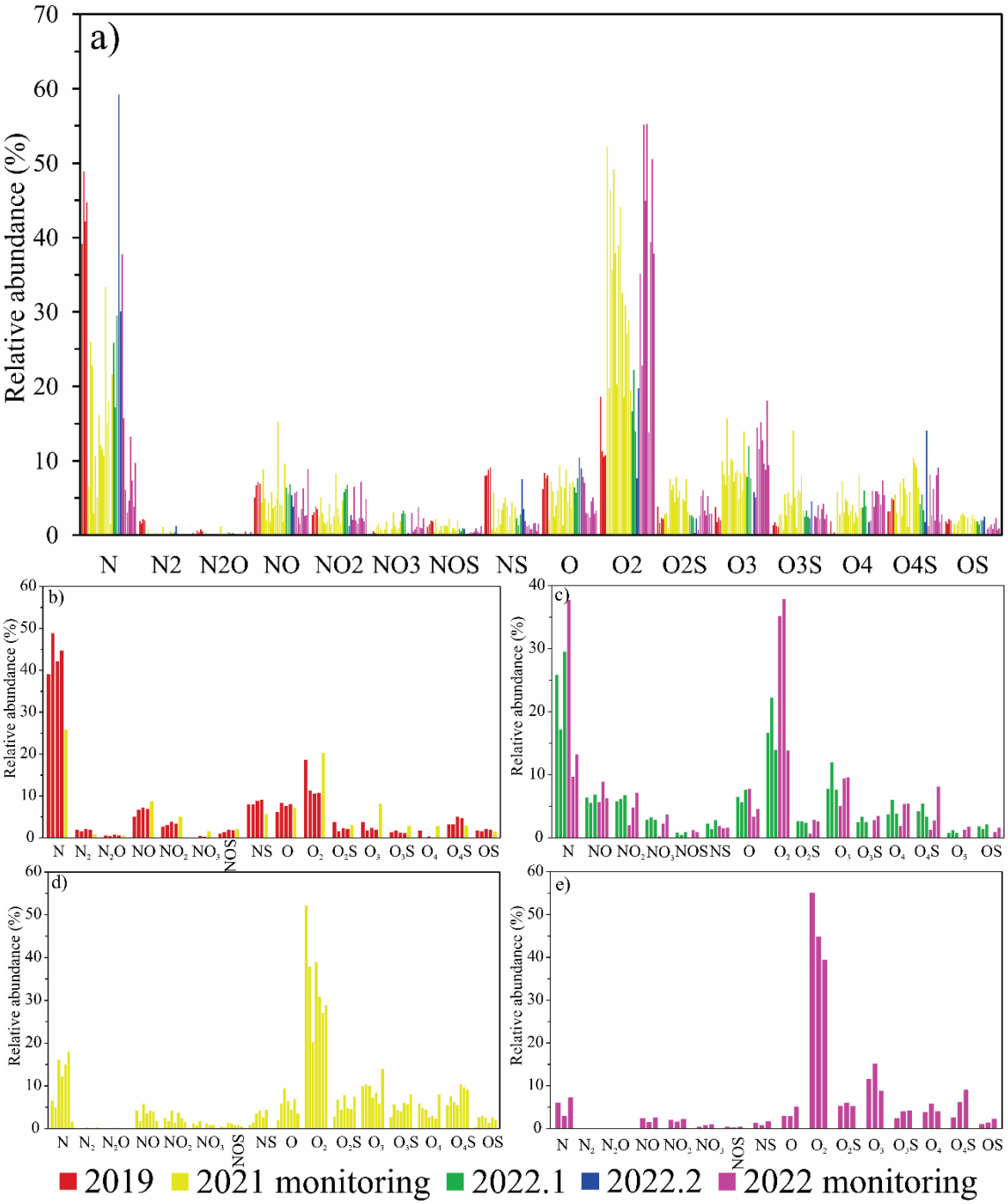

Figure 7. Heteroatom class distributions obtained by ESI(-) FT-ICR MS for the spilled oils from the 2019, 2022.1, 2022.2 events and 2021 and 2022 monitoring (a); for the four 2019 oil samples and the sample P03#2021, from the 2021 monitoring (b); for the three 2022.1 oil sample and the samples P01#2022(02), P02#2022(02), P02#2022(03) S03 from the 2022 monitoring (c); from the 2021 monitoring (d), and from the 2022 monitoring (e).

The ESI(-) FT-ICR MS results show that the class distribution of the petroleum residue samples from each of the 2021 and 2022 surveys varied significantly, corroborating the biomarker results and reflecting the different sources of oil that affected the Ceará coast in recent years. In contrast to the observed for the samples from 2019, 2022.1, and 2022.2 oil spill events, the ESI(-) class distribution for the samples from the 2021 and 2022 monitoring showed that compounds from the O_2 class are predominant in most samples (**Figure 7a**). These oily materials were probably exposed to the biodegradation process, which tends to increase the relative abundance of the O_2 class (Lima et al., 2023; Martins et al., 2017). Moreover, the predominance of the compounds with DBE 2, 3, and 4 (**Figure 8a** and **b**) corroborate this possibility since biodegradation tends to reduce the abundance of the compounds with DBE 1 (fatty acids) and increase the abundance of the compounds with DBE 2, 3, and 4 (naphthenic acids; Kim et al., 2005; Vaz et al., 2013; Martins et al., 2017).

For the N_1 class, the carbazoles (DBE 9), benzocarbazoles (DBE 12), and dibenzocarbazoles (DBE 15) are predominant for all samples (**Figure 8c** and **d**), which is expected since they are usually detected in great abundance in petroleum samples (Hughey et al., 2002). The variation in the relative abundance of the classes obtained by ESI(-) for the seven 2021 monitoring samples (P01#2021, P12#2021, P14#2021, P16#2021, P22#2021, P23#2021, P24#2021; **Figure 7d**) and for the three 2022 monitoring samples (P05E#2022(02), P06E#2022(02), and P03W#2022(03); **Figure 7e**), which

according to the biomarker profile share the same source, better display the influence of the weathering process in these samples.

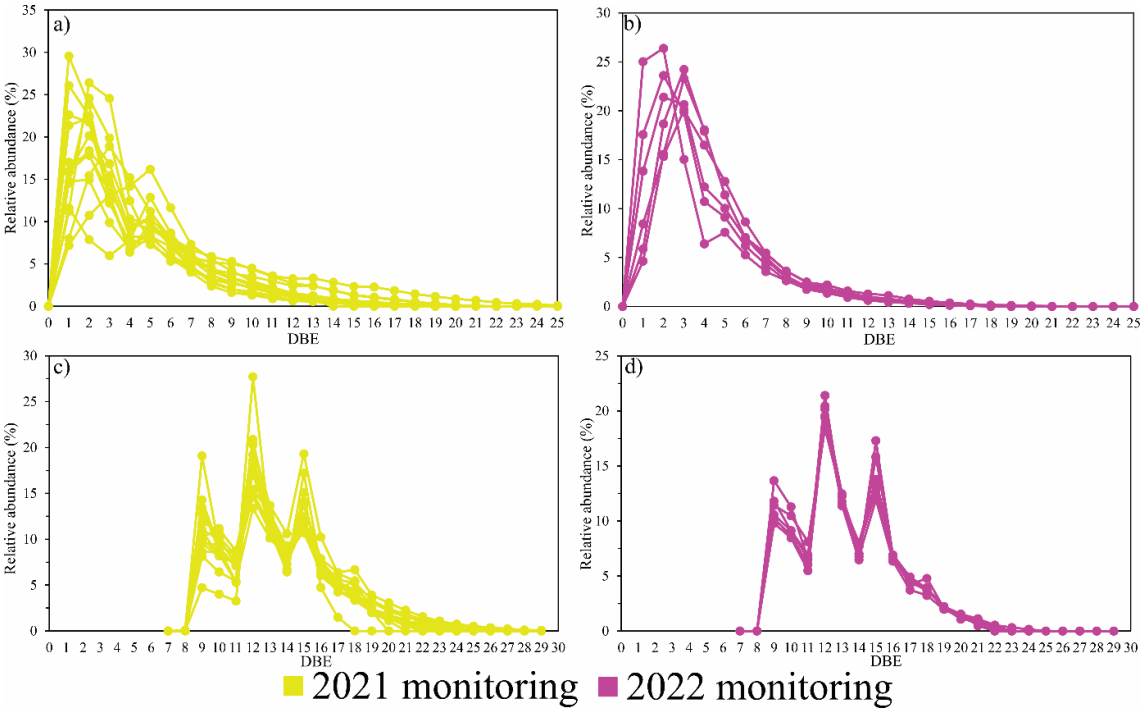

Figure 8. DBE distribution obtained from the ESI(-) FT-ICR MS for O_2 class for the samples from the a) 2021 and b) 2022 monitoring. DBE distribution obtained from the ESI(-) FT-ICR MS for N_1 class for the samples from the c) 2021 and d) 2022 monitoring.

The P03#2021 sample, which exhibits a similar biomarker profile to the 2019 oil samples, displays a high abundance of the O_2, O_3, O_3S, and O_4 classes compared to the four samples from the 2019 event (**Figure 7b**). The increase in the abundance of these classes can be attributed to photooxidation and biodegradation, which enhances the relative abundance of the highly oxygenated class upon exposure to the environment (Lima et al., 2021, 2023). This is expected since these spilled oils were exposed to weathering for approximately two years. The high abundance of the O_2 and O_4S classes (**Figure 7c**) in the three samples collected in the 2022 survey, which correlate with the 2022.1 oil

spill samples, and the detection of high oxygen species (e.g., O_6 and O_6S; **Figure S17**, **Appendence B**) also indicate the action of the process of photooxidation. These highly oxygenated species produced by exposure to sunlight can increase the toxicity of the oil in the environment (Kim et al., 2019).

3.3.2. Fuel oil evidence and assessment

The DBE vs carbon distributions for N_1 class in some of the samples from the 2021 monitoring present a high abundance in a wide range of carbon numbers from ~C20 to C40 (**Figures 9a** and **S1**, **Appendence B 8**), which is not common for crude oils. One possible explanation is that the samples that present this wide range of carbon number probably undergone some thermal process, removing the more lights compounds and increasing the relative abundance of the compounds with middle and high carbon number, something observed in the distillation process (Stanford et al., 2006; Smith et al., 2008). Moreover, the DBE vs carbon distribution for the O_2 class in some of the samples from the 2021 monitoring presents a maximum abundance in DBE 1 and 5 (**Figures 9c** and **S20**, **Appendence B**), which can possibly be attributed to the mixing of two different boiling cuts, a common practice to achieve some marine heavy fuel oil specification (Corilo et al., 2013).

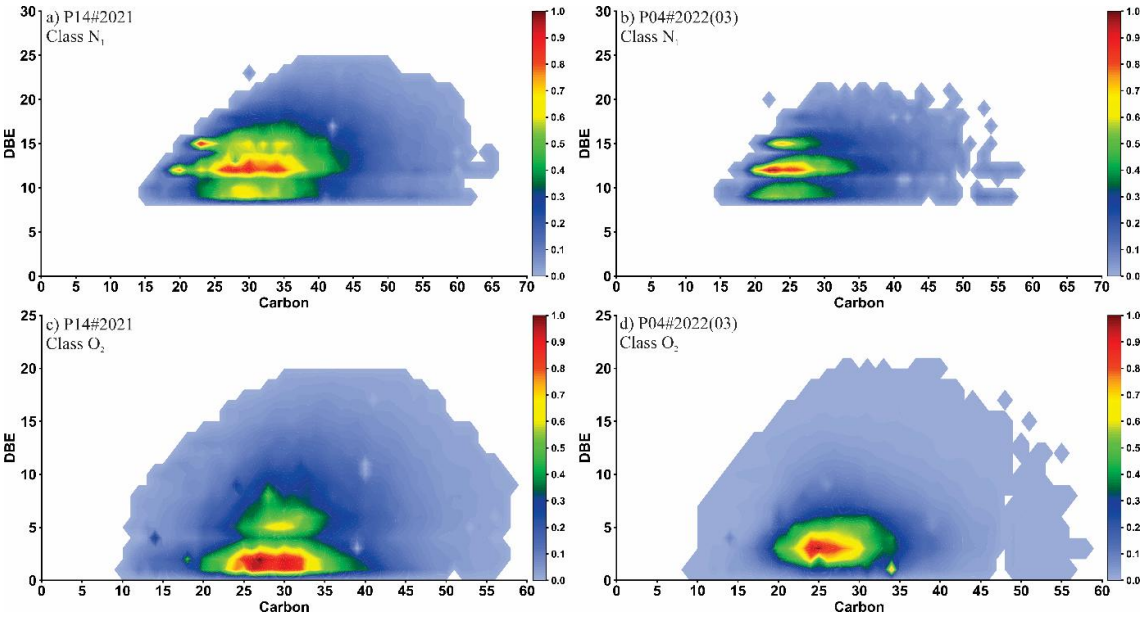

Figure 9. Isoabundance contoured plots of the double bond equivalent (DBE) vs. carbon number for the N_1 class for the samples P14#2021 (a) and P04#2022(03) (b). Isoabundance contoured plots of the double bond equivalent (DBE) vs. carbon number for the O_2 class for the samples P14#2021 (c) and P04#2022(03) (d), obtained from ESI(-) FT-ICR MS analysis of the FOS.

Furthermore, the wide amount of petroleum residue samples from the 2021 and 2022 surveys with distinct DBE vs carbon distribution for the N_1 and O_2 classes (**Figures 9** and **S20**, **Appendence B**) obtained by ESI(-) FT-ICR MS corroborate with the previous results presented in this work, that showed the high amount of samples with different sources that affected all the Ceará coast during 2021 and 2022.

3. Conclusions

This work presented a comprehensive (geo)chemical investigation of multiple petroleum residues found and collected during two surveys performed in 2021 and 2022 off the coast of Ceará, Northeastern Brazil. They present homologs series of *n*-alkanes, medium to high UCM in their gas chromatograms,

large content of saturated and aromatic biomarkers (e.g., terpanes, steranes, TPPs, and triaromatic steranes), and many heteroatom classes with homolog series of acid compounds (e.g., N_1, O_1, and O_2), confirming their petrogenic nature. The wide presence of these materials on the Brazilian coast highlights the high level of petrogenic contamination in the area with no needed control and inspection.

Unlike what was expected, the forensic geochemistry using resistant biomarkers disclosed that most of the petroleum residues collected in the 2021 survey (16 out of 19) have no correlation with the mysterious 2019 oil spill, and most of the petroleum residues collected in the 2022 survey (10 out of 13) have no correlation with the 2022.1 oil spill that occurred over the Ceará. These non-correlated oily materials have uncommon composition, including only long-chain *n*-alkanes and considerable UCM, characterizing them as paraffinic and heavy petroleum residues. They also have dissimilated among them, suggesting distinct sources and origins. These results reveal that the Brazilian coast has been contaminated by various other sources than the known oil spill events.

In addition to the low-medium *n*-alkanes, other more volatile compounds were not usually detected in the paraffinic oil residues, including the *n*-alkylcyclohexanes and light to intermediate HPAs (e.g., chrysenes, phenanthrenes), which may indicate they are related to heavy petroleum products from distillation and fractionation processes. They may be related to a mixture of petroleum residues accidentally or unintentionally discarded into the sea and brought to the Brazilian coast by the ocean currents.

The petroleomics by ESI(-) FT-ICR MS assisted in the petroleum residue chemical characterization and investigation. It corroborated the lack of correlation between most petroleum residues and known oil spill events and demonstrated the effect of weathering processes on the correlated oils after oil spills. In addition, the bimodal distribution observed in the O_2 class indicates a possible mixture of different boiling cuts, a common practice in the formulation of heavy marine fuel oil. These data reinforce the hypothesis that part of the analyzed oil residues derives from processed products and are not crude oil. Thus, this study showed how much the coast of Ceará has received a diversity of oily residues of unknown origin that have gradually and silently impacted the marine and coastal environment.

References

ALBAIGÉS, J., TORRE, L. LA., L., BAYONA, J. M., DOMÍNGUEZ, C. 2018. Chapter 15-Applications of the CEN Methodology in Multiple Oil Spills in Spanish Waters. Oil Spill Environmental Forensics Case Studies, Pages 325-343. https://doi.org/10.1016/B978-0-12-804434-6.00015-X

Aeppli, C., 2022. Recent advance in understanding photooxidation of hydrocarbons after oil spills. Curr. Opin. Chem. Eng. 36, 100763. https://doi.org/10.1016/j.coche.2021.100763

AZEVEDO, R.A., BEZERRA, K.M.M., NASCIMENTO, R.F., NELSON, R.K., REDDY, C.M., NASCIMENTO, A.P., OLIVEIRA, A.H.B., MARTINS, L.L., CAVALCANTE, R.M., 2022. Is there a similarity between the 2019 and 2022 oil spills that occurred on the coast of Ceará (Northeast Brazil)? An analysis based on forensic environmental geochemistry. Environ. Pollut. 315, 120283. https://doi.org/10.1016/j.envpol.2022.120283

AZEVEDO, D.A., GONÇALVES, M.L., SILVA, D.B., 2007. Organic Geochemistry of the Angra dos Reis Marine Sediments: Aliphatic and Polycyclic Aromatic Hydrocarbons. Environ. Forensics, 8, 245-256. https://doi.org/10.1080/15275920701506417

BASTOS, L.P.H., CAVALCANTE, D.C., ALFERES, C.L.F., SILVA, D.B.N., FERREIRA, L.O., RODRIGUES, R., PEREIRA, E., 2022. Fingerprinting an oil spill event (August of 2021) in the oceanic Fernando de Noronha archipelago using biomarkers and stable carbon isotopes. Mar. Pollut. Bull. 185, 114316. https://doi.org/10.1016/j.marpolbul.2022.114316

BONTEMPO FILHO, E.B., COUTINHO, R.Q., BARBOSA, J.A., BARCELLOS, R.L., GIACHETTI, H.L., RAMOS, G.M.S., 2022. Temporal monitoring of contamination in three sandy beaches from the 2019 oil spill near Cabo de Santo Agostinho, Northeastern Brazil. An. Acad. Bras. Cienc. 94, 1-23. https://doi.org/10.1590/0001-3765202220210513

BOUKADI. A, PHILP. R. P, THANH. N.X. Characterization of paraffinic deposits in crude oil storage tanks using high temperature gas chromatography. Applied Geochemistry, V. 20, Issue 10, pages 1831-1984(October 2005). https://doi.org/10.1016/j.apgeochem.2005.06.004

BRUM, H.D., CAMPOS-SILVA, J.V., OLIVEIRA, E.G., 2020. Brazil oil spill response: government inaction. Science 367 (6474), 155–156. https://doi.org/10.1126/ science.aba0369

CARREGOSA, J.C., SANTOS, I.R.D., DE SÁ, M.S., SANTOS, J.M., WISNIEWSKI, A., 2021. Multiple reaction monitoring tool applied in the geochemical investigation of a mysterious oil spill in northeast Brazil. An. Acad. Bras. Cienc. 93, 1–20. https://doi.org/10.1590/0001-3765202120210171

CHEN, HUAN; HOU, AIXIN; CORILO, YURI E.; LIN, QIANXIN; LU, JIE; MENDELSSOHN, IRVING A.; ZHANG, RUI; RODGERS, RYAN P.; MCKENNA, AMY M. 4 years after the Deepwater Horizon spill: molecular transformation of

Macondo well oil in Louisiana salt marsh sediments revealed by FT-ICR mass spectrometry. *Environmental Science & Technology*, v. 48, n. 10, p. 6066–6075, 2014. DOI: https://doi.org/10.1021/es500228p.

Characterization of a crude oil weathering series by ultrahigh-resolution mass spectrometry using multiple ionization modes. Sci. Total Environ. 563, 600-610. https://doi.org/10.1016/j.scitotenv.2016.03.233

CHUA. C.C, BRUNSWICK. P, KWOK. H, YAN. J, CUTHBERTSON. D, VAN AGGELEN. G , HELBING. C. C. SHANG. D. Enhanced analysis of weathered crude oils by gas chromatography-flame ionization detection, gas chromatography-mass spectrometry diagnostic ratios, and multivariate statistics. Journal of Chromatography A. Volume 1634, 20 December 2020, 461689. https://doi.org/10.1016/j.chroma.2020.461689

CARLSON, R.M.K., JACOBSON, S.R., BODUSZYNSKI, M.M., RECHSTEINER, C.A., GRUDOSKI, D.A., 1994. Applications of high temperature gas chromatography to hard-to-recover- oils and natural bitumens. In: Alemasov, V.A., Muslimov, R.K., Romanov, G.V. (Eds.), Problems of Complex Development and Production of Hard-Accesible Oils and Natural Bitumens (Production and Re®ning), (Eds. Institute of Organic and Physical Chemistry, Kazan Scienti®c Centre, Russian Academy of Sciences, Kazan, pp. 1102±1133.

CHUANYUAN WANG, C., CHEN, B., ZHANG, B., HE, S., ZHAO, M., 2013. Fingerprint and weathering characteristics of crude oils after Dalian oil spill, China. Marine Pollution Bulletin. Volume 71, Issues 1–2, 15 June 2013, Pages 64-68. https://doi.org/10.1016/j.marpolbul.2013.03.034

COTO, B.; COUTINHO, J. A. P; MARTOS, C; M, D, ROBUSTILLO; ESPADA, J. J; L. PEÑA, J. Assessment and Improvement of n-Paraffin Distribution Obtained by HTGC To Predict Accurately Crude Oil Cold Properties. *Energy & Fuels* 2011, 25, 3, 1153–1160. https://doi.org/10.1021/ef101642g

Corilo, Y. E., Podgorski, D. C., McKenna, A. M., Lemkau, K. L., Reddy, C. M., Marshall, A. G., & Rodgers, R. P. (2013). Oil spill source identification by principal component analysis of electrospray ionization Fourier transform ion cyclotron resonance mass spectra. *Analytical chemistry*, *85*(19), 9064-9069. https://doi.org/10.1021/ac401604u

CLEMENT, T. P., HAYWORTH, J. S., MULABAGAL, V., YIN, F. , & JOHN, G.F. (2012). Research brief II: impact of Hurricane Isaac onmobilizing Deepwater Horizon oil spill residues alongAlabama's coastline—a physicochemical characterizationstudy. Samuel Ginn College of Engineering, AuburnUniversity. *(PDF) Marine Tar Residues: a Review*. Available from: https://www.researchgate.net/publication/273787001_Marine_Tar_Residues_a_Review

CLEMENT, T.P., JOHN, G.F., YIN, F., 2017. Chapter 16—assessing the increase in background oil–contamination levels along Alabama's beaches resulting from the Deepwater horizon oil spill. In: Oil Spill Science and Technology, second edition. Elsevier Inc, Boston, pp. 851–888.

CORRICK, A.J., HALL, P.A., TREFRY, C., MCKIRDY, D.M., ROSS, S.G.A.S., 2021. The natural hydrocarbon loading of the South Australian coastline. Mar. Pollut. Bull. 166, 112198. https://doi.org/10.1016/j.marpolbul.2021.112198

DIEZ, S., JOVER, E., BAYONA, M, ALBAIGÉ, J. 2007. Prestige oil spill. III. Fate of aheavy oil in the marine environments. Vol. 41, nº. 9, Environmental science & technology.
https://pubs.acs.org/doi/epdf/10.1021/es0629559?ref=article_openPDF

DUAN, Y., ZHANG, H., WU, B.X., ZHENG, Z. Y., 2003. Carbon isotopic studies of individual n-alkanes in crude oils from Qaidam Basin. J.Mineral, Petrol. 23, 91-94.

DOUGLAS, G. S.; STOUT, S. A.; UHLER, A. D.; MCCARTHY, K. J.; EMSBO-MATTINGLY, S. D. Advantages of quantitative chemical fingerprinting in oil spill identification and allocation of mixed hydrocarbon contaminants. In *Standard Handbook Oil Spill Environmental Forensics*; Academic Press. 2016, pp. 789-847. https://doi.org/10.1016/B978-0-12-803832-1.00017-9

EPA. Understanding Oil Spills In Freshwater Environments Understanding Oil Spills In Freshwater Environments, 1991. www.epa.gov/sites/default/file/2018-01/documents/opguide99.pdf.

EDWARDS, D, S. DAVID M. MCKIRDY, STEVEN J.ROWLAND, DAVID J.HEATH, PATRICIA S.GRAY. Waxy bitumen stranding in southern Australia: A geochemical study of multiple oil families and their likely origins. https://doi.org/10.1016/j.orggeochem. 2017.12.010

FILEWOOD, T., KWOK, H., BRUNSWICK, P., YAN, J., OLLINIK, E, J., COTE, C., KIM, M., AGGELEN, G, V., HELBING, C., SHANG, D. Investigating the fate of polycyclic aromatic sulfur heterocycle compounds in spilled oils with a microcosm weathering experimente. *Environmental Systems Research (2022) 11:6.* https://doi.org/10.1186/s40068-022-00252-w
Fingas. M. Oil Spill Science and Technology, Second Edition – Book 2016.

GOVINDARAJAN, S.K., MISHRA, A., KUMAR, A., 2021. Oil spill in a marine environment. Requirements following an offshore oil spill. Rud. Geol. Naft. Zb. 36 (4), 1–9. https://doi.org/10.17794/rgn.2021.4.1

HARRIMAN, B., ZITO, P., PODGORSKI, D. C., TARR, M. A., & SUFLITA, J. M. (2017). Impact of photooxidation and biodegradation on the fate of oil spilled during the Deepwater Horizon incident: Advanced stages of weathering. *Environmental Science & Technology, 51*(10), 5523–5531. https://doi.org/10.1021/acs.est.7b01278

HETTITHANTHRI, OSHANI; FANG, CHIEN-LIN; LI, YING; WANG, XINYI; CHEN, YOU; JIA, FANG. A review of oil spill dynamics, impacts, and limitations

of current response methods. *Environmental Progress & Sustainable Energy*, , v. 41, n. 6, e13952, 2022. Wiley Online Library. Disponível em: https://doi.org/10.1002/ep.13952.

HASEEBA, K,P; VETHAMONY, P; VEERASINGAM, S; ABOOBACKER, V M; AL-KHAYAT, JASSIM A. A comprehensive review of oil residues in the world oceans: types, characteristics, sources and distribution. Marine Pollution Bulletin, Volume 217, Article 118106, p. 1–XX, 14 mai 2025. DOI: 10.1016/j.marpolbul.2025.118106. Disponível em: https://doi.org/10.1016/j.marpolbul.2025.118106.

HUGHEY, CHRISTINE A; RODGERS, R; MARSHALL. A. QIAN, K; ROBBINS, K. W. Identification of acidic NSO compounds in crude oils of different geochemical origins by negative ion electrospray Fourier transform ion cyclotron resonance mass spectrometry. Organic Geochemistry, v. 33, n. 7, p. 743-759, 2002. https://doi.org/10.1016/S0146-6380(02)00038-4

IBAMA, 2019. Fonte: Manchas de óleo no Nordeste. https://www.gov.br/ibama/pt-br/assuntos/fiscalizacao-e-protecao-ambiental/emergencias-mbientais/manchasdeoleo

ITOPF, 2023. Oil tanker spill statistics. https://www.itopf.org/fileadmin/uploads/itopf/data/Documents/Company_Lit/Oil_Tanker_Spill_Statistics_2023.

KAVITHA RAMADASS , SARANYA KUPPUSAMY , KADIYALA VENKATESWARLU , RAVI NAIDU & MALLAVARAPU MEGHARAJ. 2020. Unresolved complex mixtures of petroleum hydrocarbons in the environment: An overview of ecological effects and remediation approaches. https://doi.org/10.1080/10643389.2020.1813066

KIENHUIS P. G. M., HANSEN A. B., FAKSNESS L.-G., STOUT S. A., DAHLMANN G. (2016). CEN methodology for oil spill identification. In: Standard Handbook Oil Spill Environmental Forensics. Stout, S. A. & Wang, Z. eds, Second Edition, Elsevier, pp. 685-728.

KIM, DONGHWI; JUNG, H-J; HÁ, Y. NA, G. J; SHANKAR, R; KWON, H-J; YAM, H. U; KIM, H. S. Molecular level determination of water accommodated fraction with embryonic developmental toxicity generated by photooxidation of spilled oil. Chemosphere, v. 237, p. 124346, 2019. https://doi.org/10.1016/j.chemosphere.2019.124346

KIM, SUNGHWAN; STANFORD, A. L; RODGERS, P. R; MARSHALL, G. A; WALTERS, C. C; QIAN, K; WENGER, L. M; MANKIEWICZ, P. Microbial alteration of the acidic and neutral polar NSO compounds revealed by Fourier transform ion cyclotron resonance mass spectrometry. Organic Geochemistry, v. 36, n. 8, p. 1117-1134, 2005. https://doi.org/10.1016/j.orggeochem.2005.03.010

LI, P.; CAI, Q.; LIN, W.; CHEN, B.; ZHANG, B. Offshore oil spill response practices and emerging challenges. Marine. Pollution. Bulletin, Volume 110,

Issue 1,15 September 2016, Pages 6-27.
https://doi.org/10.1016/j.marpolbul.2016.06.020

LIMA, B.D., MARTINS, L.L., PEREIRA, V.B., FRANCO, D.M.M., SANTOS, I.R., SANTOS, J.M., VAZ, B.G., AZEVEDO, D.A., CRUZ, G.F., 2023. Weathering impacts on petroleum biomarker, aromatic, and polar compounds in the spilled oil at the northeast coast of Brazil over time. Mar. Pollut. Bull. 189, 114744. https://doi.org/10.1016/j.marpolbul.2023.114744

LIMA, B.D., MARTINS, L.L., SOUZA, E.S., PUDENZI, M.A., DA CRUZ, G.F., 2021. Monitoring Chemical compositional changes of simulated spilled Brazilian oils under tropical climate conditions by multiple analytical techniques. Mar. Pollut. Bull. 164, 111985. https://doi.org/10.1016/j.marpolbul.2021.111985

LIMA, B.D., MARTINS, L.L., SANTOS, L.C., SOUZA, E.S., PUDENZI, M.A., NASCIMENTO, H.L., EBERLIN, M.N., CRUZ, G.F., 2020. Geochemical Investigation of Tar Balls Collected in a Brazilian Beach Using Biomarkers, Ni/V, δ13C Ratios and Ultra-High Resolution FT-ICR Mass Spectrometry. J. Braz. Chem. Soc. 31, 673-682. https://doi.org/10.21577/0103-5053.20190231

LOBÃO, M. M., THOMAZELLI, F. F., BATISTA, E. P.M.P., OLIVEIRA, R. F., DE SOUZA, M. D.C., MATOS, N. A.V. Chronic oil spills revealed by the most important set of samples from the incident in northeastern Brazil, 2019. Anais da Academia Brasileira de Ciencias | *Annals of the Brazilian Academy of Sciences,* (2022) 94(Suppl. 2): e20210492 DOI 10.1590/0001-3765202220210492.

LOURENÇO, R.A., COMBI, T., ALEXANDRE, M.R., SASAKI, S.T., ZANARDI-LAMARDO, E., YOGUI, G.T., 2020. Mysterious oil spill along Brazil's northeast and southeast seaboard (2019–2020): Trying to find answers and filling data gaps. Mar. Pollut. Bull. 156, 111219. https://doi.org/10.1016/j.marpolbul.2020.111219

MCTI, 2022. https://www.gov.br/mcti/pt-br/acompanhe-o-mcti/noticias/2022/09/nota-tecnica-a-imprensa-residuos-de-oleo-encontrados-em-agosto-no-litoral-do-nordeste.

MARTINS, L.L., PEREIRA, V.B., NASCIMENTO, A.P., AZEVEDO, R.N.A., OLIVEIRA, A.H., TEIXEIRA, C.E.P., AZEVEDO, D.A., DA CRUZ, G.F., CAVALCANTE, R.M., GIARRIZZO, T., 2024 Forensic Geochemistry Reveals International Ship Dumping as a Source of New Oil Spill in Brazil's Coastline (Bahia) in Late 2023. Environ. Sci. Technol. 58, 9328–9338 https://doi.org/10.1021/acs.est.4c01520

MARTINS, L.L., SCHULZ, H.-M., NOAH, M., POTZ, S., RIBEIRO, H.J.P.S., CRUZ, G.F., 2021. New paleoenvironmental proxies for the Irati black shales (Paraná Basin, Brazil) based on acidic NSO compounds revealed by ultra-high resolution mass spectrometry. Org. Geochem. 151, 104152. https://doi.org/10.1016/j.orggeochem.2020.104152

MARTINS, L.L., CRUZ, G.F.D., SANTOS, L.C., PUDENZI, M.A., EBERLIN, M.N., 2019. Avaliação da extensão da biodegradação de petróleos brasileiros com ênfase nos *n*-alquilciclohexanos. Quim. Nova 42, 289-295. https://doi.org/10.21577/0100-4042.20170328

Martins, L.L., Pudenzi, M.A., da Cruz, G.F., Nascimento, H.D., Eberlin, M. N., 2017. Assessing biodegradation of Brazilian crude oils via characteristic profiles of O1 and O2 compound classes: petroleomics by negative-ion mode electrospray ionization Fourier transform ion cyclotron resonance mass spectrometry. Energy Fuel 31, 6649-6657. https://doi.org/10.1021/acs.energyfuels.7b00109

MELLO, L.C., NASCIMENTO, A.P., LOPES, B.D., LIMA, A.D.F., BEZERRA, L.E.A., MENDES, L.F., BASTOS, L.M., NOSSOLD, A.B.S., MARTINS, M.M., MARTINS, L.L., CAVALCANTE, R.M., 2023. Tarballs on the Brazilian coast in late 2022 sustain Lepas anatifera Linnaeus, 1758 (Crustacea: Cirripedia): Occurrence and risk of petroleum hydrocarbon ingestion. Sci. Total Environ. 896, 164981. https://doi.org/10.1016/j.scitotenv.2023.164981

MISRA, S., BARUAH, S., SINGH, K., 1995. Paraffin problems in crude oil production and transportation: A review. Society of Petroleum Engineers (SPE) Paper 28181, SPE Production and Facilities, pp. 50–54.

NASCIMENTO, A., AZEVEDO, R. N. A., PEREIRA, M. G. A., OLIVEIRA, A. H. B., SANTOS, J. M, CAVALCANTE, R. M., MARTINS, L. L., 2024. Forensic environmental geochemistry to reveal the extent, characteristics, and fate of waxy tarballs spilled over the northeast coast of Brazil in 2022. Mar. Environ. Res. 204, 106878. https://doi.org/10.1016/j.marenvres.2024.106878

OLIVEIRA, O.M., QUEIROZ, A.F.D.S., CERQUEIRA, J.R., SOARES, S.A., GARCIA, K.S., PAVANI FILHO, A., ROSA, M.L.S., SUZART, C.M., PINHEIRO, L.L., MOREIRA, I.T., 2020. Environmental disaster in the northeast coast of Brazil: forensic geochemistry in the identification of the source of the oily material. Mar. Pollut. Bull. 160, 111597. https://doi.org/10.1016/j.marpolbul.2020.111597

ORNITZ, B. E., CHAMP, M, A., Oil Spills First Principles: Prevention and Best Response, Elsevier Science, 2002. https://doi.org/10.1016/B978-008042814-7/50021-5

PHILP, P, R., HSIEH, M, TAHIRA, F. An overview of developments related to the characterization and significance of high molecular weight paraffins/hydrocarbons (>C40) in crude oils. Geological Society, London, Special Publications, 2015. Volume 237. Pages 37 – 51. https://doi.org/10.1144/GSL.SP.2004.237.01.04

PEREIRA, M.G.A., SANTOS, I.R., LIMA, I.F.S., COUTINHO, M.E.B., CARREGOSA, J.C., WISNIEWSKI, A., SANTOS, J.M., 2023. Geochemical Assessment of Tar Balls That Arrived in 2022 along the Northeast Coast of Brazil and Their Relationship with the 2019 Oil Spill Disaster. Energy Fuel 37, 16388–16395. https://doi.org/10.1021/acs.energyfuels.3c02472

PEREIRA, A, S;NETO, A, R, F. Estado da arte da cromatografia gasosa de alta resolução e alta temperatura. Química nova, 23(3) (2000). https://doi.org/10.1590/S0100-40422000000300014

PETERS, K.E., WALTERS, C.C., MOLDOWAN, J.M., 2005. The Biomarker Guide: Biomarkers and Isotopes in the Petroleum Exploration and Earth History, 2nd ed., University Press: Cambridge, vol. 2.

PUROHIT, B.K., TEWARI, S., PRASAD, K.S.N.V., TALARI , V. K., PANDEY N., CHOUDHURY, P., Panda, S. S., 2024. Marine oil spill clean-up: A review on technologies with recent trends and challenges. Regional Studies in Marine Science 80, 103876. https://doi.org/10.1016/j.rsma.2024.103876

PRINCE, R.C., WALTERS, C.C., 2022. Modern analytical techniques are improving our ability to follow the fate of spilled oil in the environment. Curr. Opin. Chem. Eng. 36, 1-8. https://doi.org/10.1016/j.coche.2021.100787

RADOVIĆ, J.R., AEPPLI, C., NELSON, R.K., JIMENEZ, N., REDDY, C.M., BAYONA, J.M., ALBAIGÉS, J., 2014. Assessment of photochemical processes in marine oil spill fingerprinting. Mar. Pollut. Bull. 79, 268-277. https://doi.org/10.1016/j.marpolbul.2013.11.029

REDDY, C.M., NELSON R.K., HANKE, U.M., CUI, X., SUMMONS, R.E., VALENTINE, D.L., RODGERS, R.P., CHACÓN-PATIÑO, M.L., NILES, S.F., TEIXEIRA, C.E.P., BEZERRA, L.E.A., CAVALCANTE, R.M., SOARES, M.O., OLIVEIRA, A.H.B., WHITE, H.K., SWARTHOUT, R.F., LEMKAU, K.L., RADOVIĆ, J.R., 2022. Synergy of Analytical Approaches Enables a Robust Assessment of the Brazil Mystery Oil Spill. Energy Fuel 36, 13688–13704. https://doi.org/10.1021/acs.energyfuels.2c00656

REDDY, C.M., EGLINTON, T.I., PALI´C, R., BENITEZ-NELSON, B.C., STOJANOVI´C, G., PALI´C, I., DJORDJEVI´C, S., EGLINTON, G., 2000. Even carbon number predominance of plant wax nalkanes: a correction. Org. Geochem. 31, 331–336. https://doi.org/10.1016/S0146-6380(00)00025-5

ROCHA, C. A. DA SILVA, B, J, N. Development and validation of statistically sound criteria for the match of unweathered GC-MS fingerprints in oil spill forensics. Chemosphere Volume 289, February 2022, 133085. https://doi.org/10.1016/j.chemosphere.2021.133085

SINGH, H., BHARDWAJ, N., ARYA, S.K., KHATRI, M., 2020. Environmental impacts of oil spills and their remediation by magnetic nanomaterials. Environmental Nanotechnology, Monitoring & Management. Volume 14, December 2020, 100305 https://doi.org/10.1016/j.enmm.2020.100305

SHIRNESHAN, G, BAKHTIARI, A. R., MEMARIANI, M. Identification of sources of tar balls deposited along the Southwest Caspian Coast, Iran using fingerprinting techniques. Science of The Total Environment. Volume 568, 15 October 2016, Pages 979-989.
https://doi.org/10.1016/j.scitotenv.2016.04.203

SOARES, M. O., TEIXEIRA, C. E., BEZERRA, S.V., PAIVA, T. C. L., TAVARES, T. M., GARCIA, R. M. CAVALCANTE, 2020b. Oil spill in South Atlantic (Brazil): Environmental and governmental disaster. Marine Policy, 103,879. https://doi.org/10.1016/j.marpol.2020.103879

SUARIA, G., STEFANO, A., MERLINO, S., ABBATE, M. 2018. The Occurrence of Paraffin and Other Petroleum Waxes in the Marine Environment: A Review of the Current Legislative Framework and Shipping Operational Practices. Marine Pollution, a section of the jornal Frontiers in Marine Science. March 2018, volume 5, article 94. https://doi.org/10.3389/fmars.2018.00094

STOUT, SCOTT A., ZHENDI WANG. Chemical fingerprinting methods and factors affecting petroleum fingerprints in the environment. Standard handbook oil spill environmental forensics. Academic Press, 2016. 61-129. https://doi.org/10.1016/B978-0-12-803832-1.00003-9

STOUT, S.A., WANG, Z., 2007. Chemical fingerprinting of spilled or discharged petroleum – methods and factors affecting petroleum fingerprints in the environment. Oil Spill Environmental Forensics, 1-53. https://doi.org/10.1016/B978-012369523-9.50005-7

STANFORD, L. A.; KIM, S.; RODGERS, R. P.; MARSHALL, A. G. Characterization of compositional changes in vacuum gas oil distillation cuts by electrospray ionization fourier transform− ion cyclotron resonance (FT− ICR) mass spectrometry. *Energy Fuels* 2006, 20, 1664-1673. https://doi.org/10.1021/ef060104g

SMITH, D. F.; RAHIMI, P.; TECLEMARIAM, A.; RODGERS, R. P.; MARSHALL, A. G. Characterization of Athabasca bitumen heavy vacuum gas oil distillation cuts by negative/positive electrospray ionization and automated liquid injection field desorption ionization Fourier transform ion cyclotron resonance mass spectrometry. *Energy Fuels* 2008, 22, 3118-3125. https://doi.org/10.1021/ef8000357

TERRA, W.S., MARTINS, L.L., DA CRUZ, G.F., 2019. Avaliação da Eficiência de Diferentes Solventes Orgânicos na Precipitação de Asfaltenos de Petróleos Brasileiros e Análise das Frações Asfaltênicas e Maltênicas por Diferentes Técnicas Instrumentais. Rev. Virtual Quim. 11, 1344-1363. https://doi.org/10.21577/1984-6835.20190093

K.A. BURNS, S. GARRITY, D. JORISSEN, J. MACPHERSON, M. STOELTING, J. TIERNEY, L.Y.SIMMONS, The Galeta oil spill: unexpected persistence of oil trapped inmangrove In-Chul Song a, Eun-Ji Jeon b, Song Kim b, Sun-Ju Hwang a, Jeong-Mog Seo. Oil spill fingerprint of low sulfur fuel oil in South Korea. https://doi.org/10.1016/j.marpolbul.2021.112721

VAZ, B.G., SILVA, R.C., KLITZKE, C.F., SIMAS, R.C., NASCIMENTO, H.D.L., PEREIRA, R.C.L., GARCIA, D.F., EBERLIN, M.N., Azevedo, D.A., 2013b. Assessing biodegradation in the Llanos Orientalos crude oils by electrospray ionization ultrahigh resolution and accuracy Fourier transform mass

spectrometry and chemometric analysis. Energy & Fuels 27, 1277–1284. https://doi.org/10.1021/ef301766r

WARNOCK, A.M., HAGEN, S.C., PASSERI, D.L., 2015. Marine Tar Residues: a Review. Water Air Soil Pollut 226, 1-24. https://doi.org/10.1007/s11270-015-2298-5

WANG, RUJUN; SONG, XIAOXUAN; WANG, QILIN; MA, SHUANG; WANG, BAOYU. Simulation of oil spills in inland rivers: a review. *Sustainability*, Basel, v. 15, n. 5, p. 4100, 2023. Disponível em: https://doi.org/10.3390/su15054100.

WANG, Z.D., FINGAS, M. Developments in the analysis of petroleum hydrocarbons in oils, petroleum products and oil-spill-related environmental samples by gas chromatography. J. Chromatogr. A,774 (1997), pp.51-78. https://doi.org/10.1016/S0021-9673(97)00270-7
Wang, Z., Stout, A, S. Fingerprinting and Source Identification. Standard Handbook Oil Spill Environmental Forensics. Second Edition, Elsevier 2016.

WANG, Z., STOUT, S.A., FINGAS, M., 2006. Forensic fingerprinting of biomarkers for oil spill characterization and source identification. Environ. Forensics 7, 105–146. https://doi.org/10.1080/15275920600667104

YANG, CHUN; WANG, Z; LIU, Y; YANG, Z; LI, Y. SHAH, K; ZHANG G, LANDRIAULT, M; HOLLEBONE, B; BROWN, C; LAMBERT, P; LIU, Z; TIAN, S. Aromatic steroids in crude oils and petroleum products and their applications in forensic oil spill identification. *Environmental Science & Technology*, [S. l.], v. 53, n. 22, p. 13473-13483, 2019. https://doi.org/10.1080/15275922.2013.843617

YANG. C, ZHANG. G, WANG. Z, YANG. Z, HOLLEBONE. B, LANDRIAULT. M, SHAH. K, BROWN. C. E. 2014. Development of a methodology for accurate quantitation of alkylated polycyclic aromatic hydrocarbons in petroleum and oil contaminated environmental samples. Analytical. Methods, V. 6, 7760-7771. https://doi.org/10.1039/C4AY01393J

YANG, C., YANG, Z., ZHANG, G., HOLLEBONE, B., LANDRIAULT, M., WANG, Z., LAMBERT, P., BROWN, C. E. Characterization and differentiation of chemical fingerprints of virgin and used lubricating oils for identification of contamination or adulteration sources. 2016. Fuel 163 (2016) 271–281. http://dx.doi.org/10.1016/j.fuel.2015.09.070

ZACHARIAS, D.C., FORNARO, A., 2020. Brazilian offshore oil exploration areas: an overview of hydrocarbon pollution. Revista Ambiente & Agua 15, 2569. https://doi.org/ 10.4136/ambi-água. 2569

ZHANG, H., YIN, X., ZHOU, H., WANG, J., HAN, L.2015. Weathering Characteristics of Crude Oils from Dalian Oil Spill Accident, China. Aquatic Procedia 3 (2015) 238 – 244. https://doi.org/10.1016/j.aqpro.2015.02.217

CAPÍTULO 4

4.1 CONCLUSÕES E CONSIDERAÇÕES FINAIS

Este trabalho realizou uma pesquisa abrangente sobre os mais recentes e principais derramamentos de petróleo ocorrido no nordeste do Brasil, de 2019 a 2022. A seguir, apresentam-se as principais conclusões da pesquisa:

O monitoramento realizado entre os anos de 2019 e 2022 mostrou a presença recorrente de materiais oleosos em faixas de areias e *beachrocks* de todo o litoral do Ceará, nordeste do Brasil. Pôde ser observado amostras de óleo em estado líquido como as coletadas no evento de 2019, como amostras na forma de *tarballs* coletadas no evento do final do de 2022. Também como característica dos monitoramentos obtivemos amostras muito intemperizadas, ao total foram 56 amostras de resíduos de petróleo estudadas.

O uso das técnicas cromatográficas para as análises de biomarcadores saturados e aromáticos apresentou resultados surpreendentes, dentre eles, tem-se os diferentes eventos identificados a partir dos perfis moleculares, o *fingerprinting* das amostras dos anos de 2019, 2022.1, 2022.2, indicando que essas diferenças sugerem fontes distintas para esses três grupos de óleos.

Uma surpresa nesse estudo foram os resultados das amostras monitoradas nos anos de 2021 e 2022, foram 42 amostras, onde três amostras de 2021 apresentaram similaridade com os óleos de 2019. E três amostra de 2021 apresentaram similaridade com os óleos do início do ano de 2022, isto sugere que os óleos do evento de 2019 podem ficado aprisionados no meio de forma que suas características moleculares tenham sido preservadas. Já os resíduos de 2021 podem ser da mesma fonte que foi lança em 2022, talvez a pequena quantidade não tenha sido suficiente para ser detectada no meio ambiente, porém também foi preservada. As demais amostras de 2021 e 2022, algumas apresentaram similaridade entre si e outras não, mostrando que essas amostras são de diversas fontes. Ainda como resultado encontrado, a grande maioria das amostras de 2021 e 2022, apresentam um corte em seu perfil cromatográfico o GC-FID mostra a presença somente de compostos mais pesados (*n*C31 a *n*C40), além dá não presença de compostos aromáticos

convencionais (GC-MS), estas características indicam que esses resíduos podem ter sofrido processos de térmicos.

A avaliação dos compostos polares ácidos por ESI(-) FT-ICR MS revelou que as amostras de *tarballs* (2022.2) sofreram biodegradação e fotooxidação, pelo menos na extensão inicial, apresentaram também, alta abundância de ácidos graxos (ácidos carboxílicos acíclicos), consistentes com suas características cerosas. Já para o estudo dos resíduos monitorados nos anos de 2021 e 2022, a petroleômica mostrou que a falta de correlação em grande maioria dos resíduos monitorados e os eventos ocorridos.

O intemperismo é claro nos óleos correlacionados após os eventos de 2019, 2022.1 e 2022.2. Corroborando com a questão destes resíduos de 2021 e 2022 apresentarem esse corte, a presença da classe O_2 dá indícios que esses resíduos sejam uma mistura de diferentes resíduos petrolíferos que passaram por algum processo térmico como a destilação. Esse processo é uma prática comum na formulação de óleo combustível marítimo pesado. Esses dados reforçam a hipótese de que parte dos resíduos de óleo analisados derivam de produtos processados e não são petróleo bruto.

Os resultados relacionados à presença de amostras parafínicas indicam que além das amostras dos *tarballs* parafínicos do final de 2022, as amostras de 2021 e 2022 também apresentam características parafínicas e como óleos com essas características são muito utilizados para produção de combustíveis líquidos e lubrificantes, esses resíduos após os derramamentos podem ser resíduos de processos de destilação que foram lançados intencionalmente ou não no litoral do estado do Ceará.

Por fim, este estudo destaca o quanto o litoral do Ceará tem sido suscetível a chegada de resíduos de origem petrolífera. Esses resíduos vão se acumulando e impactando silenciosamente e gradativamente o meio ambiente. Assim, é necessário que a sociedade e as autoridades constituídas priorizem estudos sobre derramamentos de petróleo, com ênfase na caracterização dos resíduos que irá contribuir para o rastreamento da origem destes. Esses estudos podem subsidiar ações mitigadoras e responsabilização jurídica ao que lançam esses resíduos intencionalmente ou não nos ambientes costeiros. Assim, é necessário

o uso de políticas públicas integradas à academia para a proteção dos ecossistemas marinhos e preservação da saúde humana frente aos impactos ocasionados pelos derramamentos de petróleo.

PRODUÇÃO CIENTÍFICA DESENVOLVIDA DURANTE O DOUTORADO

1. Artigos publicados em periódicos

AZEVEDO, R. N; **NASCIMENTO, A. P**; PEREIRA, V. B; FRACNO, D. M. M; NELSON, R. K; GONTIJO. B; Azevedo, D. A; NASCIMENTO, R. F; REDDY, C; Reddy; Rivelino M. Cavalcante, R. C; OLIVEIRA, A. H. B; MARTINS, L. L. **A Bottled High-Sulfur Fuel Oil Stranded with the Mysterious Oil Spill on the Brazilian Coast in Early 2022: Geochemical Correlation and Ocean Dumping Evidence**. Published as part of Energy & Fuels special issue "Celebrating Authors of Energy and Fuels Most-Impactful Articles (2022). : https://doi.org/10.1021/acs.energyfuels.5c01581

NASCIMENTO, ADRIANA P.; AZEVEDO, RUFINO NETO A. ; PEREIRA, MARÍLIA GABRIELA A. ; FRANCO, DANIELLE M.M. ; VAZ, BONIEK G. ; OLIVEIRA, ANDRÉ H.B. ; SANTOS, JANDYSON M. ; CAVALCANTE, RIVELINO M. ; MARTINS, LAERCIO L. . **Forensic environmental geochemistry to reveal the extent, characteristics, and fate of waxy tarballs spilled over the northeast coast of Brazil in 2022**. MARINE ENVIRONMENTAL RESEARCH, v. 204, p. 106878, 2025. http://dx.doi.org/10.1016/j.marenvres.2024.106878

LIMA, ANTÔNIA D.F. ; **NASCIMENTO, ADRIANA P.** ; MORAES, ALESSANDRA S.B. ; COSTA, ANA B. ; SANTOS, RAFAEL P. ; BEZERRA, LUÍS E.A. ; GIARRIZZO, TOMMASO ; MARTINS, LAERCIO L. ; CAVALCANTE, RIVELINO M. **. Lepas anatifera as a biomonitor of ocean health, ecological impacts, and cancer risk in a new frontier of exploration (Brazilian Equatorial Margin)**. ENVIRONMENTAL RESEARCH JCR, v. 274, p. 121226, 2025. http://dx.doi.org/10.1016/j.envres.2025.121226

MARTINS, LAERCIO L. ; PEREIRA, VINÍCIUS B. ; **NASCIMENTO, ADRIANA P.** ; AZEVEDO, RUFINO NETO A. ; OLIVEIRA, ANDRÉ H. B. ; TEIXEIRA, CARLOS EDUARDO P. ; AZEVEDO, DÉBORA A. ; DA CRUZ, GEORGIANA F. ; CAVALCANTE, RIVELINO M. ; GIARRIZZO, TOMMASO . **Forensic Geochemistry Reveals International Ship Dumping as a Source of New Oil Spill in Brazil's Coastline (Bahia) in late 2023**. ENVIRONMENTAL SCIENCE & TECHNOLOGY, v. 58, p. 9328-9338, 2024. http://dx.doi.org/10.1021/acs.est.4c01520

FEITOSA, ALICE F. ; MENEZES, ÍCARO B.H.M.P. ; DUARTE, OSCAR S. ; S'B' SALMITO-VANDERLEY, CARMINDA ; CARNEIRO, PEDRO B.M. ; AZEVEDO, RUFINO N.A. ; OLIVEIRA, ANDRÉ H.B. ; LUZ, ANA C.S. ; **NASCIMENTO, ADRIANA P.** ; NASCIMENTO, RONALDO F. ; MARTINS, LAERCIO L. ; CAVALCANTE, RIVELINO M. ; FEITOSA, CAROLINE V. . **The impact of chronic and acute problems on sea turtles: The consequences of the oil spill and ingestion of anthropogenic debris on the tropical semi-arid coast of Ceará, Brazil**. AQUATIC TOXICOLOGY, v. 269, p. 106867, 2024. http://dx.doi.org/10.1016/j.aquatox.2024.106867

BRABO, LUCIO ; MARTINS, LAERCIO L. ; ANDRADES, RYAN ; TEIXEIRA, CARLOS E.P. ; **DO NASCIMENTO, ADRIANA PEREIRA** ; DE AZEVEDO, RUFINO NETO ANDRADE ; BEZERRA, LUÍS E.A. ; CAVALCANTE, RIVELINO M. ; COTTENS, KELLY FERREIRA ; SOARES, ROMULO ALEXANDRE ; DE OLIVEIRA SOUSA, PAULO

HENRIQUE GOMES ; MONT'ALVERNE, TARIN F. ; SOARES, MARCELO O. ; GIARRIZZO, TOMMASO . **A transcontinental threat: Plastic waste from Africa invades Brazil's coast**. SCIENCE OF THE TOTAL ENVIRONMENT, v. 954, p. 176599, 2024. http://dx.doi.org/10.1016/j.scitotenv.2024.176599

MELLO, LUIZA C. ; **NASCIMENTO, ADRIANA P.** ; LOPES, BEATRIZ D. ; LIMA, ANTÔNIA D.F. ; BEZERRA, LUÍS E.A. ; MENDES, LIANA DE F. ; BASTOS, LUCIANA M. ; NOSSOL, ARLENE B.S. ; MARTINS, MÁRIO M. ; MARTINS, LAERCIO L. ; CAVALCANTE, RIVELINO M. . **Tarballs on the Brazilian coast in late 2022 sustain Lepas anatifera Linnaeus, 1758 (Crustacea: Cirripedia): Occurrence and risk of petroleum hydrocarbon ingestion**. SCIENCE OF THE TOTAL ENVIRONMENT, v. 896, p. 164981, 2023. http://dx.doi.org/10.1016/j.scitotenv.2023.164981

AZEVEDO, RUFINO N.A. ; BEZERRA, KAMYLLA M.M. ; NASCIMENTO, RONALDO F. ; NELSON, ROBERT K. ; REDDY, CHRISTOPHER M. ; **NASCIMENTO, ADRIANA P.** ; OLIVEIRA, ANDRÉ H.B. ; MARTINS, LAERCIO L. ; CAVALCANTE, RIVELINO M. **Is there a similarity between the 2019 and 2022 oil spills that occurred on the coast of Ceará (Northeast Brazil)? An analysis based on forensic environmental geochemistry**. ENVIRONMENTAL POLLUTION, v. 314, p. 120283-7, 2022. http://dx.doi.org/10.1016/j.envpol.2022.120283

2. Resumos publicados em anais de congressos

Adriana P, Nascimento; Azevedo, R. N. A; Moraes, A. S. B; Pereira, V. B; Azevedo, A. Debora; Oliveira, A. H. B; Giarrizzo, T; Cavalcante, R. M; Martins, L. L. **Monitoring spilled oils along the coast of Ceará (2021-2022) to estimate the extent of environmental pollution after the 2019 oil spill: forensic geochemistry**, foi apresentado na forma de pôster durante a 48ª Reunião Anual da Sociedade Brasileira de Química, 2025.

MARTINS, L. L. ; PEREIRA, V. B. ; CAVALCANTE, R. M. ;**NASCIMENTO, ADRIANA P. DO**; AZEVEDO, DÉBORA A. ; AZEVEDO, RUFINO NETO A. ; OLIVEIRA, ANDRÉ H. B. ; CRUZ, G. F. ; TEIXEIRA, C. E. P. ; GIARRIZZO, T. **Assessing the origin and fate of tarballs on the coast of Brazil in late 2023 by forensic environmental geochemistry: disclosing international oil dumping**. In: Reunião Anual da SBQ, 2024, São Paulo. A centralidade da química na educação do cidadão e na inovação científica e tecnológica, 2024.

BRABO, L. ; MARTINS, L. L. ; ANDRADES, R. C. ; TEIXEIRA, C. E. P. ; **NASCIMENTO, ADRIANA P.** ; AZEVEDO, RUFINO N.A. ; CAVALCANTE, R. M. ; CARNEIRO, T. Y. C. ; COTTENS, K. F. ; DANTAS, A. D. ; SANTOS JUNIOR, O. S. ; LIMA, E. R. ; SOARES, R. A. ; SOUSZA, P. H. G. O. ; SOUZA, F. D. L. ; SOUSA, G. N. ; MONTALVERNE, T. F. ; SOARES, M. O. ; GIARRIZZO, T. **. Poluição marinha por plástico: o caso dos resíduos africanos no litoral semiárido brasileiro**. In: 20º CONGRESSO LATINO-AMERICANO DE CIÊNCIAS DO MAR COLACMAR 2024 e do 8º CONGRESSO BRASILEIRO DE OCEANOGRAFIA CBO 2024, Itajaí. 20º CONGRESSO LATINO-AMERICANO DE CIÊNCIAS DO MAR COLACMAR 2024 e do 8º CONGRESSO BRASILEIRO DE OCEANOGRAFIA CBO 2024, 2024. v. 1.

LIMA, E. R. ; BRABO, L. ; **NASCIMENTO, ADRIANA P. DO** ; AZEVEDO, RUFINO N.A. ; DANTAS, A. D. ; SOUZA, F. D. L. ; CARNEIRO, T. Y. C. ; SANTOS JUNIOR, O. S. ; SOUSA, G. N. ; MONTALVERNE, T. F. ; MARTINS, L. L. ; GIARRIZZO, T. **Rastreando a poluição costeira: auditoria de marcas para monitorar resíduos estrangeiros no litoral semiárido do Ceará**. In: 20º CONGRESSO LATINO-AMERICANO DE CIÊNCIAS DO MAR COLACMAR 2024 e do 8º CONGRESSO BRASILEIRO DE OCEANOGRAFIA ? CBO 2024, 2024, Itajaí. 20º CONGRESSO LATINO-AMERICANO DE CIÊNCIAS DO MAR COLACMAR 2024 e do 8º CONGRESSO BRASILEIRO DE OCEANOGRAFIA ? CBO 2024, 2024.

NASCIMENTO, ADRIANA P. DO; AZEVEDO, RUFINO N.A. ; PEREIRA, VINÍCIUS B. ; AZEVEDO, DÉBORA A. ; Oliveira Gadelha ; CAVALCANTE, R. M. ; MARTINS, L. L. . **Assessment of oily materials beached over the coast of Ceará by forensic geochemistry: a chronic environmental problem**. In: 21º Encontro Nacional de Química Analítica (ENQA) e o 9º Congresso Ibero Americano de Química Analítica (CIAQA), 2024, Belém. 21º Encontro Nacional de Química Analítica (ENQA) e o 9º Congresso Ibero Americano de Química Analítica (CIAQA), 2024.

OLIVEIRA, A. H. B. ; AZEVEDO, RUFINO N.A. **NASCIMENTO, ADRIANA P. DO** ; PEREIRA, V. B. ; AZEVEDO, D. A. ; NASCIMENTO, RONALDO F. ; CAVALCANTE, R. M. ; MARTINS, L. L. . **Stranded oil on the coast of Ceará revealed as heavy fuel oil by gas chromatography**. In: 21º Encontro Nacional de Química Analítica (ENQA) e o 9º Congresso Ibero Americano de Química Analítica (CIAQA), 2024, Belém. 21º Encontro Nacional de Química Analítica (ENQA) e o 9º Congresso Ibero Americano de Química Analítica (CIAQA), 2024.

AZEVEDO, RUFINO N.A. ; **NASCIMENTO, ADRIANA P. DO** ; PEREIRA, V. B. ; FRANCO, D. M. M. ; AZEVEDO, D. A. ; NELSON, ROBERT K. ; REDDY, CHRISTOPHER M. ; NASCIMENTO, RONALDO F. ; VAZ, BONIEK G. ; CAVALCANTE, RIVELINO M. ; OLIVEIRA, ANDRÉ H. B. ; MARTINS, LAERCIO L. . **FT-ICR MS to assess the foreign origin and fuel characteristics of the spilled oil on the coast of Ceará, Brazil, in early 2022**. In: 4th Iberoamerican Conference on Mass Spectrometry, 2024, Foz do Iguaçu. 4th Iberoamerican Conference on Mass Spectrometry, 2024., 2024, Foz do Iguaçu. 4th Iberoamerican Conference on Mass Spectrometry, 2024, Foz do Iguaçu. 4th Iberoamerican Conference on Mass Spectrometry, 2024., 2024.

AZEVEDO, RUFINO N.A. ; **NASCIMENTO, Adriana Pereira do** ; PEREIRA, V. B. ; AZEVEDO, DÉBORA A. ; CAVALCANTE, RIVELINO M. ; MARTINS, LAERCIO L. ; OLIVEIRA, ANDRÉ H. B. . **ORIGEM E CARACTERÍSTICAS DE COMBUSTÍVEL DO ÓLEO DERRAMADO NO ESTADO DO CEARÁ NO INÍCIO DE 2022**: UMA ABORDAGEM GEOQUÍMICA AMBIENTAL FORENSE. In: XV semana da Química & VIII workshop da Pós-graduação em Química, 2024, Fortaleza. XV semana da Química & VIII workshop da Pós-graduação em Química, 2024.

MARIANO, P. ; **NASCIMENTO, ADRIANA P. DO** ; AZEVEDO, RUFINO N.A. ; BRABO, LUCIO ; CAVALCANTE, RIVELINO M. ; GIARRIZZO, TOMMASO ; MARTINS, LAERCIO L. ; OLIVEIRA, ANDRÉ H. B. **INVESTIGAÇÃO DA FREQUÊNCIA E ORIGEM DE ÓLEOS ENCALHADOS NA COSTA DO CEARÁ EM 2023 E 2024: GEOQUÍMICA AMBIENTAL FORENSE E ANÁLISE QUÍMICA MOLECULAR ABRANGENTE**. In: Encontros Universitários 202, 2024. Encontros Universitários 2024, 2024.

SOUZA, F. D. L. ; LIMA, E. R. ; BRABO, LUCIO ; AZEVEDO, RUFINO N.A. ; **NASCIMENTO, ADRIANA P. DO** ; CARNEIRO, T. Y. C. ; SANTOS JUNIOR, O. S. ; SOARES, MARCELO O. ; GIARRIZZO, T. . **Do macro ao micro: fragmentos macroplásticos como potencializadores da poluição marinha**. In: Semana Nacional de Oceanografia, 2024, Rio de Janeiro. IV Simpos Oceano, 2024.

NASCIMENTO, ADRIANA P. DO; AZEVEDO, RUFINO N.A. ; FARIAS, M. T. A. R. ; MARTINS, LAERCIO L. ; OLIVEIRA, ANDRÉ H.B. ; CAVALCANTE, R. M. **Geoquímica Orgânica para desvendar os múltiplos derramamentos de óleo no litoral cearense: uma problemática crônica, porém silenciosa**. In: Encontros Universitários 2023, 2023, Fortaleza. Encontros Universitários 2023, 2023.

NASCIMENTO, ADRIANA P. DO; AZEVEDO, RUFINO N.A. ; OLIVEIRA, ANDRÉ H.B. ; MARTINS, L. L. ; CAVALCANTE, R. M. ; PEREIRA, M. G. A. ; SANTOS, J. M. **. Is there a correlation between the waxy tarballs stranded on the coast of northeast Brazil in late 2022 with previous oil spills?**. In: XVI Latin American Congress on Organic Geochemistry (ALAGO 2023), 2023, Aracaju-SE, 2023, Aracaju. Annals - XVI Latin American Congress on Organic Geochemistry (ALAGO 2023), 2023. v. 1. p. 205-206.

NASCIMENTO, ADRIANA P. DO; CAVALCANTE, R. M. ; MARTINS, L. L. ; PEREIRA, M. G. A. ; SANTOS, J. M. ; AZEVEDO, RUFINO N.A. ; OLIVEIRA, ANDRÉ H.B. **O uso da química forense aplicada na investigação dos múltiplos derramamentos de óleo (2019 a 2022) no litoral do nordeste brasileiro**. In: XIV Semana da Química e VII Workshop da Pós-Graduação em Química da Universidade Federal do Ceará, 2023, Fortaleza. XIV Semana da Química, 2023.

NASCIMENTO, ADRIANA P. DO; AZEVEDO, RUFINO N.A. ; OLIVEIRA, ANDRÉ H. B. ; MARTINS, LAERCIO L. ; CAVALCANTE, RIVELINO M. ; PEREIRA, MARÍLIA GABRIELA A. ; SANTOS, JANDYSON M. **Is there a correlation between the waxy tarballs stranded on the coast of northeast Brazil in late 2022 with previous oil spills?**. In: XVI Latin American Congress on Organic Geochemistry (ALAGO 2023), 2023, Aracaju. Annals - XVI Latin American Congress on Organic Geochemistry (ALAGO 2023), 2023.

NASCIMENTO, ADRIANA P. DO; AZEVEDO, RUFINO N.A. ; PEREIRA, M. G. A. ; SANTOS, J. M. ; FRANCO, D. M. M. ; VAZ, BONIEK G. ; OLIVEIRA, A. H. B. ; CAVALCANTE, RIVELINO M. ; MARTINS, L. L. . **The use of mass spectrometry techniques to investigate oil spills in Northeast Brazil in the years 2019 to 2022**. In: 4a Escola de Espectrometria de Massas - 2023, 2023, em alto mar- Porto de Santos. 4a Escola de Espectrometria de Massas - 2023, 2023.

LUZ, A. C. S. ; OLIVEIRA, ANDRÉ H.B. ; CAVALCANTE, RIVELINO M. ; AZEVEDO, RUFINO N.A. ; **NASCIMENTO, ADRIANA P.** ; FEITOSA, A. F. ; FEITOSA, C. V. ; FRANCO, D. M. M. ; COVAS, T. R. ; VAZ, B. G. ; MARTINS, LAERCIO L. **Assessment of petroleum compounds in sea turtles from the coast of the state of Ceará, Brazil, after the 2019 oil spill using ESI(-) FT-ICR MS**. In: 3rd Iberoamerican Conference on Mass Spectrometry - Ibero Rio 2022, 2022, Rio de Janeiro. III IberoAmerican Conference on Mass Spectrometry, 2022. v. 1. p. 3-619.

NASCIMENTO, ADRIANA P.; CAVALCANTE, RIVELINO M. ; OLIVEIRA, ANDRÉ H.B. ; AZEVEDO, RUFINO N.A. ; FRANCO, D. M. M. ; COVAS, T. R. ; VAZ, B. G. ; MARTINS, LAERCIO L. . **Forensic environmental geochemistry by petroleomics to investigate the frequent oil spills reaching the coast of Brazil since 2019**. In: 3rd Iberoamerican Conference on Mass Spectrometry - Ibero Rio 2022, 2022, Rio de Janeiro. III IberoAmerican Conference on Mass Spectrometry, 2022. v. 1. p. 434-435.

NASCIMENTO, ADRIANA P.; CAVALCANTE, RIVELINO M. ; AZEVEDO, RUFINO N.A. ; FRANCO, D. M. M. ; COVAS, T. R. ; VAZ, B. G. ; MARTINS, LAERCIO L. . **Assessment of weathering processes on the spilled oils stranded on the coast of ceará, brazil, in 2022 by esi(-) FT-ICR/MS.** In: 5th Fortaleza Austral Spring School, 2022, Fortaleza. 5th Fortaleza Austral Spring School, 2022. v. 1. p. 1-1.

AZEVEDO, RUFINO N.A. ; BEZERRA, KAMYLLA M.M. ; NASCIMENTO, RONALDO F. ; OLIVEIRA, ANDRÉ H.B. ; **NASCIMENTO, ADRIANA P. DO** ; MARTINS, LAERCIO L. ; CAVALCANTE, RIVELINO M. . **Existe semelhança entre os derramamentos de óleo de 2019 e 2022 ocorridos no litoral do Ceará (Nordeste do Brasil)? Uma análise baseada em geoquímica ambiental forense**. In: XIII Semana da Química UFC, 2022, Fortaleza. Química: Ciência Essencial para o Desenvolvimento Sustentável, 2022, Fortaleza. XIII Semana da Química UFC, 2022, 2022.

APÊNDICE A

Material suplementar do artigo 1: *Publicado em https://ars.els-cdn.com/content/image/1-s2.0-S0141113624005397-mmc1.pdf*

SUPPLEMENTARY MATERIAL

Forensic environmental geochemistry to reveal the extent, characteristics, and fate of waxy tarballs spilled over the northeast coast of Brazil in 2022

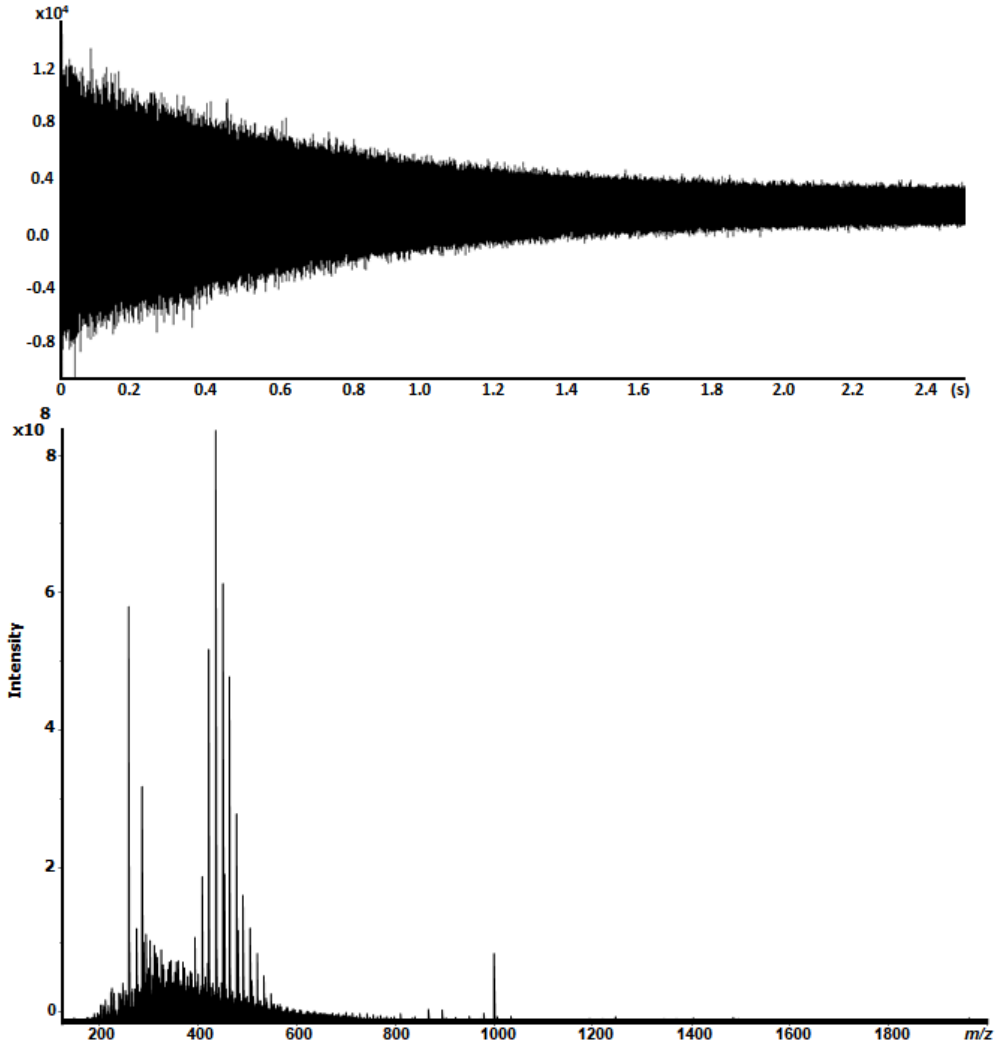

Fig. S1. Top: time domain of transient acquisition time. Bottom: Spectra in magnitude mode, sample P01#22.2(09).

Fig. S2. Test of fluctuation of the waxy tarball, collected in late 2022 at the State of Ceará, Brazil, on sea water.

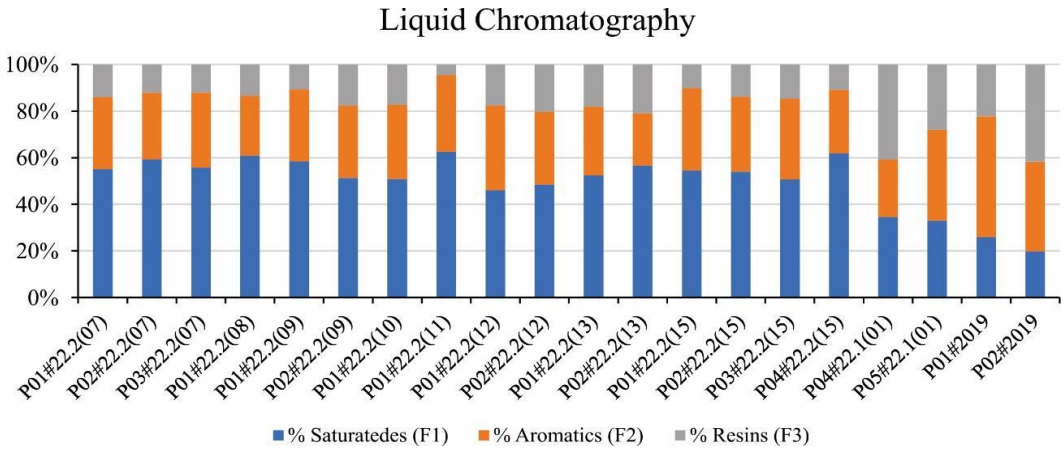

Fig. S3. Percentage of the saturated, aromatic, and resin fractions of the maltene obtained by liquid chromatography.

Fig. S4. Approximately 2.8 kg of tarballs collected in 200 m of extension at the Future beach, State of Ceará, Brazil, on September 23, 2022.

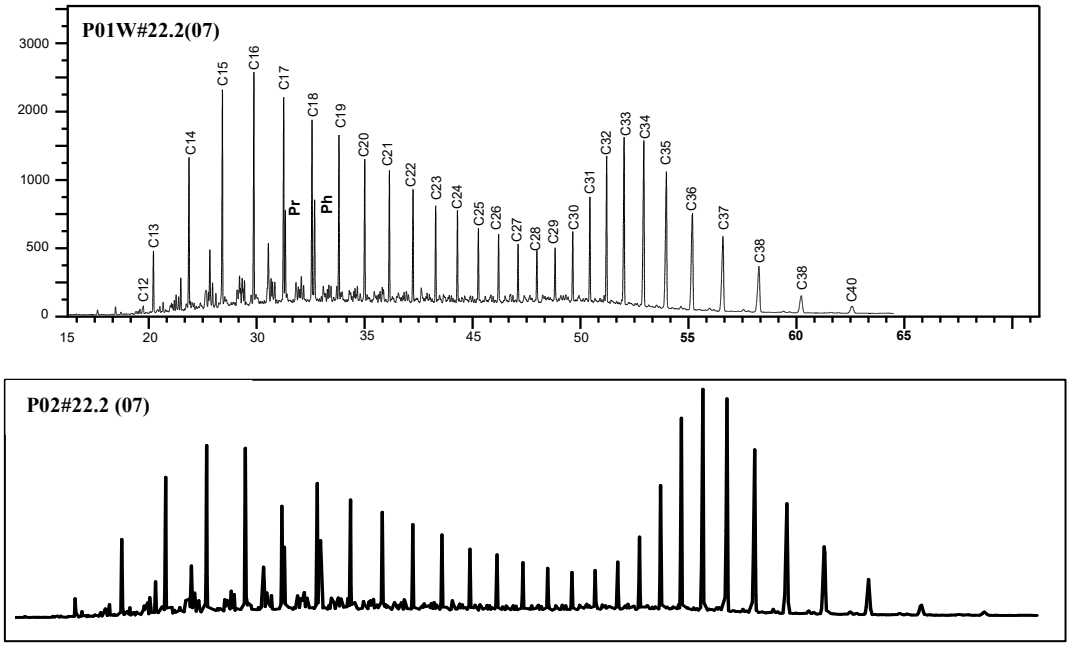

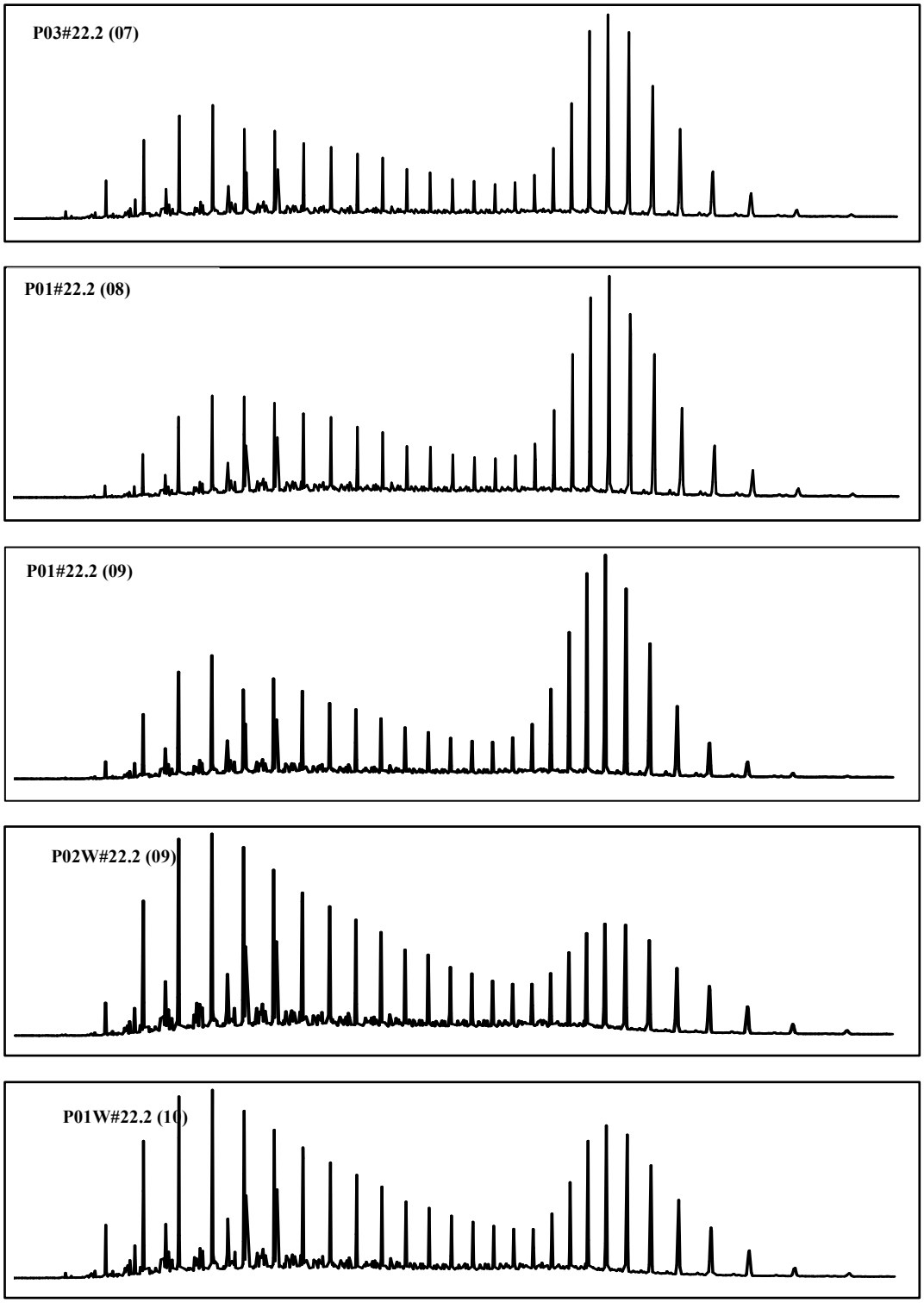
P03#22.2 (07)
P01#22.2 (08)
P01#22.2 (09)
P02W#22.2 (09)
P01W#22.2 (10)

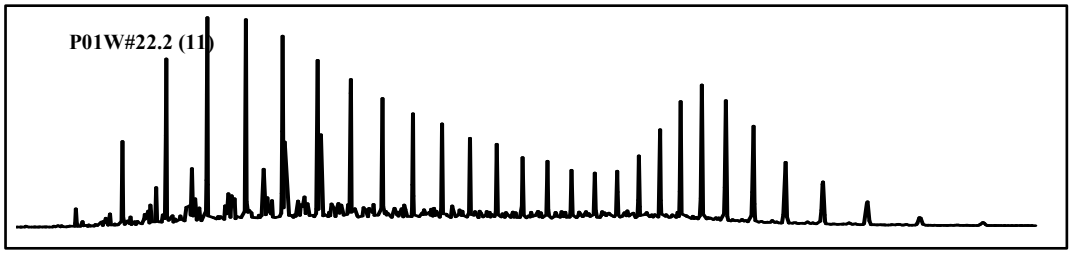
P01W#22.2 (11)

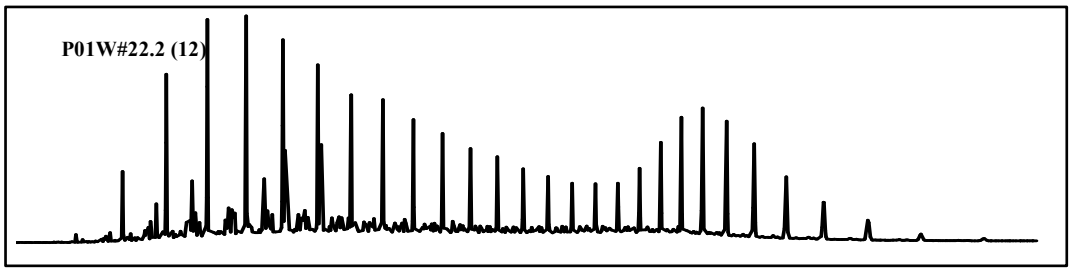
P01W#22.2 (12)

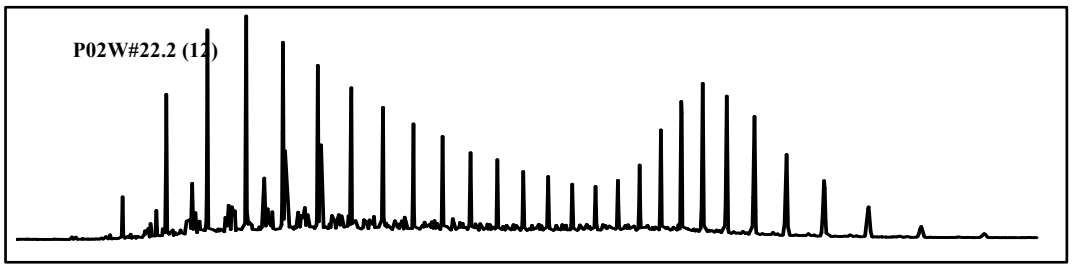
P02W#22.2 (12)

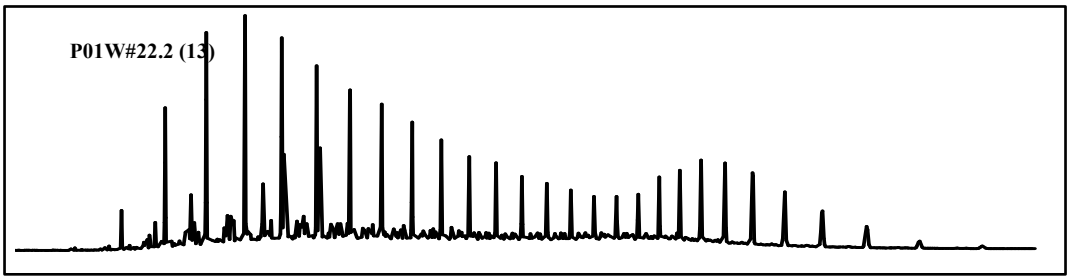
P01W#22.2 (13)

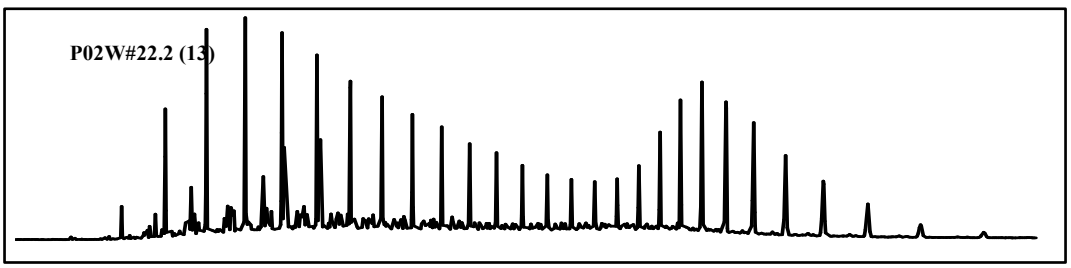
P02W#22.2 (13)

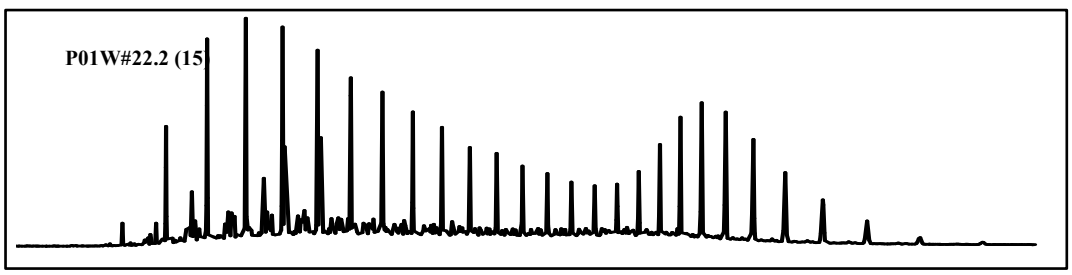
P01W#22.2 (15)

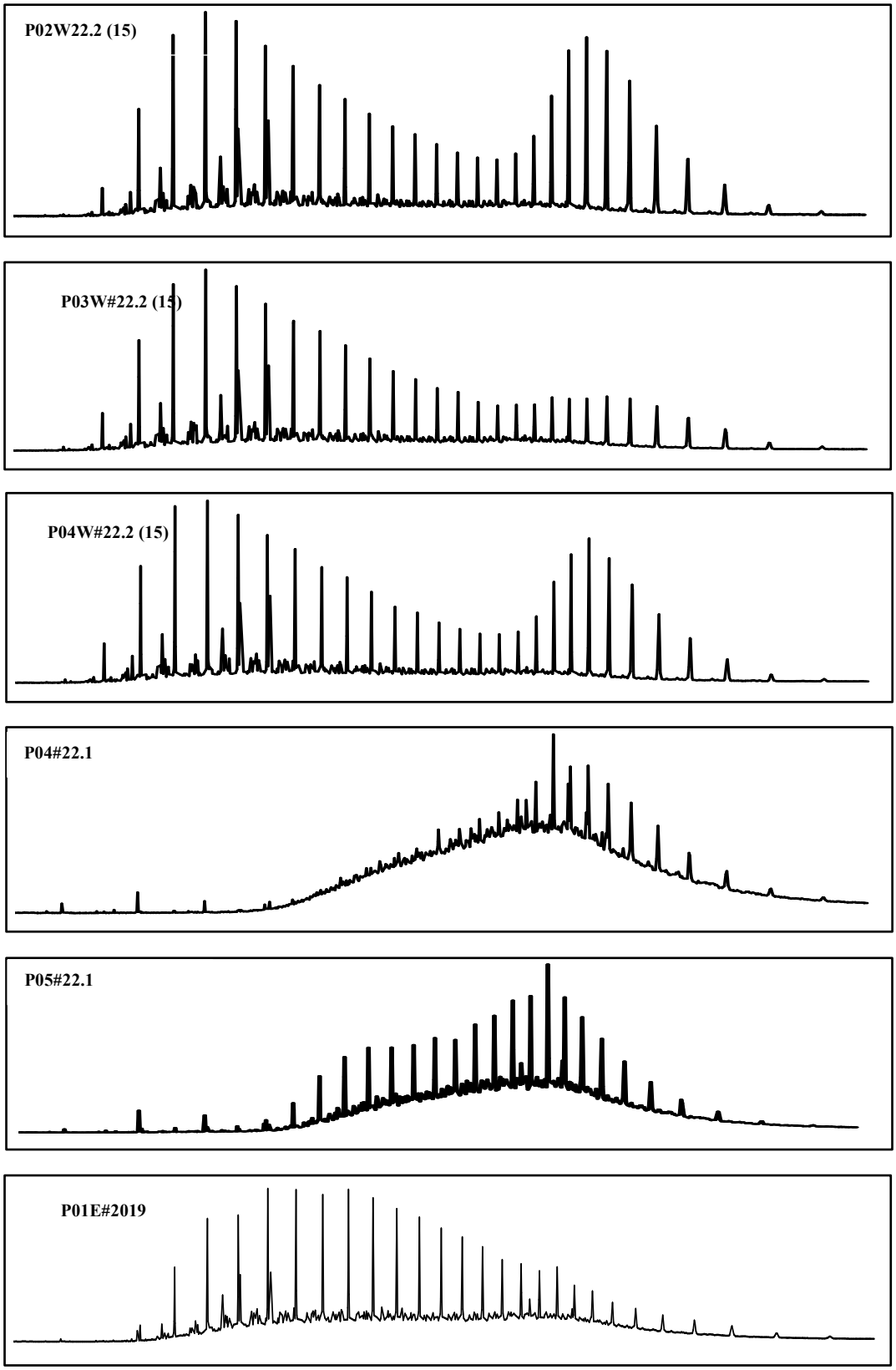
P02W22.2 (15)
P03W#22.2 (15)
P04W#22.2 (15)
P04#22.1
P05#22.1
P01E#2019

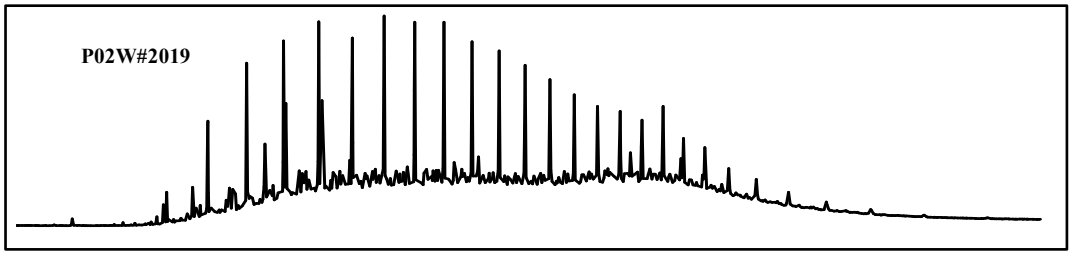

Fig. S4. GC-FID chromatograms of the 16 tarball samples collected in late 2022, in addition to the two spilled oils collected in early 2022 and the two spilled oils collected in 2019.

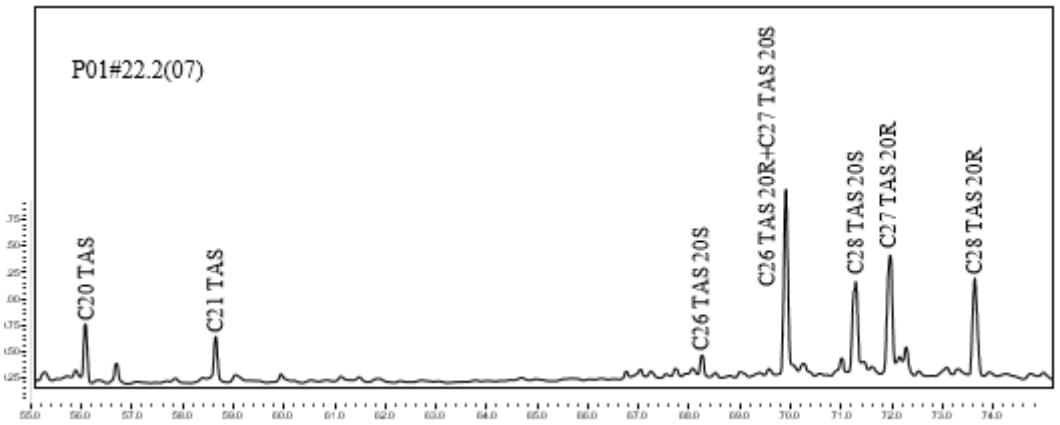
P01#22.2(07)
C20 TAS
C21 TAS
C26 TAS 20S
C26 TAS 20R+C27 TAS 20S
C28 TAS 20S
C27 TAS 20R
C28 TAS 20R

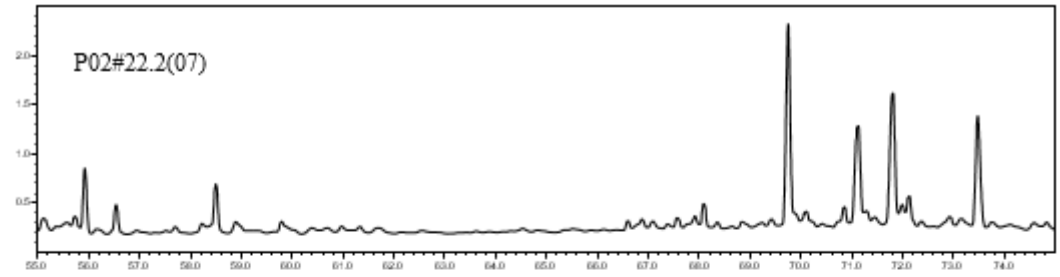
P02#22.2(07)

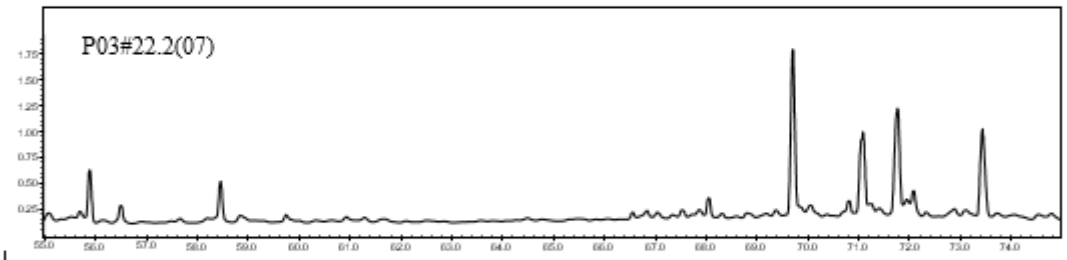
P03#22.2(07)

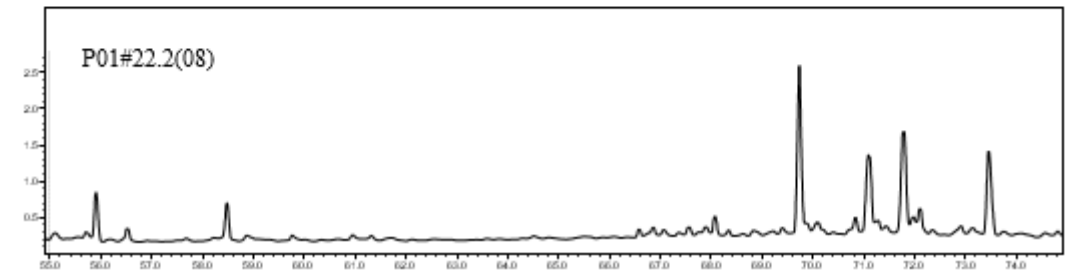
P01#22.2(08)

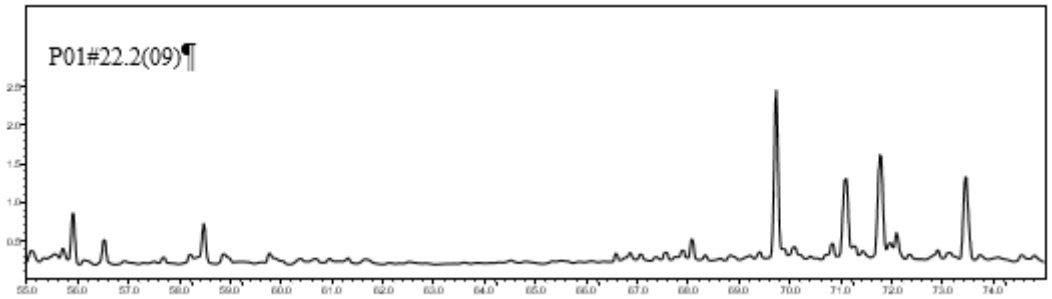
P01#22.2(09)¶

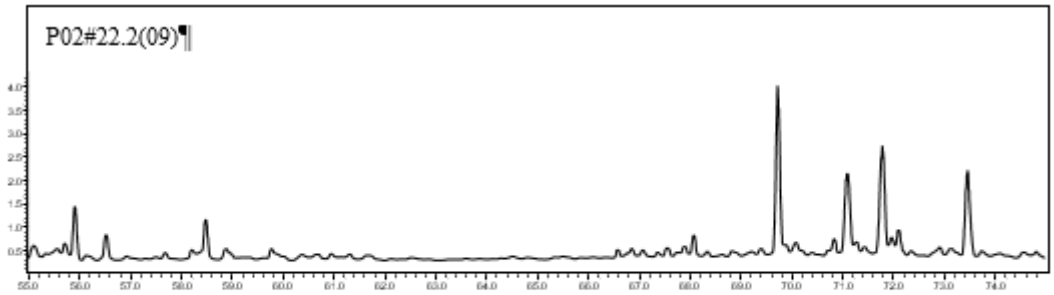
P02#22.2(09)¶

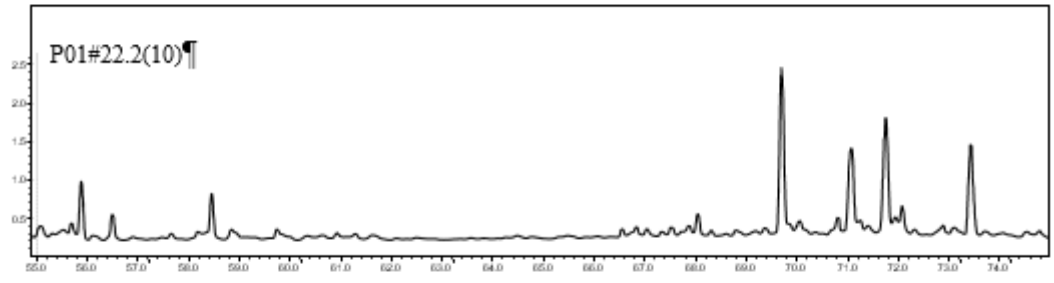
P01#22.2(10)¶

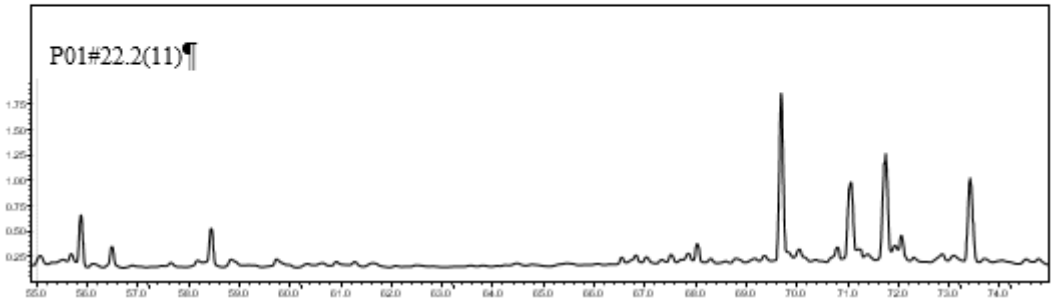
P01#22.2(11)¶

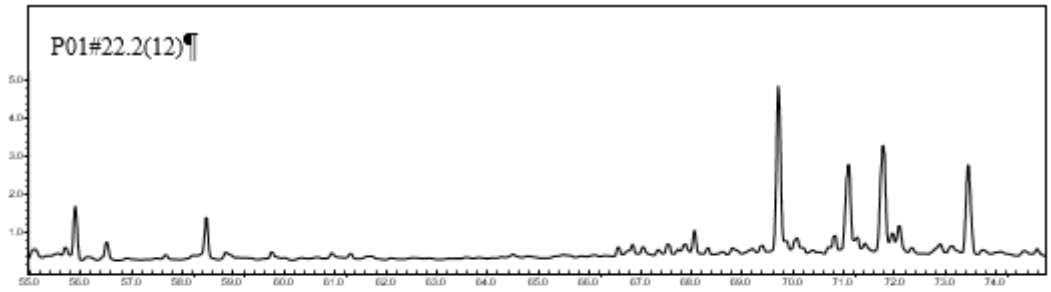
P01#22.2(12)¶

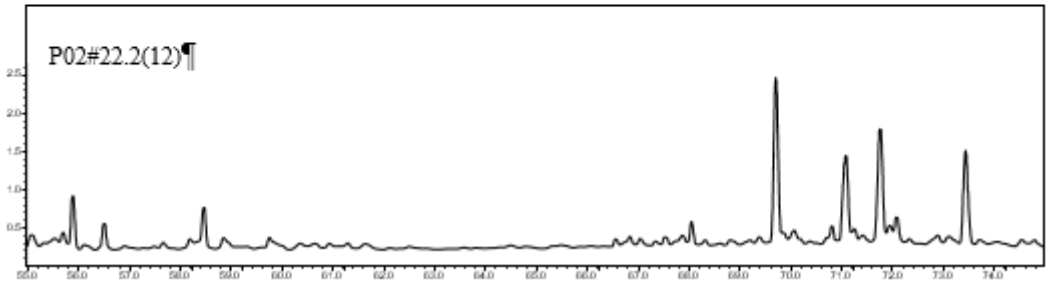
P02#22.2(12)¶

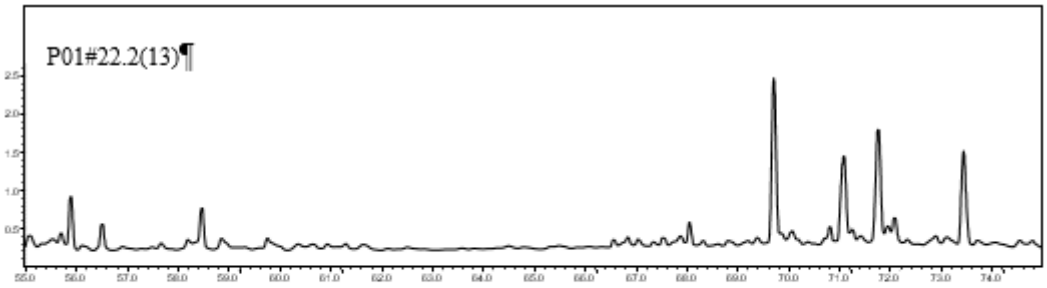
P01#22.2(13)¶

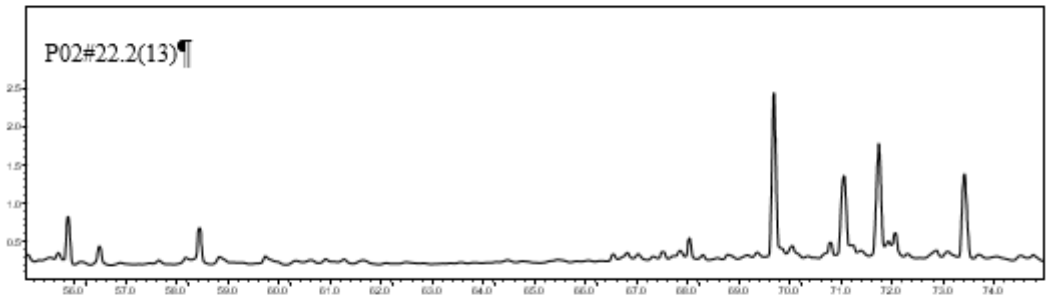
P02#22.2(13)¶

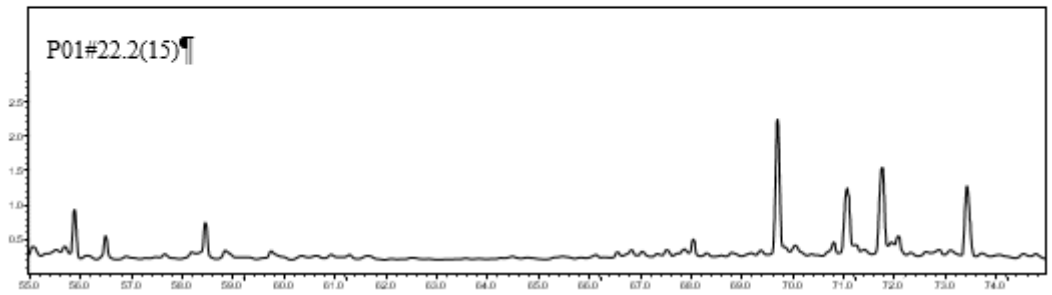
P01#22.2(15)¶

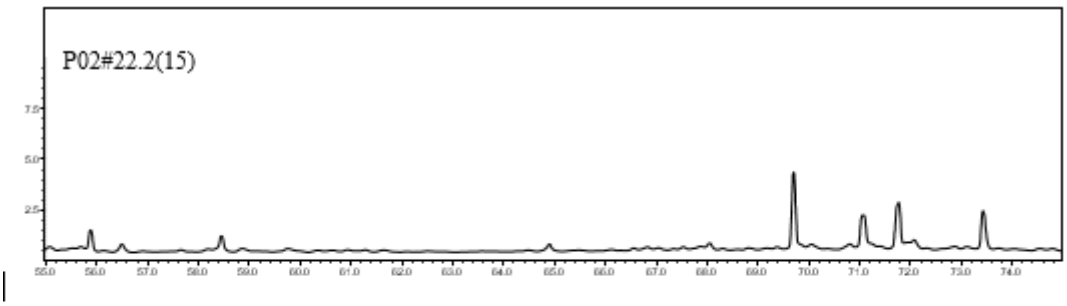
P02#22.2(15)

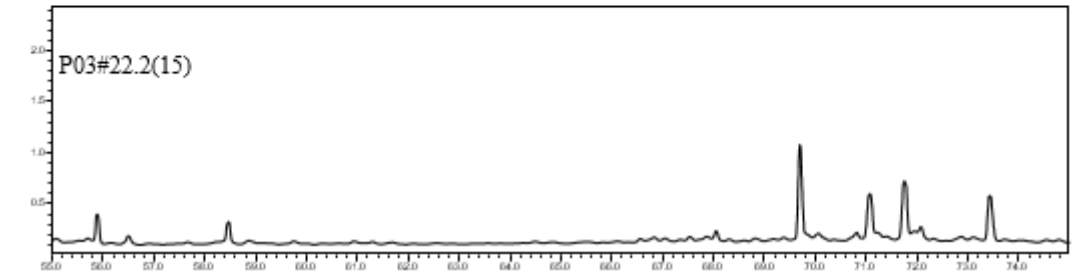
P03#22.2(15)

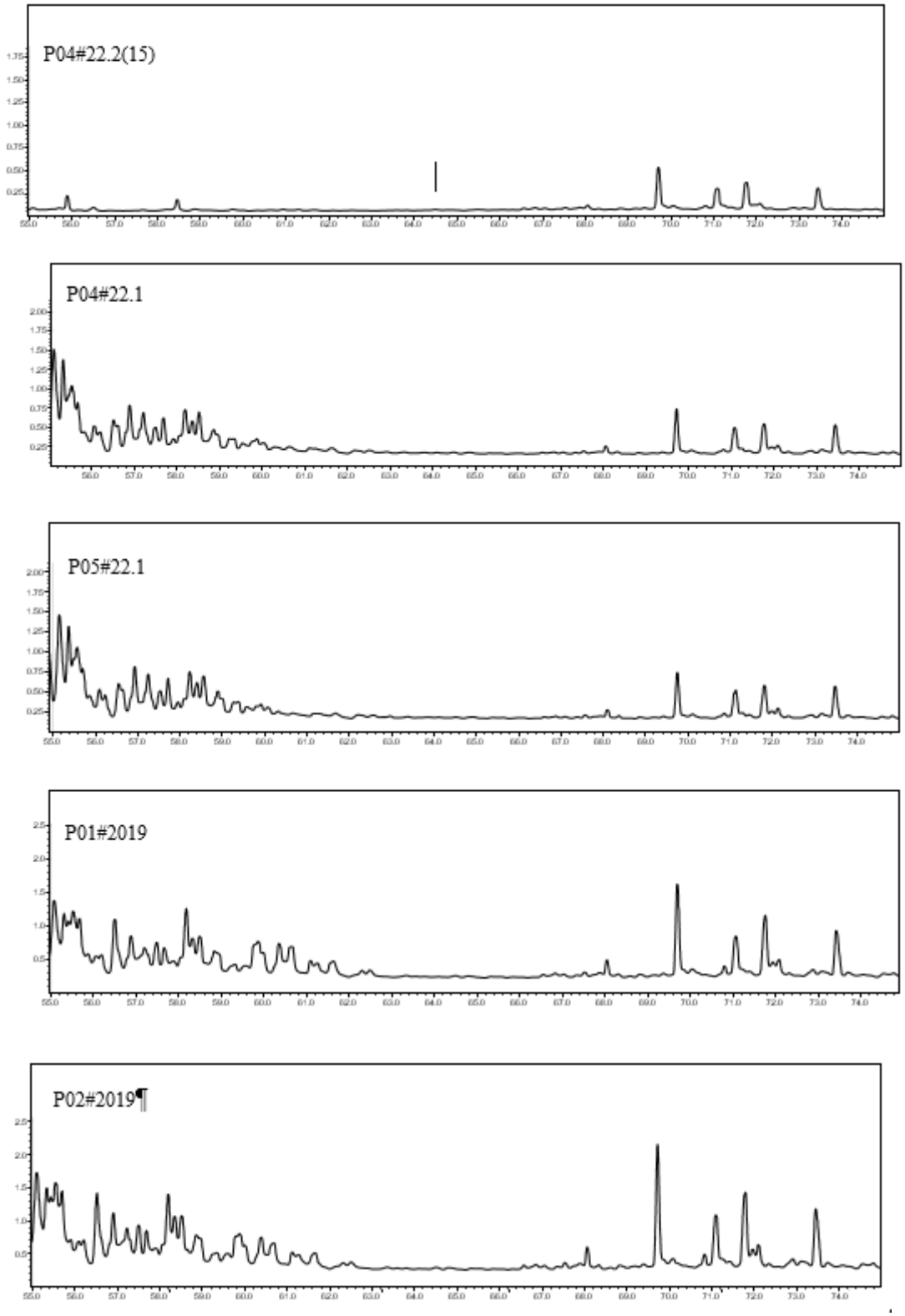

Fig. S6. Chromatograms *m/z* 231 of the 16 tarball samples collected in late 2022, in addition to the two spilled oils collected in early 2022 and the two spilled oils collected in 2019.

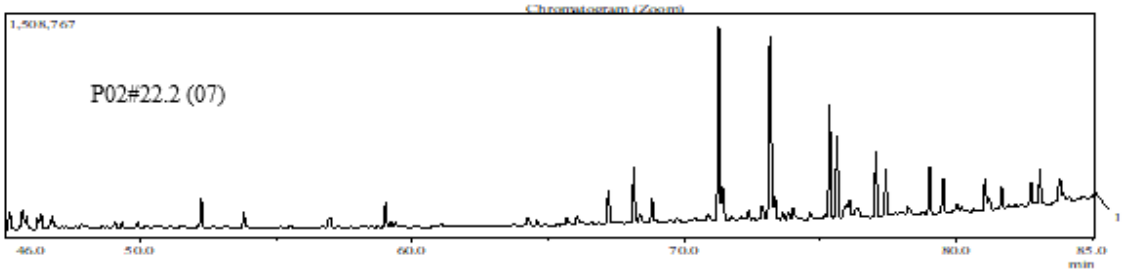
Chromatogram (Zoom)
1,508,767
P02#22.2 (07)
46.0
50.0
60.0
70.0
80.0
85.0
min

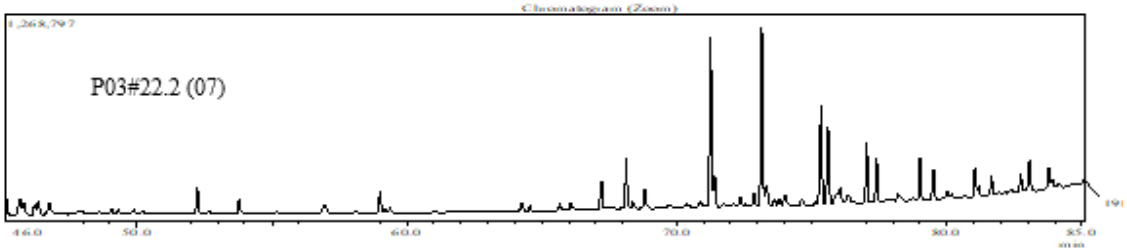
Chromatogram (Zoom)
1,268,797
P03#22.2 (07)
46.0
50.0
60.0
70.0
80.0
85.0
min

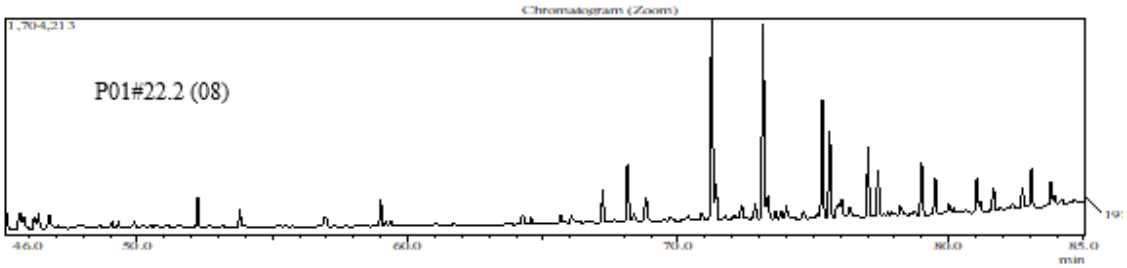
Chromatogram (Zoom)
1,704,213
P01#22.2 (08)
46.0
50.0
60.0
70.0
80.0
85.0
min

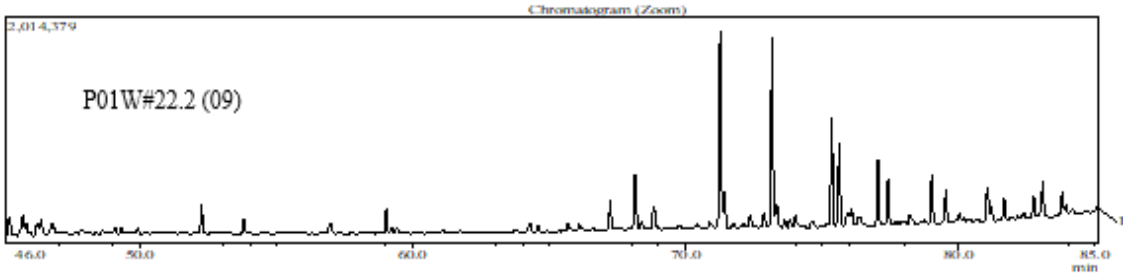
Chromatogram (Zoom)
2,014,379
P01W#22.2 (09)
46.0
50.0
60.0
70.0
80.0
85.0
min

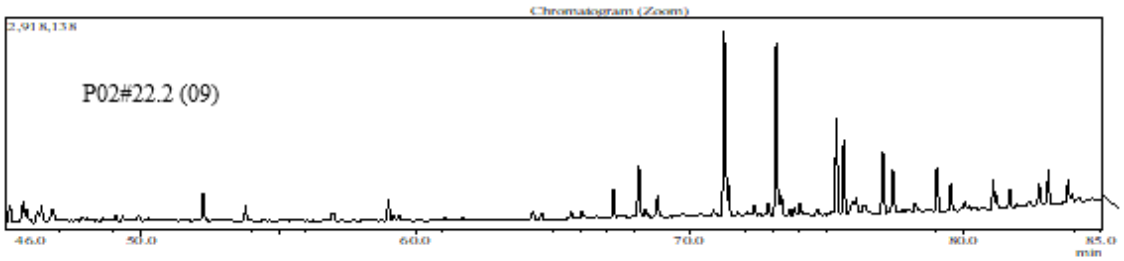
Chromatogram (Zoom)
2,918,138
P02#22.2 (09)
46.0
50.0
60.0
70.0
80.0
85.0
min

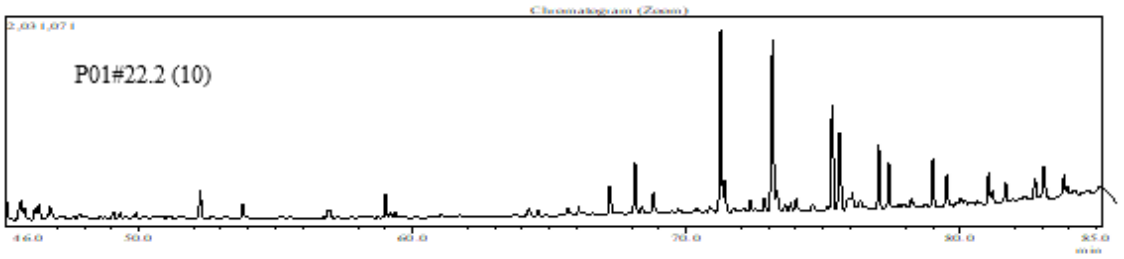
Chromatogram (Zoom)
2,031,071
P01#22.2 (10)
46.0
50.0
60.0
70.0
80.0
85.0
min

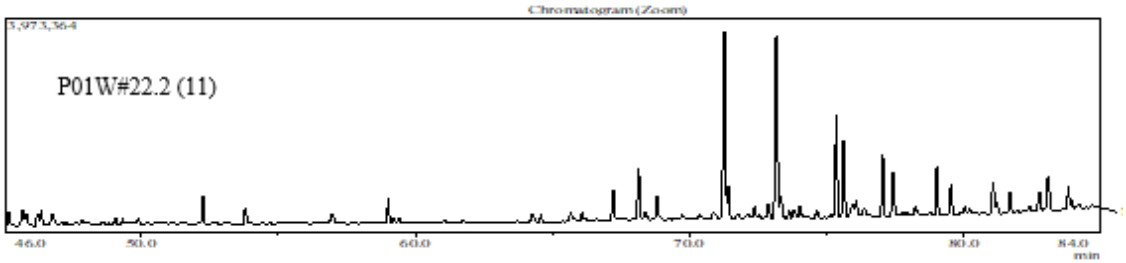
Chromatogram (Zoom)
3,973,364
P01W#22.2 (11)
46.0
50.0
60.0
70.0
80.0
84.0
min

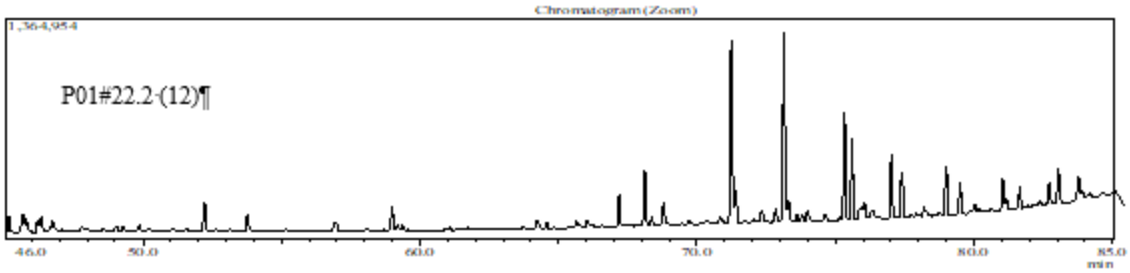
Chromatogram (Zoom)
1,364,954
P01#22.2·(12)¶
46.0
50.0
60.0
70.0
80.0
85.0
min

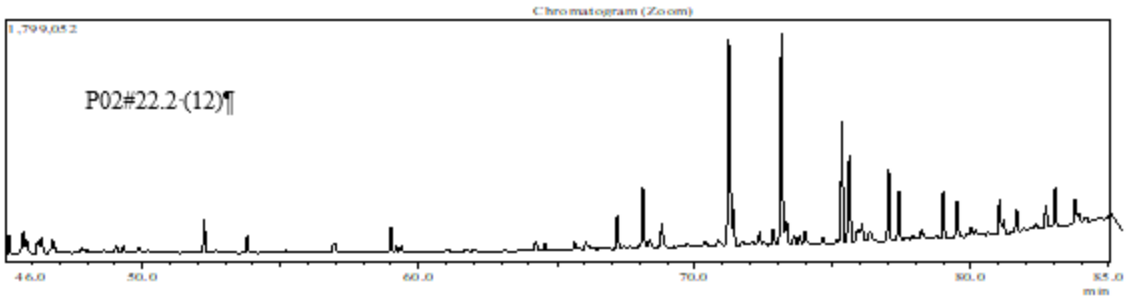
Chromatogram (Zoom)
1,799,052
P02#22.2·(12)¶
46.0
50.0
60.0
70.0
80.0
85.0
min

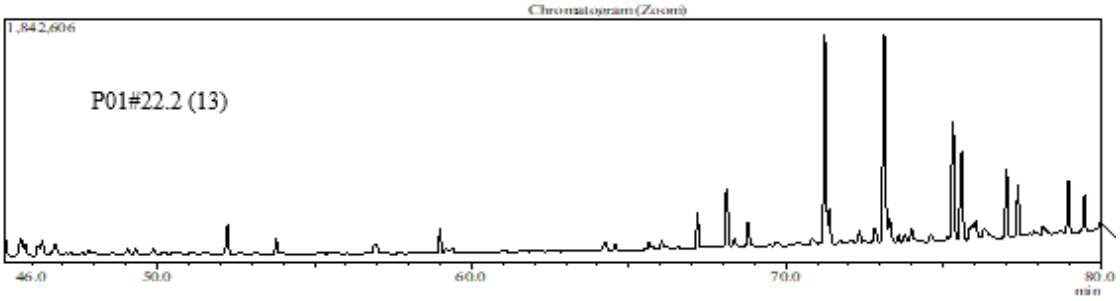
Chromatogram (Zoom)
1,842,606
P01#22.2 (13)
46.0
50.0
60.0
70.0
80.0
min

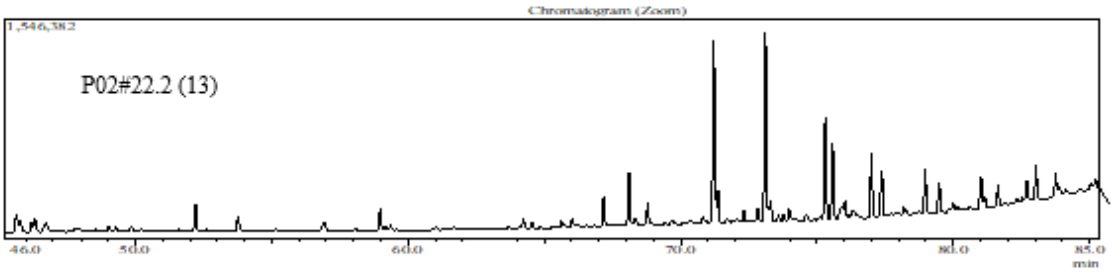
Chromatogram (Zoom)
1,546,382
P02#22.2 (13)
46.0
50.0
60.0
70.0
80.0
85.0
min

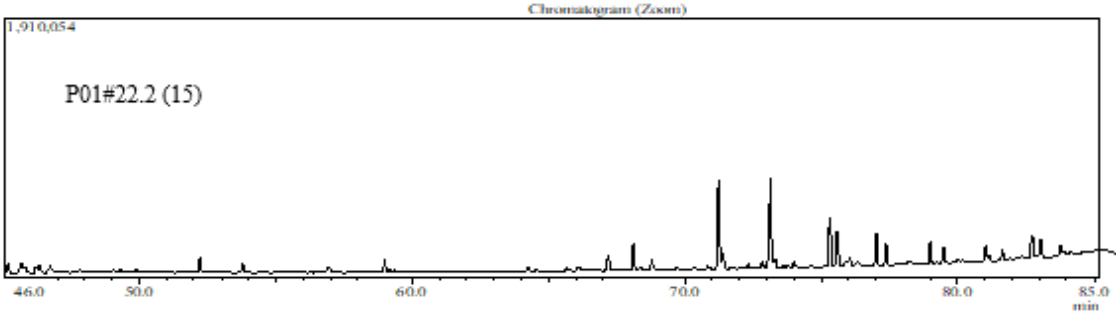
Chromatogram (Zoom)
1,910,054
P01#22.2 (15)
46.0
50.0
60.0
70.0
80.0
85.0
min

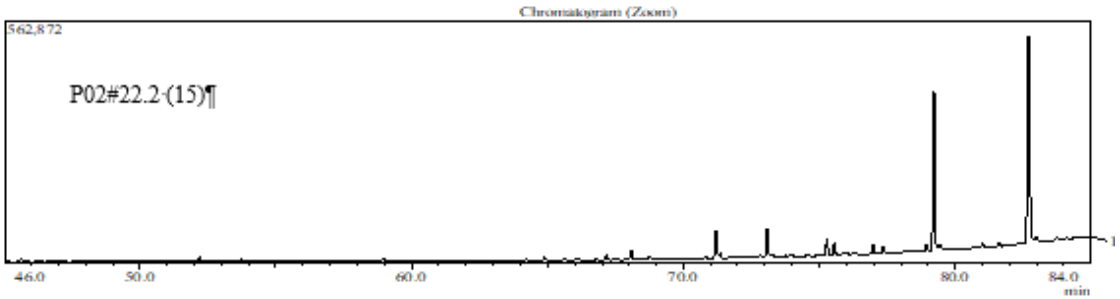
Chromatogram (Zoom)
562,872
P02#22.2-(15)¶
46.0
50.0
60.0
70.0
80.0
84.0
min

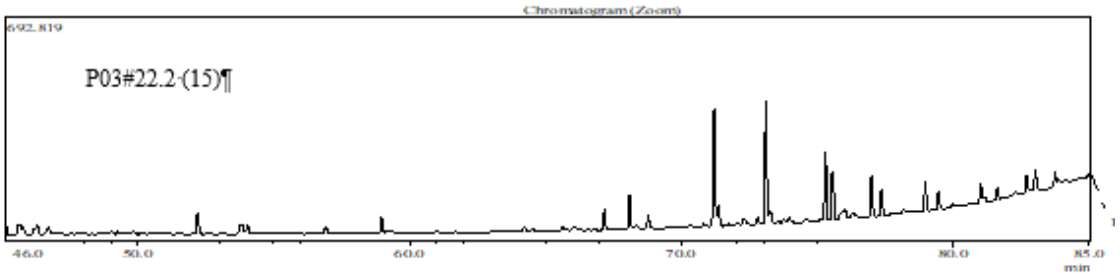
Chromatogram (Zoom)
692,819
P03#22.2-(15)¶
46.0
50.0
60.0
70.0
80.0
85.0
min

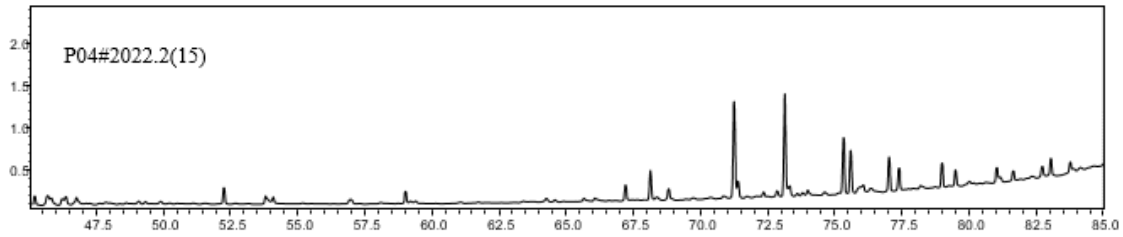
P04#2022.2(15)
2.0
1.5
1.0
0.5
47.5
50.0
52.5
55.0
57.5
60.0
62.5
65.0
67.5
70.0
72.5
75.0
77.5
80.0
82.5
85.0

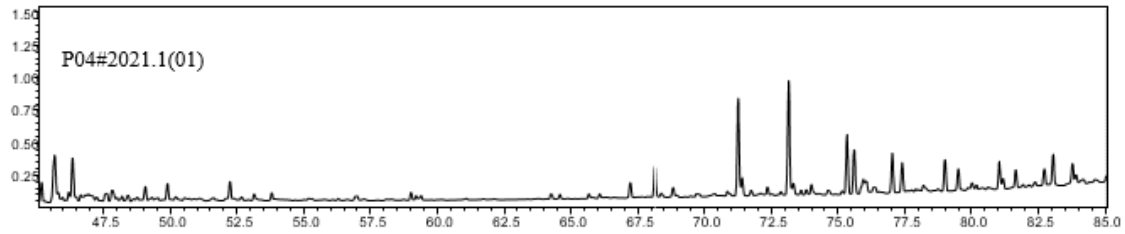
P04#2021.1(01)
1.50
1.25
1.00
0.75
0.50
0.25
47.5
50.0
52.5
55.0
57.5
60.0
62.5
65.0
67.5
70.0
72.5
75.0
77.5
80.0
82.5
85.0

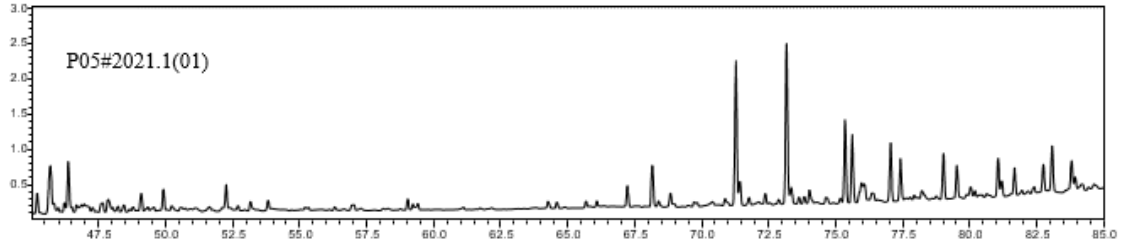
P05#2021.1(01)
3.0
2.5
2.0
1.5
1.0
0.5
47.5
50.0
52.5
55.0
57.5
60.0
62.5
65.0
67.5
70.0
72.5
75.0
77.5
80.0
82.5
85.0

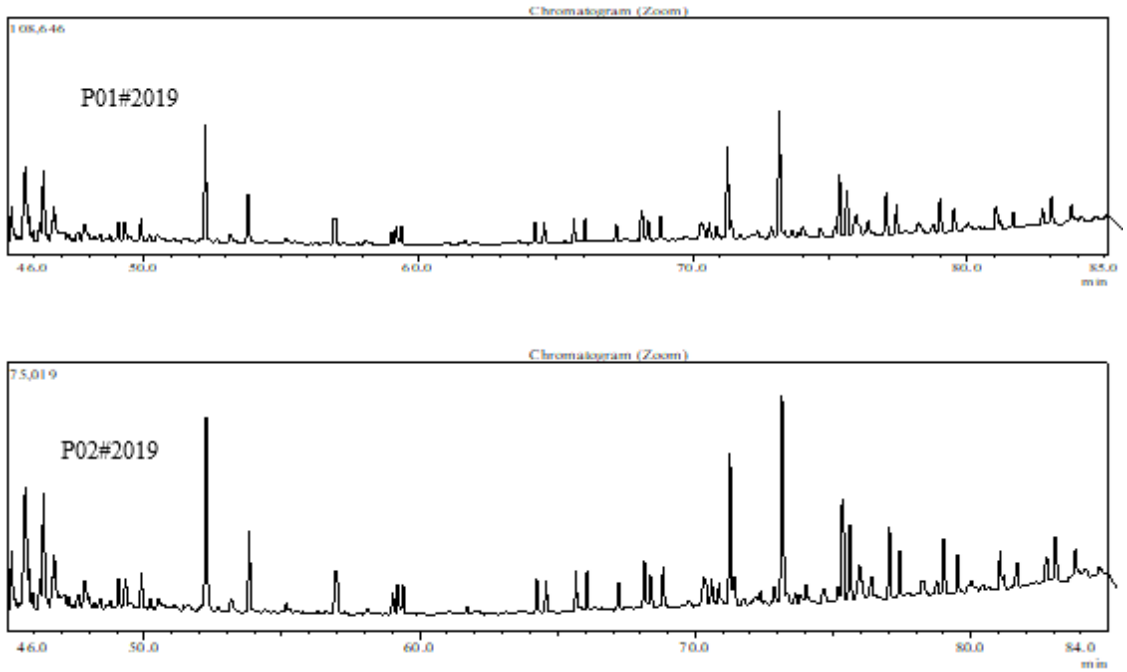

Fig. S7. Chromatograms *m/z* 191 of the 16 tarball samples collected in late 2022, in addition to the two spilled oils collected in early 2022 and the two spilled oils collected in 2019.

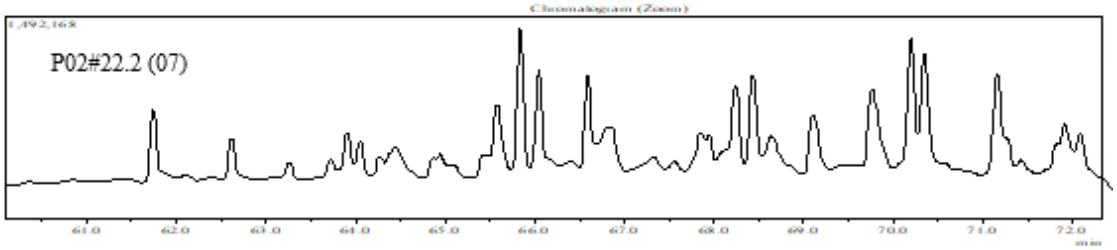
Chromatogram (Zoom)
1,492,168
P02#22.2 (07)
61.0
62.0
63.0
64.0
65.0
66.0
67.0
68.0
69.0
70.0
71.0
72.0
min

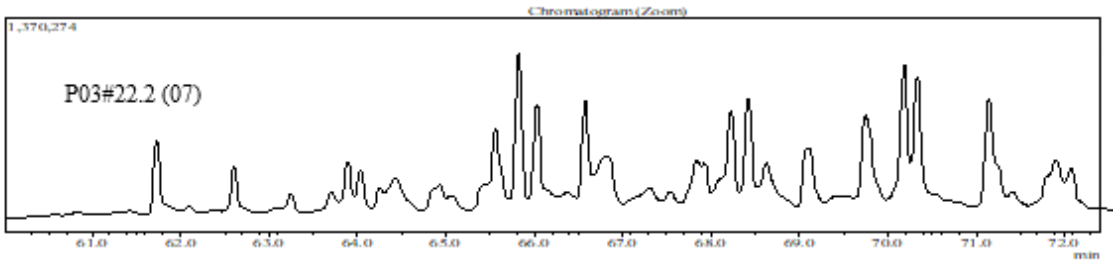
Chromatogram (Zoom)
1,370,274
P03#22.2 (07)
61.0
62.0
63.0
64.0
65.0
66.0
67.0
68.0
69.0
70.0
71.0
72.0
min

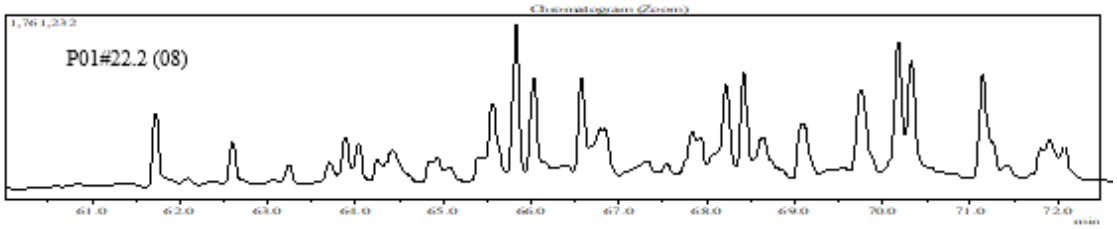
Chromatogram (Zoom)
1,761,232
P01#22.2 (08)
61.0
62.0
63.0
64.0
65.0
66.0
67.0
68.0
69.0
70.0
71.0
72.0
min

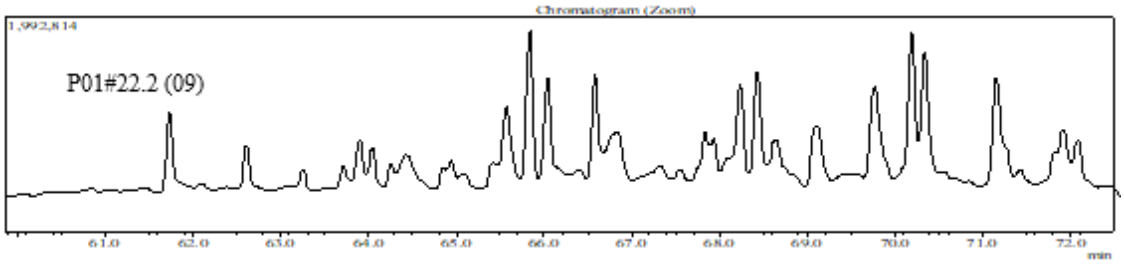
Chromatogram (Zoom)
1,992,814
P01#22.2 (09)
61.0
62.0
63.0
64.0
65.0
66.0
67.0
68.0
69.0
70.0
71.0
72.0
min

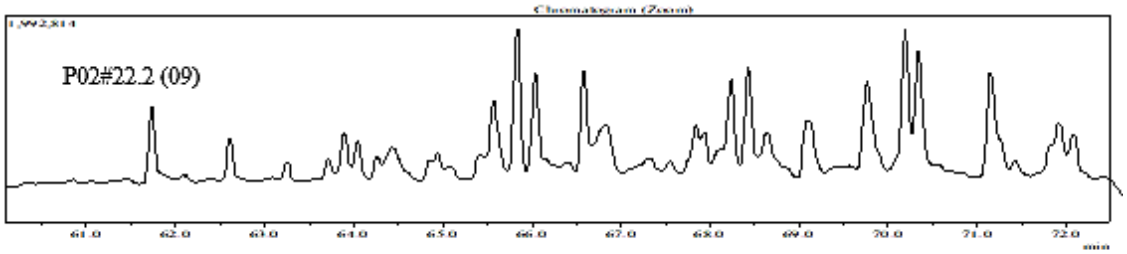
Chromatogram (Zoom)
P02#22.2 (09)
61.0
62.0
63.0
64.0
65.0
66.0
67.0
68.0
69.0
70.0
71.0
72.0
min

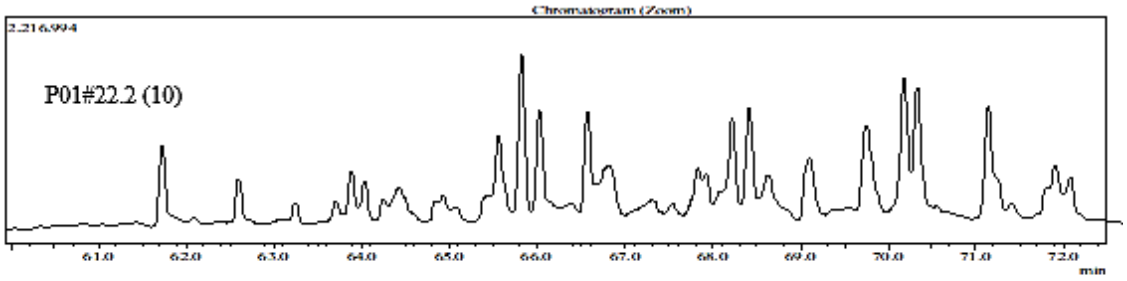
Chromatogram (Zoom)
2,216,994
P01#22.2 (10)
61.0
62.0
63.0
64.0
65.0
66.0
67.0
68.0
69.0
70.0
71.0
72.0
min

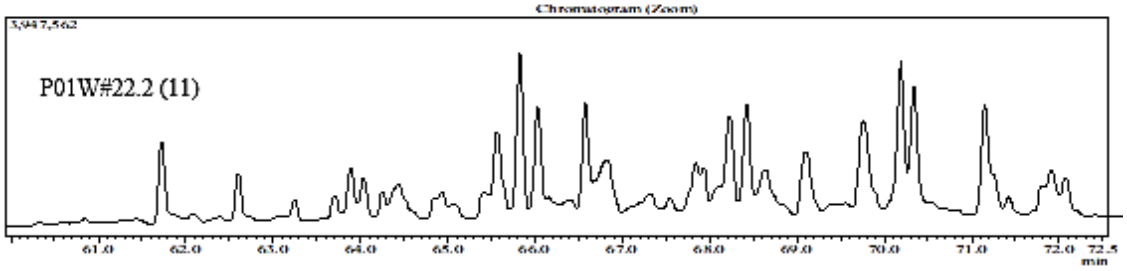
Chromatogram (Zoom)
3,947,562
P01W#22.2 (11)
61.0
62.0
63.0
64.0
65.0
66.0
67.0
68.0
69.0
70.0
71.0
72.0
72.5
min

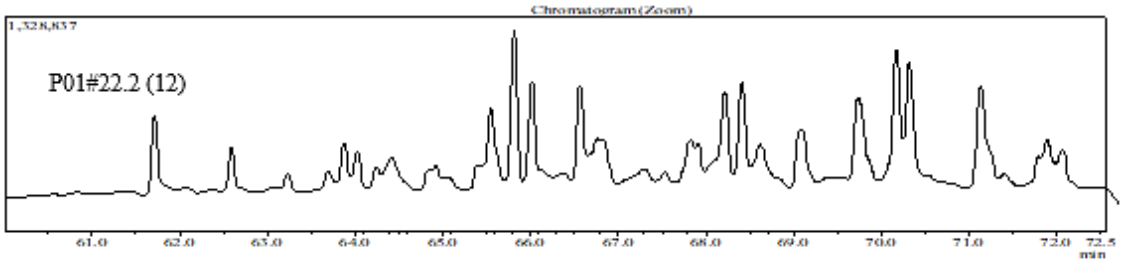
Chromatogram (Zoom)
1,328,837
P01#22.2 (12)
61.0
62.0
63.0
64.0
65.0
66.0
67.0
68.0
69.0
70.0
71.0
72.0
72.5
min

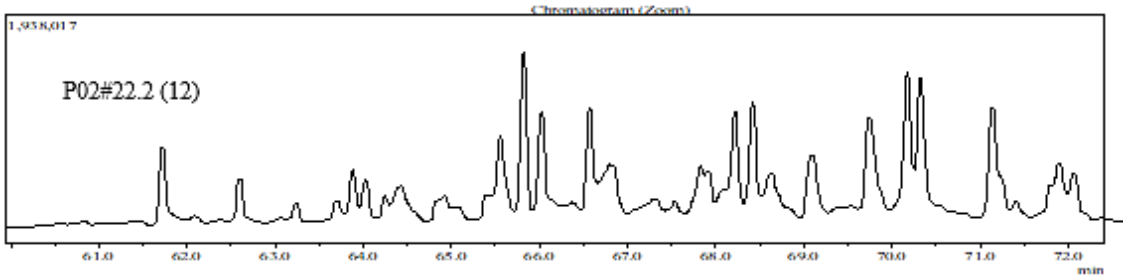
Chromatogram (Zoom)
1,938,017
P02#22.2 (12)
61.0
62.0
63.0
64.0
65.0
66.0
67.0
68.0
69.0
70.0
71.0
72.0
min

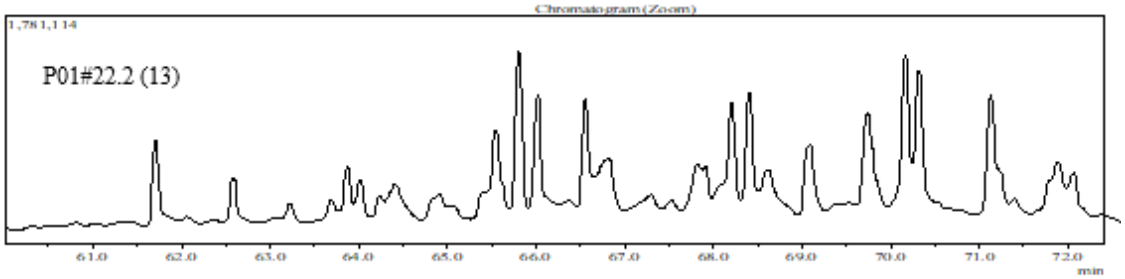
Chromatogram (Zoom)
1,781,114
P01#22.2 (13)
61.0 62.0 63.0 64.0 65.0 66.0 67.0 68.0 69.0 70.0 71.0 72.0
min

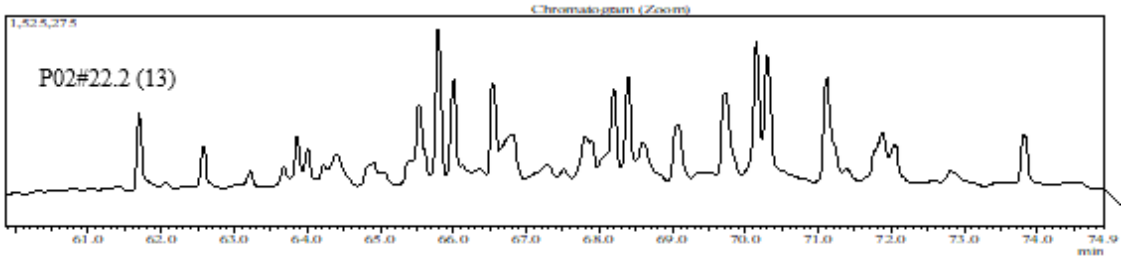
Chromatogram (Zoom)
1,525,275
P02#22.2 (13)
61.0 62.0 63.0 64.0 65.0 66.0 67.0 68.0 69.0 70.0 71.0 72.0 73.0 74.0 74.9
min

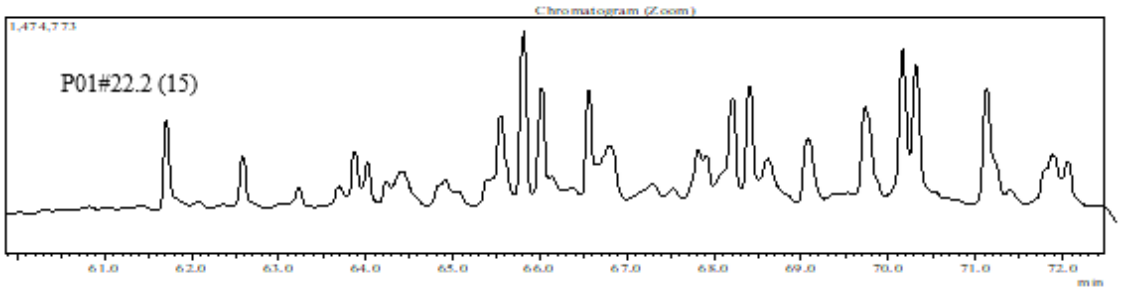
Chromatogram (Zoom)
1,474,773
P01#22.2 (15)
61.0 62.0 63.0 64.0 65.0 66.0 67.0 68.0 69.0 70.0 71.0 72.0
min

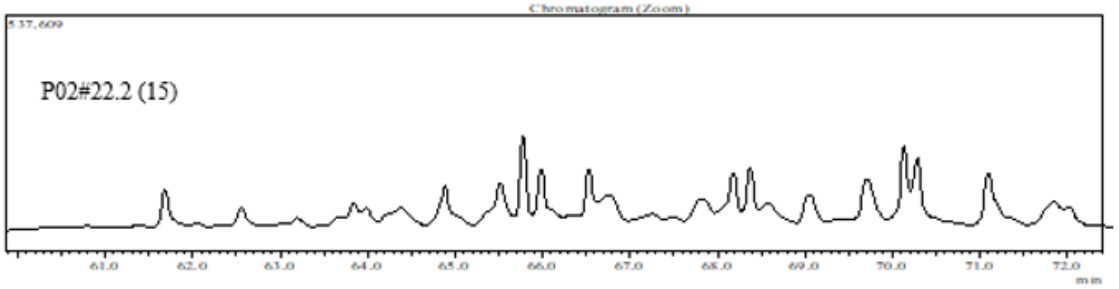
Chromatogram (Zoom)
537,609
P02#22.2 (15)
61.0 62.0 63.0 64.0 65.0 66.0 67.0 68.0 69.0 70.0 71.0 72.0
min

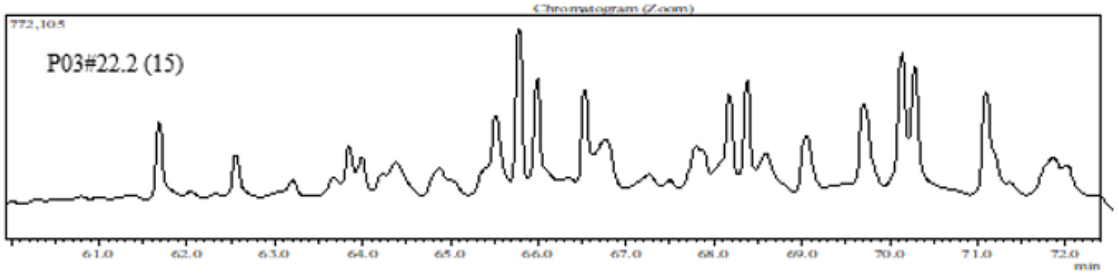
Chromatogram (Zoom)
772,105
P03#22.2 (15)
61.0 62.0 63.0 64.0 65.0 66.0 67.0 68.0 69.0 70.0 71.0 72.0
min

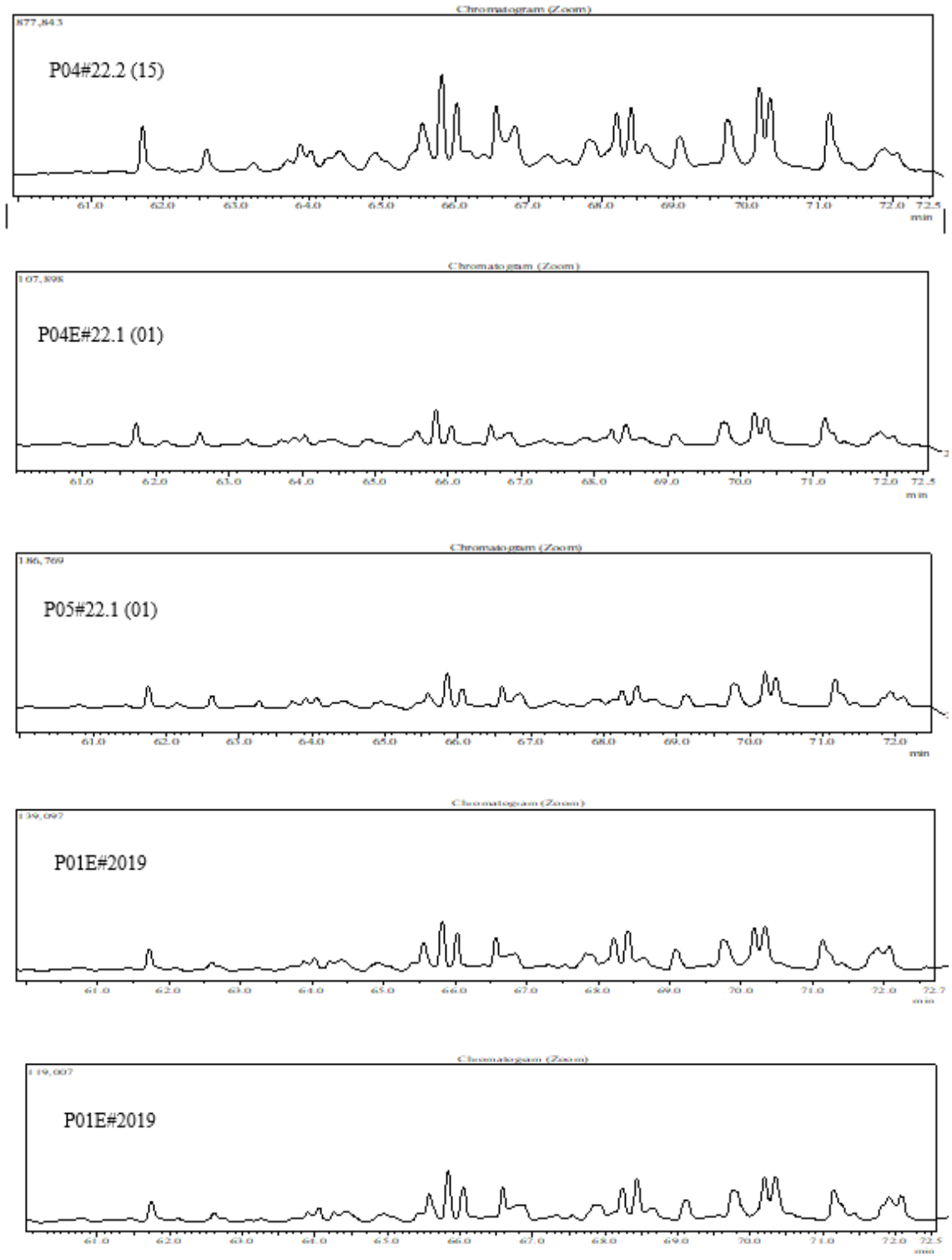

Fig. S8. Chromatograms *m/z* 217 of the 16 tarball samples collected in late 2022, in addition to the two spilled oils collected in early 2022 and the two spilled oils collected in 2019.

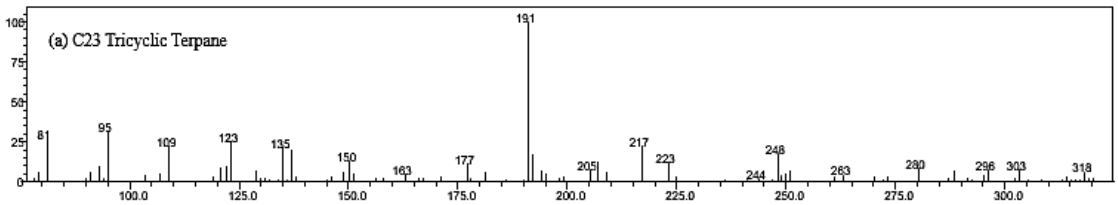
(a) C23 Tricyclic Terpane

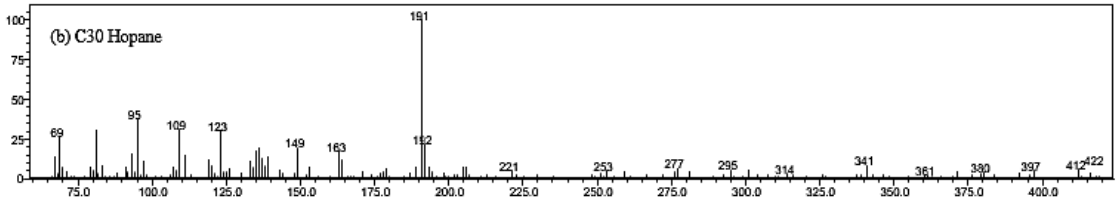
(b) C30 Hopane

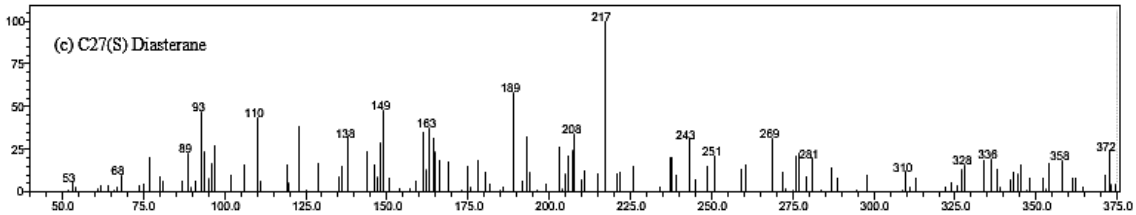
(c) C27(S) Diasterane

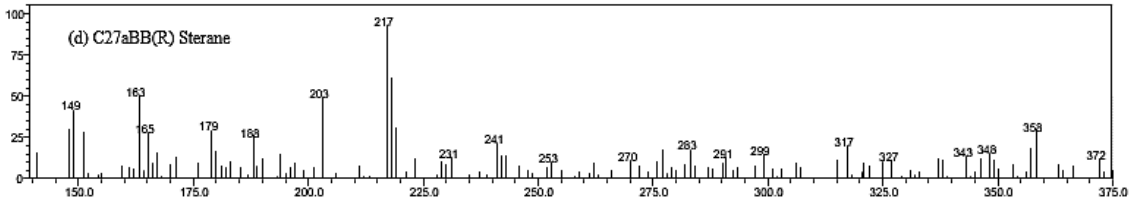
(d) C27aBB(R) Sterane

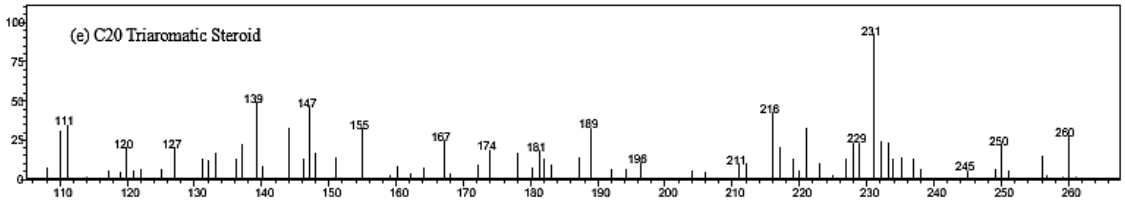
(e) C20 Triaromatic Steroid

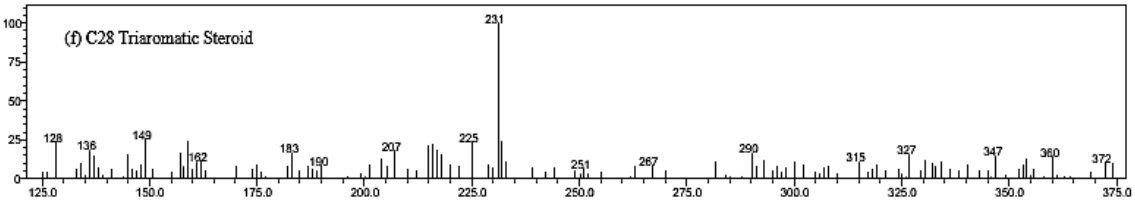
(f) C28 Triaromatic Steroid

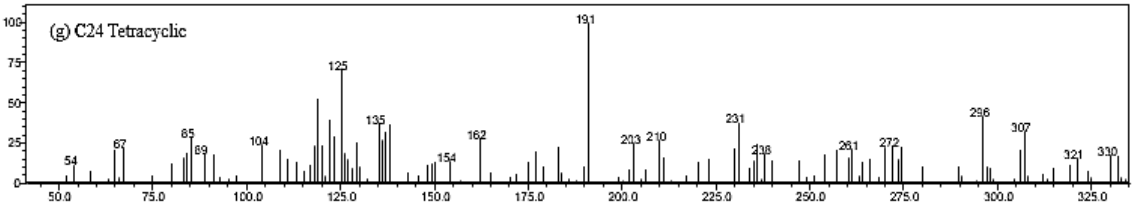
(g) C24 Tetracyclic

Fig. S9. Representative mass spectra of each family of biomarkers: C23 Tricyclic terpane, obtained from sample P01#2019 (a); C30 Hopane, obtained from sample P04#22.1(01) (b); C27 Diasterane, obtained from sample P01#22.2(07) (c); C27 Sterane, obtained from sample P01#22.2(07) (d); C20 Triaromatic Steroid, obtained from sample P01#22.2(10) (e); C28 Triaromatic Steroid, obtained from sample P01#22.2(10) (f); and C24 Tetracyclic Terpane, obtained from sample P04#22.1(01) (g).

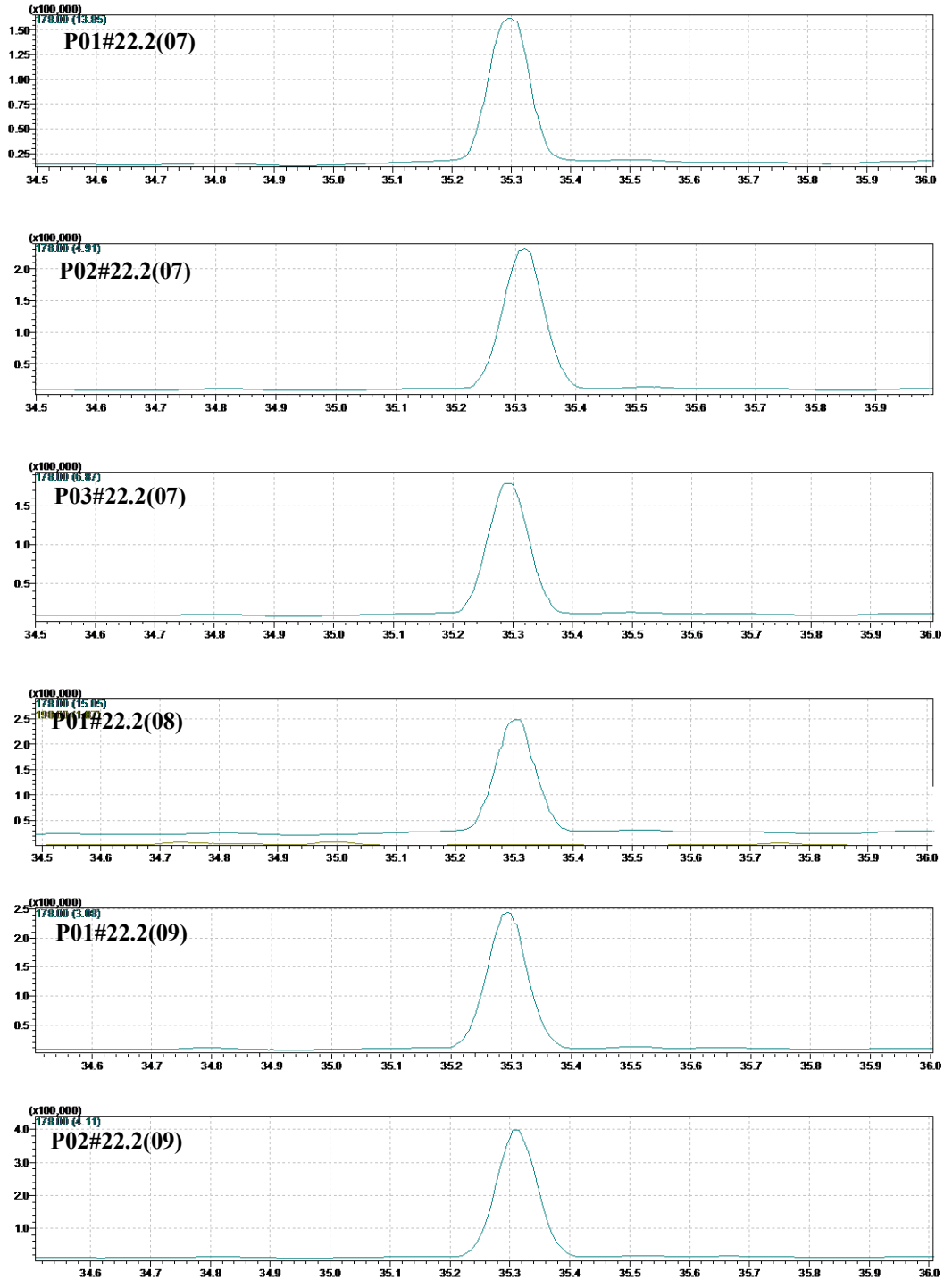

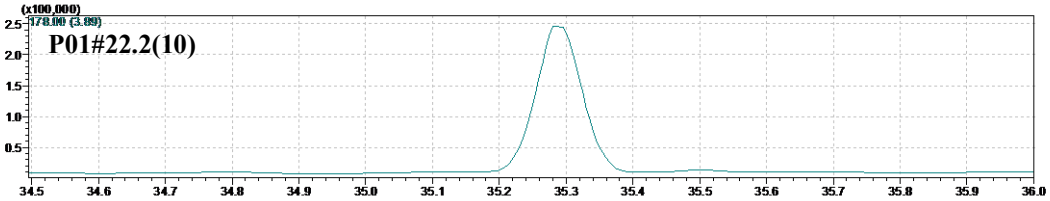
(x100,000)
178.00 (3.89)
P01#22.2(10)

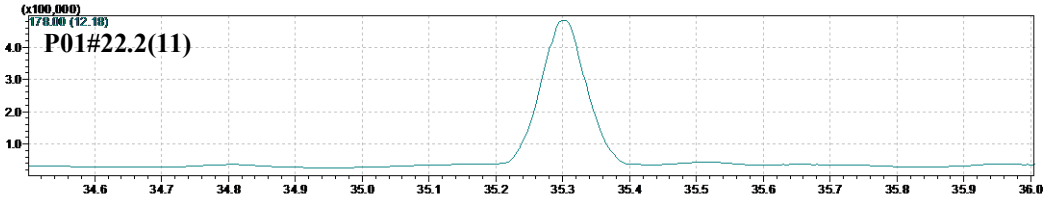
(x100,000)
178.00 (12.18)
P01#22.2(11)

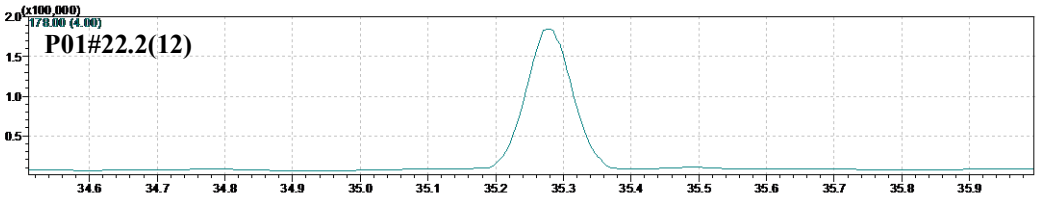
(x100,000)
178.00 (4.00)
P01#22.2(12)

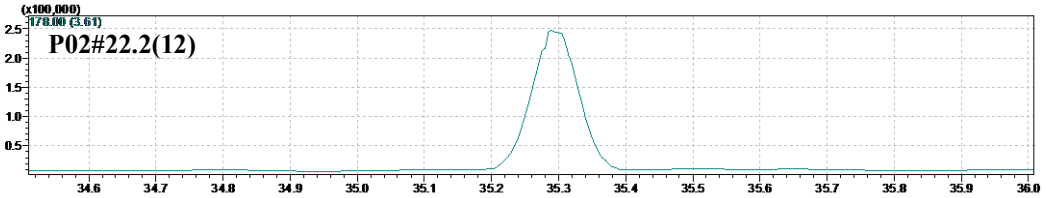
(x100,000)
178.00 (3.61)
P02#22.2(12)

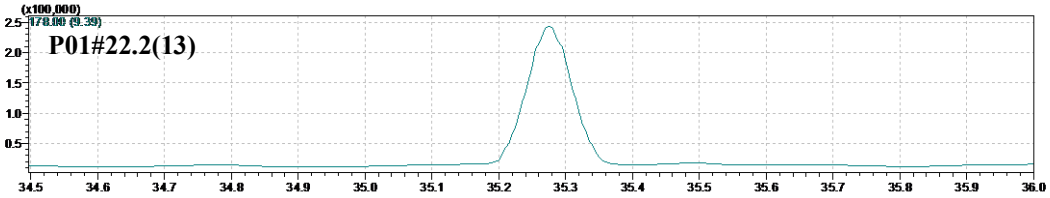
(x100,000)
178.00 (9.39)
P01#22.2(13)

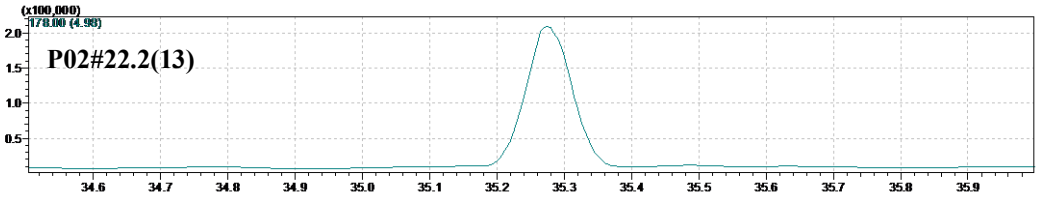
(x100,000)
178.00 (4.98)
P02#22.2(13)

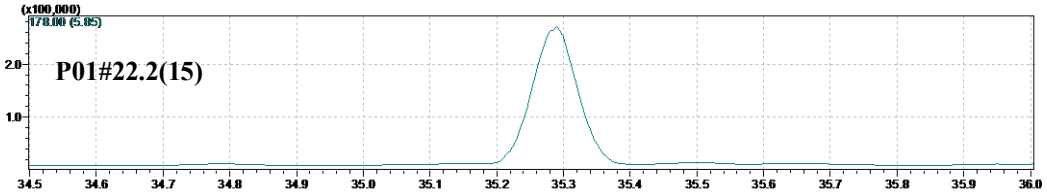
(x100,000)
178.00 (5.85)
P01#22.2(15)

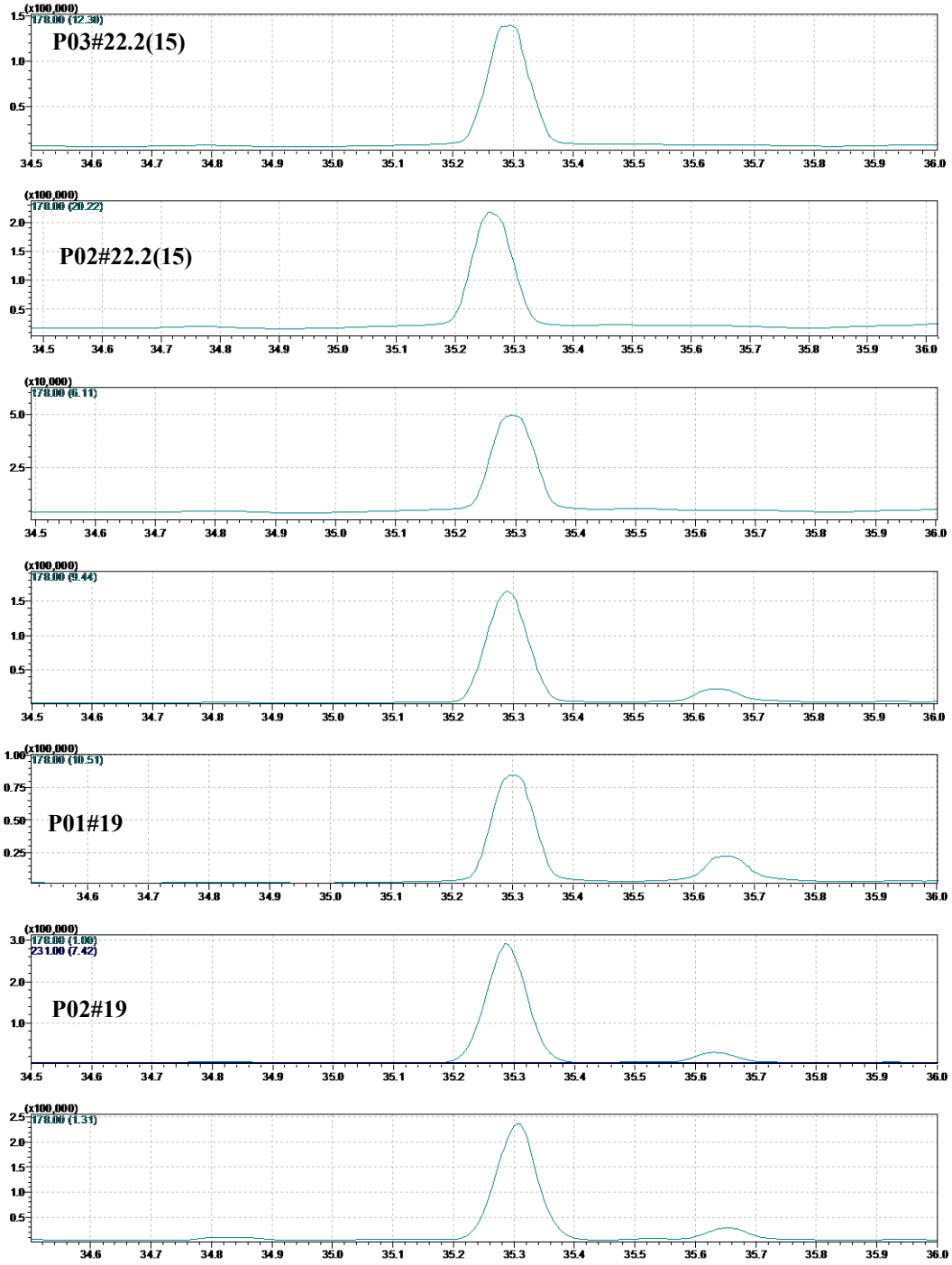

Fig. S10. Chromatograms *m/z* 178 of the 16 tarball samples collected in late 2022, in addition to the two spilled oils collected in early 2022 and the two spilled oils collected in 2019.

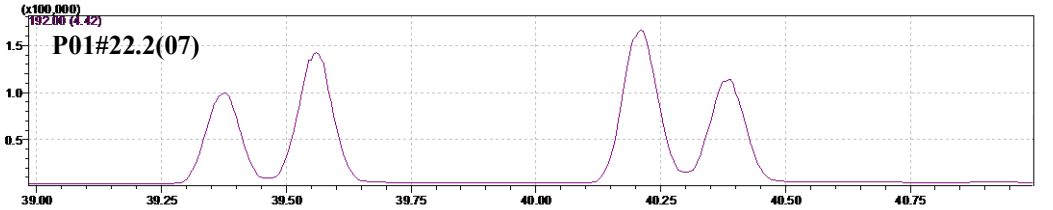
(x100,000)
192.00 (4.42)
P01#22.2(07)
1.5
1.0
0.5
39.00
39.25
39.50
39.75
40.00
40.25
40.50
40.75

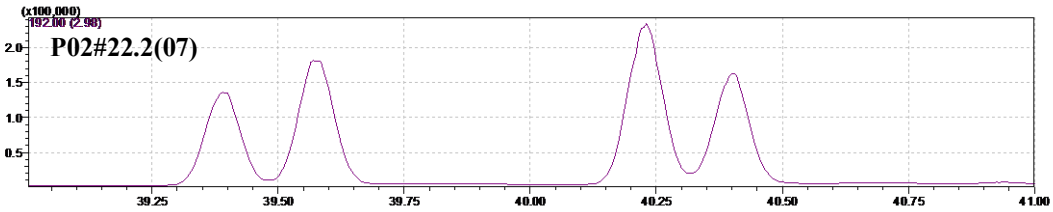
(x100,000)
192.00 (2.98)
P02#22.2(07)
2.0
1.5
1.0
0.5
39.25
39.50
39.75
40.00
40.25
40.50
40.75
41.00

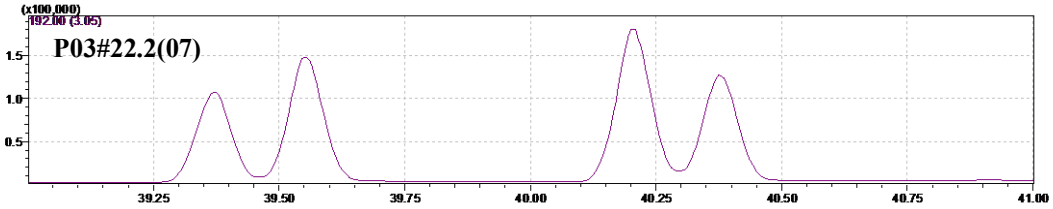
(x100,000)
192.00 (3.05)
P03#22.2(07)
1.5
1.0
0.5
39.25
39.50
39.75
40.00
40.25
40.50
40.75
41.00

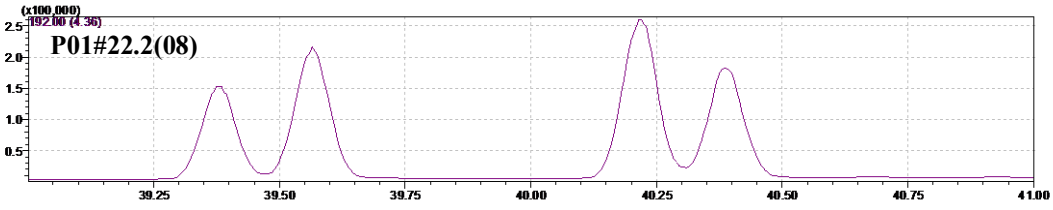
(x100,000)
192.00 (4.36)
P01#22.2(08)
2.5
2.0
1.5
1.0
0.5
39.25
39.50
39.75
40.00
40.25
40.50
40.75
41.00

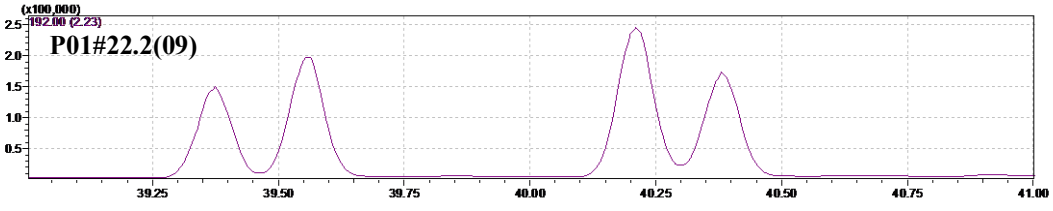
(x100,000)
192.00 (2.23)
P01#22.2(09)
2.5
2.0
1.5
1.0
0.5
39.25
39.50
39.75
40.00
40.25
40.50
40.75
41.00

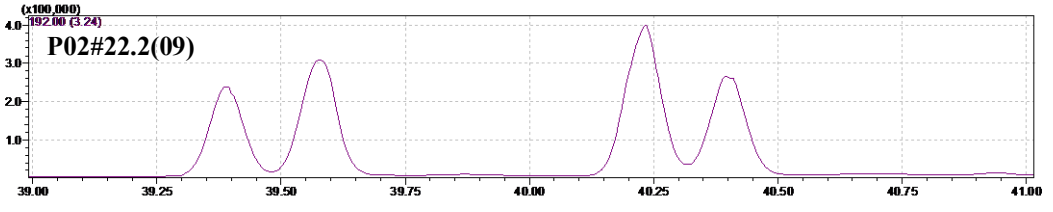
(x100,000)
192.00 (3.24)
P02#22.2(09)
4.0
3.0
2.0
1.0
39.00
39.25
39.50
39.75
40.00
40.25
40.50
40.75
41.00

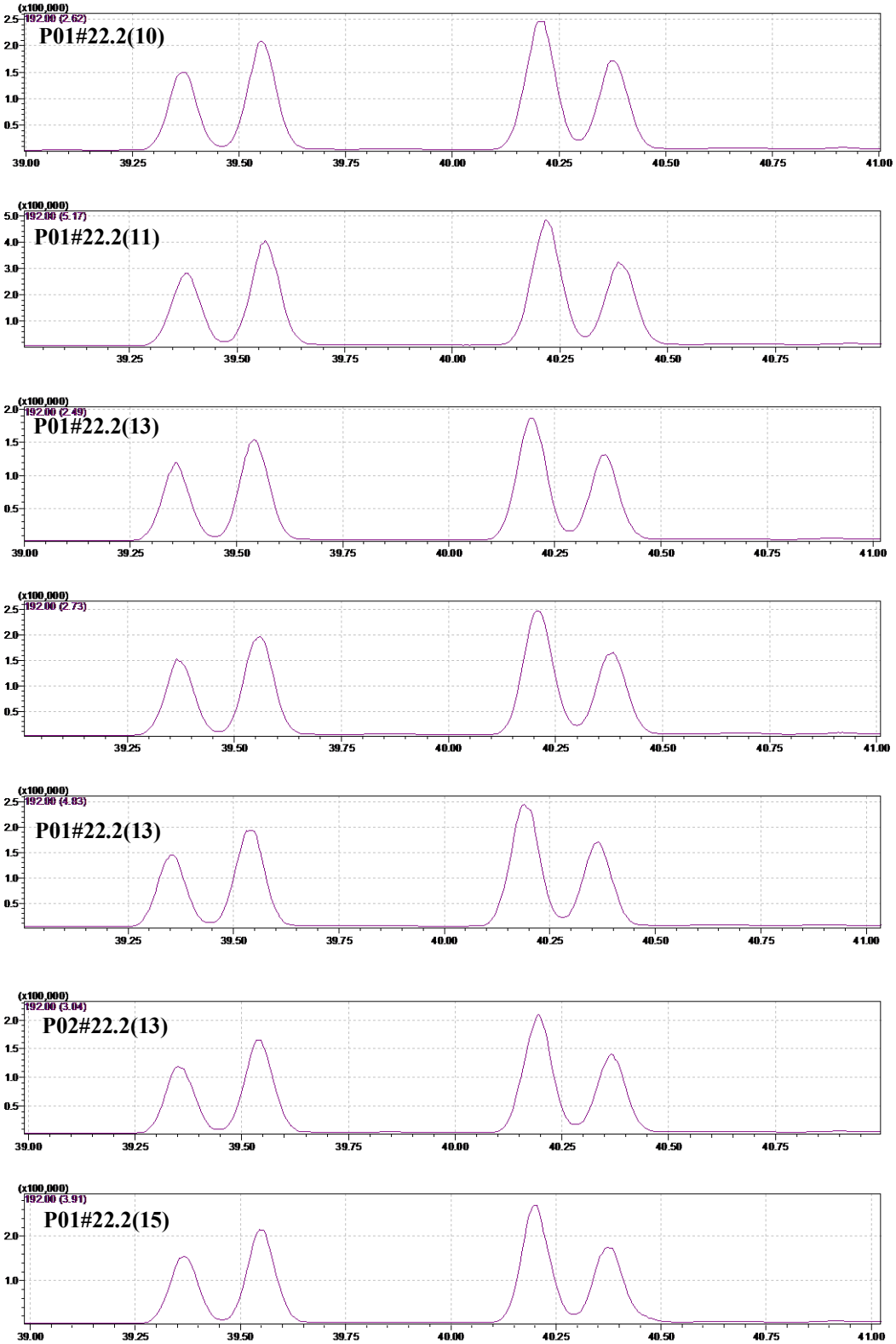
(x100,000)
192.00 (2.62)
P01#22.2(10)
(x100,000)
192.00 (5.17)
P01#22.2(11)
(x100,000)
192.00 (2.49)
P01#22.2(13)
(x100,000)
192.00 (2.73)
(x100,000)
192.00 (4.83)
P01#22.2(13)
(x100,000)
192.00 (3.04)
P02#22.2(13)
(x100,000)
192.00 (3.91)
P01#22.2(15)

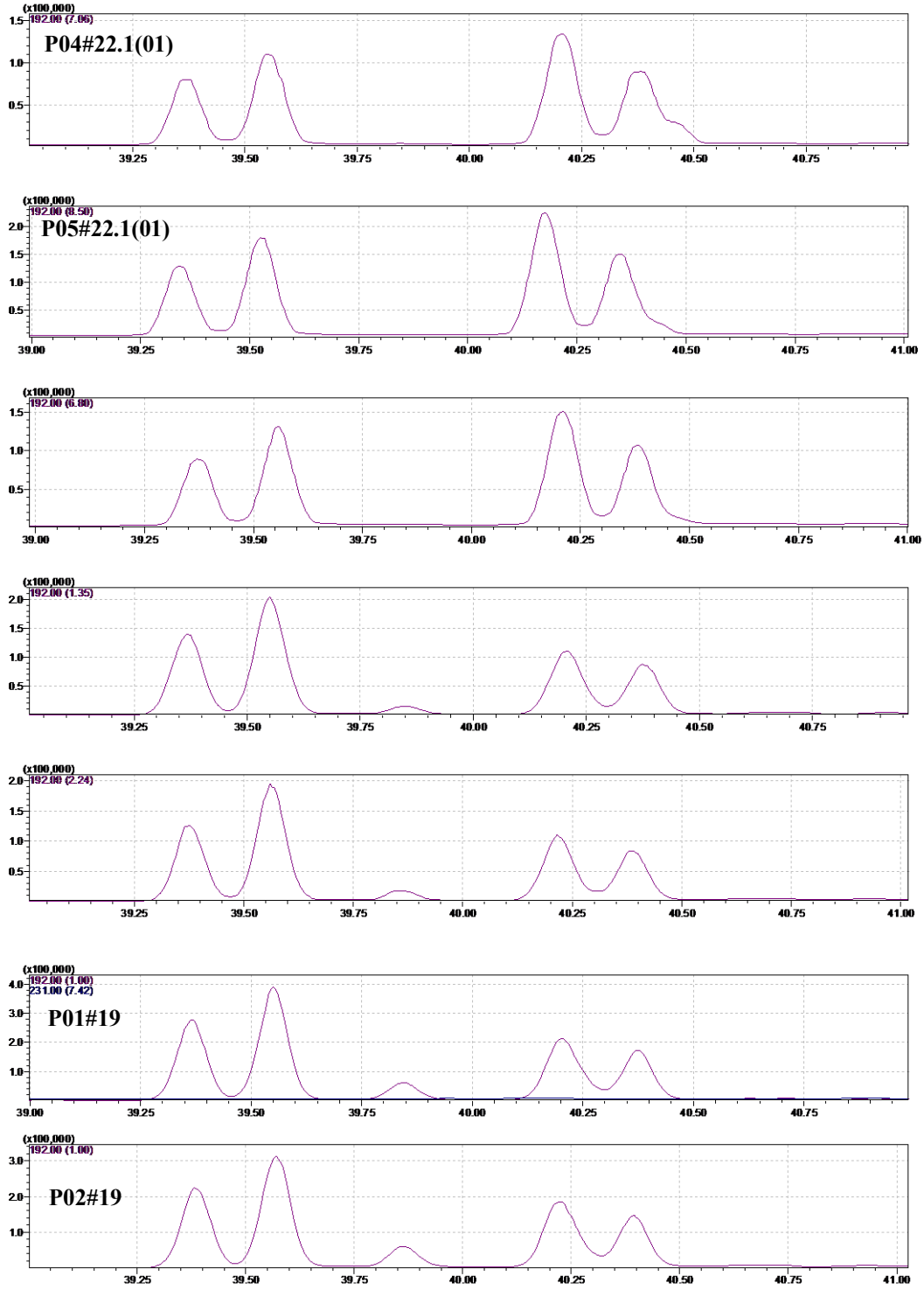

Fig. S11. Chromatograms *m/z* 192 of the 16 tarball samples collected in late 2022, in addition to the two spilled oils collected in early 2022 and the two spilled oils collected in 2019.

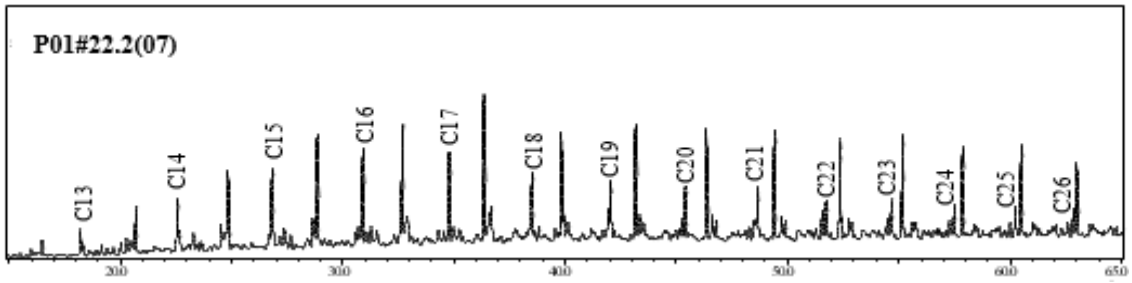
P01#22.2(07)
C13
C14
C15
C16
C17
C18
C19
C20
C21
C22
C23
C24
C25
C26
200
300
400
500
600
650

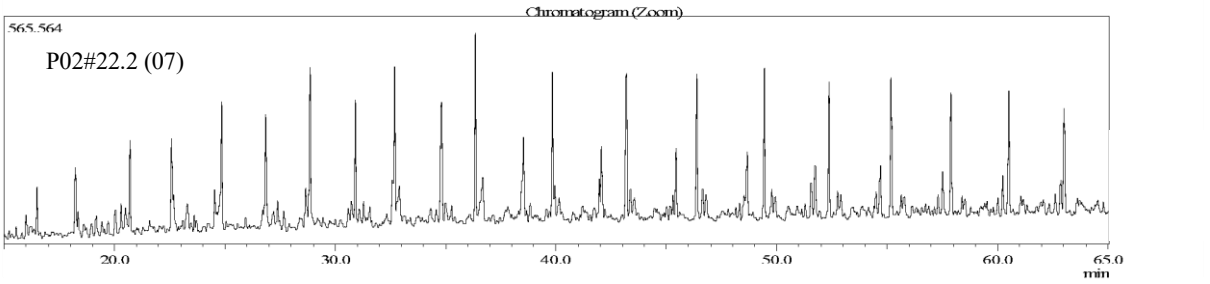
Chromatogram (Zoom)
565.564
P02#22.2 (07)
20.0
30.0
40.0
50.0
60.0
65.0
min

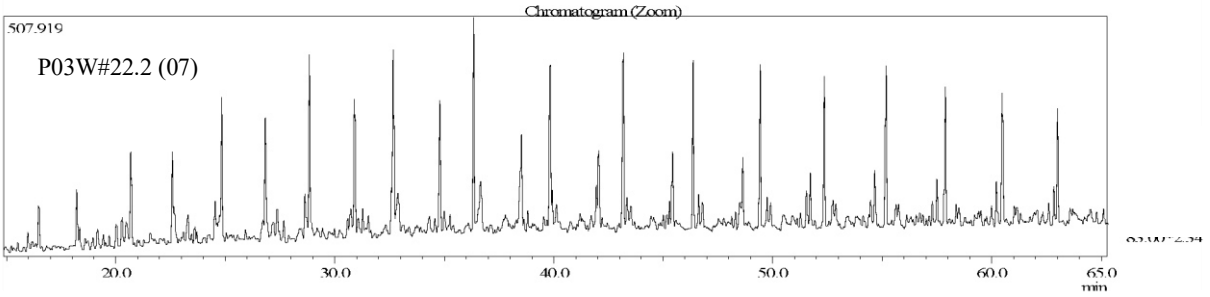
Chromatogram (Zoom)
507.919
P03W#22.2 (07)
20.0
30.0
40.0
50.0
60.0
65.0
min

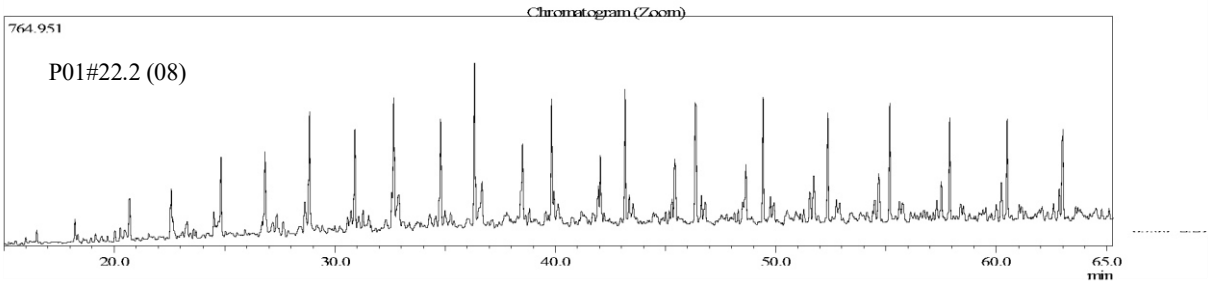
Chromatogram (Zoom)
764.951
P01#22.2 (08)
20.0
30.0
40.0
50.0
60.0
65.0
min

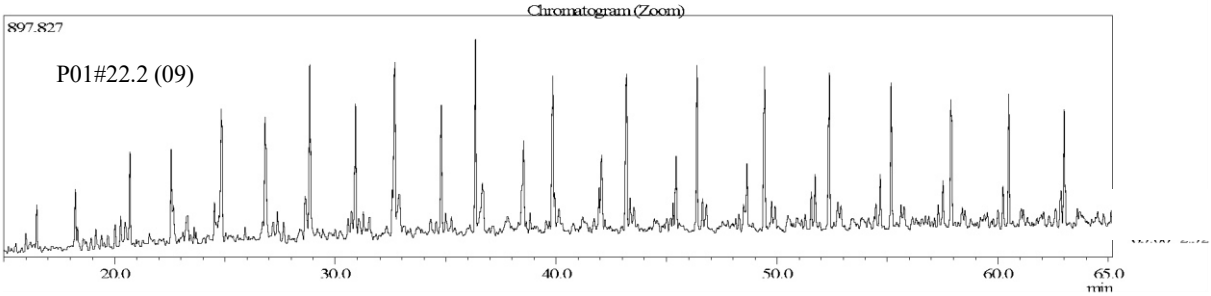
Chromatogram (Zoom)
897.827
P01#22.2 (09)
20.0
30.0
40.0
50.0
60.0
65.0
min

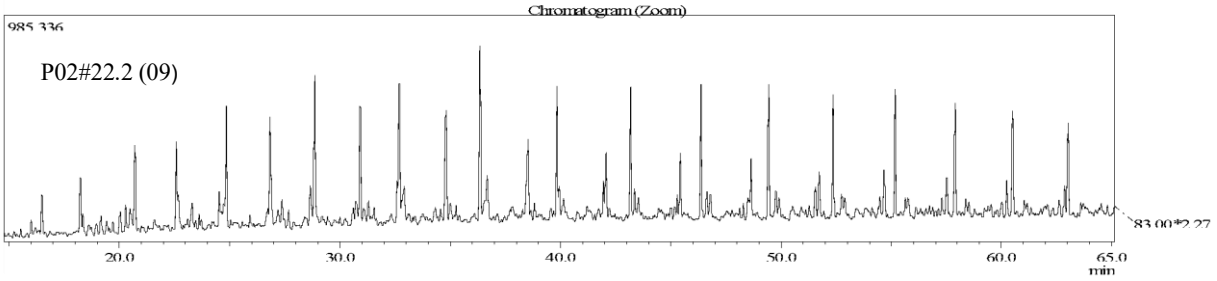
Chromatogram (Zoom)
985.336
P02#22.2 (09)
83.00*2.27
20.0
30.0
40.0
50.0
60.0
65.0
min

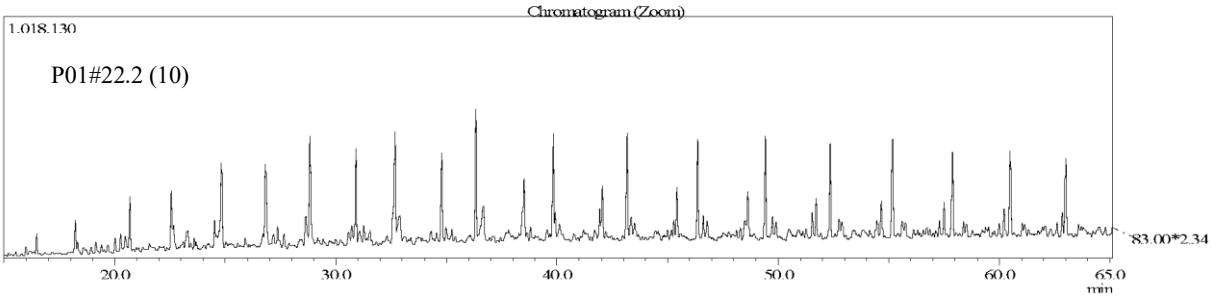
Chromatogram (Zoom)
1.018.130
P01#22.2 (10)
83.00*2.34
20.0
30.0
40.0
50.0
60.0
65.0
min

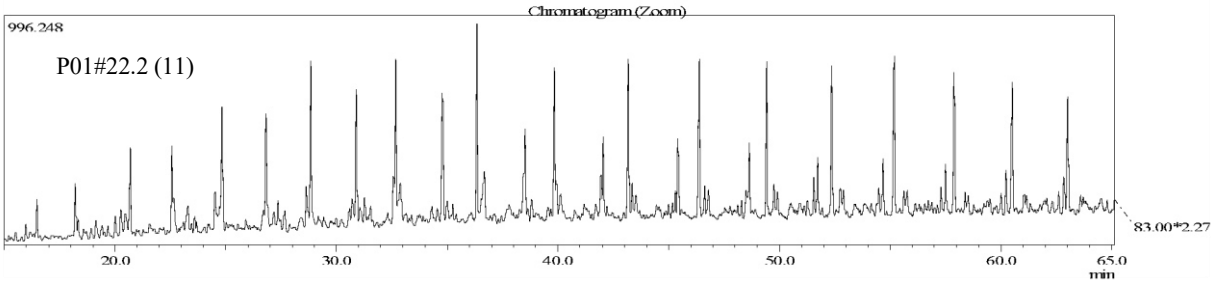
Chromatogram (Zoom)
996.248
P01#22.2 (11)
83.00*2.27
20.0
30.0
40.0
50.0
60.0
65.0
min

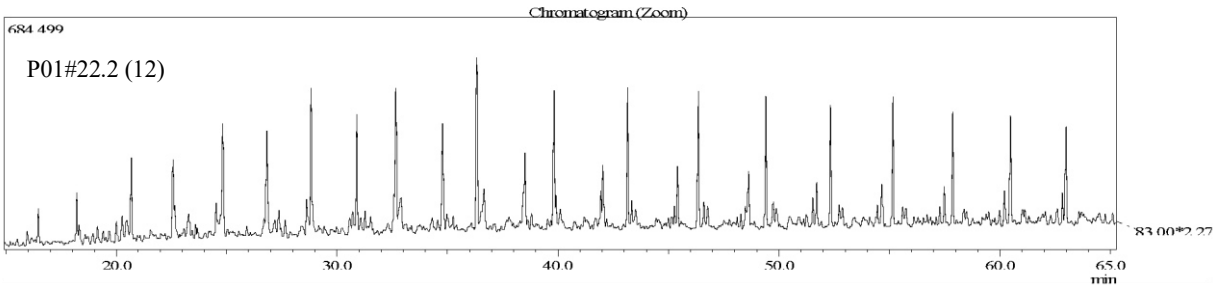
Chromatogram (Zoom)
684.499
P01#22.2 (12)
83.00*2.27
20.0
30.0
40.0
50.0
60.0
65.0
min

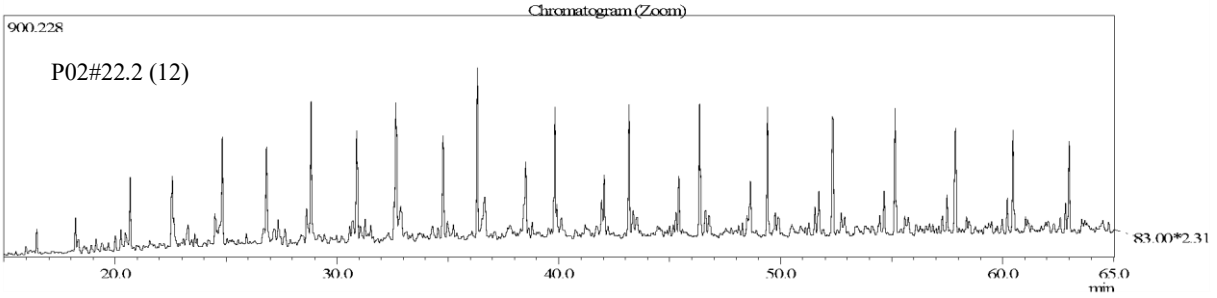
Chromatogram (Zoom)
900.228
P02#22.2 (12)
83.00*2.31
20.0
30.0
40.0
50.0
60.0
65.0
min

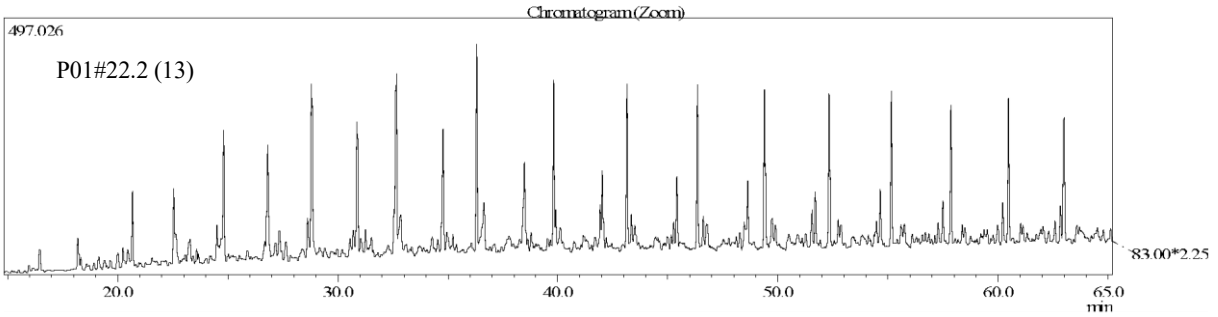
Chromatogram (Zoom)
497.026
P01#22.2 (13)
83.00*2.25
20.0
30.0
40.0
50.0
60.0
65.0
min

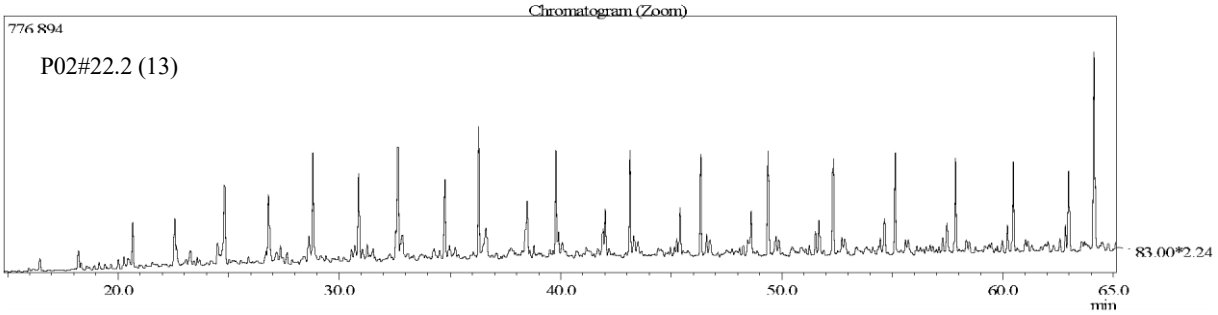
Chromatogram (Zoom)
776.894
P02#22.2 (13)
83.00*2.24
20.0
30.0
40.0
50.0
60.0
65.0
min

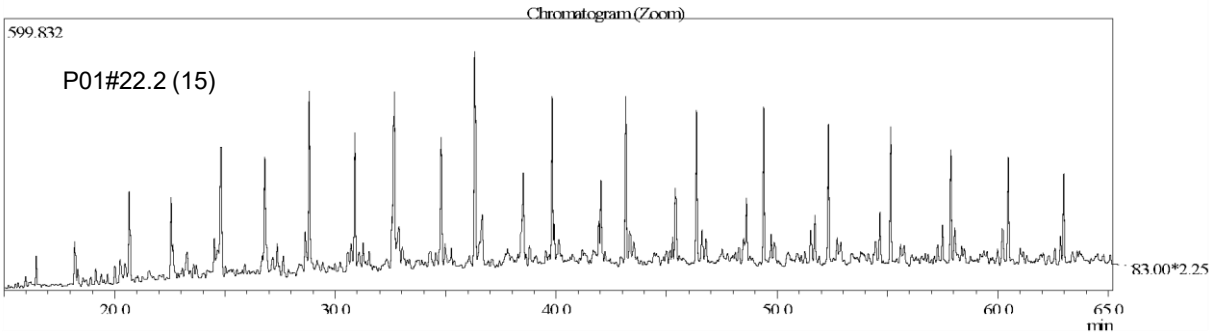
Chromatogram (Zoom)
599.832
P01#22.2 (15)
83.00*2.25
20.0
30.0
40.0
50.0
60.0
65.0
min

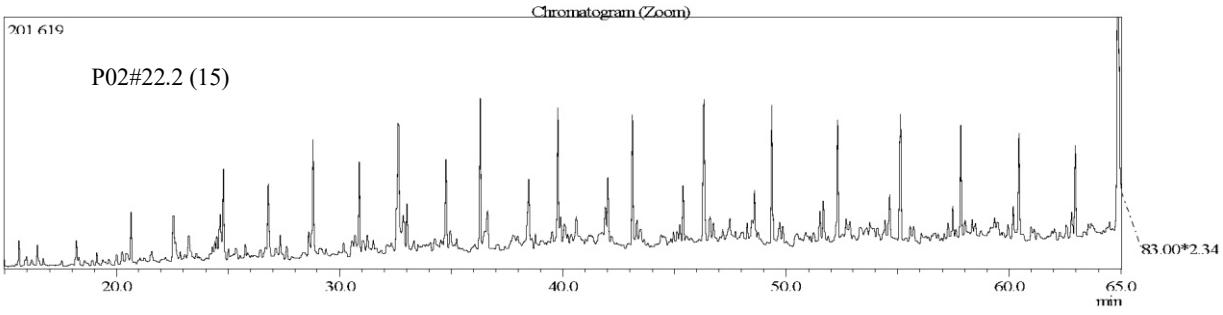
Chromatogram (Zoom)
201.619
P02#22.2 (15)
83.00*2.34
20.0
30.0
40.0
50.0
60.0
65.0
min

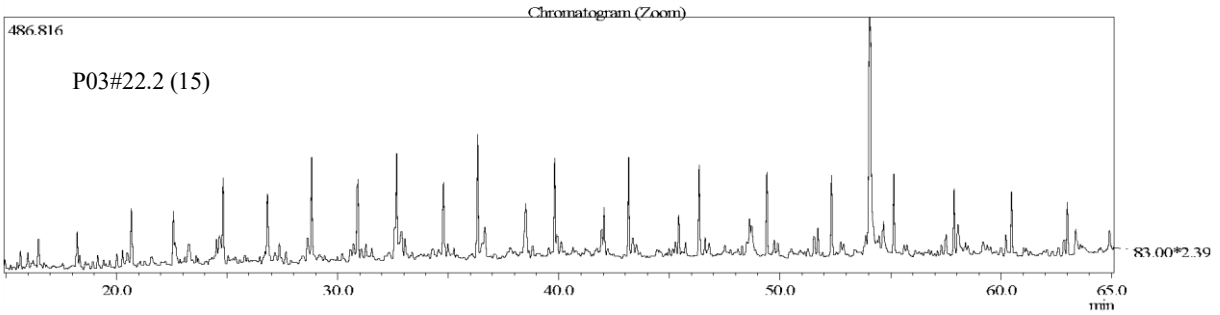
Chromatogram (Zoom)
486.816
P03#22.2 (15)
83.00*2.39
20.0
30.0
40.0
50.0
60.0
65.0
min

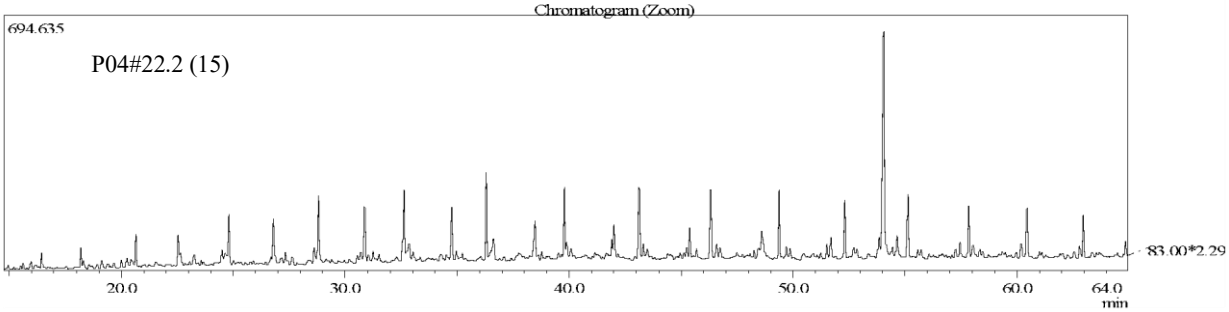
Chromatogram (Zoom)
694.635
P04#22.2 (15)
83.00*2.29
20.0
30.0
40.0
50.0
60.0
64.0
min

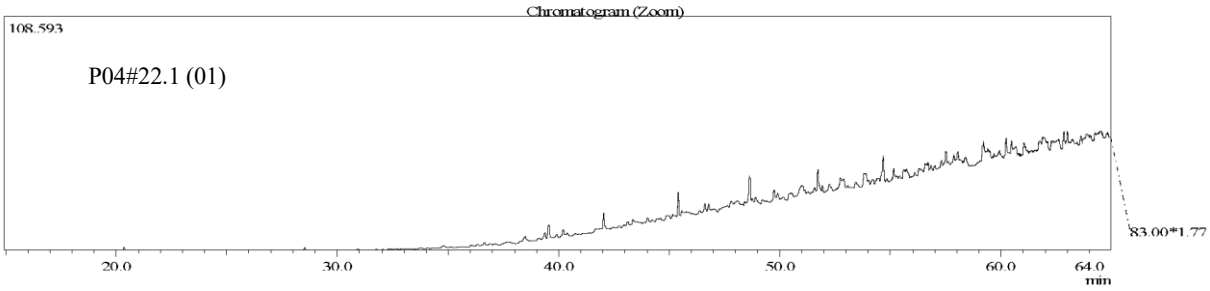
Chromatogram (Zoom)
108.593
P04#22.1 (01)
83.00*1.77
20.0
30.0
40.0
50.0
60.0
64.0
min

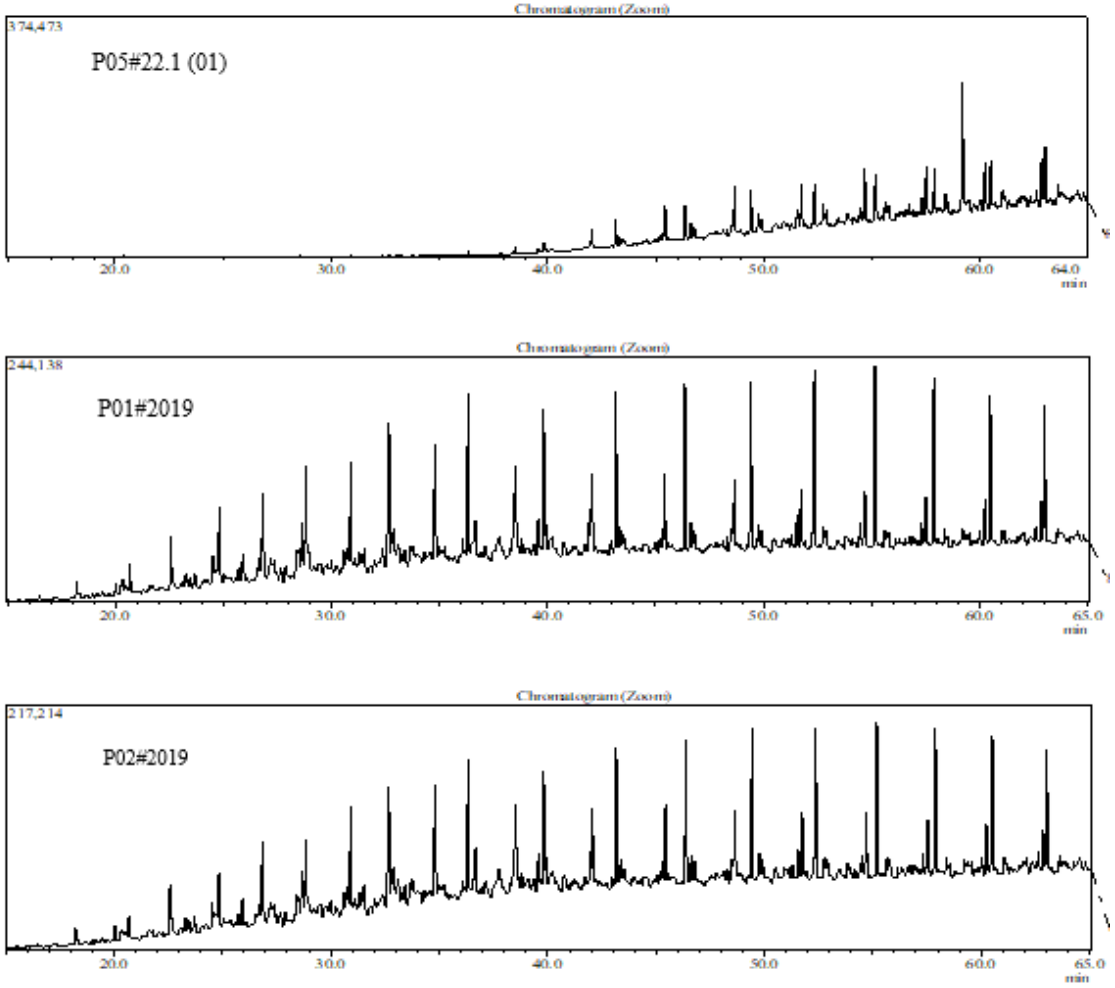

Fig. S12. Chromatograms *m/z* 83 of the 16 tarball samples collected in late 2022, in addition to the two spilled oils collected in early 2022 and the two spilled oils collected in 2019.

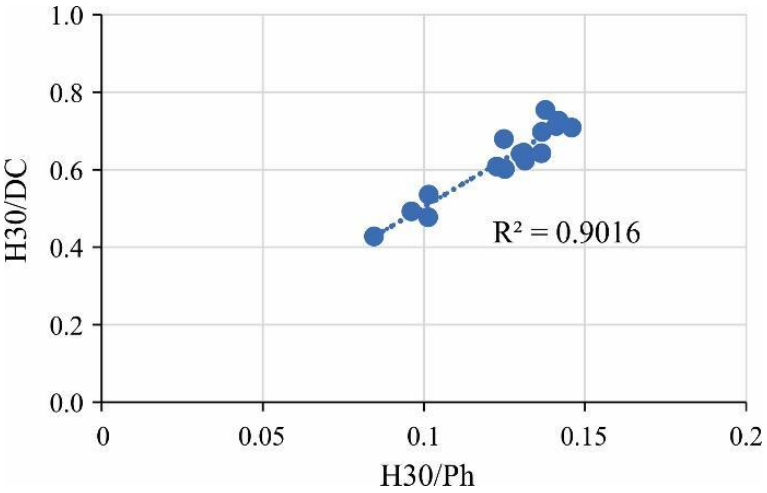

Fig. S13. Plot of the H30/Ph against the H30/DC from the GC-MS results.

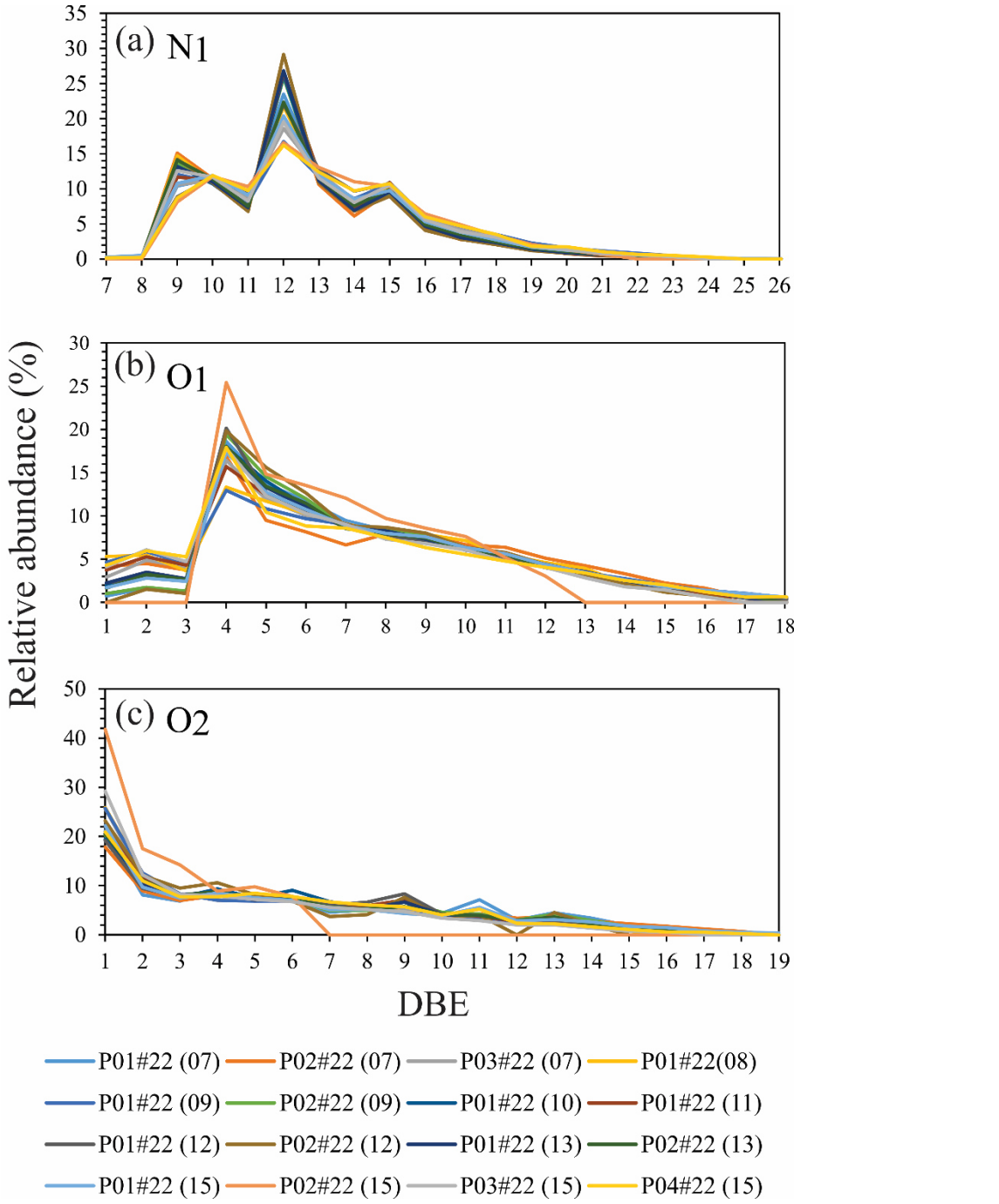

Figure S14. DBE distribution of the N_1 (a), O_1, and O_2 (c) classes in the waxy tarball samples.

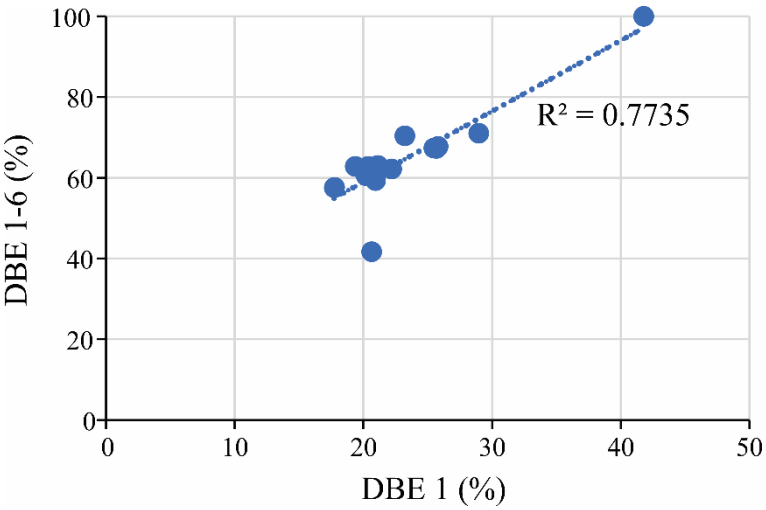

Fig. S15. Plots of the modified SA Index against the A/C ratio (c) and modified A/C ratio (d), which are biodegradation parameters based on O_2 compounds. In addition, plot of the DBE 1 (%) against the DBE 1-6 (%).

Table S1. Sample codes, collection date and the locality information, including the beach, state, and coordinates.

Sample code	Collection date	Locality		
		Beach	State	UTM Coordinates
P01#22.2(07)	24/09/2022	Icaraí	Ceará	537757mE 9594342mN
P02#22.2(07)	24/09/2022	Cumbuco	Ceará	533316mE 9597660mN
P03#22.2(07)	24/09/2022	Pecém	Ceará	518881mE 9607612mN
P01#22.2(08)	01/10/2022	Futuro	Ceará	562182mE 9584381mN
P01#22.2(09)	03/10/2022	Flecheiras	Ceará	468892Me 9644085mN
P02#22.2(09)	03/10/2022	Almofala	Ceará	408870mE 9676111mN
P01#22.2(10)	27/09/2022	Paracuru	Ceará	498889mE 9624193mN
P01#22.2(11)	01/10/2022	Peroba	Ceará	671931mE 9484730mN
P01#22.2(12)	17/10/2022	Albino	Bahia	506432mE 8276415mN
P02#22.2(12)	17/10/2022	Costa	Bahia	501079mE 8420201mN
P01#22.2(13)	15/09/2022	Barra Formosa	Rio Grande do Norte	939154mE 9301473mN
P02#22.2(13)	15/09/2022	Tabatinga	Rio Grande do Norte	930791mE 9329725mN
P01#22.2(15)	27/08/2022	Candeias	Pernambuco	949758mE 9091305mN
P02#22.2(15)	30/08/2022	Olinda	Pernambuco	957692mE 9111175mN
P03#22.2(15)	03/10/2022	Maragogi	Alagoas	915741mE 9000784mN

P04#22.2(15)	22/10/2022	Pina	Pernambuco	954299mE 9103451mN
P04#22.1(01)	28/01/2022	Cumbe	Ceará	639794mE 9505801mN
P05#22.1(01)	28/01/2022	Canoa Quebrada	Ceará	644223mE 9500265mN
P01#2019	01/11/2022	Mangue do Rio Jaguaribe	Ceará	641512mE 9503285mN
P02#2019	07/11/2019	Cumbuco	Ceará	642645mE 9501869mN

Table S2. Geochemical ratios based on the *n*-alkanes and isoprenoids pristane (Pr) and phytane (Ph) assessed by GC-FID.

Sample code	Pr/Ph[a]	Pr/*n*C17[b]	Ph/*n*C18[c]	TAR[d]	CPI[e]	WI[h]	Σ*n*C9-40 (ppm)[f]	Resolved/UCM (%)[g]
P01#22.2(07)	0.77	0.41	0.58	0.42	1.02	0.50	13481.58	46.8
P02#22.2(07)	0.84	0.46	0.63	0.58	1.41	0.68	6611.63	54.7
P03#22.2(07)	0.88	0.45	0.62	0.76	1.42	0.47	4864.1	61.3
P01#22.2(08)	0.80	0.51	0.69	1.06	1.4	0.21	11173.7	101.0
P01#22.2(09)	0.86	0.5	0.66	0.9	1.04	0.34	5868.59	57.42
P02#22.2(09)	0.83	0.45	0.61	0.37	1.26	0.44	6318.7	38.26
P01#22.2(10)	0.80	0.46	0.64	0.44	1.04	0.33	6285.9	41.14
P01#22.2(11)	0.80	0.43	0.62	0.42	1.28	0.59	6169.57	40.25
P01#22.2(12)	0.84	0.43	0.58	0.40	1.09	0.53	6329.71	32.81
P02#22.2(12)	0.86	0.43	0.58	0.43	1.3	0.47	6247.9	44.84
P01#22.2(13)	0.85	0.43	0.58	0.32	1.0	0.44	4449.65	33.39
P02#22.2(13)	0.79	0.43	0.62	0.46	1.0	0.33	6329.71	36.88
P01#22.2(15)	0.83	0.44	0.6	0.40	1.51	0.33	6236.32	39.04
P02#22.2(15)	0.83	0.45	0.61	0.51	1.05	0.34	7598.37	45.32
P03#22.2(15)	0.80	0.46	0.65	0.32	1.18	0.40	4271.22	32.37
P04#22.2(15)	0.85	0.46	0.62	0.45	2.62	0.44	5849.37	39.78
P04#22.1(01)	0.17	0.85	9.27	24.22	1.42	0.07	594.1	12,64
P05#22.1(01)	0.02	0.02	0.67	9.21	1.24	0.02	973.48	94.40
P01#2019	0.99	0.46	0.45	0.64	1.08	0.041	1752.93	15.69
P02#2019	0.77	0.47	0.65	0.65	1.07	0.065	806.91	8.93

[a]Pristane/Phytane; [b]Pristane/*n*C17; [c]Fitane/*n*C18; [d]TAR (Terrigenous aquatic ratio) = (*n*C15 + *n*C17 + *n*C19)/(*n*C27 + *n*C29 + *n*C31); [e]CPI (carbon preference index) = 1/2[(*n*C25 + *n*C27 + *n*C29 + *n*C31 + *n*C33)/(*n*C24 + *n*C26 + *n*C28 + *n*C30 + *n*C32) + (*n*C25 + *n*C27 + *n*C29 + *n*C31 + *n*C33)/(*n*C26 + *n*C28 + *n*C30 + *n*C32 + *n*C34)]; [f]Σ*n*C9-40(ppm); [g]Resolved/UCM (%); [h]WI (Weathering Index) = (*n*C10 + *n*C12 + *n*C14)/(*n*C22 + *n*C24 + *n*C26 + *n*C28).

Table S3. Part 1: Parameters based on monoaromatic steroids (*m/z* 231), terpanes (*m/z* 191), and steranes (*m/z* 217) for similarity assessment.

Sample code	21/23 Tri[a]	23/24 Tri[b]	26/25 Tri[c]	Tet24/26 Tri[d]	Ts/(Ts+Tm)[e]	H29/H30[f]	H31R/H30[g]	H31(S)/H31(R)[h]	23 Tri/C30H[i]
P01#22.2(07)	0.08	2.04	0,42	3.65	0.36	0.98	0.46	1.30	0.14
P02#22.2(07)	0.14	2.07	0.47	3.34	0.36	1.00	0.47	1.27	0.15
P03#22.2(07)	0.13	2.03	0.45	3.42	0.36	0.97	0.46	1.29	0.14
P01#22.2(08)	0.11	1.97	0.52	2.92	0.36	0.99	0.46	1.29	0.15
P01#22.2(09)	0.18	2.10	0.54	3.00	0.36	1.00	0.45	1.31	0.15
P02#22.2(09)	0.18	1.98	0.50	3.06	0.37	0.98	0.45	1.32	0.15
P01#22.2(10)	0.14	2.03	0.52	3.04	0.37	0.96	0.43	1.33	0.15
P01#22.2(11)	0.12	1.96	0.57	2.70	0.36	1.00	0.45	1.32	0.15
P01#22.2(12)	0.13	1.99	0.45	3.61	0.36	0.97	0.44	1.33	0.14
P02#22.2(12)	0.18	2.10	0.47	3.25	0.36	1.01	0.46	1.31	0.14
P01#22.2(13)	0,13	2.17	0.36	4.56	0.36	0.98	0.46	1.28	0.13
P02#22.2(13)	0,13	2.07	0.49	3.54	0.36	0.99	0.44	1.32	0.13
P01#22.2(15)	0.13	2.03	0.45	3.54	0.36	0.99	0.44	1.34	0.16
P02#22.2(15)	0.04	2.35	0.13	10.91	0.34	1.00	0.43	1.41	0.14
P03#22.2(15)	0.06	1.28	0.34	4,25	0.35	1.00	0.44	1.31	0.16
P04#22.2(15)	0.02	1.80	0.22	7,11	0.35	1.03	0.44	1.35	0.17
P04#22.1(01)	0.91	2.67	0.75	1.68	0.31	0.83	0.40	1.25	0.13
P05#22.1(01)	0.74	2.65	0.71	1.45	0.32	0.84	0.44	1.22	0.14
P01#2019	0.19	2.56	0.51	0.58	0.34	0.68	0.39	1.33	0.91
P02#2019	0.24	2.47	0.61	0.55	0.35	0.68	0.39	1.33	0.87

[a]C21/C23 Tricyclic Terpane; [b]C23/C24 Tricyclic Terpane; [c]C26/C25 Tricyclic Terpane; [d]C24 tetracyclic/C23 Tricyclic Terpane; [e]18α(H)-30-Norneohopane/(18α(H)-30-Norneohopane + 17α(H)-22,29,30-Trisnorhopane); [f]17α(H),21β(H)-30-Norhopane/17α(H),21β(H)-Hopane; [g]17α(H),21β(H)-Hopane (22R)/17α(H),21β(H)-Hopane; [h]17α(H),21β(H)-30-Homohopane (22S)/ 17α(H),21β(H)-Hopane (22R); [i]C23 Tricyclic Terpane/17α(H),21β(H)-Hopane

Table S3. Part 2: Parameters based on monoaromatic steroids (*m/z* 231), terpanes (*m/z* 191), and steranes (*m/z* 217) for similarity assessment.

Sample code	C27/C29[a]	C29ββ/(C29 ββ +C29⟨⟨)[b]	C27 ββ /C29 ββ[c]	C30H/C27⟨⟨ ⟨[d]	C27 diasterane/C 27 steranes[e]	Steranes/T erpanes[f]	Dia 27R/Dia 27S[g]	C29αββ(S)/ C30H[h]	C29αββ(R)/C30H[i]
P01#22.2(07)	0.96	0.41	1.28	4.79	0.24	0.37	0.54	0.11	0.19
P02#22.2(07)	0.90	0.41	1.17	4.87	0.24	0.38	0.55	0.13	0.20
P03#22.2(07)	0.94	0.41	1.24	4.80	0.24	0.37	0.55	0.12	0.19
P01#22.2(08)	0.94	0.40	1.26	4.76	0.24	0.38	0.56	0.11	0.20

P01#22.2(09)	0.90	0.40	1.21	4.62	0.23	0.40	0.59	0.13	0.21
P02#22.2(09)	0.91	0.41	1.21	4.38	0.26	0.42	0.47	0.13	0.21
P01#22.2(10)	0.95	0.41	1.27	4.61	0.24	0.39	0.52	0.12	0.20
P01#22.2(11)	0.94	0.41	1.23	4.46	0.23	0.41	0.55	0.12	0.21
P01#22.2(12)	0.94	0.39	1.32	4.56	0.24	0.39	0.53	0.11	0.20
P02#22.2(12)	0.91	0.40	1.21	4.45	0.24	0.40	0.53	0.13	0.21
P01#22.2(13)	0.92	0.41	1.23	4.69	0.22	0.39	0.52	0.12	0.20
P02#22.2(13)	0.90	0.41	1.20	4.62	0.23	0.39	0.59	0.13	0.20
P01#22.2(15)	0.92	0.41	1.20	4.51	0.25	0.40	0.56	0.12	0.20
P02#22.2(15)	1.03	0.37	1.55	3.59	0.27	0.39	0.52	0.09	0.18
P03#22.2(15)	1.00	0.40	1.36	3.47	0.27	0.39	0.58	0.10	0.19
P04#22.2(15)	1.00	0.40	1.34	3.37	0.26	0.40	0.56	0.11	0.19
P04#22.1(01)	0.71	0.37	1.08	9.10	0.33	0.17	0.53	0.05	0.09
P05#22.1(01)	0.71	0.35	1.12	8.74	0.35	0.17	0.56	0.05	0.10
P01#2019	0.82	0.37	1.39	6.88	0.20	0.32	0.28	0.09	0.13
P02#2019	0.93	0.37	1.41	7.03	0.17	0.32	0.32	0.09	0.14

[a]C27 (R+S)/C29 (R+S) steranes; [b]C29ββ/(C29ββ + C29⟨⟨) (S+R) steranes; [c]C27ββ/C29ββ (R+S) steranes; [d]17α(H),21β(H)-Hopane /C27⟨⟨⟨ (R+S) steranes; [e]C27 (R+S) Diasteranes/C27 (R+S) sterane; [f]C27, C28, C29 (⟨⟨⟨, ββ, ⟨ββ) (R+S) /17α(H),21β(H)-30-Norhopane + 17α(H),21β(H)-Hopane + 17α(H),21β(H)-30-Homohopane (R+S); 17α(H),21β(H)-30-Bishomohopane (R+S) + 17α(H),21β(H)-30-trishomohopane (R+S) [g]C27R/C27S diasterane; [h]C29ααββ(S) sterane/ 17α(H),21β(H)-Hopane; [i]C29ααββ(R) sterane/17α(H),21β(H)-Hopane.

Table S3. Part 3: Parameters based on monoaromatic steroids (*m/z* 231), terpanes (*m/z* 191), and steranes (*m/z* 217) for similarity assessment.

Sample code	**C20 /C28 20R TAS[a]**	**C28 20S/C28 20R TAS[b]**	**C27 20R/C28 20R TAS[c]**	**C20 TAS/C30H[d]**	**C28 TAS 20S/C30H[e]**	**C20 TAS/C21 TAS[f]**	**C20/C26R + C27S TAS[g]**	**C26S/C26R + C27S TAS[h]**	**C28S/C26R + C27S TAS[i]**	**C28R/C26R + C27S TAS[j]**	**C27R/C26R + C27S TAS[k]**
P01#22.2(07)	0.42	0.94	1.19	0.12	0.26	1.18	0.27	0.09	0.60	0.63	0.75
P02#22.2(07)	0.44	0.94	1.20	0.15	0.31	1.36	0.28	0.10	0.60	0.64	0.77
P03#22.2(07)	0.41	0.92	1.20	0.13	0.29	1.39	0.26	0.10	0.59	0.64	0.77
P01#22.2(08)	0.41	0.94	1.21	0.12	0.27	1.18	0.26	0.10	0.60	0.65	0.78
P01#22.2(09)	0.43	0.94	1.20	0.14	0.31	1.38	0.27	0.10	0.60	0.64	0.76
P02#22.2(09)	0.46	0.95	1.21	0.15	0.31	1.45	0.29	0.11	0.61	0.64	0.78
P01#22.2(10)	0.46	0.95	1.22	0.14	0.29	1.46	0.29	0.10	0.60	0.63	0.77
P01#22.2(11)	0.44	0.93	1.20	0.13	0.27	1.27	0.28	0.11	0.60	0.64	0.78
P01#22.2(12)	0.44	0.91	1.19	0.14	0.28	1.24	0.28	0.10	0.58	0.64	0.76
P02#22.2(12)	0.44	0.95	1.21	0.14	0.30	1.43	0.28	0.10	0.60	0.63	0.76
P01#22.2(13)	0.41	0.93	1.20	0.12	0.28	1.55	0.26	0.10	0.60	0.64	0.77
P02#22.2(13)	0.60	0.91	1.16	0.03	0.04	1.41	0.31	0.11	0.46	0.50	0.59

P01#22.2(15)	0.49	0.94	1.21	0.15	0.29	1.26	0.30	0.09	0.59	0.62	0.75
P02#22.2(15)	0.45	0.94	1.20	0.14	0.30	1.53	0.27	0.08	0.58	0.61	0.74
P03#22.2(15)	0.44	0.93	1.19	0.14	0.30	1.28	0.28	0.08	0.60	0.64	0.77
P04#22.2(15)	0.45	0.93	1.19	0.13	0.26	1.09	0.28	0.08	0.57	0.61	0.73
P04#22.1(01)	0.13	0.83	0.95	0.02	0.12	0.44	0.10	0.14	0.68	0.82	0.78
P05#22.1(01)	0.16	0.85	0.98	0.02	0.13	0.47	0.12	0.13	0.65	0.76	0.75
P01#2019	0.07	0.77	1.15	0.05	0.54	0.18	0.05	0.14	0.49	0.63	0.73
P02#2019	0.05	0.80	1.13	0.02	0.26	0.14	0.03	0.14	0.51	0.63	0.71

[a]C20 triaromatic steroid/C28 20R triaromatic steroid; [b]C28 20S triaromatic steroid/C28 20R triaromatic steroid; [c]C27 20R triaromatic steroid/C28 20R triaromatic steroid; [d]C20 triaromatic steroids/17α(H),21β(H)-Hopane; [e]C28 triaromatic steroid (20S)/17α(H),21β(H)-Hopane; [f]C20 triaromatic steroid/C21 triaromatic steroid; [g]C20 triaromatic steroid/C26R + C27S triaromatic steroid; [h]C26S triaromatic steroid/C26R + C27S triaromatic steroid; [i]C28S triaromatic steroid/C26R + C27S triaromatic steroid; [j]C28R triaromatic steroid/C26R + C27S triaromatic steroid; [k]C27R triaromatic steroid/C26R + C27S triaromatic steroid.

Table S4. Parameters based on *n*-alkanes (*m/z* 85), terpanes (*m/z* 191), and steranes (*m/z* 217) for thermal maturity assessment (organic geochemistry characteristics).

Sample Code	H31S/(H31S + H31R)[a]	H32S/(H32S + H32R)[b]	Ts/(Ts + Tm)[c]	C29 20S/(20S + 20R)[d]	C29 ββ/(ββ + αα)[e]	CPI[f]
P01#22.2(07)	0.57	0.59	0.36	0.46	0.41	0.97
P02#22.2(07)	0.56	0.59	0.36	0.48	0.41	0.99
P03#22.2(07)	0.56	0.60	0.36	0.47	0.41	1.00
P01#22.2(08)	0.56	0.59	0.36	0.47	0.40	0.97
P01#22.2(09)	0.57	0.59	0.36	0.48	0.40	0.99
P02#22.2(09)	0.57	0.59	0.37	0.48	0.41	0.98
P01#22.2(10)	0.57	0.59	0.37	0.46	0.41	1.00
P01#22.2(11)	0.57	0.60	0.36	0.45	0.41	1.00
P01#22.2(12)	0.57	0.59	0.36	0.48	0.39	0.98
P02#22.2(12)	0.57	0.60	0.36	0.47	0.40	1.06
P01#22.2(13)	0.56	0.60	0.36	0.47	0.41	0.97
P02#22.2(13)	0.57	0.60	0.36	0.47	0.41	1.02
P01#22.2(15)	0.57	0.60	0.36	0.48	0.41	1.00
P02#22.2(15)	0.59	0.60	0.34	0.48	0.37	0.99
P03#22.2(15)	0.57	0.60	0.35	0.46	0.40	0.97
P04#22.2(15)	0.57	0.60	0.35	0.47	0.40	1.00
P04#22.1(01)	0.56	0.59	0.31	0.50	0.37	1.12
P05#22.1(01)	0.57	0.59	0.32	0.50	0.35	1.04
P01#2019	0.57	0.45	0.34	0.53	0.37	1.06
P02#2019	0.57	0.60	0.35	0.52	0.37	1.06

[a]17α(H),21β(H)-30-Homohopane(S)/(17α(H),21β(H)-30-Homohopane(S+R); [b]17α(H),21β(H)-30, 31-Bishomohopane(S)/(17α(H),21β(H)-30, 31-bishomohopane(S+R); [c]18α(H)-30-Norneohopane/(18α(H)-30-Norneohopane + 17α(H)-22,29,30-Trisnorhopane); [d]C29 20S Sterane/C29 20 (S+R) steranes; [e]C29 ββ (R+S) steranes/(C29 ββ+αα) (R+S) steranes; [f]CPI (carbon preference index) = 1/2[(*n*C25 + *n*C27 + *n*C29 + *n*C31 + *n*C33)/(*n*C24 + *n*C26 + *n*C28 + *n*C30 + *n*C32) + (*n*C25 + *n*C27 + *n*C29 + *n*C31 + *n*C33)/(*n*C26 + *n*C28 + *n*C30 + *n*C32 + *n*C34)]

Table S5. Parameters based on *n*-alkanes (*m/z* 85), isoprenoids (*m/z* 183), terpanes (*m/z* 191), and steranes (*m/z* 217), TPPs (*m/z* 259) for genesis assessment (organic geochemistry characteristics).

Sample Code	TAR[a]	Pr/Ph[b]	21/23Tri[c]	Hop/Ste[d]	H31R/H30[e]	TPP/ (TPP+DIA27)[f]	H29/H30[g]	HH35(s)/ HH34(s)[h]	C27/C29[i]	G/H[j]	DIA27/C27[h]
P01#22.2(07)	0.55	0.60	0.08	3.78	0.46	0.29	0.98	0.89	0.96	0.04	0.24
P02#22.2(07)	0.57	0.64	0.14	3.70	0.47	0.28	1.00	0.89	0.90	0.02	0.24
P03#22.2(07)	0.64	0.62	0.13	3.89	0.46	0.27	0.97	0.73	0.94	0.02	0.24
P01#22.2(08)	0.61	0.60	0.11	3.71	0.46	0.28	0.99	0.71	0.94	0.00	0.24
P01#22.2(09)	0.61	0.61	0.18	3.60	0.45	0.27	1.00	0.67	0.90	0.01	0.23
P02#22.2(09)	0.53	0.62	0.18	3.46	0.45	0.28	0.98	0.80	0.91	0.01	0.26
P01#22.2(10)	0.76	0.58	0.14	3.77	0.43	0.28	0.96	0.75	0.95	0.04	0.24
P01#22.2(11)	0.64	0.64	0.12	3.46	0.45	0.28	1.00	0.67	0.94	0.01	0.23
P01#22.2(12)	0.59	0.62	0.13	3.75	0.44	0.28	0.97	0.86	0.94	0.00	0.24
P02#22.2(12)	0.60	0.60	0.18	3.56	0.46	0.28	1.01	0.73	0.91	0.03	0.24
P01#22.2(13)	0.55	0.63	0.13	3.74	0.46	0.31	0.98	0.82	0.92	0.01	0.22
P02#22.2(13)	0.71	0.62	0.13	3.77	0.44	0.30	0.99	0.69	0.90	0.00	0.23
P01#22.2(15)	0.49	0.63	0.13	3.57	0.44	0.33	0.99	1.86	0.92	0.01	0.25
P02#22.2(15)	0.63	0.70	0,04	3.90	0.43	0.30	1.00	n.d.	1.03	0.00	0.27
P03#22.2(15)	0.57	0.62	0.06	3.68	0.44	0.31	1.00	1.40	1.00	0.00	0.27
P04#22.2(15)	0.49	0.63	0.02	3.56	0.44	0.29	1.03	0.89	1.01	0.01	0.26
P04#22.1(01)	65.32	0.01	0.91	10.75	0.40	0.32	0.83	0.69	0.71	0.02	0.33
P05#22.1(01)	16.07	0.01	0.74	10.06	0.44	0.28	0.84	0.86	0.71	0.02	0.35
P01#2019	0.72	0.71	0.19	7.22	0.39	0.89	0.68	2.12	0.82	0.33	0.20
P02#2019	0.85	0.72	0.24	5.25	0.39	0.87	0.68	0.84	0.93	0.16	0.17

[a]TAR (Terrigenous aquatic ratio) = (*n*C15 + *n*C17 + *n*C19)/(*n*C27 + *n*C29 + *n*C31); [b]Pristane/Phytane; [c]C21/C23 Tricyclic Terpane; [d]Hopanes/Steranes; [e]17α(H),21β(H)-Homohopane (22R)/17α(H),21β(H)-Hopane; [f]C30 Tetracyclic Polyprenoid 18⟨(H)/(C30 Tetracyclic Polyprenoid 18⟨(H) + C27 (S+R) diasteranes) [g]17α(H),21β(H)-30-Norhopane/17α(H),21β(H)-Hopane; [h]17α(H),21β(H)-30,31,32,33,34-pentakishomohopane(22S)/17α(H),21β(H)-30,31,32,33-Tetrakishomohopane (22S); [i]C27 (R+S)/C29 (R+S) steranes; [j]Gammacerane /17α(H),21β(H)-Hopane; [h]C27 (R+S) Diasteranes/C27 (R+S) steranes.

Table S6. Parameters based on phenanthrene (Ph; *m/z* 178), and methylphenanthrenes (MP) and 2-methylanthracene (2MA; *m/z* 192) for type of oil assessment.

Sample code	(3 + 2)/(9/4 + 1)MP[a]	2-MA/3-MP[b]	2-MA/1-MP[c]	2-MA/(2 + 3-MP)[d]	2-MA/(9/4 + 1-MP)[e]	2MA/∑MP[f]
P01#22.2(07)	0.87	0.00	0.00	0.00	0.00	0.00
P02#22.2(07)	0.86	0.00	0.00	0.00	0.00	0.00
P03#22.2(07)	0.86	0.00	0.00	0.00	0.00	0.00
P01#22.2(08)	0.84	0.00	0.00	0.00	0.00	0.00
P01#22.2(09)	0.85	0.00	0.00	0.00	0.00	0.00
P02#22.2(09)	0.86	0.00	0.00	0.00	0.00	0.00
P01#22.2(10)	0.86	0.00	0.00	0.00	0.00	0.00
P01#22.2(11)	0.86	0.00	0.00	0.00	0.00	0.00

P01#22.2(12)	0.88	0.00	0.00	0.00	0.00	0.00
P02#22.2(12)	0.87	0.00	0.00	0.00	0.00	0.00
P01#22.2(13)	0.88	0.00	0.00	0.00	0.00	0.00
P02#22.2(13)	0.87	0.00	0.00	0.00	0.00	0.00
P01#22.2(15)	0.86	0.00	0.00	0.00	0.00	0.00
P02#22.2(15)	0.79	0.01	0.00	0.00	0.00	0.00
P03#22.2(15)	0.83	0.01	0.01	0.00	0.00	0.00
P04#22.2(15)	0.85	0.00	0.00	0.00	0.00	0.00
P04#22.1(01)	1.85	0.08	0.15	0.03	0.06	0.02
P05#22.1(01)	1.81	0.11	0.20	0.05	0.08	0.03
P01#2019	1.86	0.21	0.42	0.09	0.17	0.05
P02#2019	1.79	0.26	0.50	0.11	0.19	0.06

(3 + 2-methylphenanthrene)/(9/4 + 1-methylphenanthrene); [b]2-methylantracene/3-methylphenanthrene; [c]2-methylantracene/1-methylphenanthrene; [d]2-methylantracene/(3 + 2-methylphenanthrene); [e]2-methylantracene/(9/4 + 1-methylphenanthrene); [f]2-methylantracene/(3 + 2 +9/4 + 1-methylphenanthrene).

Table S7. Part 1: Parameters based on *n*-alkane and isoprenoids (GC-FID), *n*-alkylcyclohexanes (*m/z* 83), triaromatic steroids (*m/z* 231), and methylphenanthrenes (MP, *m/z* 192) for the evaluation of weathering processes.

Sample Code	C17/Pr[a]	C18/Ph[b]	9 MP/3MP[c]	9 MP/2MP[d]	C20 TAS/C30H[e]	C28 TAS 20S/C30H[f]	H30/Pr[g]	H30/Ph[h]
P01#22.2(07)	2.41	1.71	1.71	1.17	0.12	0.26	0.15	0.10
P02#22.2(07)	2.17	1.59	1.68	1.23	0.15	0.31	0.22	0.14
P03#22.2(07)	2.21	1.62	1.66	1.20	0.13	0.29	0.22	0.14
P01#22.2(08)	1.97	1.46	1.72	1.21	0.12	0.27	0.23	0.14
P01#22.2(09)	2.02	1.52	1.69	1.25	0.14	0.31	0.22	0.14
P02#22.2(09)	2.24	1.63	1.69	1.23	0.15	0.31	0.20	0.13
P01#22.2(10)	2.15	1.57	1.68	1.21	0.14	0.29	0.22	0.13
P01#22.2(11)	2.31	1.61	1.71	1.20	0.13	0.27	0.20	0.13
P01#22.2(12)	2.33	1.71	1.66	1.19	0.14	0.28	0.21	0.13
P02#22.2(12)	2.32	1.72	1.69	1.23	0.14	0.30	0.20	0.12
P01#22.2(13)	2.35	1.72	1.66	1.19	0.12	0.28	0.23	0.15
P02#22.2(13)	2.33	1.62	1.69	1.22	0.14	0.29	0.23	0.14
P01#22.2(15)	2.27	1.67	1.67	1.22	0.15	0.29	0.16	0.10
P02#22.2(15)	2.24	1.65	1.74	1.24	0.14	0.30	0.18	0.12
P03#22.2(15)	2.16	1.54	1.73	1.22	0.14	0.30	0.16	0.10
P04#22.2(15)	2.18	1.62	1.71	1.21	0.13	0.26	0.13	0.08

[a]*n*C17/Pristane; [b]*n*C18/Phytane; [c]9/4-Methylphenanthrene/3-Methylphenanthrene; [d]9/4-Methylphenanthrene/2-Methylphenanthrene; [e]C20 triaromatic steroid/17α(H),21β(H)-Hopane; [f]C28 20S triaromatic steroid/17α(H),21β(H)-Hopane; [g]17α(H),21β(H)-Hopane/Pristane; [h]17α(H),21β(H)-Hopane/Phytane.

Table S7. Part 2: Parameters based on *n*-alkane and isoprenoids (GC-FID), *n*-alkylcyclohexanes (*m/z* 83), triaromatic steroids (*m/z* 231), and methylphenanthrenes (MP, *m/z* 192) for the evaluation of weathering processes.

Sample Code	H30/C17[a]	H30/C18[b]	H30/DC[c]	H30/AC[d]	C30H/9-MP[e]	C30H/1-MP[f]	C30H/2-MP[g]	C30H/3-MP[h]
P01#22.2(07)	0.05	0.05	0.49	0.05	1.44	2.22	1.68	2.46
P02#22.2(07)	0.07	0.08	0.73	0.08	1.02	1.58	1.25	1.72
P03#22.2(07)	0.07	0.07	0.70	0.08	1.22	1.84	1.47	2.04
P01#22.2(08)	0.08	0.09	0.75	0.08	1.61	2.43	1.96	2.78
P01#22.2(09)	0.07	0.07	0.64	0.07	1.05	1.63	1.31	1.77
P02#22.2(09)	0.06	0.07	0.60	0.07	0.91	1.43	1.12	1.54
P01#22.2(10)	0.08	0.08	0.64	0.07	0.97	1.50	1.17	1.63
P01#22.2(11)	0.07	0.07	0.64	0.07	1.48	2.30	1.77	2.53
P01#22.2(12)	0.06	0.07	0.62	0.07	1.02	1.58	1.21	1.69
P02#22.2(12)	0.06	0.07	0.61	0.07	0.97	1.59	1.19	1.64
P01#22.2(13)	0.07	0.07	0.71	0.08	0.88	1.37	1.05	1.46
P02#22.2(13)	0.07	0.08	0.71	0.08	1.01	1.60	1.23	1.70
P01#22.2(15)	0.05	0.05	0.48	0.06	0.83	1.27	1.01	1.38
P02#22.2(15)	0.05	0.07	0.68	0.07	0.92	1.23	1.15	1.61
P03#22.2(15)	0.06	0.06	0.54	0.06	1.15	1.70	1.41	1.99
P04#22.2(15)	0.05	0.05	0.43	0.05	1.03	1.57	1.24	1.76

[a]17α(H),21β(H)-Hopane/*n*C17; [b]17α(H),21β(H)-Hopane/*n*C18; [c]17α(H),21β(H)-Hopane/ΣC13-C26 *n*-alkylcyclohexanes; [d]17α(H),21β(H)-Hopane/C16 *n*-alkylcyclohexane; [e]17α(H),21β(H)-Hopane/9/4-Methylphenanthrene; [f]17α(H),21β(H)-Hopane/1-Methylphenanthrene; [g]17α(H),21β(H)-Hopane/2-Methylphenanthrene; [h]17α(H),21β(H)-Hopane/3-Methylphenanthrene.

Table S8. Part 1: Relative abundance (%) for heteroatom classes obtained from the analysis by ESI(-) FT-ICR MS.

Sample code	HC	N	N2	N2O	N2O5	N2OS3	N2S2	N2S3	N3	N3O2	N3O3
P01#22.2(07)	0.00	61.37	1.30	0.24	0.00	0.00	0.00	0.00	0.00	0.00	0.00
P02#22.2(07)	0.41	51.08	0.83	0.67	0.00	0.00	0.00	0.00	0.00	0.00	0.00
P03#22.2(07)	0.00	29.82	0.72	0.43	0.00	0.00	0.00	0.00	0.00	0.00	0.00
P01#22.2(08)	0.11	34.63	0.00	0.00	0.00	0.00	0.00	0.00	0.00	0.00	1.70
P01#22.2(09)	0.55	28.66	0.88	0.44	0.00	0.45	0.28	0.00	0.00	0.00	2.68
P02#22.2(09)	0.00	59.25	1.04	0.00	0.00	0.00	0.00	0.00	0.00	0.00	0.00
P01#22.2(10)	0.00	51.96	0.96	0.00	0.00	0.00	0.00	0.00	0.00	0.00	0.00
P01#22.2(11)	0.00	42.23	0.52	0.00	0.00	0.00	0.58	0.00	0.00	0.00	0.00
P01#22.2(12)	0.17	51.57	1.28	0.37	0.49	0.00	0.95	0.00	0.15	0.17	0.00
P02#22.2(12)	0.00	71.81	0.38	0.00	0.00	0.00	0.00	0.00	0.00	0.00	0.00
P01#22.2(13)	0.00	52.70	0.84	0.00	0.00	0.00	0.00	0.00	0.00	0.00	0.00
P02#22.2(13)	0.00	51.46	1.04	0.30	0.00	0.00	0.00	0.00	0.00	0.00	0.00
P01#22.2(15)	0.00	50.52	1.36	0.49	0.12	0.00	0.34	0.00	0.00	0.00	0.00
P02#22.2(15)	0.00	64.37	0.00	0.00	0.00	0.00	0.00	0.00	0.00	0.00	0.00

P03#22.2(15)	0.00	26.77	0.28	0.00	0.00	0.00	0.00	0.00	0.00	0.00	0.00
P04#22.2(15)	0.56	23.26	0.52	0.34	0.00	0.00	0.59	0.28	0.00	0.00	0.46

Table S8. Part 2: Relative abundance (%) for heteroatom classes obtained from the analysis by ESI(-) FT-ICR MS.

Sample code	N3O2S	N3O2S2	N3O3S	N3O4S	N3S3	NO	NO2	NO2S	NO3	NOS	NS
P01#22.2(07)	0.00	0.00	0.00	0.00	0.00	5.57	1.30	0.00	0.00	0.88	7.82
P02#22.2(07)	0.00	0.00	0.00	0.00	0.00	11.67	4.00	0.00	0.62	2.20	6.70
P03#22.2(07)	0.00	0.00	0.00	0.00	0.00	7.30	3.82	0.00	1.01	1.30	4.93
P01#22.2(08)	0.00	0.00	0.00	0.00	0.00	4.44	3.17	0.00	0.34	0.00	4.05
P01#22.2(09)	0.00	0.00	0.37	0.00	0.00	5.76	4.17	0.27	1.45	1.30	4.63
P02#22.2(09)	0.00	0.00	0.00	0.00	0.00	5.91	1.35	0.00	0.00	0.91	7.41
P01#22.2(10)	0.00	0.00	0.00	0.00	0.00	4.96	2.41	0.00	0.23	0.86	6.24
P01#22.2(11)	2.99	1.23	0.96	0.78	0.00	4.78	2.97	0.00	0.46	0.74	4.37
P01#22.2(12)	0.00	0.00	0.00	0.00	0.00	4.75	1.98	0.00	0.00	0.97	5.73
P02#22.2(12)	0.00	0.00	0.00	0.00	0.00	3.35	0.34	0.00	0.00	0.00	7.23
P01#22.2(13)	0.00	0.00	0.00	0.00	0.00	6.31	2.57	0.00	0.00	1.02	6.38
P02#22.2(13)	0.00	0.00	0.00	0.00	0.00	5.37	2.63	0.00	0.37	1.15	6.65
P01#22.2(15)	0.00	0.00	0.00	0.00	0.00	5.47	2.29	0.00	0.00	1.33	7.00
P02#22.2(15)	0.00	0.00	0.00	0.00	0.00	3.38	0.00	0.00	0.00	0.00	6.36
P03#22.2(15)	0.51	0.00	0.00	0.00	0.00	4.46	3.25	0.00	0.85	0.57	3.66
P04#22.2(15)	1.72	1.22	1.14	0.88	0.25	5.79	4.17	0.00	1.09	0.97	3.58

Table S8. Part 3: Relative abundance (%) for heteroatom classes obtained from the analysis by ESI(-) FT-ICR MS.

Sample code	NS2	O	O2*	O2S	O3	O3S	O4	O4S	O5S	OS	S
P01#22.2(07)	0.00	10.84	4.17	0.26	0.00	2.37	0.00	1.80	0.00	2.06	0.00
P02#22.2(07)	0.00	5.52	7.02	0.94	1.88	2.09	0.00	2.79	0.00	1.59	0.00
P03#22.2(07)	0.00	9.28	12.19	2.12	4.45	6.08	1.42	11.10	0.62	2.88	0.54
P01#22.2(08)	0.06	10.37	22.76	2.61	6.70	5.24	0.00	0.00	0.00	2.95	0.89
P01#22.2(09)	0.00	10.63	17.63	3.44	6.51	4.75	0.00	0.00	0.00	3.91	1.24
P02#22.2(09)	0.00	10.91	5.05	0.48	0.80	2.17	0.00	2.84	0.00	1.87	0.00
P01#22.2(10)	0.00	10.09	7.50	1.30	2.73	2.78	0.70	4.55	0.00	2.74	0.00
P01#22.2(11)	0.00	9.11	9.32	1.73	3.64	3.62	0.71	5.47	0.00	3.24	0.55

P01#22.2(12)	0.34	11.32	7.08	1.15	2.65	3.38	0.00	1.69	0.00	3.17	0.62
P02#22.2(12)	0.00	10.33	2.94	0.00	0.00	1.14	0.00	1.27	0.00	1.22	0.00
P01#22.2(13)	0.00	9.88	7.25	1.17	2.36	2.93	0.35	3.83	0.00	2.39	0.00
P02#22.2(13)	0.00	9.75	6.49	1.42	2.33	3.25	0.43	4.67	0.00	2.69	0.00
P01#22.2(15)	0.00	11.15	6.34	1.35	1.73	2.99	0.25	4.16	0.00	3.13	0.00
P02#22.2(15)	0.00	11.27	6.04	0.00	0.00	0.00	0.00	8.57	0.00	0.00	0.00
P03#22.2(15)	0.00	8.69	12.61	2.17	4.85	9.65	1.47	15.85	0.91	2.88	0.57
P04#22.2(15)	0.00	9.83	12.04	2.71	4.64	8.18	1.10	8.40	0.94	4.01	1.34

The mass spectral peaks that appeared pronounced in the ESI(-) mode, $C_{16}H_{30}O_2$ (DBE 2), $C_{16}H_{32}O_2$ (DBE 1), $C_{18}H_{34}O_2$ (DBE 2), and $C_{18}H_{36}O_2$ (DBE 1), may reflect common contaminants (Tian et al., 2022). Because these compounds present a homologous series (Kim et al., 2005), they were calculated through the mean between C15 and C17 for compounds C16 of DBE 1 and DBE 2 and between C17 and C19 for compounds C18 of DBE 1 and DBE 2.

Table S9. Relative abundance (%) for elemental classes obtained from the analysis by ESI(-) FT-ICR MS.

Sample code	Ox	Ny	Sz	OxNy	OxSz	NySz	OxNySz
P01#22.2(07)	15.01	62.67	0.00	7.11	6.50	7.82	0.88
P02#22.2(07)	14.48	52.12	0.00	17.02	7.44	6.73	2.20
P03#22.2(07)	27.34	30.54	0.54	12.56	22.79	4.93	1.30
P01#22.2(08)	39.86	34.67	0.89	9.66	10.81	4.11	0.00
P01#22.2(09)	34.96	29.71	1.24	14.58	12.17	4.94	2.41
P02#22.2(09)	16.77	60.29	0.00	7.26	7.37	7.41	0.91
P01#22.2(10)	21.02	52.92	0.00	7.60	11.36	6.24	0.86
P01#22.2(11)	22.78	42.75	0.55	8.21	14.06	4.95	6.70
P01#22.2(12)	21.09	53.09	0.62	7.78	9.41	7.04	0.97
P02#22.2(12)	13.27	72.19	0.00	3.68	3.63	7.23	0.00
P01#22.2(13)	19.84	53.54	0.00	8.89	10.32	6.38	1.02
P02#22.2(13)	19.00	52.51	0.00	8.67	12.03	6.65	1.15
P01#22.2(15)	19.46	51.88	0.00	8.37	11.63	7.33	1.33
P02#22.2(15)	17.31	64.37	0.00	3.38	8.57	6.36	0.00
P03#22.2(15)	27.62	27.06	0.57	8.55	31.46	3.66	1.07
P04#22.2(15)	27.76	23.92	1.35	11.92	24.37	4.73	5.95

Table S10. Parameters based on acidic polar compounds obtained from the analysis by ESI(-) FT-ICR MS for the evaluation of weathering processes.

Sample code	NO_3/NO_2	$NO_3/(NO+NO_2)$	NO_x/N_1	$(O_4+O_3)/(O_2+O_1)$	$O_4/(O_2+O_1)$	O_3/O_2	$O_{x>2}/O_1$	SO_x/SO	SO_x/N_1
P01#22.2(07)	0.00	0.00	0.11	0.00	0.00	0.00	0.00	3.15	0.11
P02#22.2(07)	0.16	0.04	0.32	0.15	0.00	0.27	1.88	4.66	0.15
P03#22.2(07)	0.27	0.09	0.41	0.27	0.07	0.37	4.60	7.92	0.76
P01#22.2(08)	0.11	0.05	0.23	0.20	0.00	0.29	6.70	3.66	0.31
P01#22.2(09)	0.35	0.15	0.40	0.23	0.00	0.37	6.51	3.09	0.42
P02#22.2(09)	0.00	0.00	0.12	0.05	0.00	0.16	0.80	3.93	0.12
P01#22.2(10)	0.09	0.03	0.15	0.19	0.04	0.36	2.80	4.15	0.22
P01#22.2(11)	0.15	0.06	0.19	0.24	0.04	0.39	3.72	4.34	0.33
P01#22.2(12)	0.00	0.00	0.13	0.14	0.00	0.37	2.65	2.97	0.18
P02#22.2(12)	0.00	0.00	0.05	0.00	0.00	0.00	0.00	2.98	0.05
P01#22.2(13)	0.00	0.00	0.17	0.16	0.02	0.33	2.40	4.31	0.20
P02#22.2(13)	0.14	0.05	0.16	0.17	0.03	0.36	2.38	4.48	0.23
P01#22.2(15)	0.00	0.00	0.15	0.11	0.01	0.27	1.75	3.72	0.23
P02#22.2(15)	0.00	0.00	0.05	0.00	0.00	0.00	0.00	0.00	0.13
P03#22.2(15)	0.26	0.11	0.32	0.30	0.07	0.38	5.02	10.94	1.18
P04#22.2(15)	0.26	0.11	0.48	0.26	0.05	0.39	4.76	6.05	1.04

References

Tian, Y., Jiang, B., Chen, J., Zhan, Z.W., Yang, C., Zou, Y.R., 2022. Characterisation by ESI FT-ICR MS of heteroatomic compounds in catalytic hydropyrolysates released from marine crude oil asphaltenes. Org. Geochem. 167, 104391. https://doi.org/10.1016/j.orggeochem.2022.104391

APÊNDICE B

Supplementary Material

Material suplementar do artigo 2: Monitoring petroleum residues along the Ceará coast in 2021 and 2022: Forensic geochemistry to assess chronic seashore pollution in Brazil after the 2019 oil spill

Table S1. Code, collection date, and locality information, including the beach, state, and coordinates of the beached petroleum residue samples from the 2021 and 2022 surveys.

Survey	Sample code	Collection date	Locality		
			Beach	State	Coordinates
2021	P01#21	23/07/2021	Barra Velha	Ceará	-4.068898, -38,173206
	P03#21	24/07/2021	Pontal de Maceió	Ceará	-4.395502 -37.766495
	P04#21	24/07/2021	Pontal de Maceió	Ceará	-4,406538 -37.767475
	P06#21	25/07/2021	Canto Verde	Ceará	-4.533824 -37.686238
	P07#21	10/08/2021	Iguape	Ceará	-3.943579 -38.275587
	P08#21	10/08/2021	Sabiaguaba	Ceará	-3.778348 -38.426251
	P10#21	24/07/2021	Pecém	Ceará	-3.547169 -38.806706
	P11#21	10/08/2021	Iguape	Ceará	-3.946129 -38.271525
	P12#21	27/07/2021	Pecém	Ceará	-3.548363 -38.806858
	P14#21	07/10/2021	Taíba	Ceará	-3.460652 -38.933276
	P16#21	08/10/2021	Lagoinha	Ceará	-3.349089 -39.111768
	P17#21	08/10/2021	Lagoinha	Ceará	-3.342730 -39.123993
	P20#21	04/11/2021	Apiques	Ceará	-3.110456 -39.501801
	P21#21	04/11/2021	Caetanos	Ceará	-3.080615 -39.559479
	P22#22	05/11/2021	Caetanos	Ceará	-3.074150 -39.568155
	P23#21	04/11/2021	Icaraizinho de Amontada	Ceará	-3.042388 -39.608993
	P24#21	04/11/2021	Bitupitá	Ceará	-2.866729 -41.255910
	P28#21	06/11/2021	Jericoacoara	Ceará	-2.771067 -40.336370
	P34#21	06/11/2021	Caetanos	Ceará	-3.076038 -39.561762

2022	P01#2022(04)S01	13/07/2022	Bitupitá	Ceará	-2.889087 -41.252678
	P01#22(04)S05	13/07/2022	Bitupitá	Ceará	-2.891472 -41.233314
	P01#22(03)S03	17/07/2022	Bitupitá	Ceará	-2.891088 -41.274399
	P01#22(05)S01	11/09/2022	Jericoacoara	Ceará	-2.791111 -40.519444
	P01#22(05)S03	13/07/2022	Jericoacoara	Ceará	-2.791667 -40.520278
	P01#22(03)	30/06/2022	Cumbuco	Ceará	-3.592107 -38.804093
	P04#22(03)	30/06/2022	Flecheiras	Ceará	-3.169372 -39.584056
	P03#22(03)	30/06/2022	Paracuru	Ceará	-3.398907 -39.011062
	P02#22(03)S03	30/06/2022	Taíba	Ceará	-3.447096 -38.898457
	P01#22(02)	03/05/2022	Sabiaguaba	Ceará	-3.782708 -38.427554
	P02#22(02)	03/05/2022	Porto das Dunas	Ceará	-3.818905 -38.404423
	P06#22(02)	03/05/2022	Canto Verde	Ceará	-4.155022 -38.122778
	P05#22(02)	03/05/2022	Canoa Quebrada	Ceará	-4.031948 -38.254763

Table S2. Code, collection date, and locality information, including the beach, state, and coordinates of the beached petroleum residue samples from the 2019, 2022.1, and 2022.2 events.

Event	Sample code	Collection date	Locality		
			Beach	**State**	**Coordinates**
2019	P01#2019	01/11/2019	Mangue do Rio Jaguaribe	Ceará	-4.440677 -37.778097
	P02#2019	07/11/2019	Cumbuco	Ceará	-3.621241 -38.738776
	P03#2019	08/11/2019	Paracuru (Quebra Mar)	Ceará	-38.738776 -38.990374
	P04#2019	08/11/2019	Paracuru (Boca do Poço)	Ceará	-3.404193 -39.025663
2022.1	P01#22.1(01)	28/01/2022	Sabiaguaba		-3,377797 -38,430343
	P04#22.1(01)	28/01/2022	Cumbe	Ceará	-4.472713 -37.740430
	P05#22.1(01)	28/01/2022	Canoa Quebrada	Ceará	-4.519647 -37.700726
2022.2	P01#22.2(07)	24/09/2022	Icaraí	Ceará	3.674444 -38.664444
	P01#22.2(08)	01/10/2022	Futuro Beach	Ceará	-3.763055 -38.439444
	P01#22.2(06)	23/09/2022	Futuro Beach		-3.747436 -38.447813

Table S3. Diagnostic ratios based on tricyclic and pentacyclic terpanes (*m/z* 191), steranes (*m/z* 217), and TPPs (*m/z* 259) for similarity evaluation of the oils of the 2019 event and 2021 survey

Ratios	2019 Event				2021 Survey			
	P01	P02	P03	P04	P03	P07	P08	RSD
Tr26/Tet24[1]	2.22	2.50	2.54	2.21	2.25	1.97	2.20	8.8
Tr25/Tr26[2]	1.66	1.39	1.48	1.53	1.56	1.60	1.48	5.8
Ts/Tm[3]	0.57	0.51	0.46	0.47	0.50	0.45	0.53	8.0
H29/H30[4]	0.69	0.74	0.75	0.73	0.67	0.63	0.75	6.1
H31R/H30[5]	0.45	0.43	0.46	0.41	0.46	0.41	0.40	5.7
C32HH(S)/C32HH(S + R)[6]	0.63	0.59	0.62	0.62	0.35	0.59	0.34	22.3
H35/H34[7]	1.08	1.07	1.04	0.92	1.06	0.99	0.94	6.1
C29 20S/(20S + 20R) Ste[8]	0.37	0.43	0.41	0.43	0.25	0.39	0.12	29.8
C28 20S/(20S + 20R) Ste[9]	0.47	0.22	0.29	0.39	0.37	0.39	0.34	22.0
C27 20S/(20S + 20R) Ste1[0]	0.41	0.38	0.47	0.44	0.43	0.33	0.89	42.9
C27/C29 Ste[11]	1.14	1.12	0.97	1.05	1.06	0.91	1.00	7.7
TPP/(TPP+Dia27)[12]	0.80	0.78	0.81	0.78	0.81	0.76	0.81	2.6

[1]C26tricyclic terpane/ tetracyclic terpane ; [2]C25 Tricyclic Terpane/ C26 Tricyclic Terpae; [3]C27 18α-trisnorneohopane/C27 17α-trisnorhopane; [4]C29 hopane /C30 hopane; [5]17α(H), 21β(H)-Homohopane(R)/C30 17α(H), 21β(H) Hopane ; [6]17α(H),21β(H)-30, 31-Bishomohopane(S)/17α(H),21β(H)-30, 31-bishomohopane(S + R); [7]C35 hopane (S + R)/C34 hopane (S + R); [8] C29 βαS/(20S + 20R) = 13α(H),17α(H)- diacholestanes 20R and 20S; [9]C28 βαS/(20S + 20R) = 13α(H),17α(H)- diacholestanes 20R and 20S; ; [10] C27 βαS/(20S + 20R) = 13α(H),17α(H)-diacholestanes 20R and 20S;[11]©(5α(H),14α(H),17α(H) Cholestane (20S); [12](C30 tetracyclic polyprenoids/[C30 tetracyclic polyprenoids + C27diasterane βα (S + R)].

Table S4. Diagnostic ratios based on tricyclic and pentacyclic terpanes and steranes (*m/z* 191), steranes (*m/z* 217), and TPPs (*m/z* 259) for similarity evaluation from the oils of the 2022.1 Event and 2022 survey

Ratios	2022.1 Event			2022 Survey			
	P04 (01)	P05 (01)	P01(01)	P01 (02)	P02 (02)	P02 (03)S03	DSR %
Tr26/Tet24[1]	0.86	0.88	0.75	0.93	0.86	0.88	7.05
Tr25/Tr26[2]	1.07	1.00	1.14	0.98	1.12	0.92	8.14
Ts/Tm[3]	0.51	0.50	0.43	0.44	0.45	0.46	6.55
H29/H30[4]	0.71	0.89	0.74	0.78	0.75	0.75	8.06
H31R/H30[5]	0.40	0.45	0.36	0.39	0.39	0.38	7.47
C32HH(S)/C32HH(S + R)[6]	0.62	0.59	0.58	0.57	0.42	0.55	12.25
H35/H34[7]	1.07	1.10	1.04	1.03	1.21	1.20	7.05
C29 20S/(20S + 20R) Ste[8]	0.41	0.45	0.39	0.46	0.45	0.43	5.87
C28 20S/(20S + 20R) Ste[9]	0.46	0.26	0.48	0.52	0.24	0.25	29.45

C27 20S/(20S + 20R) Ste[10]	0.35	0.37	0.38	0.38	0.38	0.22	14.78
C27/C29 Steranes[11]	0.77	0.80	0.74	0.81	0.86	1.23	11.36
TPP/(TPP+Dia27)[12]	0.59	0.59	0.56	0.56	0.56	0.50	5.84

[1]C26 tricyclic terpane/ tetracyclic terpane ; [2]C25 Tricyclic Terpane/ C26 Tricyclic Terpae; [3]C27 18α-trisnorneohopane/C27 17α-trisnorhopane; [4]C29 hopane /C30 hopane; [5]17α(H), 21β(H)-Homohopane(R)/C30 17α(H), 21β(H) Hopane ; [6]17α(H),21β(H)-30, 31-Bishomohopane(S)/17α(H),21β(H)-30, 31-bishomohopane(S + R); [7]C35 hopane (S + R)/C34 hopane (S + R); [8] C29 βαS/(20S + 20R) = 13α(H),17α(H)- diacholestanes 20R and 20S; [9]C28 βαS/(20S + 20R) = 13α(H),17α(H)-diacholestanes 20R and 20S; ; [10] C27 βαS/(20S + 20R) = 13α(H),17α(H)- diacholestanes 20R and 20S;[11]©(5α(H),14α(H),17α(H) Cholestane (20S); [12](C30 tetracyclic polyprenoids/[C30 tetracyclic polyprenoids + C27diasterane βα (S + R)].

Table S5. Diagnostic ratios based on tricyclic and pentacyclic terpanes and steranes (*m/z* 191), steranes (*m/z* 217), and TPPs (*m/z* 259) for similarity evaluation from the oils of the 2022.1 event and 2022

	2021 Survey																
Ratios	**P01**	**P04**	**P06**	**P10**	**P11**	**P12**	**P14**	**P16**	**P17**	**P20**	**P21**	**P22**	**P23**	**P24**	**P28**	**P34**	**DPR**
Tr26/Tet24[1]	0.58	3.05	0.12	0.10	0.22	0.21	0.40	0.13	2.05	1.35	1.30	0.32	0.22	0.16	0.25	2.24	116.4
Tr25/Tr26[2]	0.40	0.83	2.96	2.36	1.18	1.51	1.54	1.48	1.05	1.58	0.84	2.05	1.98	1.37	1.20	0.75	45.4
Ts/Tm[3]	0.25	1.19	0.34	1.75	1.18	0.50	0.58	0.32	0.33	0.72	0.30	0.53	0.41	0.30	1.12	1.53	68.5
H29/H30[4]	1.58	0.38	1.19	0.75	1.05	1.03	0.94	1.26	0.67	0.57	0.42	0.81	1.10	1.26	1.09	0.42	38.6
H31R/H30[5]	0.40	0.17	0.44	0.42	0.54	0.45	0.44	0.47	0.36	0.40	0.22	0.43	0.47	0.48	0.49	0.18	28.2
C32HH(S)/C32HH(S + R)[6]	0.56	0.64	0.62	0.59	0.60	0.63	0.60	0.58	0.60	0.60	0.58	0.62	0.56	0.57	0.60	0.60	3.9
H35/H34[7]	1.36	0.50	0.88	0.85	0.91	1.01	1.09	0.92	1.03	1.25	0.77	0.92	0.93	1.11	0.86	0.31	27.8
C29 20S/(20S + 20R) Ste[8]	0.40	0.41	0.46	0.30	0.46	0.42	0.46	0.45	0.50	0.47	0.47	0.46	0.42	0.48	0.42	0.28	14.2
C28 20S/(20S + 20R) Ste[9]	0.45	0.43	0.43	0.34	0.52	0.49	0.49	0.56	0.35	0.44	0.30	0.33	0.36	0.53	0.39	0.45	18.2
C27 20S/(20S + 20R) Ste[10]	0.42	0.44	0.43	0.34	0.46	0.44	0.41	0.47	0.39	0.51	0.35	0.49	0.50	0.46	0.44	0.32	13.3
C27/C29 Ste[11]	0.73	0.45	0.29	1.11	0.65	0.82	0.85	0.67	1.57	0.86	1.39	0.60	0.56	0.70	0.69	0.51	42.9
TPP/(TPP+Dia27)[12]	0.57	0.92	0.84	0.39	0.53	0.52	0.37	0.63	0.76	0.47	0.90	0.53	0.59	0.64	0.45	0.94	30.1

[1]C26 tricyclic terpane/ tetracyclic terpane ; [2]C25 Tricyclic Terpane/ C26 Tricyclic Terpae; [3]C27 18α-trisnorneohopane/C27 17α-trisnorhopane; [4]C29 hopane /C30 hopane; [5]17α(H), 21β(H)-Homohopane(R)/C30 17α(H), 21β(H) Hopane ; [6]17α(H),21β(H)-30, 31-Bishomohopane(S)/17α(H),21β(H)-30, 31-bishomohopane(S + R); [7]C35 hopane (S + R)/C34 hopane (S + R); [8] C29 βαS/(20S + 20R) = 13α(H),17α(H)- diacholestanes 20R and 20S; [9]C28 βαS/(20S + 20R) = 13α(H),17α(H)- diacholestanes 20R and 20S; ; [10] C27 βαS/(20S + 20R) = 13α(H),17α(H)- diacholestanes 20R and 20S;[11]©(5α(H),14α(H),17α(H) Cholestane (20S); [12](C30 tetracyclic polyprenoids/[C30 tetracyclic polyprenoids + C27diasterane βα (S + R)].

Table S6. Diagnostic ratios based on tricyclic and pentacyclic terpanes and steranes (*m/z* 191), steranes (*m/z* 217), and TPPs (*m/z* 259) for similarity evaluation from the oils of 2022.1 and 2022.

Ratios	2022 Survey													
	P01(04)S01	P01(04)S05	P01(05)S01	P01(05)S03	P01(03)	P05(02)	P01(02)	P02(02)	P01(03)S03	P04(03)	P02(03)S03	P03(03)	P06(02)	DPR
[1]Tr26/Tet24[1]	1.42	0.13	1.41	0.55	0.17	0.29	0.93	0.86	0.47	0.76	0.88	0.27	0.25	80.06
[2]Tr25/Tr26[2]	1.63	1.30	1.20	1.64	1.81	1.63	0.98	1.12	1.64	1.44	0.92	1.56	1.39	19.52
[3]Ts/Tm[3]	0.57	1.77	0.69	0.79	0.36	0.84	0.44	0.45	0.66	0.56	0.46	0.60	0.55	63.39
[4]H29/H30[4]	0.62	0.84	0.61	0.75	1.02	0.88	0.78	0.75	0.80	0.95	0.75	1.02	1.03	17.68
[5]H31R/H30[5]	0.42	0.43	0.41	0.34	0.37	0.48	0.39	0.39	0.44	0.41	0.38	0.39	0.39	8.59
[6]C32HH(S)/C32HH(S + R)[6]	0.64	0.60	0.60	0.61	0.59	0.58	0.57	0.42	0.61	0.56	0.55	0.59	0.61	8.95
[7]H35/H34[7]	1.25	0.95	1.22	0.92	1.16	1.17	1.03	1.21	1.00	0.88	1.20	0.94	0.99	12.92
[8]C29 20S/(20S + 20R) Ste[8]	0.44	0.39	0.45	0.46	0.46	0.45	0.46	0.45	0.45	0.48	0.43	0.44	0.40	5.40
[9]C28 20S/(20S + 20R) Ste[9]	0.22	0.50	0.23	0.29	0.35	0.35	0.52	0.24	0.48	0.58	0.25	0.50	0.42	35.96
[10]C27 20S/(20S + 20R) Ste[10]	0.57	0.33	0.43	0.42	0.46	0.36	0.38	0.38	0.41	0.43	0.22	0.44	0.38	19.37
[11]C27/C29 Ste[11]	0.60	0.78	1.02	0.79	0.61	0.76	0.81	0.86	0.90	0.66	1.23	0.92	0.84	21.11
[12]TPP/(TPP+Dia27)[12]	0.56	0.38	0.53	0.53	0.65	0.45	0.56	0.56	0.37	0.66	0.50	0.48	0.49	16.51

[1] C26 tricyclic terpane/ tetracyclic terpane ; [2]C25 Tricyclic Terpane/ C26 Tricyclic Terpae; [3]C27 18α-trisnorneohopane/C27 17α-trisnorhopane; [4]C29 hopane /C30 hopane; [5]17α(H), 21β(H)-Homohopane(R)/C30 17α(H), 21β(H) Hopane ; [6]17α(H),21β(H)-30, 31-Bishomohopane(S)/17α(H),21β(H)-30, 31-bishomohopane(S + R); [7]C35 hopane (S + R)/C34 hopane (S + R); [8] C29 βαS/(20S + 20R) = 13α(H),17α(H)- diacholestanes 20R and 20S; [9]C28 βαS/(20S + 20R) = 13α(H),17α(H)- diacholestanes 20R and 20S; ; [10] C27 βαS/(20S + 20R) = 13α(H),17α(H)- diacholestanes 20R and 20S;[11]©(5α(H),14α(H),17α(H) Cholestane (20S); [12](C30 tetracyclic polyprenoids/[C30 tetracyclic polyprenoids + C27diasterane βα (S + R)].

Table S7. Conventional oil HPAs present in monitoring samples carried out on the coast of the State of Ceará in 2021

2021 Survey																				
m/z	**Compounds**	**P01**	**P03**	**P04**	**P06**	**P07**	**P08**	**P10**	**P11**	**P12**	**P14**	**P16**	**P17**	**P20**	**P21**	**P22**	**P23**	**P24**	**P28**	**P34**
142	**C1N(1)**	Nd	Nd	Nd	Nd	Nd	Nd	Nd	Nd	Nd	Nd	Nd	Nd	Nd	Nd	Nd	Nd	Nd	Nd	Nd
	C1N(2)	Nd	Nd	Nd	Nd	Nd	Nd	Nd	Nd	Nd	Nd	Nd	Nd	Nd	Nd	Nd	Nd	Nd	Nd	Nd
156	**C2N(1)**	Nd	Nd	Nd	Nd	Nd	Nd	Nd	Nd	Nd	Nd	Nd	Nd	Nd	Nd	Nd	Nd	Nd	Nd	Nd
	C2N(2)	Nd	Nd	Nd	Nd	Nd	Nd	Nd	Nd	Nd	Nd	Nd	Nd	Nd	Nd	Nd	Nd	Nd	Nd	Nd
	C2N(3)	Nd	Nd	Nd	Nd	Nd	Nd	Nd	Nd	Nd	Nd	Nd	Nd	Nd	Nd	Nd	Nd	Nd	Nd	Nd
	C2N(4)	Nd	Nd	Nd	Nd	Nd	Nd	Nd	Nd	Nd	Nd	Nd	Nd	Nd	Nd	Nd	Nd	Nd	Nd	Nd
	C2N(5)	Nd	Nd	Nd	Nd	Nd	Nd	Nd	Nd	Nd	Nd	Nd	Nd	Nd	Nd	Nd	Nd	Nd	Nd	Nd
184	**DBTO**	Nd	x	Nd	Nd	x	Nd	Nd	Nd	Nd	Nd	Nd	Nd	Nd	Nd	Nd	Nd	Nd	Nd	Nd
178	**Ph**	Nd	x	Nd	Nd	x	Nd	Nd	Nd	Nd	Nd	Nd	Nd	Nd	Nd	Nd	Nd	Nd	Nd	Nd
	An	Nd	x	Nd	Nd	Nd	Nd	Nd	Nd	Nd	Nd	Nd	Nd	Nd	Nd	Nd	Nd	Nd	Nd	Nd
198	**4MeDBT**	Nd	x	Nd	Nd	x	x	Nd	Nd	Nd	Nd	Nd	Nd	Nd	Nd	Nd	Nd	Nd	Nd	Nd
	3+2MeDBT	Nd	x	Nd	Nd	x	x	Nd	Nd	Nd	Nd	Nd	Nd	Nd	Nd	Nd	Nd	Nd	Nd	Nd
	1MeDBT	Nd	x	Nd	Nd	x	x	Nd	Nd	Nd	Nd	Nd	Nd	Nd	Nd	Nd	Nd	Nd	Nd	Nd
192	**3-MP**	Nd	x	Nd	Nd	x	x	Nd	Nd	Nd	Nd	Nd	Nd	Nd	Nd	Nd	Nd	Nd	Nd	Nd
	2-MP	Nd	x	Nd	Nd	x	x	Nd	Nd	Nd	Nd	Nd	Nd	Nd	Nd	Nd	Nd	Nd	Nd	Nd
	2-MA	Nd	x	Nd	Nd	x	x	Nd	Nd	Nd	Nd	Nd	Nd	Nd	Nd	Nd	Nd	Nd	Nd	Nd
	9/4-MA	Nd	x	Nd	Nd	x	x	Nd	Nd	Nd	Nd	Nd	Nd	Nd	Nd	Nd	Nd	Nd	Nd	Nd
	1-MA	Nd	x	Nd	Nd	x	x	Nd	Nd	Nd	Nd	Nd	Nd	Nd	Nd	Nd	Nd	Nd	Nd	Nd
206	**P2**	Ba	x	Nd	Nd	Nd	x	Nd	Nd	Nd	Nd	Nd	Nd	Nd	Nd	Nd	Nd	Nd	Nd	Nd
212	**C2-DBT**	Nd	x	Nd	Nd	Nd	x	Nd	Nd	Nd	Nd	Nd	Nd	Nd	Nd	Nd	Nd	Nd	Nd	Nd
226	**C3-DBT**	Nd	x	Nd	Nd	Nd	x	x	Nd	Nd	Nd	Nd	Nd	Nd	Nd	Nd	Nd	Nd	Nd	Nd
242	**C1C**	**Nd**	x	x	x	x	x	x	x	x	x	x	x	x	x	x	x	x	x	x
256	**C2C**	**Nd**	x	Nd	Nd	x	x	x	x	x	x	x	x	x	x	Nd	x	x	x	x

Nd: Not detected or low abundance; x: Detected

Table S8. Conventional oil PAHs present in monitoring samples carried out on the coast of the State of Ceará in 2022

2022 Survey											
m/z	**Compounds**	**P01#22(04)S01**	**P01#22(04)S05**	**P01#22(05)S01**	**P01#22(05)S03**	**P01#22(03)S01**	**P05#22(02)**	**P01#22(03)S03**	**P04#22 (03)**	**P03#22(03)**	**P06#22(02)**
142	**C1N(1)[1]**	Nd	Nd	Nd	Nd	Nd	Nd	Nd	Nd	Nd	Nd
	C1N(2)[2]	Nd	Nd	Nd	Nd	Nd	Nd	Nd	Nd	Nd	Nd
156	**C2N(1)**	Nd	Nd	Nd	Nd	Nd	Nd	Nd	Nd	Nd	Nd
	C2N(2)	Nd	Nd	Nd	Nd	Nd	Nd	Nd	Nd	Nd	Nd
	C2N(3)	Nd	Nd	Nd	Nd	Nd	Nd	Nd	Nd	Nd	Nd
	C2N(4)	Nd	Nd	Nd	Nd	Nd	Nd	Nd	Nd	Nd	Nd
	C2N(5)	Nd	Nd	Nd	Nd	Nd	Nd	Nd	Nd	Nd	Nd
184	**DBTO**	Nd	Nd	Nd	Nd	Nd	Nd	Nd	Nd	Nd	Nd
178	**Ph**	Nd	Nd	Nd	Nd	Nd	Nd	Nd	Nd	Nd	Nd
	An	Nd	Nd	Nd	Nd	Nd	Nd	Nd	Nd	Nd	Nd
198	**4MeDBT**	Nd	Nd	Nd	Nd	Nd	Nd	Nd	Nd	Nd	Nd
	3+2MeDBT	Nd	Nd	Nd	Nd	Nd	Nd	Nd	Nd	Nd	Nd
	1MeDBT	Nd	Nd	Nd	Nd	Nd	Nd	Nd	Nd	Nd	Nd
192	**3-MP**	Nd	Nd	Nd	Nd	Nd	Nd	Nd	Nd	Nd	Nd
	2-MP	Nd	Nd	Nd	Nd	Nd	Nd	Nd	Nd	Nd	Nd
	2-MA	Nd	Nd	Nd	Nd	Nd	Nd	Nd	Nd	Nd	Nd
	9/4-MA	Nd	Nd	Nd	Nd	Nd	Nd	Nd	Nd	Nd	Nd
	1-MA	Nd	Nd	Nd	Nd	Nd	Nd	Nd	Nd	Nd	Nd
206	**P2**	Nd	Nd	Nd	Nd	Nd	x	Nd	x	Nd	Nd
212	**C2-DBT**	Nd	Nd	Nd	Nd	Nd	Nd	Nd	x	Nd	Nd
226	**C3-DBT**	Nd	Nd	Nd	Nd	Nd	Nd	Nd	x	Nd	x
242	**C1C**	Nd	x	Nd	x	x	x	x	x	x	Nd
256	**C2C**	Nd	x	Nd	Nd	x	x	x	x	x	Nd

Nd: Not detected or very low abundance; x: Detected

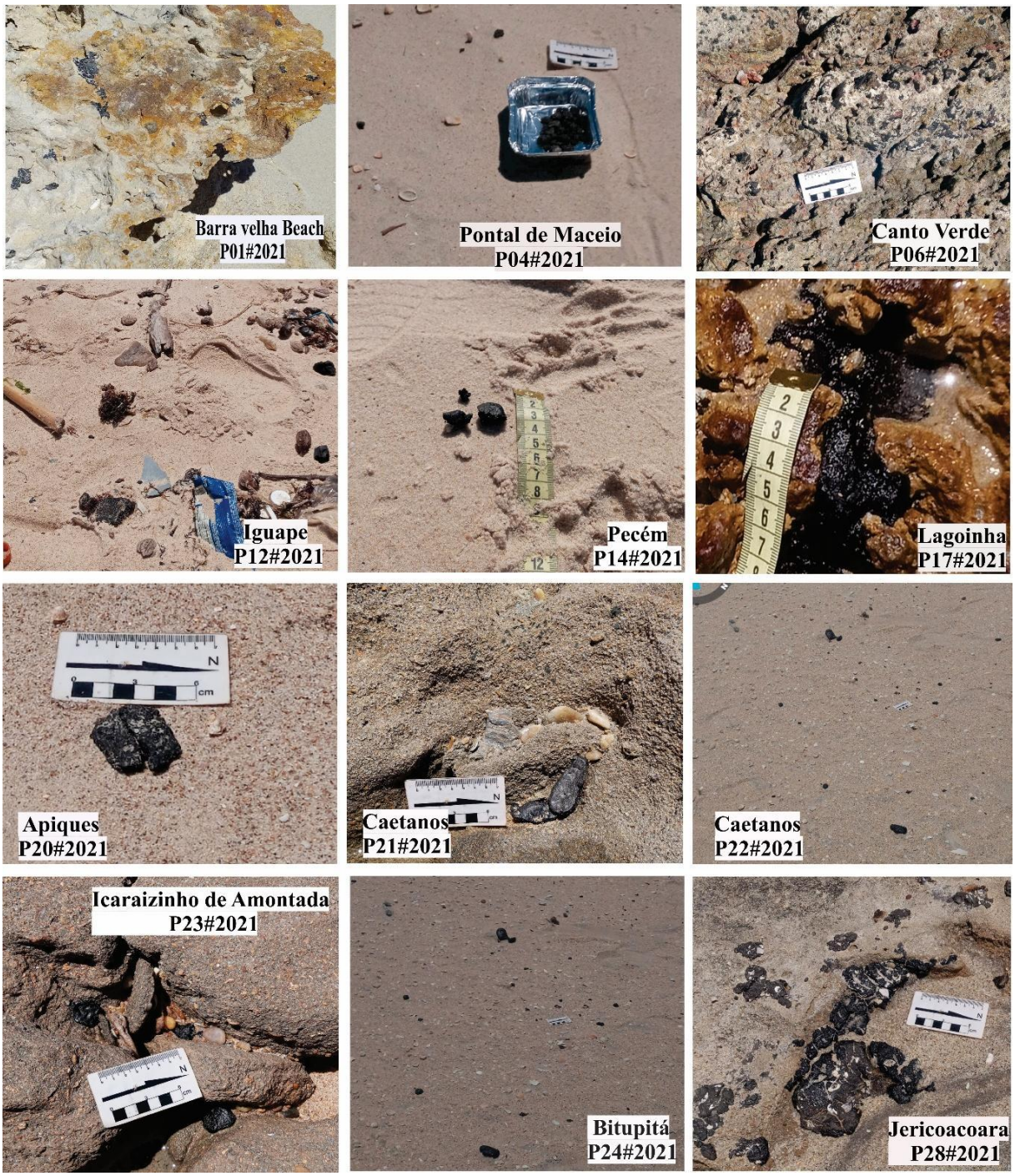

Figure S1. Pictures of oil residue samples right before being collected during the 2021 survey over the coast of the State of Ceará, Northeastern Brazil.

Figure S2. Pictures of oil residue samples right before being collected during the 2022 survey over the coast of the State of Ceará, Northeastern Brazil.

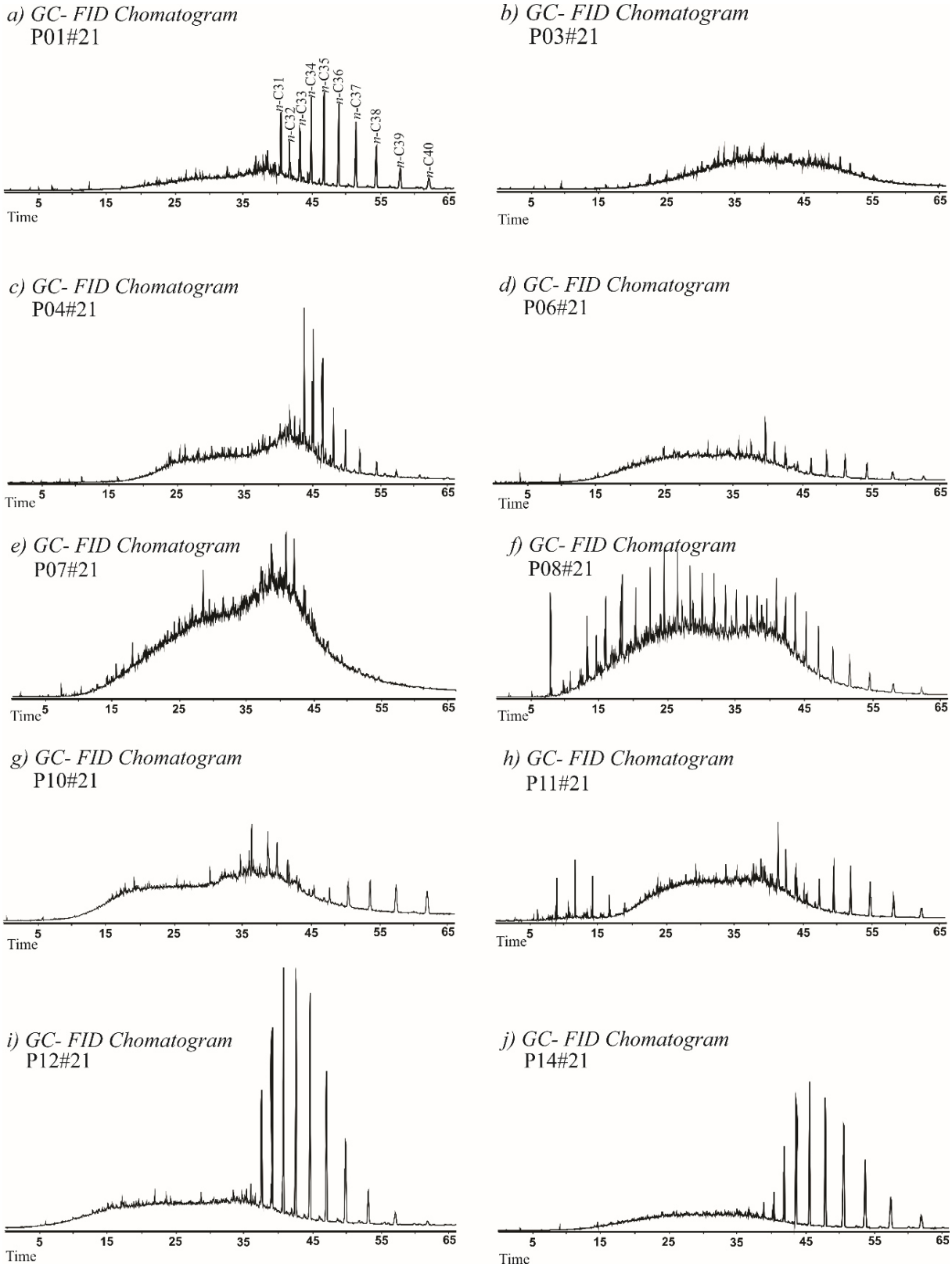

Figure S3 (Part 1). GC-FID chromatograms for the petroleum residue samples collected over the state of Ceará, Northeastern Brazil, during the 2021 survey.

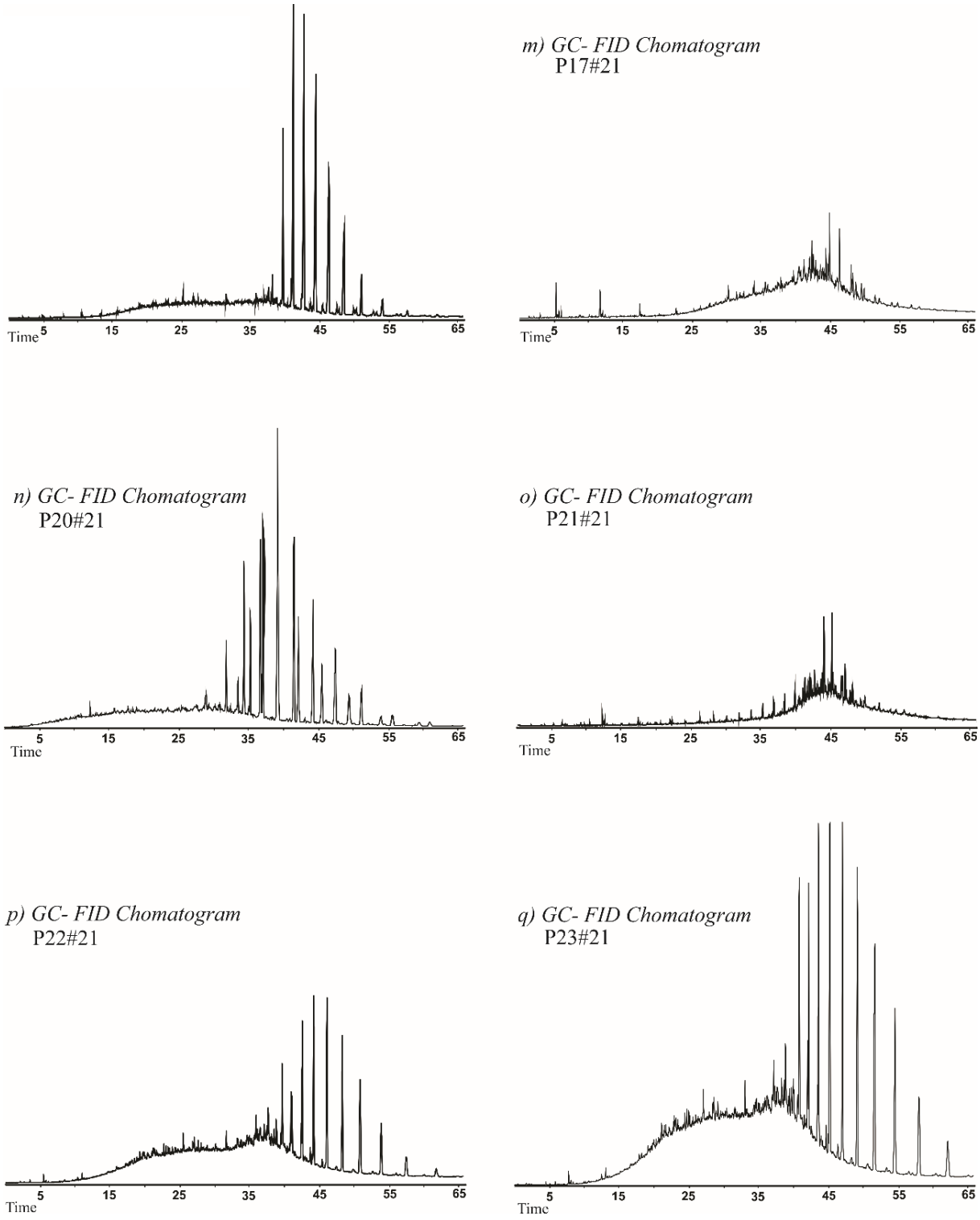

Figure S3 (Part 2). GC-FID chromatograms for the petroleum residue samples collected over the state of Ceará, Northeastern Brazil, during the 2021 survey.

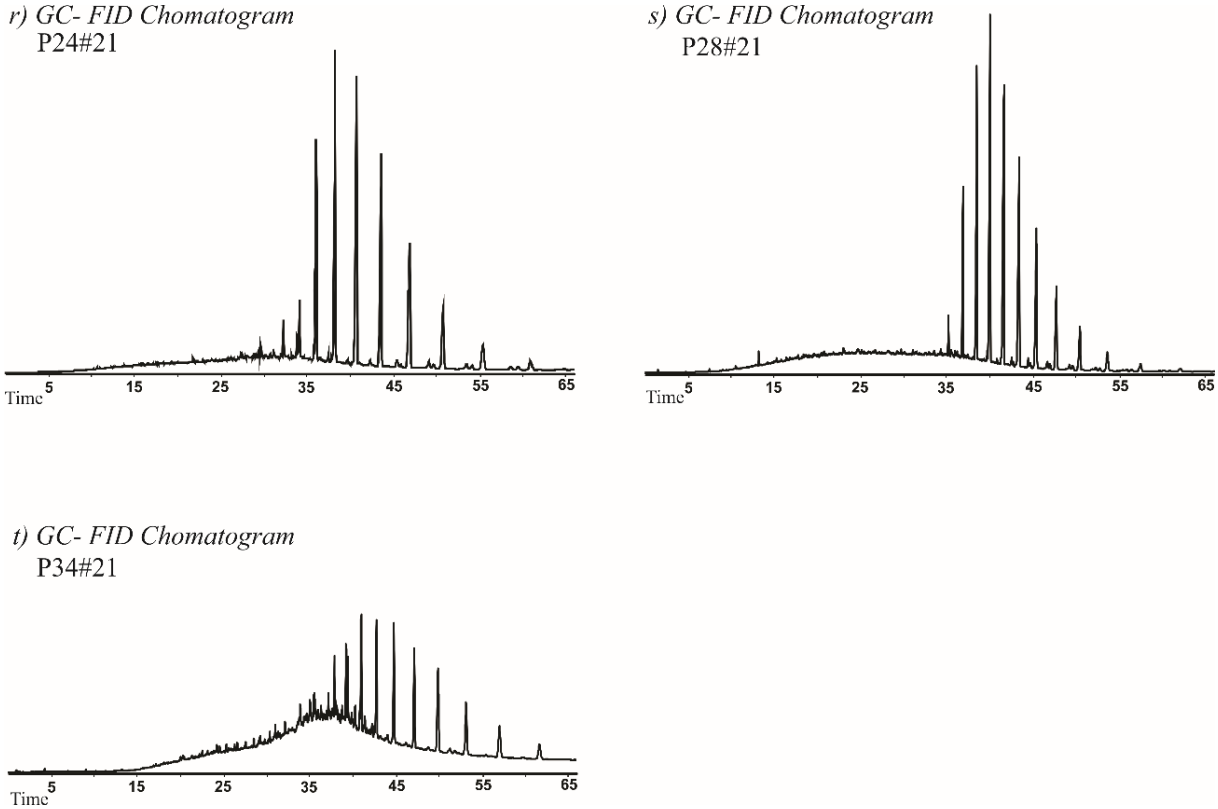

Figure S3 (Part 3). GC-FID chromatograms for the petroleum residue samples collected over the state of Ceará, Northeastern Brazil, during the 2021 survey.

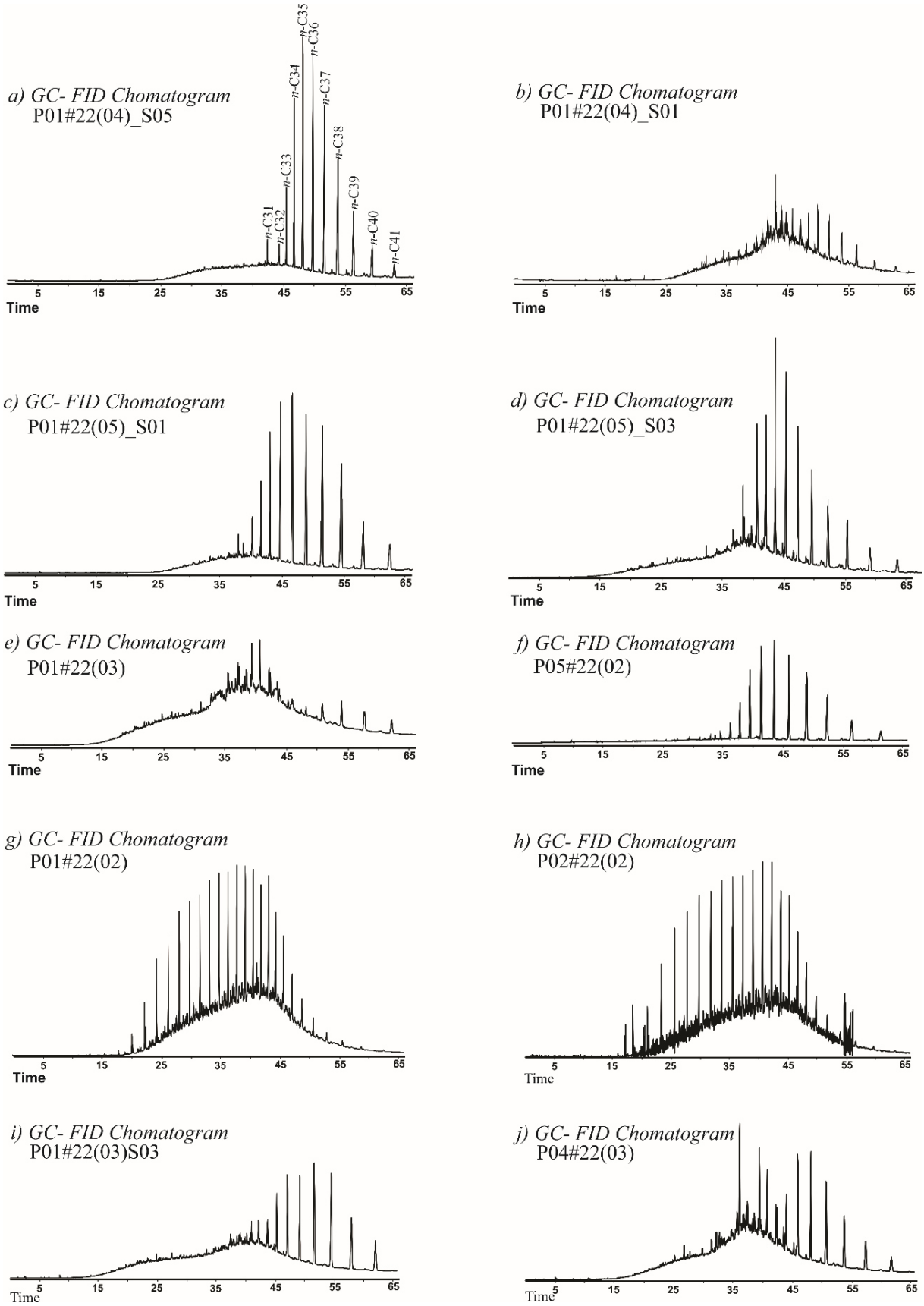

Figure S4 (Part 1). GC-FID chromatograms for the petroleum residue samples collected over the state of Ceará, Northeastern Brazil, during the 2022 survey.

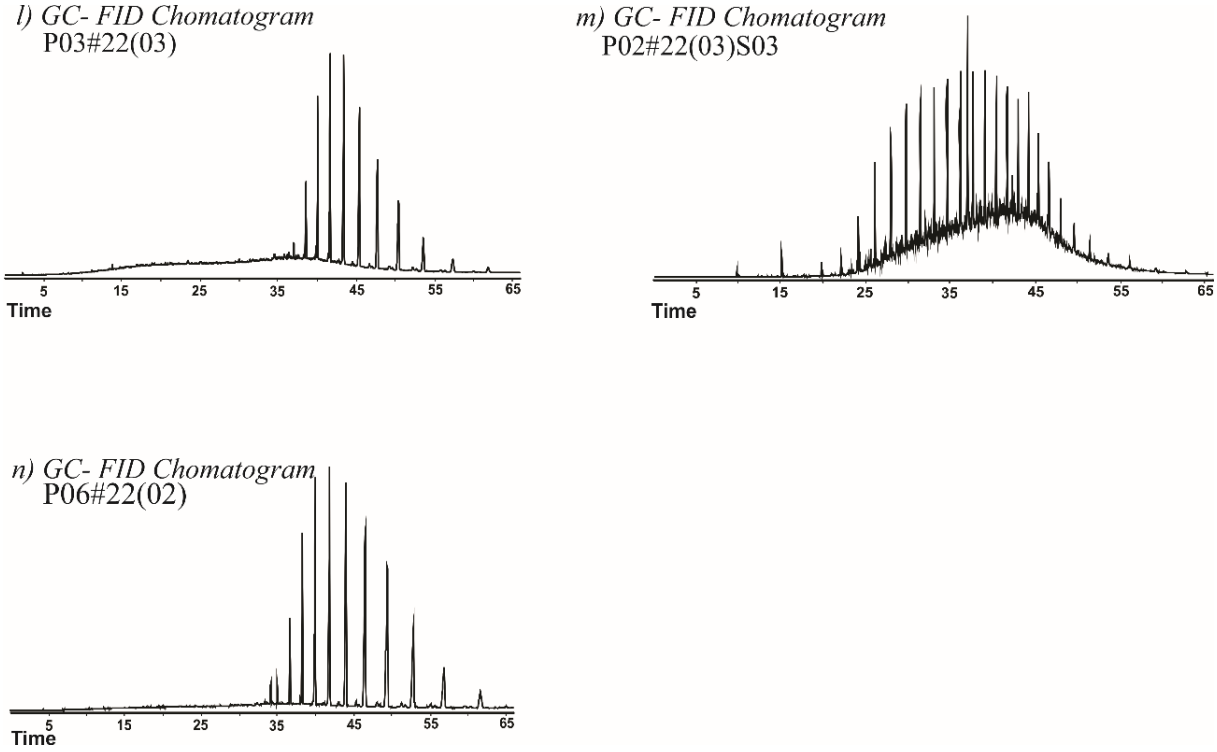

Figure S4 (Part 2). GC-FID chromatograms for the petroleum residue samples collected over the state of Ceará, Northeastern Brazil, during the 2022 survey.

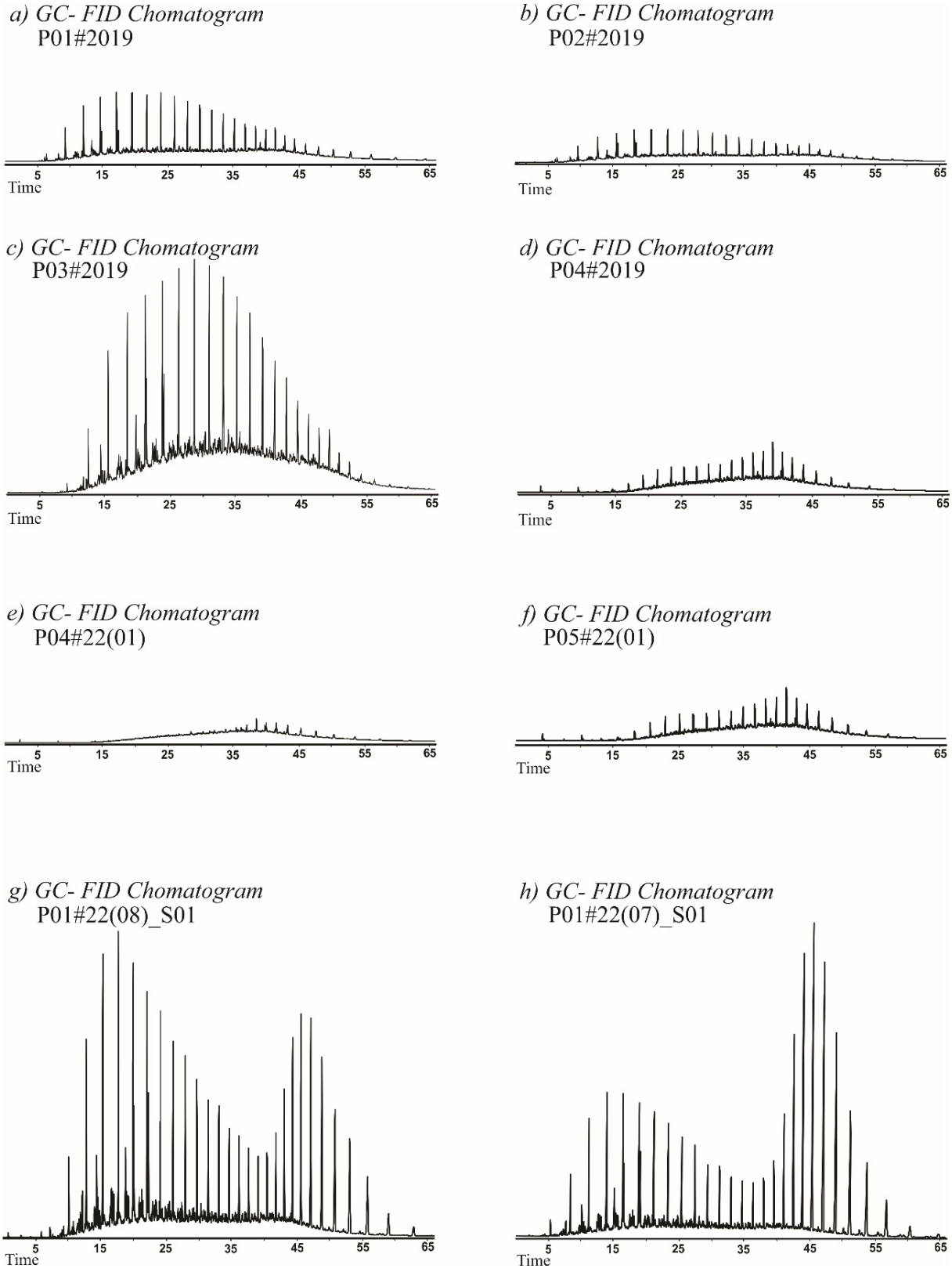

Figure S5. GC-FID chromatograms for the spilled oil samples collected from the state of Ceará coast, Northeastern Brazil, related to the 2019, 2022.1 and 2022.2 events.

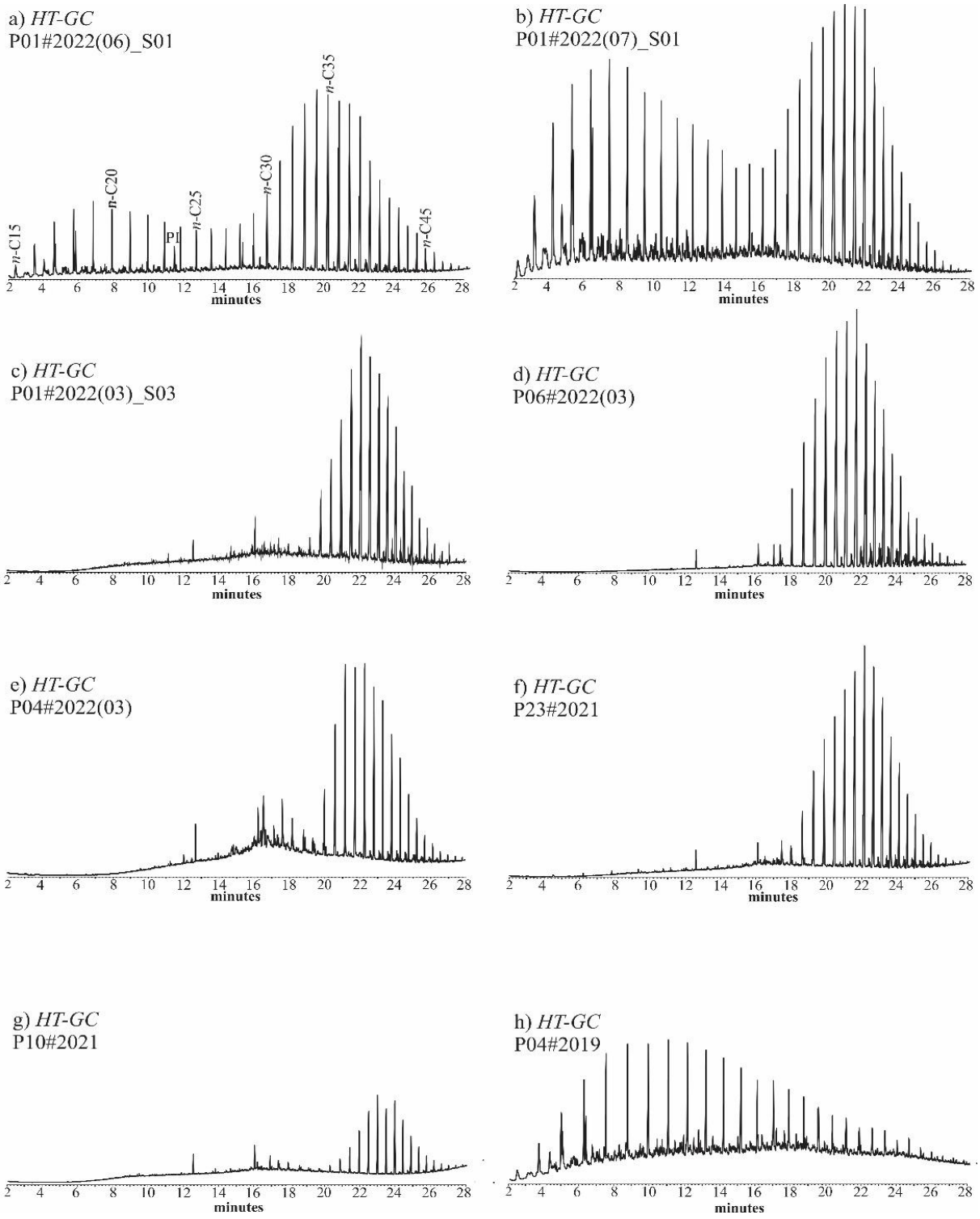

Figure S6. HT-GC chromatograms of the samples monitoring of the 2021, 2022 and events of the 2022.2 and 2019.

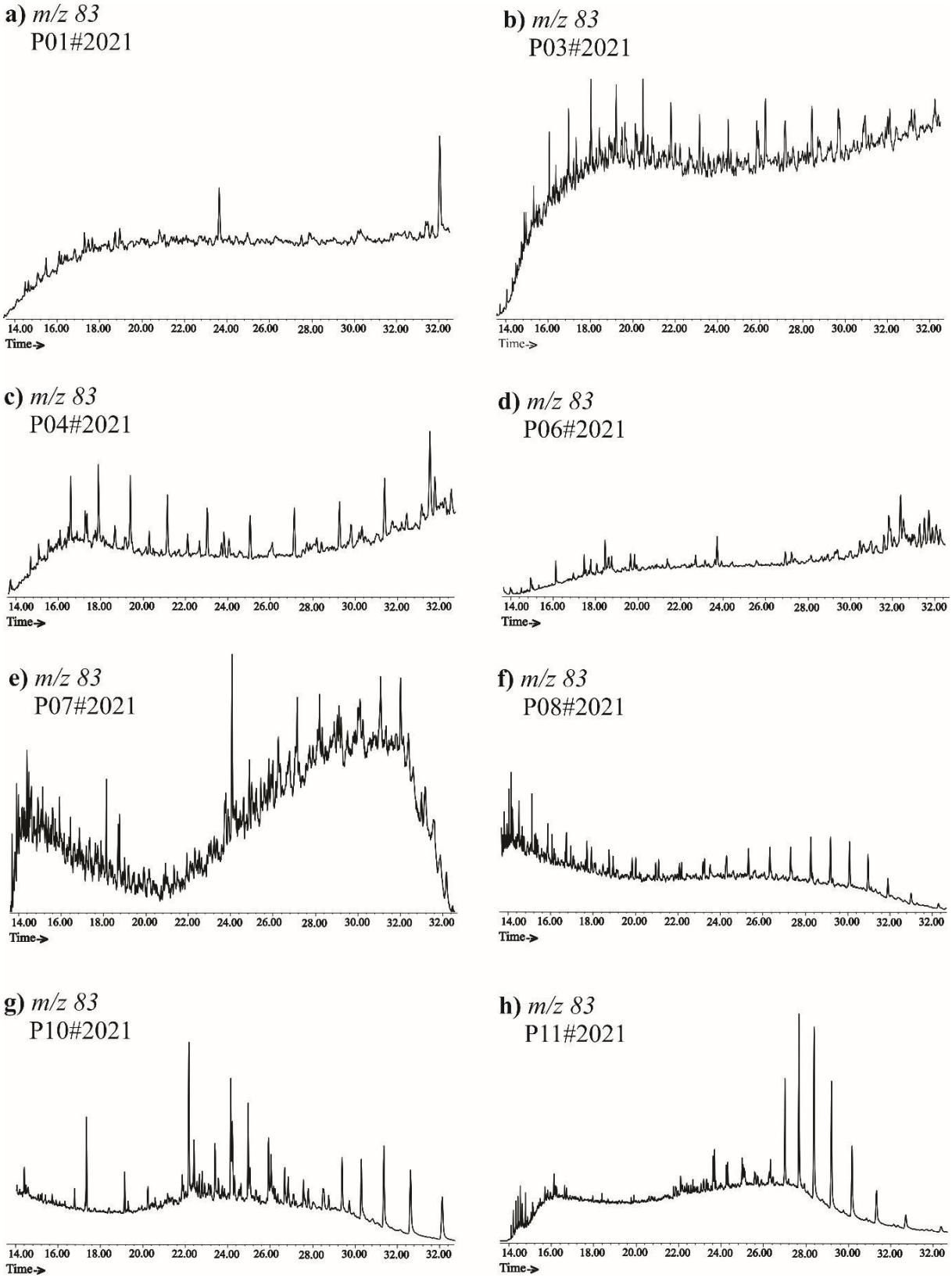

Figure S7 (Part 1). GC-MS chromatograms *m/z* 83 for the *n*-alkylcyclohexanes assessment in the samples collected in the 2021 survey.

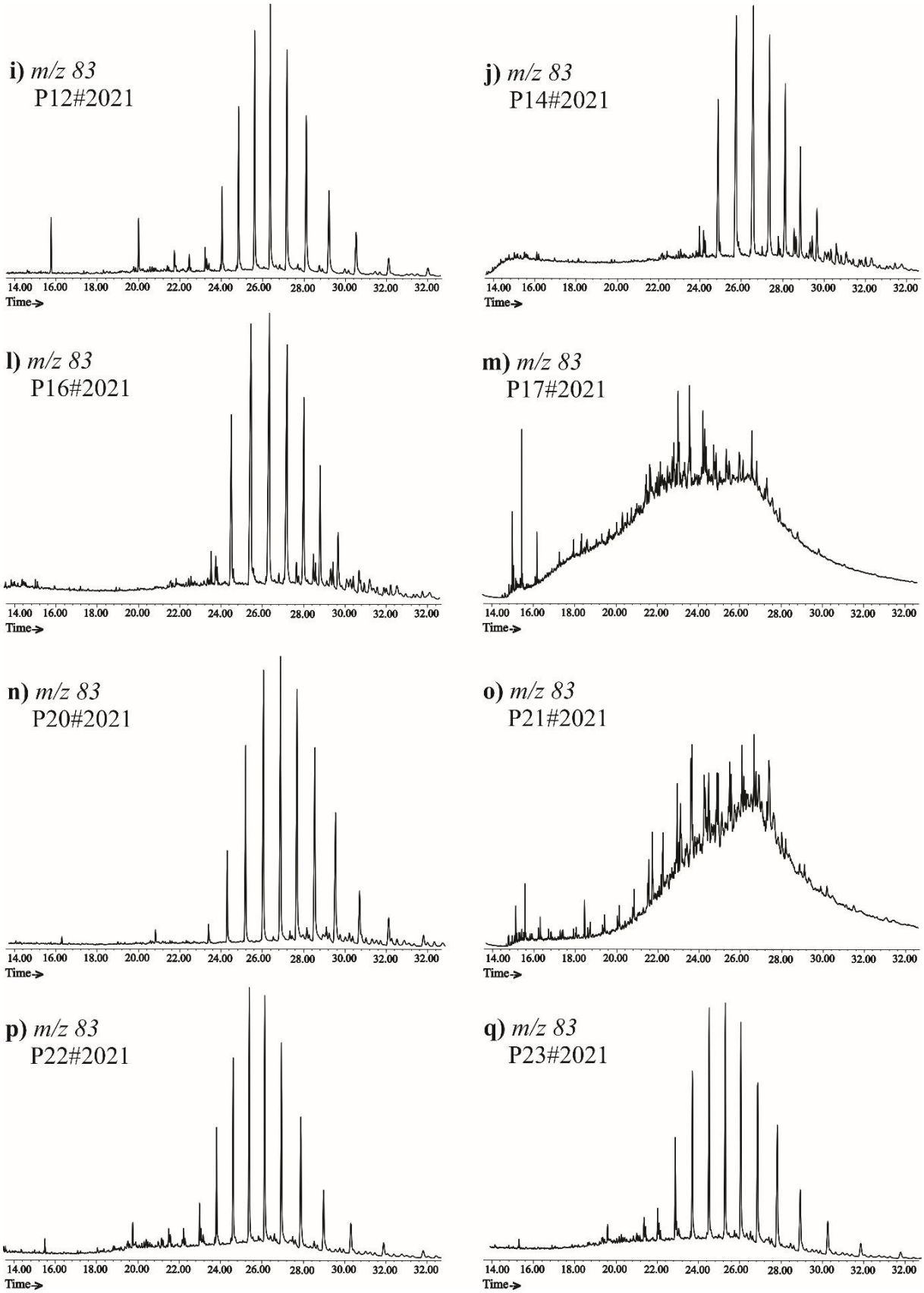

Figure S7 (Part 2). GC-MS chromatograms *m/z* 83 for the *n*-alkylcyclohexanes assessment in the samples collected in the 2021 survey.

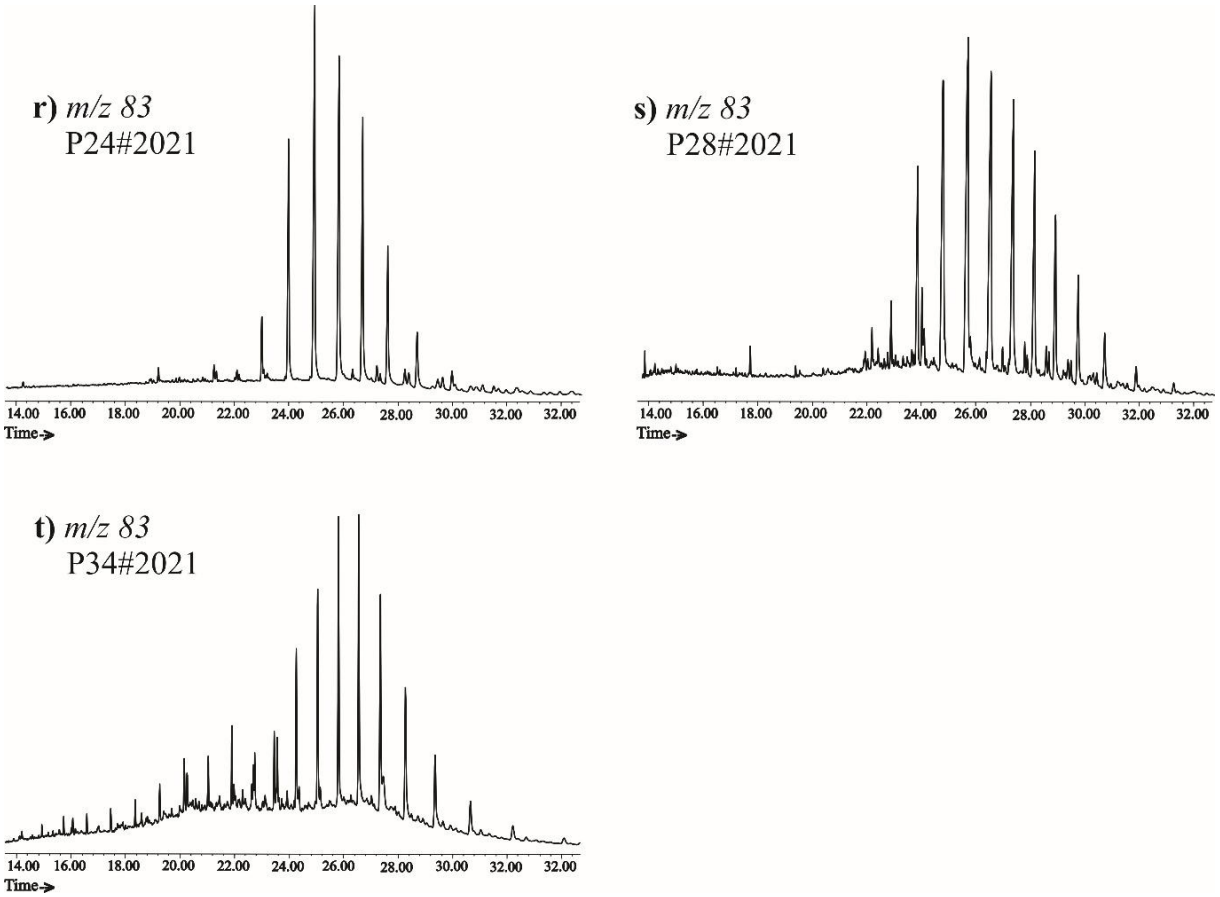

Figure S7 (Part 3). GC-MS chromatograms *m/z* 83 for the *n*-alkylcyclohexanes assessment in the samples collected in the 2021 survey.

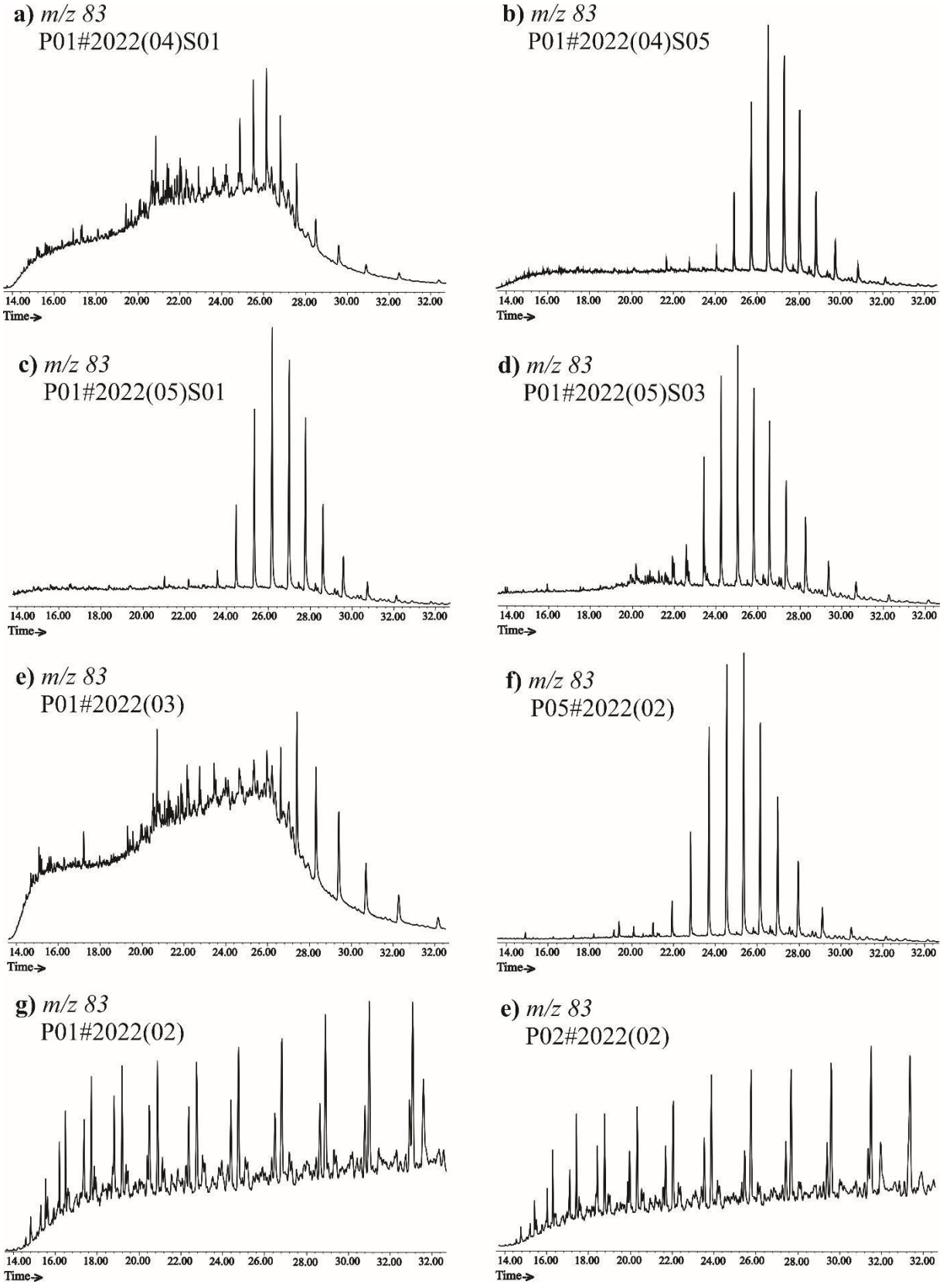

Figure S8 (Part 1). GC-MS chromatograms *m/z* 83 for the *n*-alkylcyclohexanes assessment in the samples collected in the 2022 survey.

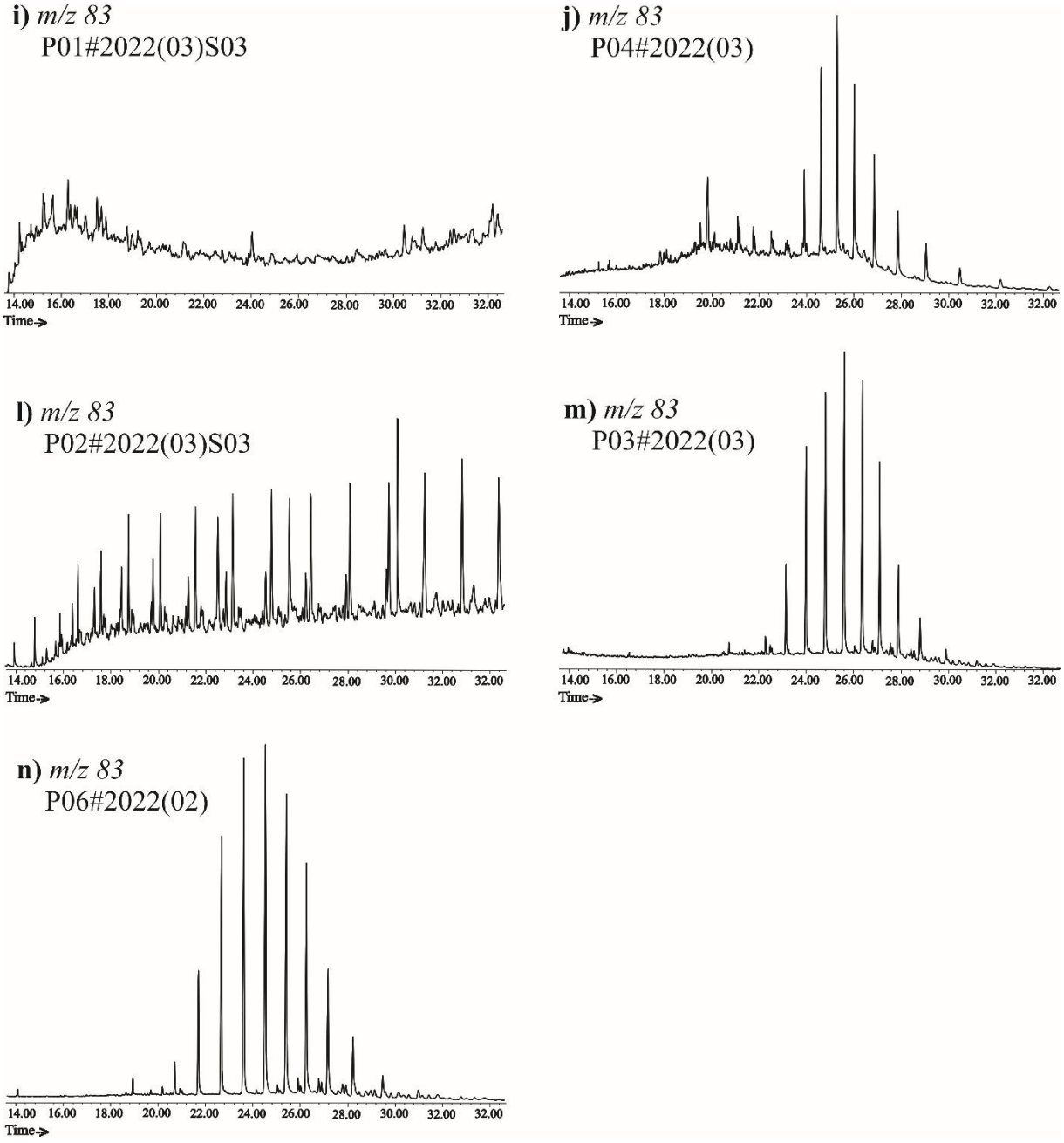

Figure S8 (Part 2). GC-MS chromatograms *m/z* 83 for the *n*-alkylcyclohexanes assessment in the samples collected in the 2022 survey.

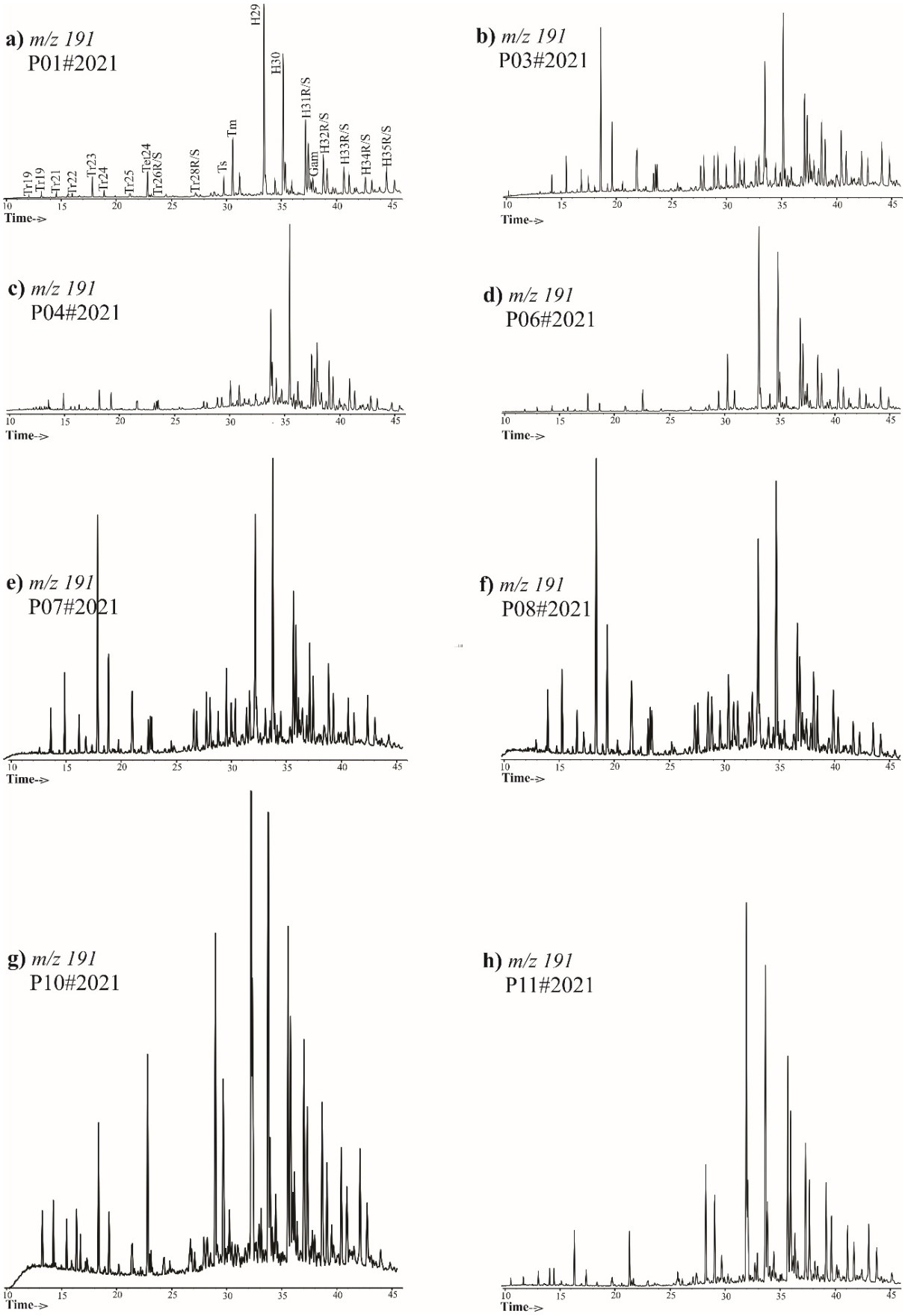

Figure S9 (Part 1). GC-MS chromatograms *m/z* 191 of the samples collected in the 2021 survey.

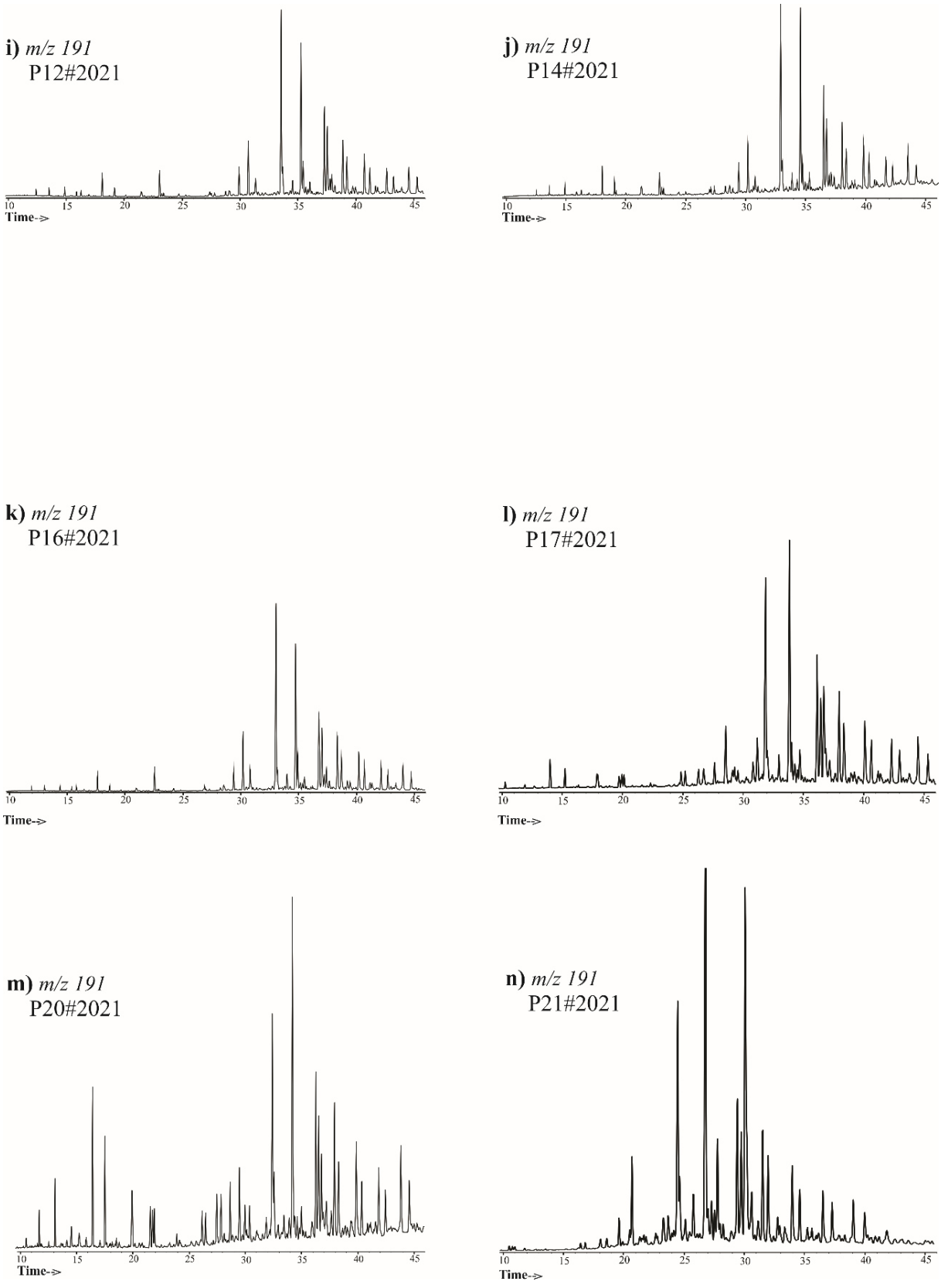

Figure S9 (Part 2). GC-MS chromatograms *m/z* 191 of the samples collected in the 2021 survey.

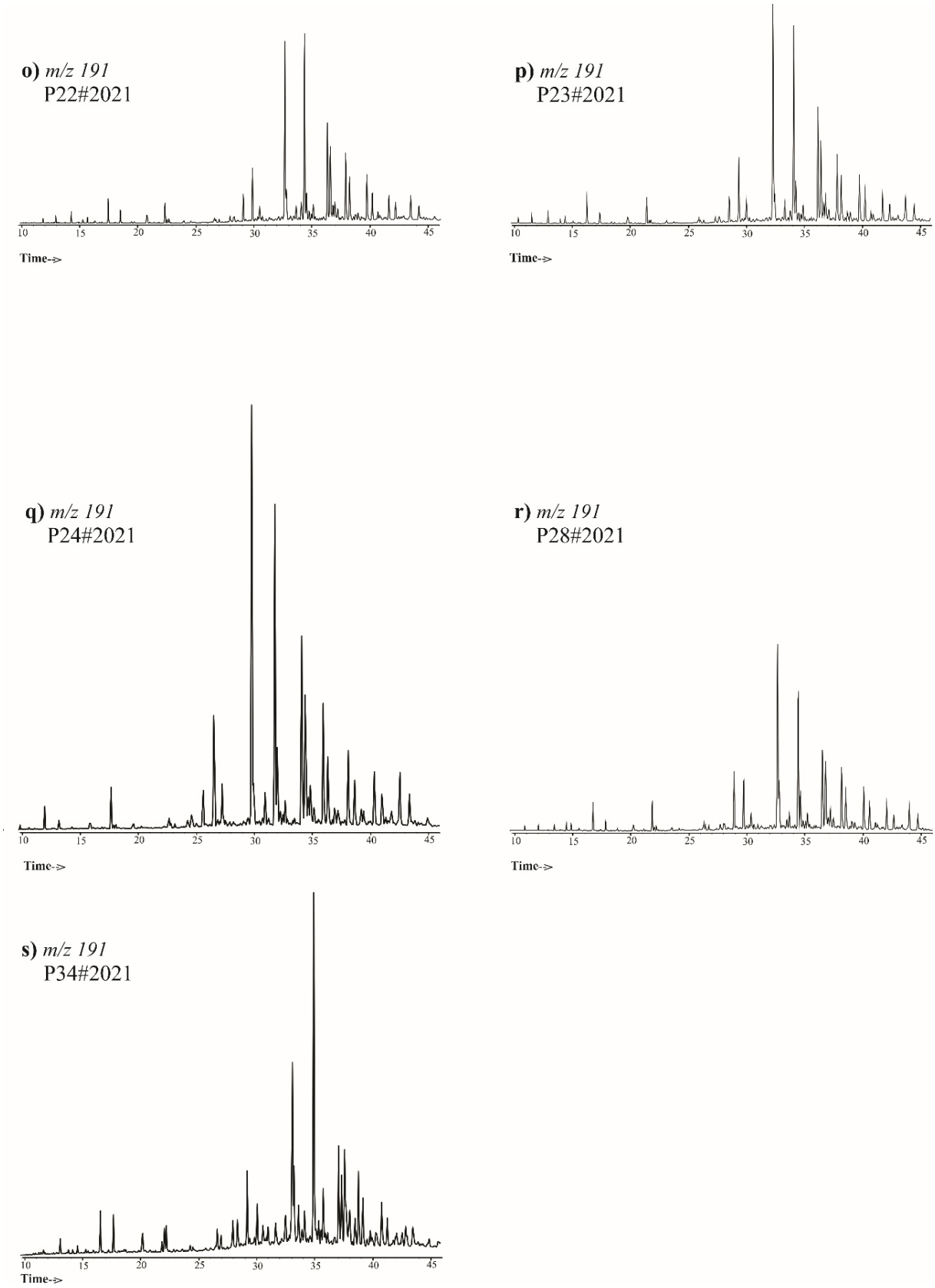

Figure S9 (Part 3). GC-MS chromatograms *m/z* 191 of the samples collected in the 2021 survey.

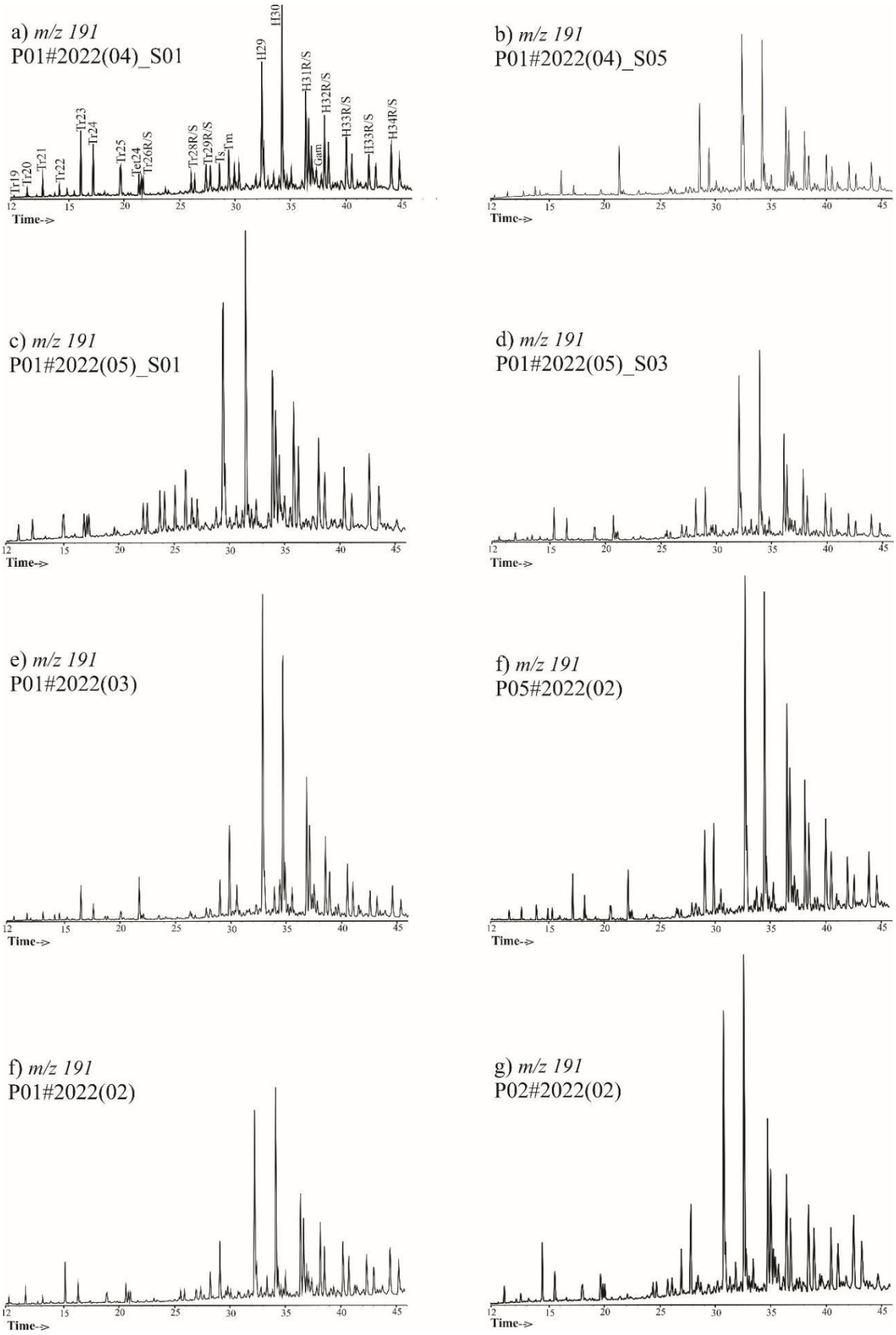

Figure S10 (Part. 1). GC-MS chromatograms *m/z* 191 of the samples monitoring of the 2022.

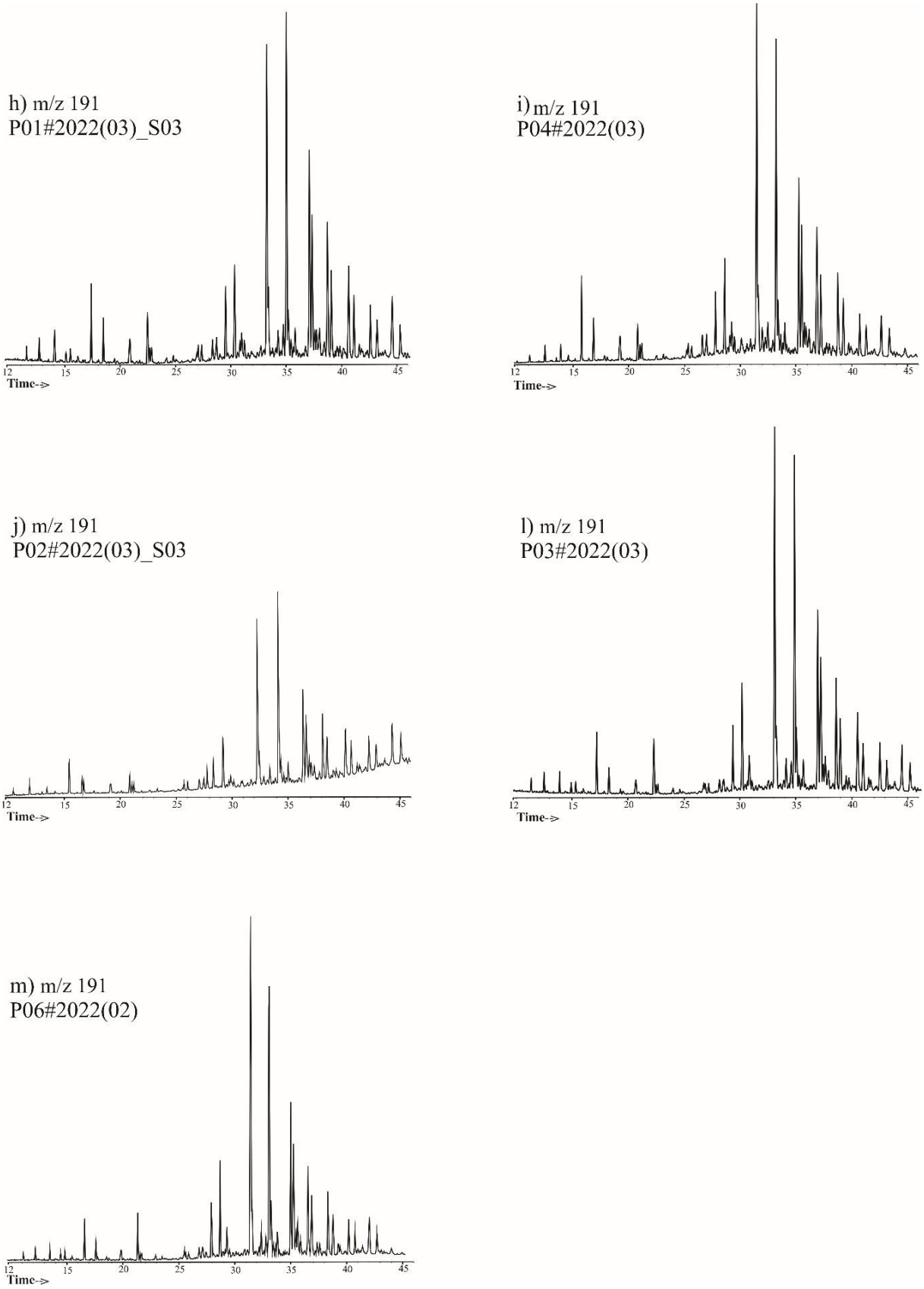

Figure S10 (Part. 2). GC-MS chromatograms *m/z* 191 of the samples monitoring of the 2022.

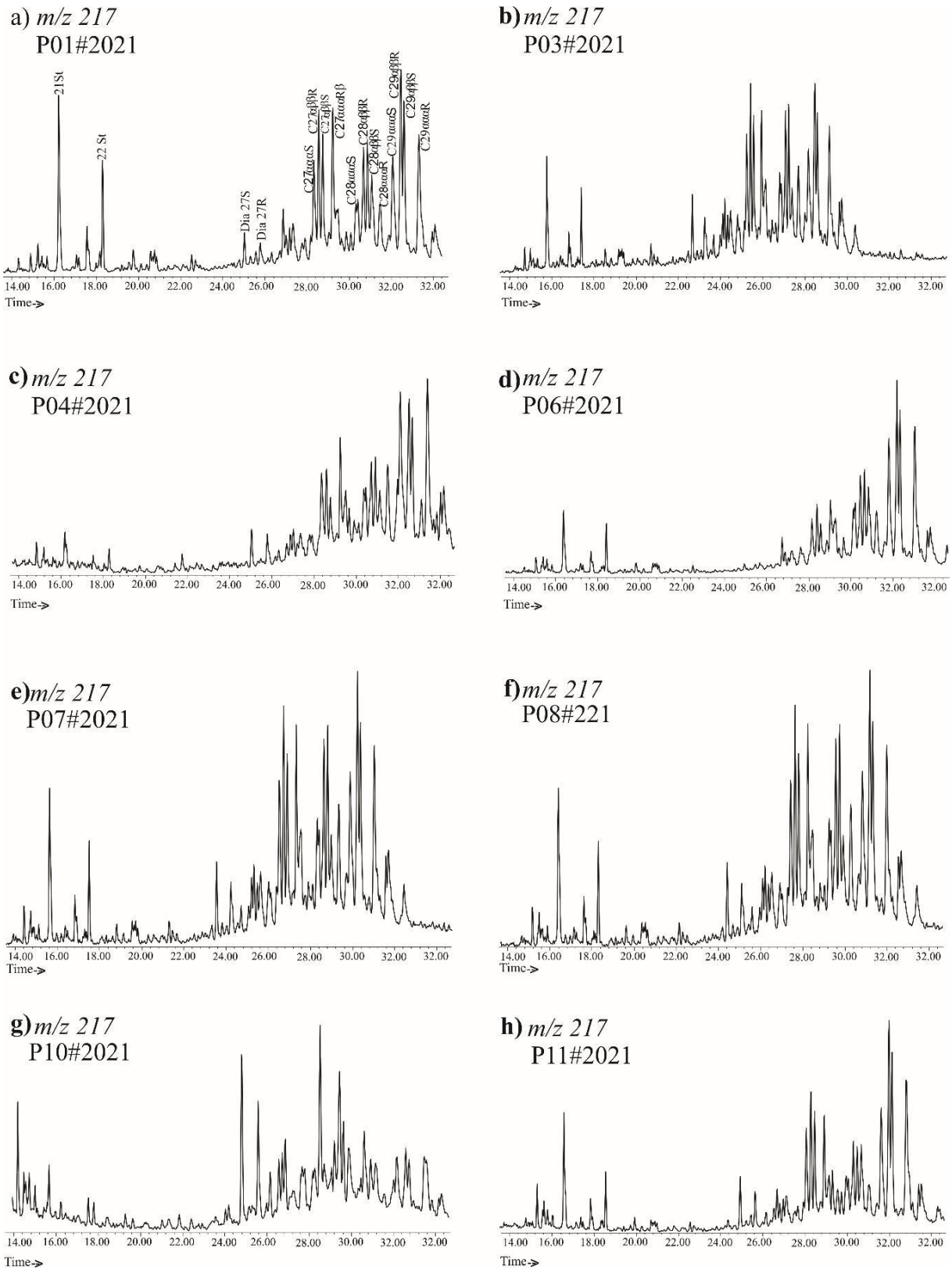

Figure S11 (Part. 1). GC-MS chromatograms *m/z* 217 of the samples monitoring of the 2021.

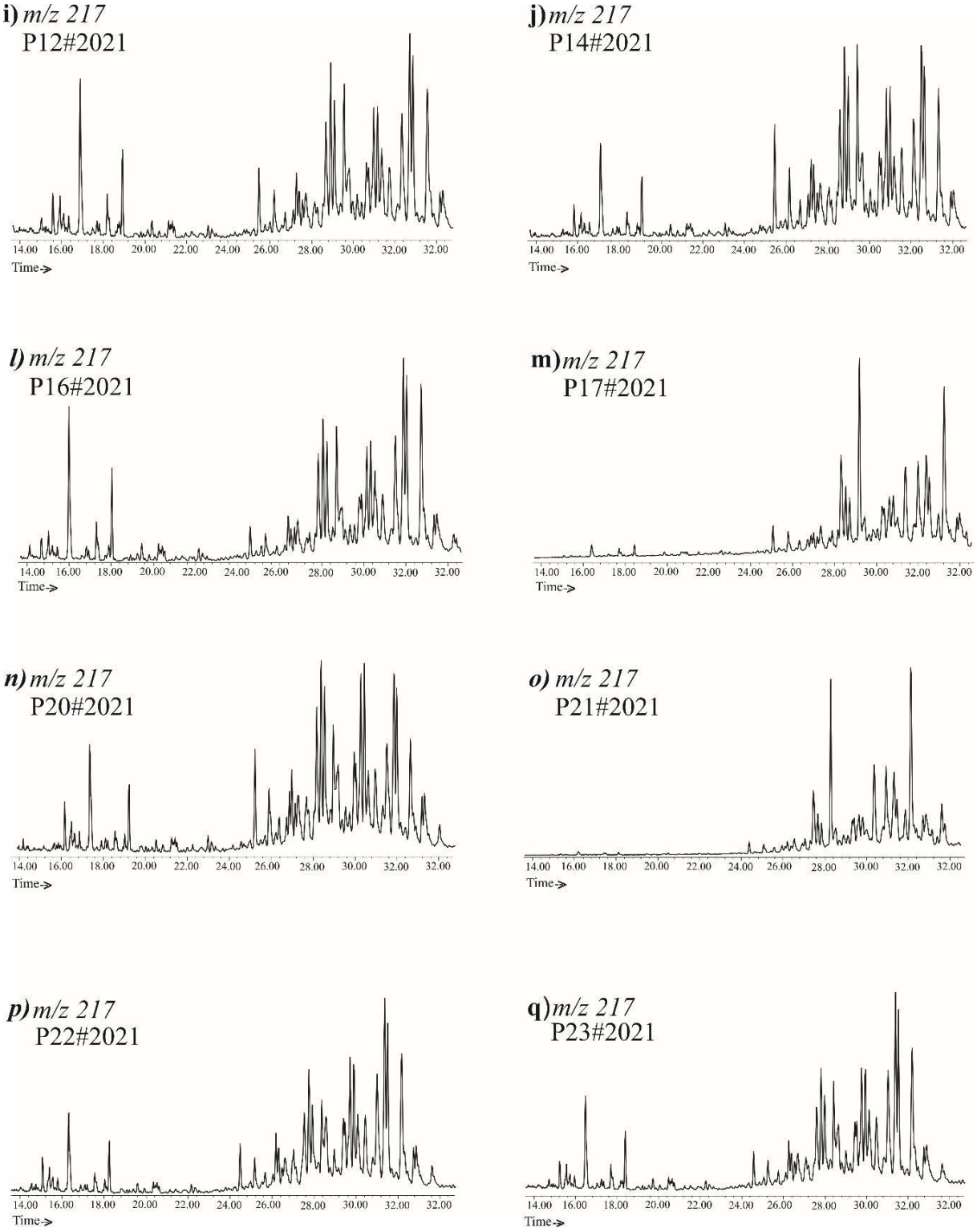

Figure S11 (Part. 2). GC-MS chromatograms *m/z* 217 of the samples monitoring of the 2021.

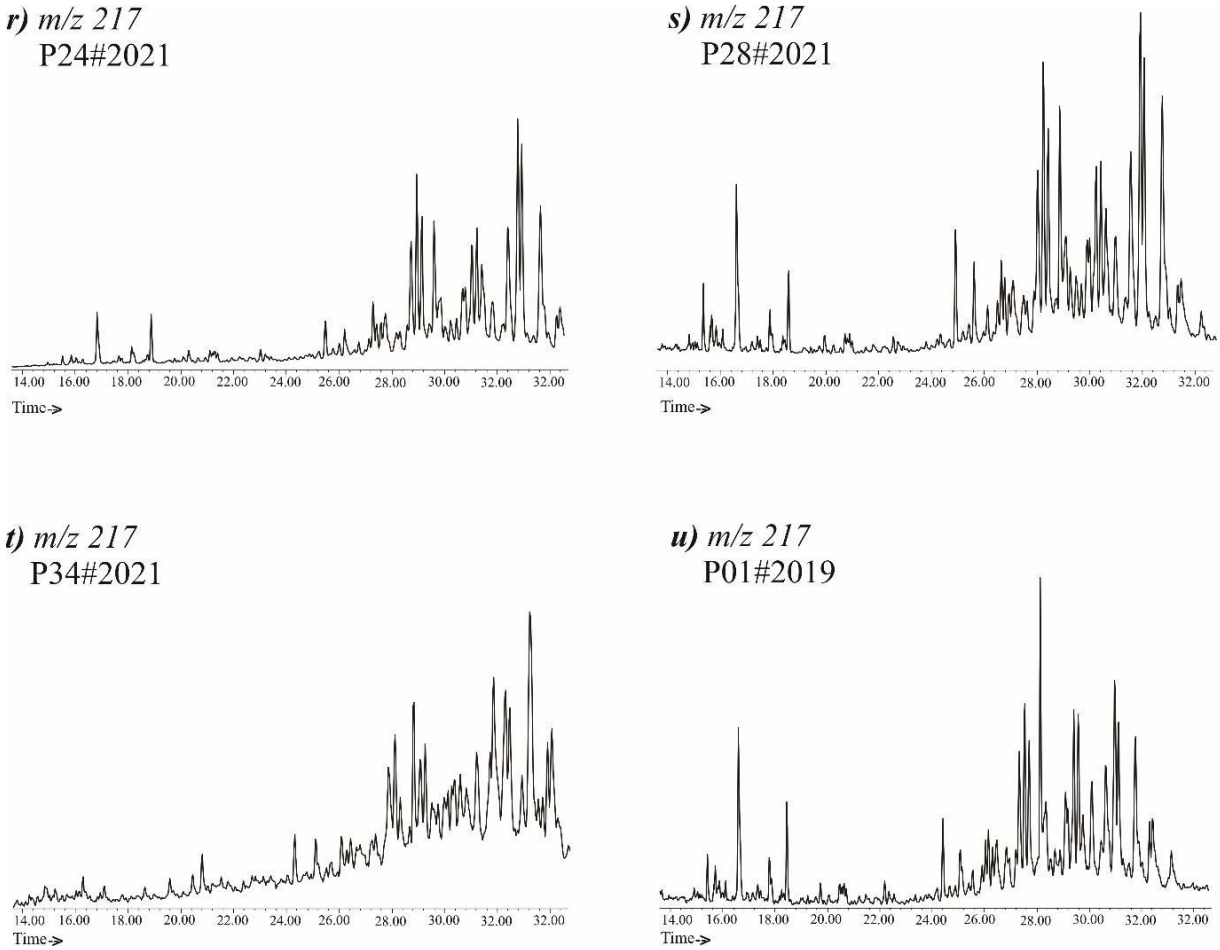

Figure S11(Part. 3). GC-MS chromatograms *m/z* 217 of the samples monitoring of the 2021 and 2019.

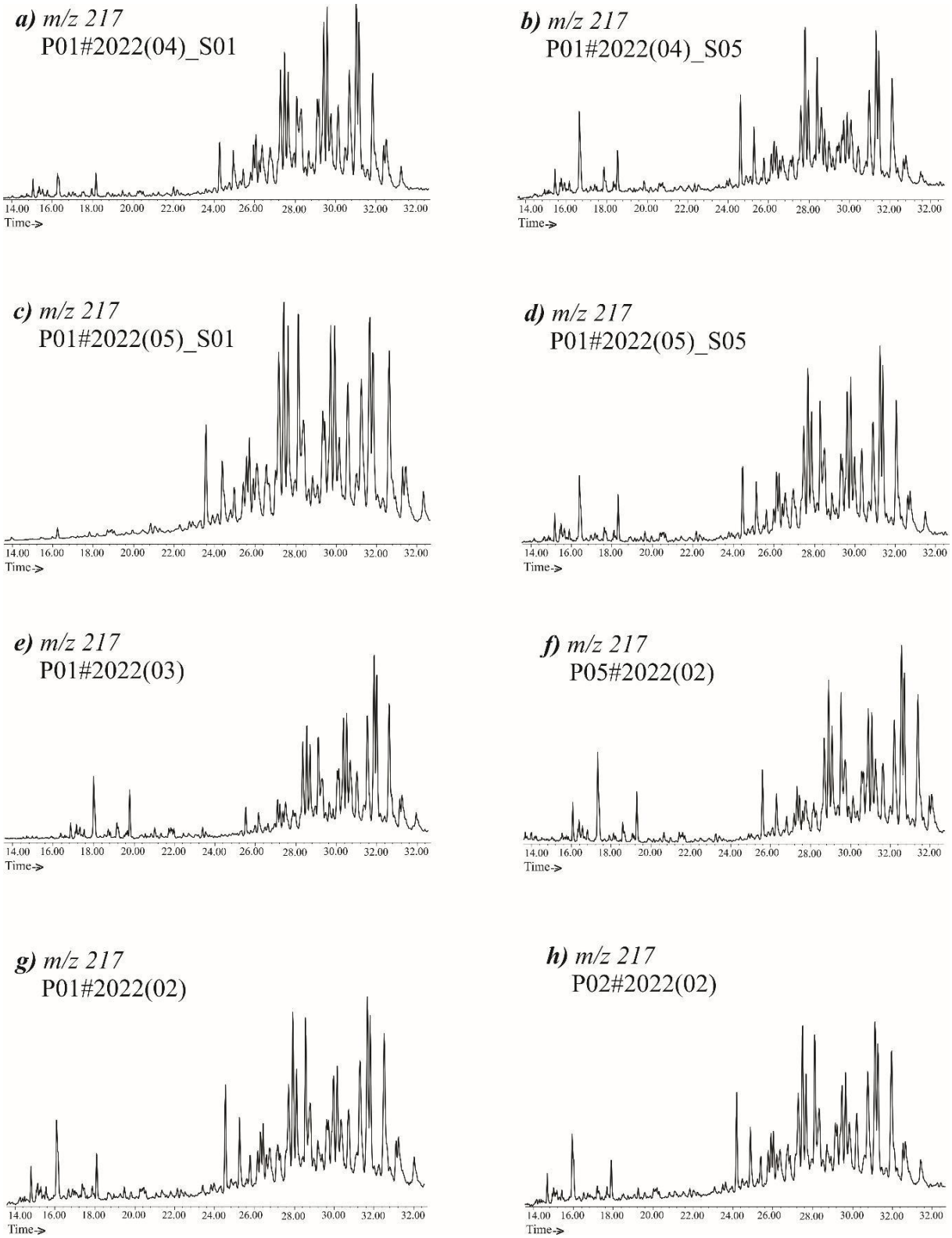

Figure S12 (Part. 1). GC-MS chromatograms *m/z* 217 of the samples monitoring of the 2022.

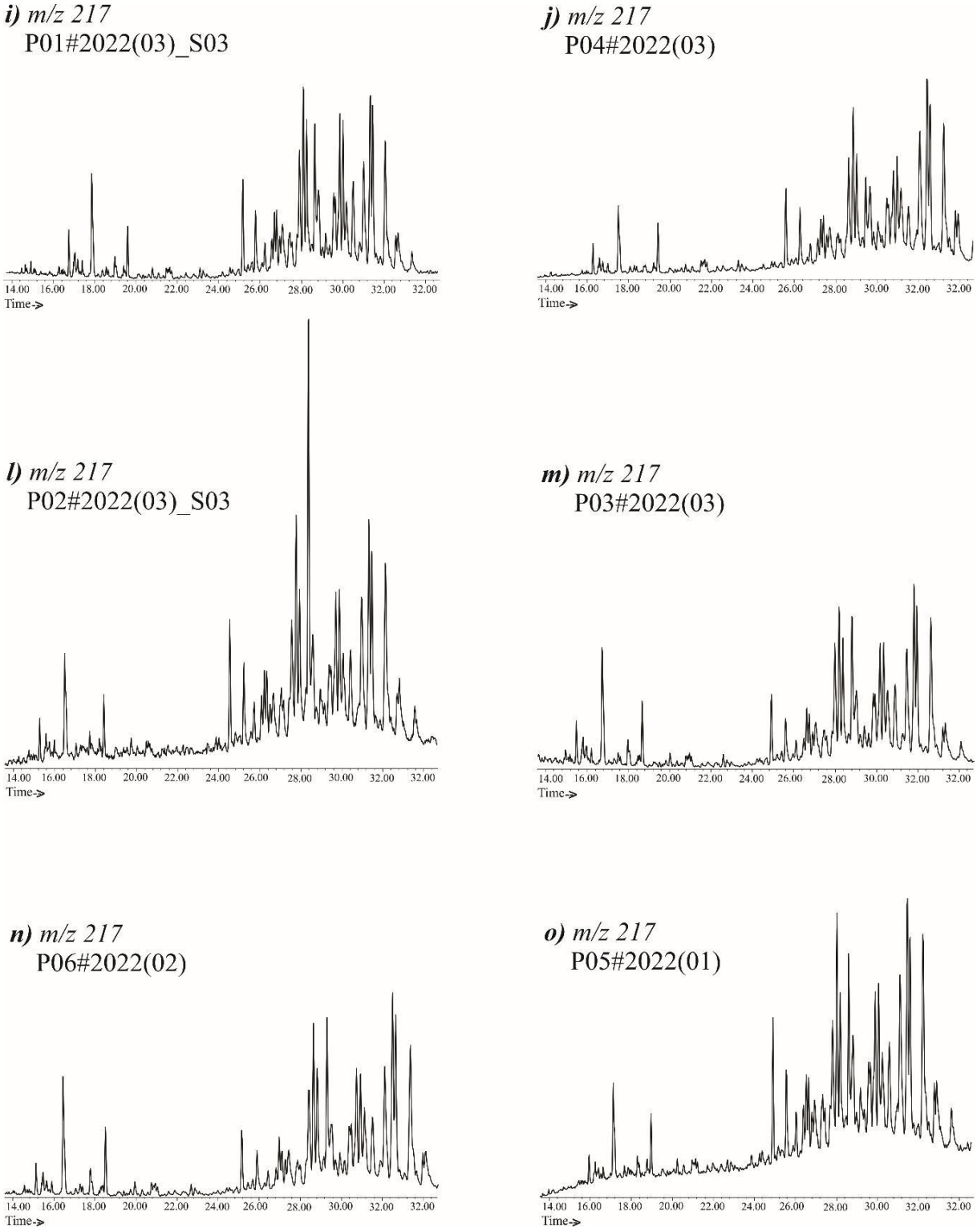

Figure S12 (Part.2). GC-MS chromatograms *m/z* 217 of the samples monitoring of the 2021 and 2022.1.

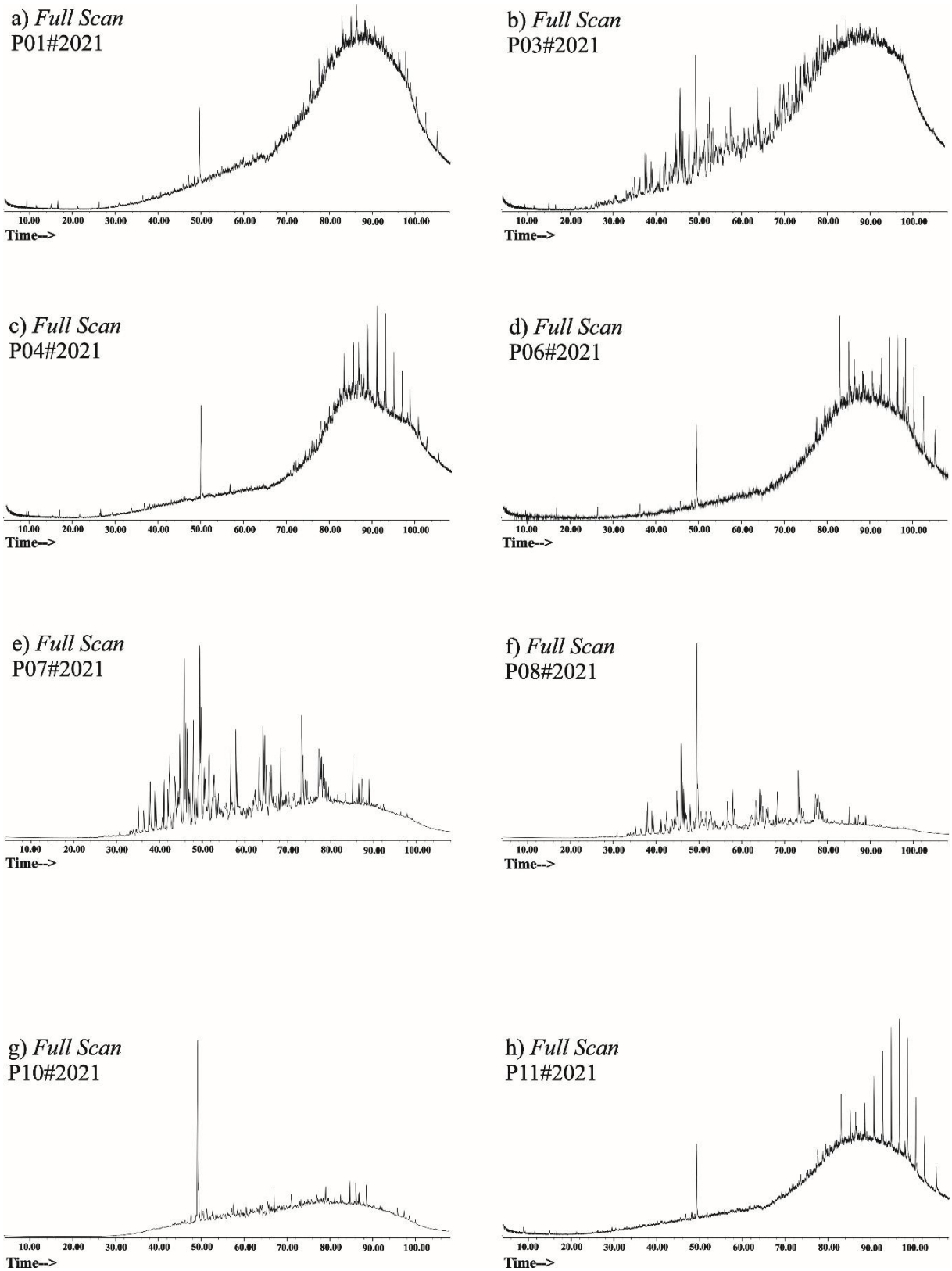

Figure S13 (Part. 1). Total ion current chromatograms (TICC) for the aromatic fraction of the oil residues collected in the 2021 survey.

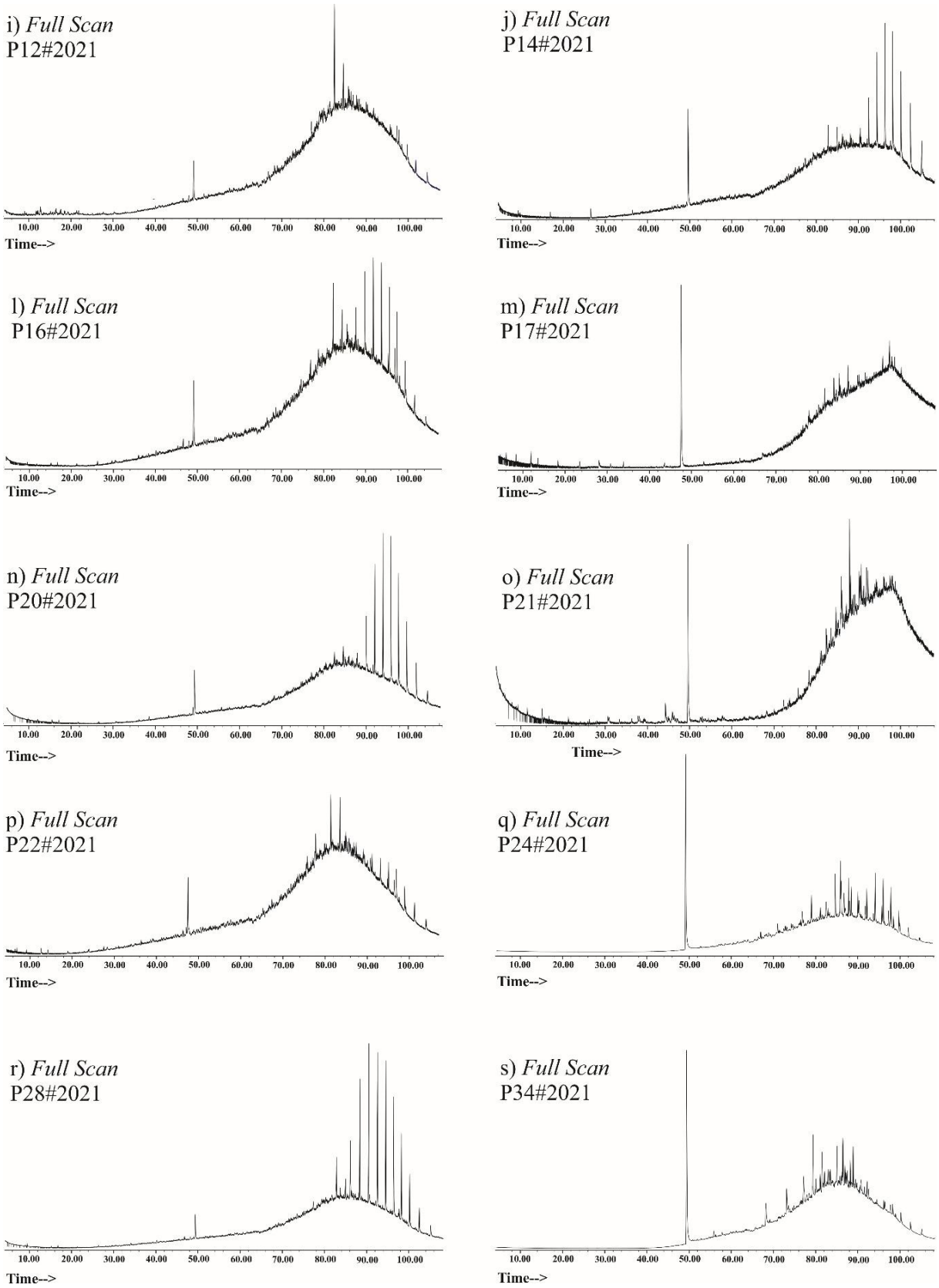

Figure S13 (Part. 2). Total ion current chromatograms (TICC) for the aromatic fraction of the oil residues collected in the 2021 survey.

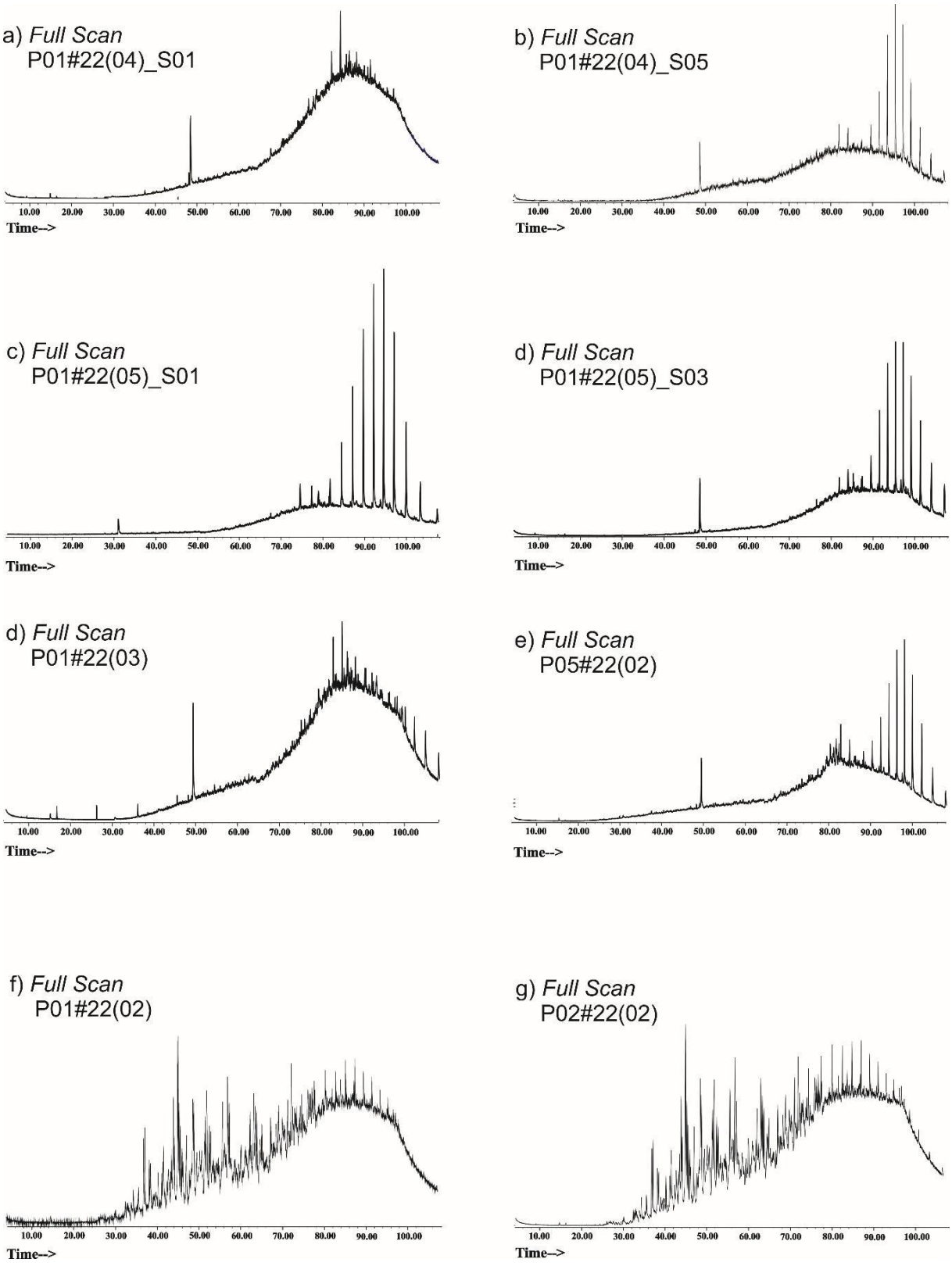

Figure S14 (Part. 1). Total ion current chromatograms (TICC) for the aromatic fraction of the oil residues collected in the 2022 survey.

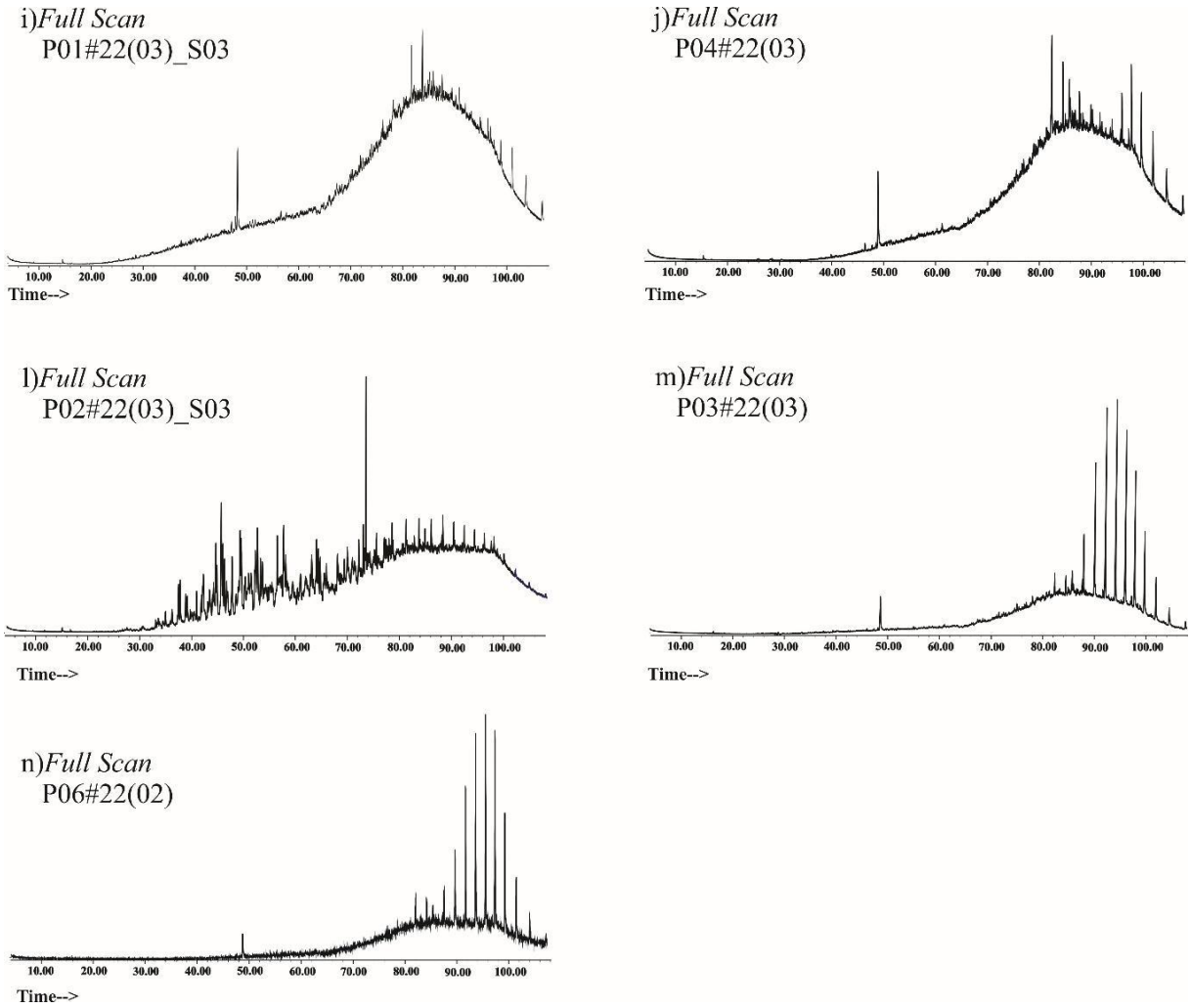

Figure S14 (Part. 2). Total ion current chromatograms (TICC) for the aromatic fraction of the oil residues collected in the 2021 survey.

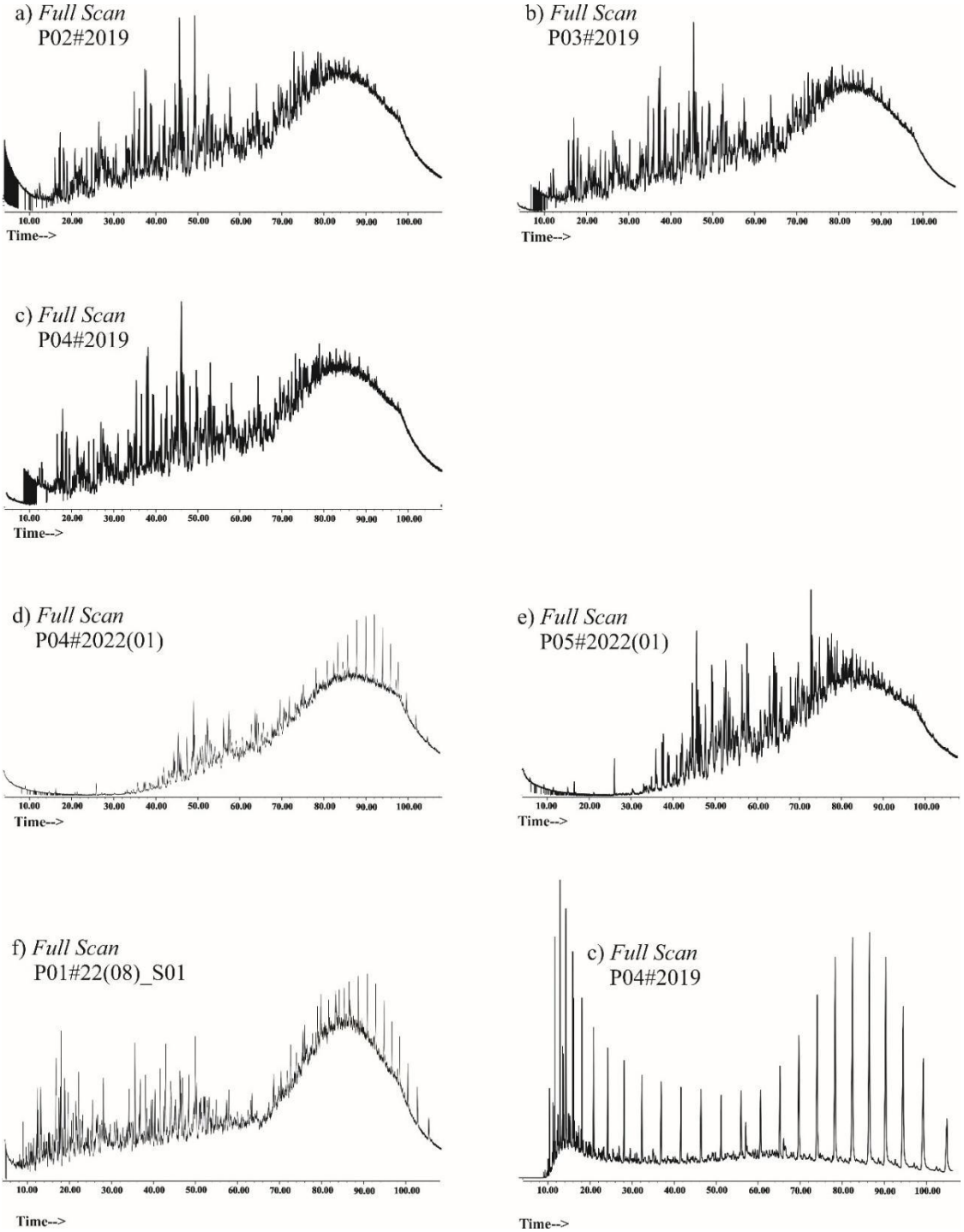

Figure S15. Total ion current chromatograms (TICC) for the events from the years 2019, 2022.1, and 2022.2 survey.

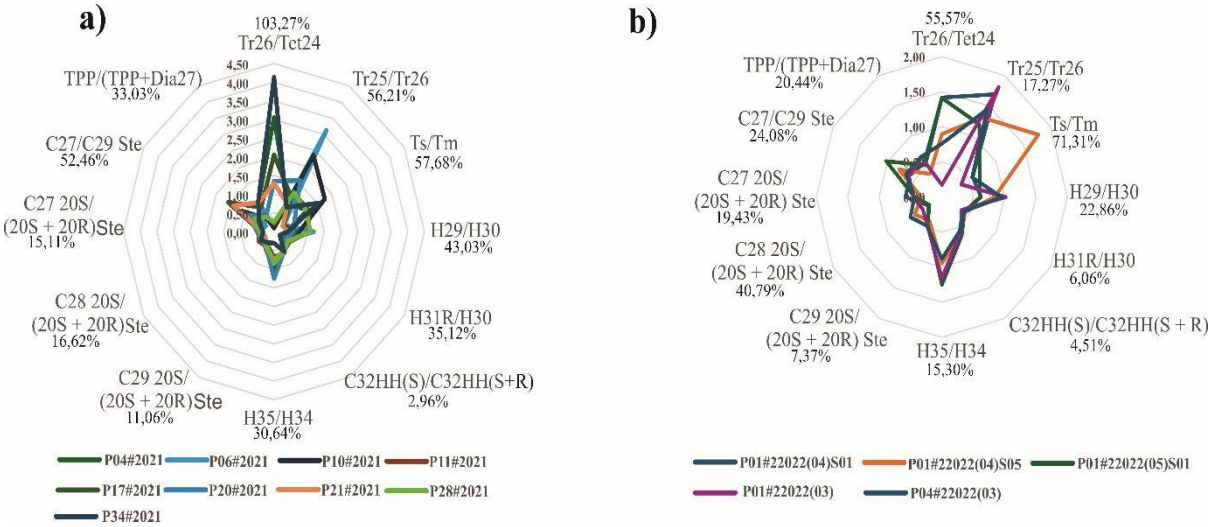

Figure S16. Mass chromatogram *m/z* 191, 217, and 259 obtained from GC-MS analysis, showing the distribution of terpanes and steranes for the 2021 and 2022 survey samples that did not obtain similarity with any sample.

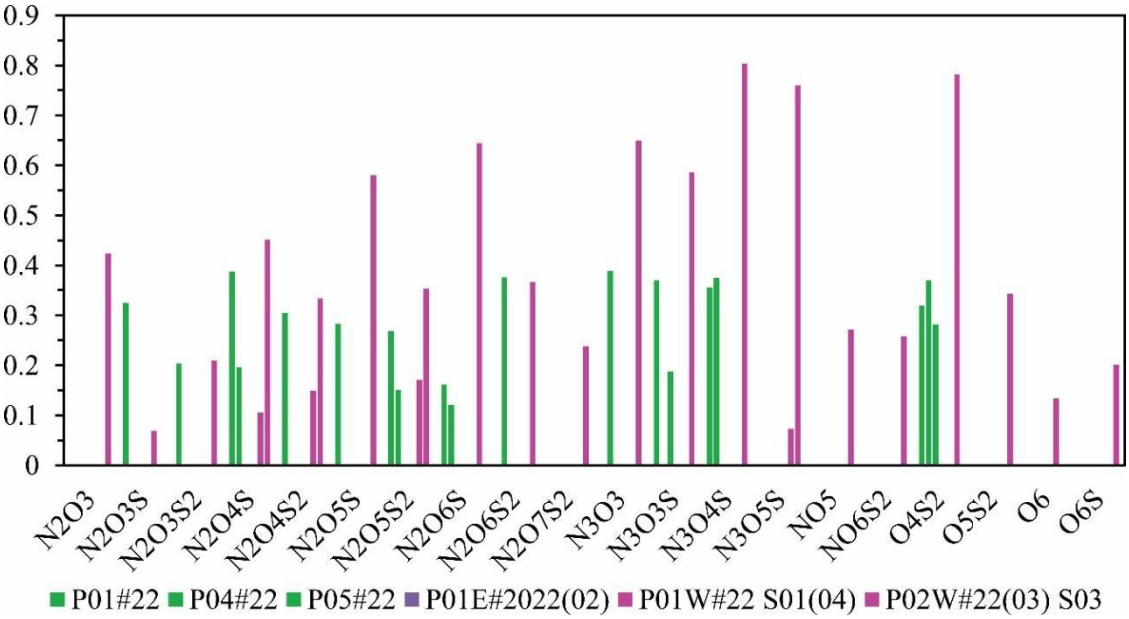

Figure S17. Distribution of heteroatom classes of oil residues monitored in 2021 and 2022 evaluated by ESI(-) FT-ICR MS

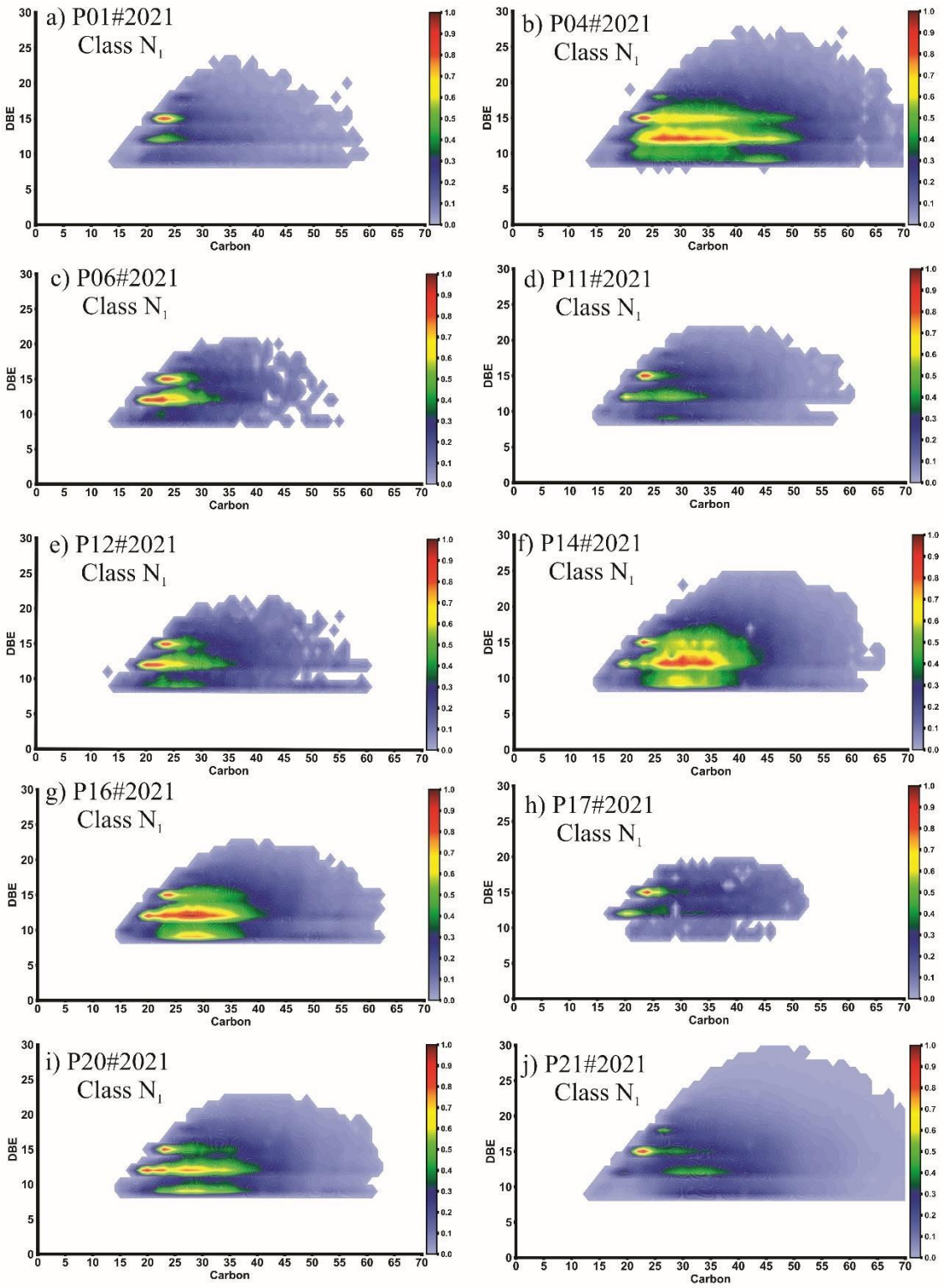

Figure S18 (Part. 1). Isoabundance contoured plots of the double bond equivalent (DBE) vs. carbon number for the N_1 class for the samples monitored in the year 2021.

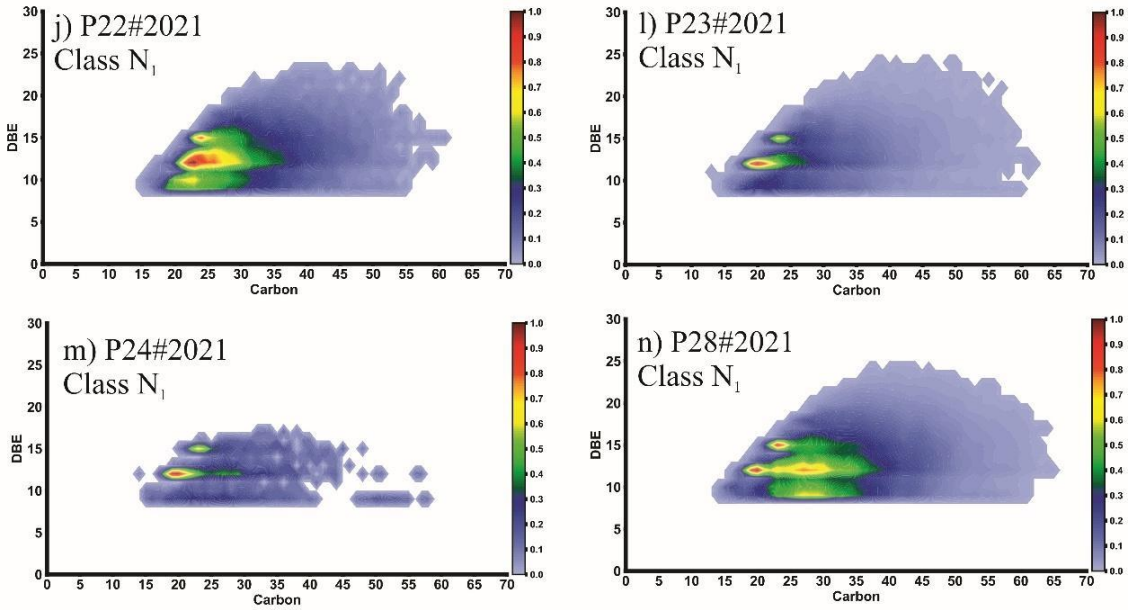

Figure S18 (Part. 2). Isoabundance contoured plots of the double bond equivalent (DBE) vs. carbon number for the N_1 class for the samples monitored in the year 2021.

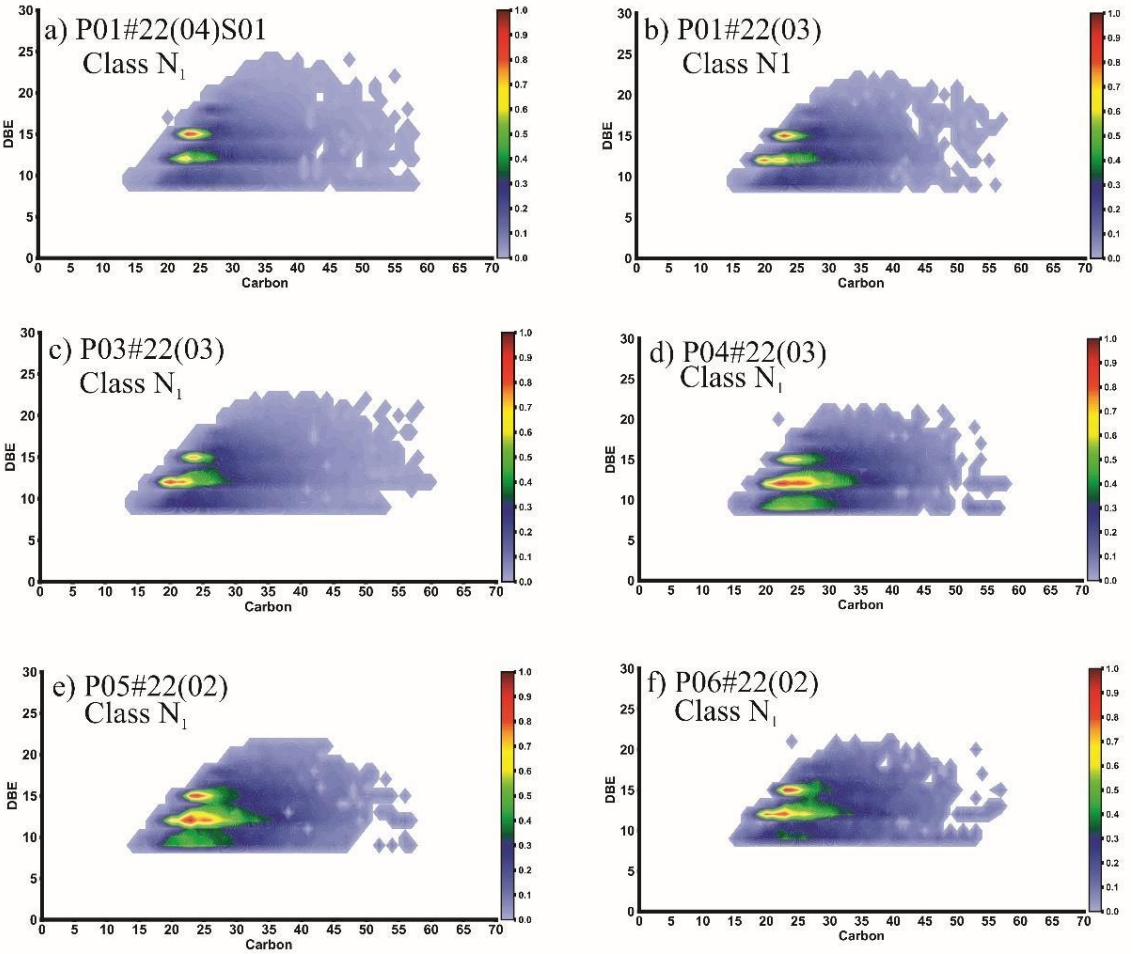

Figure S19 (Part. 1). Isoabundance contoured plots of the double bond equivalent (DBE) vs. carbon number for the N_1 class for the samples monitored in the year 2021.

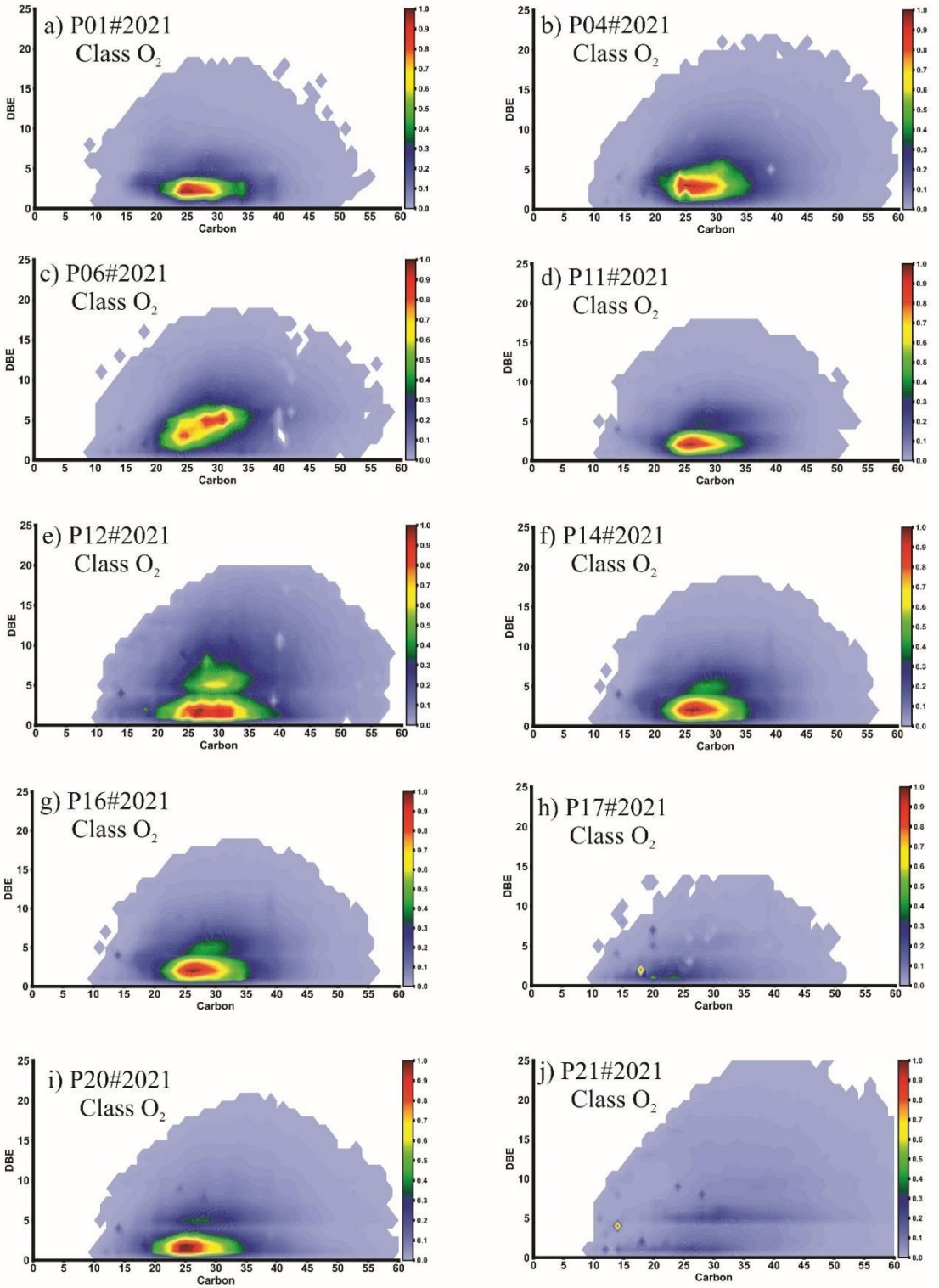

Figure S20 (Part. 1). Isoabundance contoured plots of the double bond equivalent (DBE) vs. carbon number for the O_2 class for the samples monitored in the year 2022.

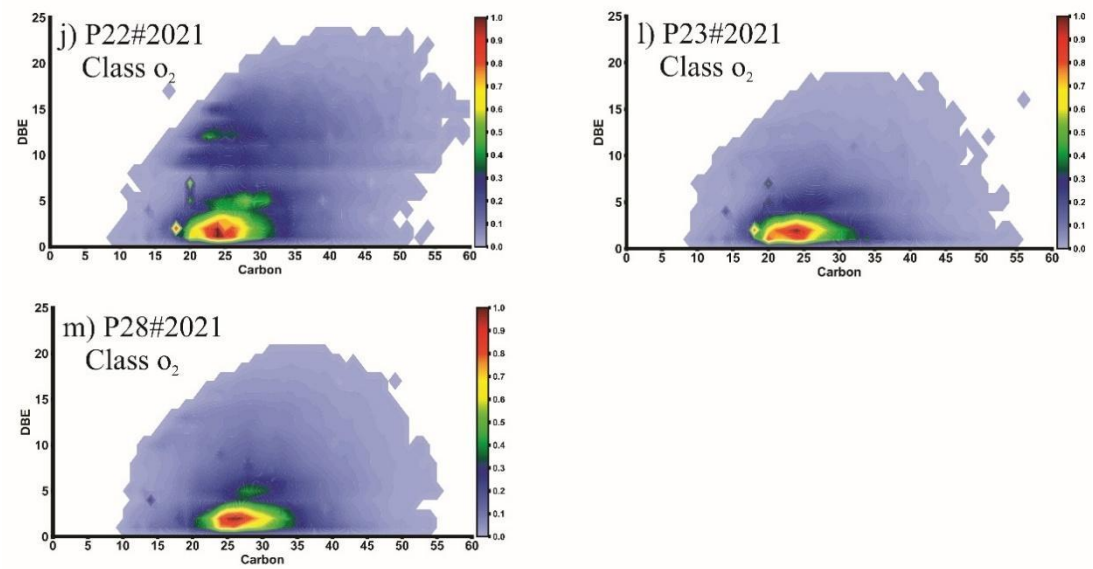

Figure S20(Part. 2). Isoabundance contoured plots of the double bond equivalent (DBE) vs. carbon number for the O_2 class for the samples monitored in the year 2022.

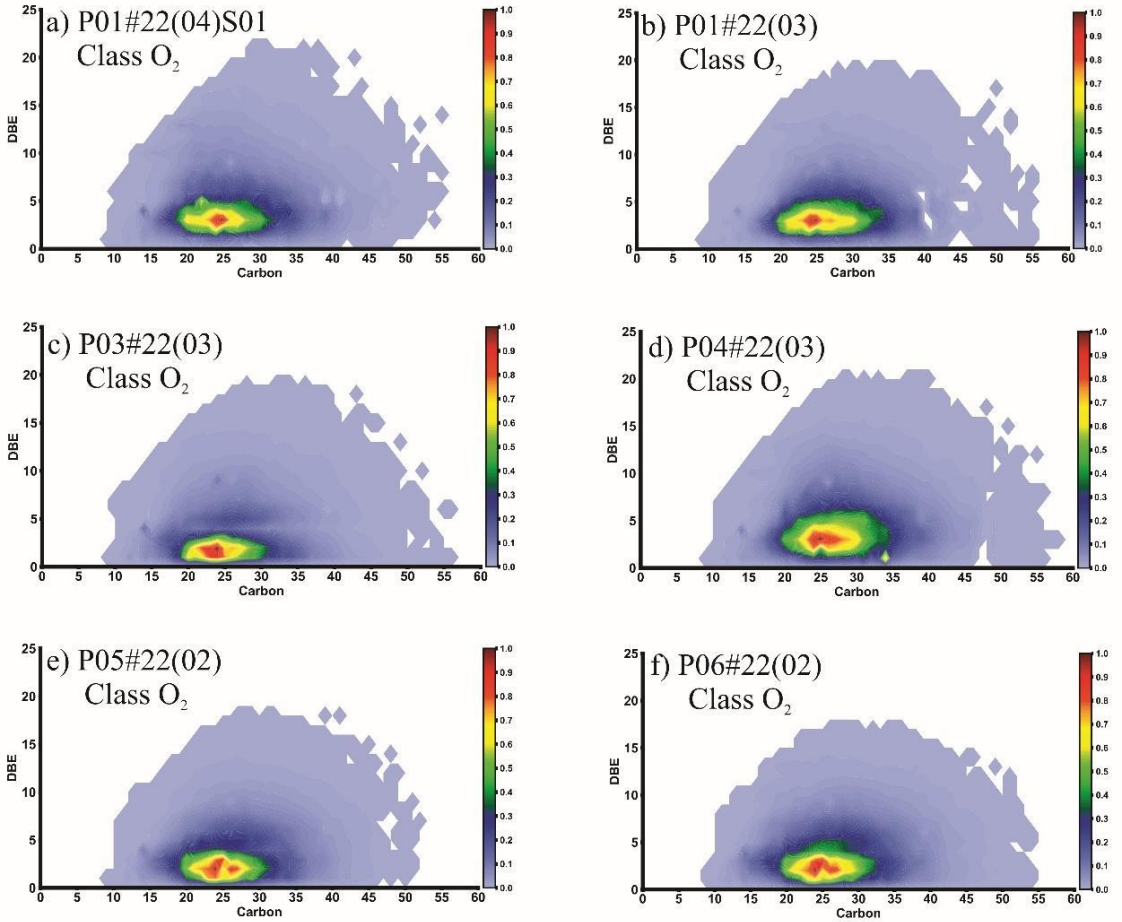

Figure S21. Isoabundance contoured plots of the double bond equivalent (DBE) vs. carbon number for the O_2 class for the samples monitored in the year 2022.